Percorso dottorale sviluppato con il sostegno finanziario di NextGenerationEU:

Missione 4, Componente 1, Investimento 4.1, CUP B63C22000810001

Borsa MUR exDM351/2022 Ricerche PNRR

Dipartimento di Biotecnologie, Chimica e Farmacia

Dottorato in Chemical and Pharmaceutical Sciences

38° Ciclo

Coordinatore: Prof. Maurizio Taddei

New approaches to the modulation of Hedgehog signalling pathway with small molecules and bioconjugates

Settore scientifico disciplinare: CHEM/05 – Organic Chemistry

Candidata

Demetra Zambardino

Sede di attività

Università degli Studi di Siena

Firma digitale del/della candidato/a

Firmato digitalmente da Demetra Zambardino
Data: 05.03.2026 15:16:08 CET

Supervisore

Prof.ssa Elena Petricci

Ente di appartenenza
Università degli Studi di Siena

Anno accademico di conseguimento del titolo di Dottore di ricerca

2025/26

“Anche ad essere s’impara”

Italo Calvino, Il cavaliere inesistente

ABSTRACT

Antibody-Drug Conjugates (ADCs) are at the forefront of targeted therapy, designed to enhance the therapeutic index of drugs. This approach leverages the high selectivity of a monoclonal antibody (mAb) to deliver a payload, covalently bound by a linker, to a specific target, thereby reducing off-target toxicity and improving pharmacokinetics. It is now recognized that the use of highly cytotoxic payloads is not essential for ADC efficacy, a realization that has expanded interest to a new range of payloads with diverse pharmacological activities. In this context, our efforts focused on the Hedgehog (Hh) signalling pathway, whose aberrant activation is implicated in a variety of human cancers by promoting proliferation and invasion of cancer cells. While few Hh inhibitors are approved for Hh-dependent diseases, the rapid emergence of drug resistance is a significant clinical challenge. Our research group has developed a library of Hh inhibitors active against resistant receptor mutants; however, these compounds display suboptimal pharmacokinetic profiles.

Therefore, the first section of this thesis details the design, synthesis, and evaluation of novel ADCs. This work centered on the development of conjugates incorporating in-house payloads, specifically Hh pathway inhibitors, ProTide-Gemcitabine systems, and ERK inhibitors, to overcome pharmacokinetic limitations and enhance therapeutic efficacy by targeted delivery.

Additionally, the modulation of Hh can also play a role in promoting the repair of tissues and osteogenesis processes. In this context, agonists of the Hh pathway can find application in regenerative medicine. Our research group has developed Hh agonists that were evaluated on mesenchimal cells for their osteogenic potential.

The second section of this thesis investigates a distinct project in green chemistry: the use of Sulfur Hexafluoride (SF_6) as a fluorinating agent. This work, carried out in the research group of Prof. Tanja Gulder at Saarland University, was driven by the need to find applications for SF_6, a potent yet non-toxic and chemically inert greenhouse gas. A novel photochemical methodology was developed and optimized to exploit SF_6 as a reagent for the nucleophilic fluorination of organic compounds. A preliminary substrate scope evaluation yielded promising data and established future perspectives for the valorization of this abundant gas.

INDEX

LIST OF ABBREVIATIONS

2-HG	D-2-hydroxyglutarate
5-FU	5-Fluorouracil
7TM	Seven-transmembrane
AAC	Antibody-antibiotic conjugate
ADA	Anti-drug antibody
ADC	Antibody-drug conjugate
ADCC	Antibody-dependent cellular cytotoxicity
ADME	Absorption, distribution, metabolism, and excretion
ALCL	Anaplastic large-cell lymphoma
ALP	Alkaline phosphatase
AML	Acute myeloid leukaemia
APL	Acute promyelocytic leukaemia
ARS	Alizarin red S
ATO	Arsenic trioxide
BC	Bodipy-cyclopamine
BCC	Basal cell carcinoma
BCN	Bicyclononyne
bs	Broad singlet
CAST	Cancer Stromal Targeting
CatB	Cathepsin B
CD	Cluster of differentiation
CDC	Complement-dependent cytotoxicity
CDR	Complementarity-determining region
CE	Capillary electrophoresis
CGNP	Cerebellar granule neuron precursor
CL_{int}	Intrinsic clearance
CRC	Colorectal cancer
CSF-1R	Colony-stimulating factor 1 receptor
CTC	2-Chlorotrityl chloride resin
Ctx	Cetuximab
CuAAC	Copper-catalyzed azide-alkyne cycloaddition
CYP	Cytochrome P
Cys	Cysteine
d	Doublet
DAR	Drug-antibody ratio
DAST	Diethylaminosulfur trifluoride
DBCO	Dibenzocyclooctyne amine
DCE	1,2-dichloroethane
dd	Doublet of doublets
ddd	Doublet of doublets of doublets
dddd	Doublet of doublets of doublets of doublets
DDI	Drug-drug interaction
Deoxo-Fluor	Bis(2-methoxyethyl)aminosulfur trifluoride
DHh	Desert Hedeghog
DIBAC	Aza-dibenzocyclooctyne
DIBALH	Diisobutylaluminum hydride

DIBO	Dibenzoannulated cyclooctyne
DIPEA	*N*,*N*-diisopropylethylamine
DLS	Dynamic light scattering
DM1	Mertansine or emtansine
DM4	Ravtansine or soravtansine
DMAP	4-dimethylaminopyridine
DMF	Dimethylformamide
DMSO	Dimethyl sulfoxide
DNA	Deoxyribonucleic acid
DPR	Diaminopropionic acid
DTT	Dithiothreitol
EC_{50}	Half-maximal effective concentration
ECD	*N*-terminal extracellular domain
ECL	Extracellular loop
EDC·HCl	1-Ethyl-3- (3-dimethylaminopropyl)carbodiimide hydrochloride
EGFR	Epidermal growth factor receptor
EMSA	Electrophoretic mobility shift assays
EMT	Epithelial-mesenchymal transition
ERK	Extracellular signal-regulated kinases
ESI	Electrospray ionization
EtOAc	Ethyl acetate
Fab	Fragment antigen binding
FAP	Fibroblast activation protein
Fc	Fragment crystallizable region
FcγR	Fcγ receptor
FDA	Food and Drug Administration
Fmoc	Fluorenylmethoxycarbonyl
GC-MS	Gas chromatography-mass spectrometry
GlaB	Glabrescione B
GLI-A	Activator GLI
GLI-R	Repressor GLI
GP	General procedure
GPCR	G protein-coupled receptor
GSH	Reduced glutathione
HAMA	Human anti-mouse antibody
HAT	Hydrogen atom transfer
HDAC	Histone deacetylase
HER	Human epidermal growth factor receptor
Hh	Hedgehog
HIC	Hydrophobic interaction chromatography
HIPS	Hydrazino-iso-Pictet-Spengler
HL	Hodgkin's lymphoma
HMPO	5-(hydroxymethyl)pyrogallol orthoester
HPLC	High-performance liquid chromatography
HPV	Human papillomavirus
HRMS	High-resolution mass analysis
I/E	Influx/efflux
IAA	Indole-3-acetic acid

iADC/ISAC	Immune-stimulating antibody conjugate
IC_{50}	Half maximal inhibitory concentration
ICBs	Immune checkpoint blockades
IDH	Isocitrate dehydrogenase
IEDDA	Inverse electron-demand Diels-Alder
IFT80	Intraflagellar transport protein 80
Ig	Immunoglobulin
IHh	Indian Hedgehog
ISCT	International society for cell therapy
LC-MS	Liquid chromatography - mass spectrometry
LiHDMS	Lithium bis(trimethylsilyl)amide
Lys	Lysine
m	Multiplet
mAb	Monoclonal antibody
MALDI	Matrix-assisted laser desorption/ionization
MC	Maleimidocaproic acid
MCC	*N*-maleimidomethylcyclohexane-1-carboxylate
MCR	Multicomponent reaction
MDR	Multidrug-resistance
MeCN	Acetonitrile
MM	Malignant mesothelioma
MMAE	Monomethyl auristatin E
MMAF	Monomethyl auristatin F
mQ	MilliQ water
mRNA	Messenger ribonucleic acid
MSC	Mesenchymal stem cell
MTGase	Microbial transglutaminase
MTX	Methotrexate
MW	Microwave
NAs	Nucleoside Analogues
ncAA	Noncanonical aminoacid
NFSI	*N*-fluorobenzenesulfonimide
NHC	*N*-heterocyclic carbene
NHS	*N*-hydroxysuccinimide
NK	Natural killer
NMR	Nuclear magnetic resonance
ORR	Overall response rate
OS	Overall survival
P3	Passage 3
PABA	*p*-aminobenzyl alcohol
pAcF	*p*-acetylphenylalanine
PBD	Pyrrolobenzodiazepine
PBS	Phosphate-buffer saline
PC	Primary cilium
PDB	Protein data bank
PE	Petroleoum ether
PEG	Polyethylene glycol
PFS	Progression-free survival

PgP	P-glycoprotein
PI3K	Phosphatidylinositol 3-kinase
PK	Pharmacokinetics
PPO	Protoporphyrinogen oxidase
ppt	Parts per trillion
PSAR	Polysarcosine
pTLC	Preparative thin-layer chromatography
PTCH	Patched
Py	Pyridine
q	Quartet
QM	Quinone methide
qPCR	Quantitative polymerase chain reaction
RIC	Radioimmunoconjugate
RNAi	Ribonucleic acid interference
R_t	Retention time
r.t.	Room temperature
RT-qPCR	Real-time polymerase chain reaction
s	Singlet
S-NHS	Sulpho-*N*-hydroxysuccinimide
SAHA	Vorinostat, suberanilohydroxamic acid
SAR	Structure–activity relationship
SCC	Squamous cell carcinoma
SDHI	Succinate dehydrogenase inhibitor
SEC	Size-exclusion chromatography
SER	Single-electron reduction
SET	Single-electron transfer
SHh	Sonic Hedgehog
SMAC	Sortase-mediated antibody conjugation
SMC	Smooth muscle cell
SMO	Smoothened
S_NAr	Nucleophilic aromatic substitution
SPAAC	Strain-promoted azide-alkyne cycloaddition
SrtA	Sortase A
STING	Stimulator of interferon genes
SuFu	Suppressor of Fused
t	Triplet
T3P	Propylphosphonic anhydride
TAM	Tumour-Associated Macrophage
TBAF	Tetrabutylammonium fluoride
TBAI	Tetrabutylammonium iodide
TCEP	Tris(2-carboxyethyl)phosphine
TDAE	Tetrakis(dimethylamino)ethylene
TEMPO	2,2,6,6-Tetramethylpiperidin-1-oxyl
TFA	Trifluoroacetic acid
TFF	Tangential flow filtration
TFMP	Trifluoromethylpyridine
THF	Tetrahydrofuran
TI	Therapeutic index

TLC	Thin-layer chromatography
TLR	Toll-like receptor
TMDD	Target-mediated drug disposition
TME	Tumour microenvironment
TNBC	Triple-negative breast cancer
TOF	Time of flight
TsCl	*p*-toluenesulphonyl chloride
T-DM1	Trastuzumab emtansine
UV-Vis	Ultraviolet-visible spectroscopy
Val-Cit	Valine-citrulline
VEGF	Vascular endothelial growth factor
WTA	Wall teichoic acid

SECTION A - DEVELOPMENT OF BIOCONJUGATION STRATEGIES FOR THE SYNTHESIS OF NOVEL ANTIBODY-DRUG CONJUGATES

CHAPTER 1. INTRODUCTION

1.1. CANCER IN THE WORLD AND FUTURE TRENDS

With improving prevention for cardiovascular diseases, changing demographic and risk factors have led to today's observation that cancer is the first or second leading cause of premature death (i.e. at ages 30-69 years) in 134 of 183 countries, and it ranks third or fourth in an additional 45 countries.[1] Despite advances in early detection and treatment, the global incidence of cancer continues to rise. The combination of population growth and increasing life expectancy has led to a steady increase in the absolute number of cancer cases and deaths worldwide (**Figure 1**).

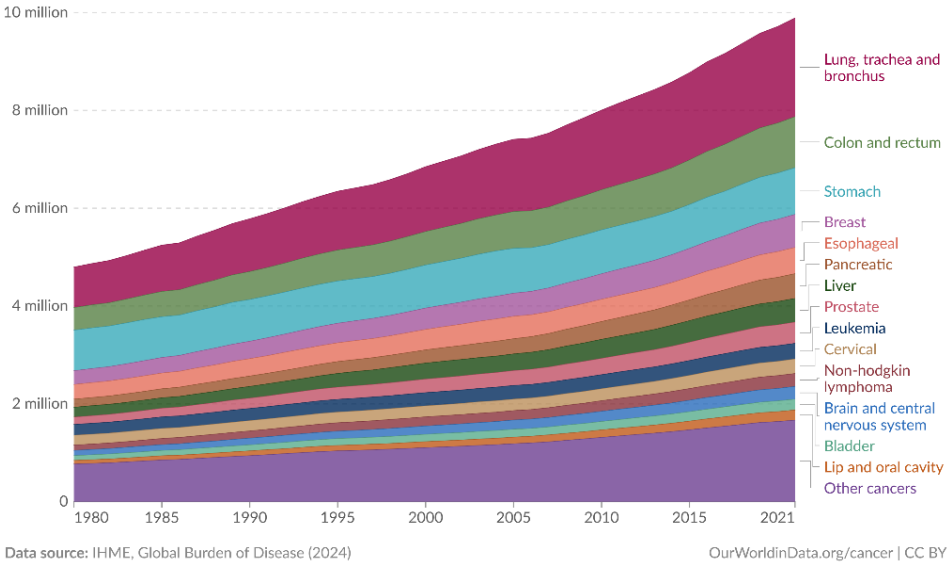

Figure 1. Cancer deaths by type, world.[2]

According to the World Health Organization, new cancer cases are expected to increase from approximately 20 million in 2022 to over 35 million by 2050 (**Figure 2**), a rise of around 77%.[3]

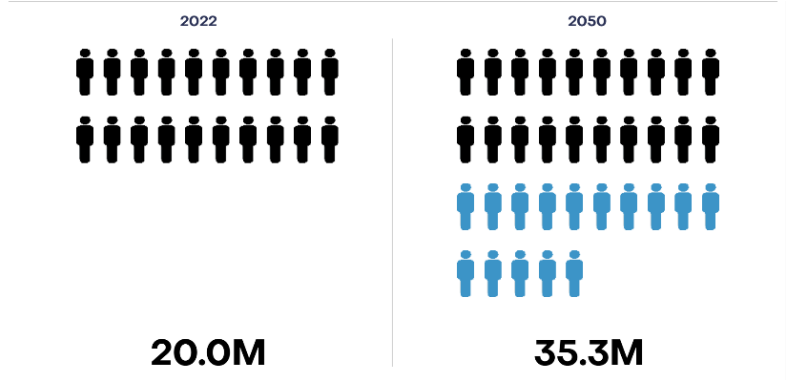

Figure 2. Estimated number of new cases of cancer worlwide from 2022 to 2050, both sexes, age 0-85+.[4]

While some malignancies are associated with well-characterized risk factors, such as infections by *Helicobacter pylori*, human papillomavirus (HPV), or hepatitis viruses, a large proportion of cancers are still of multifactorial or unknown origin. It is estimated that only 5-10% of all cancers result from inherited genetic mutations, whereas the remaining 90-95% are linked to environmental exposures and a variety of risk factors. These include tobacco use, excessive alcohol consumption, unhealthy diet, obesity, sedentary behaviour, and chronic infections. Notably, infection-related cancers account for roughly 13% of cases globally, with higher rates observed in low-income regions, highlighting the importance of vaccination and antimicrobial interventions. Other carcinogenic agents, such as ionizing radiation, ultraviolet rays, or exposure to industrial chemicals and air pollution, also play a role in cancer development.[1]

Taken together, these data underscore the complex and multifactorial nature of cancer. Demographic changes and the growing prevalence of high-risk lifestyles in industrialized societies are expected to drive a further increase in cancer burden in the coming decades. This evolving scenario calls for the development of more targeted and effective therapeutic strategies, and reinforce the importance of interdisciplinary approaches in oncology research, particularly at the intersection of chemistry, biology, and pharmaceutical innovation.

1.1.1. Conventional therapies and challenges

The standard treatment for cancer consists of generally validated therapeutic approaches widely accepted and applied in long-term clinical practice, including surgery, radiotherapy and chemotherapy, which are frequently combined to enhance their respective efficacies. However, although conventional therapies have high initial response rates, the proliferation and

progression mechanisms of tumors, and the overall complexity of these malignancies, often result in several complications, such as treatment resistance and tumor relapse, exposing the limits of these traditional approaches.[5]

Surgical resection is the primary approach for managing solid tumors. Nevertheless, this approach may not be adequate to achieve the desired therapeutic outcomes in cases of highly invasive and metastatic malignancies, making it the best option only for the treatment of cancer in its early stages.

Radiotherapy is a highly efficacious strategy for treating cancer, as the process of irradiation can result in direct DNA damage, which subsequently leads to apoptosis, necrosis and mitotic abnormalities in cancer cells.[6] However, it is important to note that tumor resistance and relapse are frequently observed following radiotherapy, a phenomenon that can be attributed to the presence of "radiation-resistant mechanisms" within tumor cells. Indeed, tumor cells demonstrate increased self-repair capabilities, thus enabling them to effectively repair radiation-induced DNA damage.[7] In addition, in cases such as hypoxic or highly differentiated tumors, sensitivity to radiation is diminished.[8,9] Furthermore, the efficacy of radiation treatment can be influenced by the location and size of the tumor. Tumors in hard-to-reach areas or with large volumes are challenging to eradicate completely using radiotherapy. Finally, a great issue of radiotherapy is also its low selectivity, leading to damages to healthy cells, tissues, and organs.

Radiotherapy and surgery were the predominant approaches for cancer management in the 1960s. However, as micrometastases and the recurrence of cancer after surgery and radiation therapy became evident, there was an increasing interest in combination chemotherapy.[10] The term “chemotherapy” was coined in the early 1900s by the German chemist Paul Ehrlich, who investigated the use of chemicals to treat diseases.[11] Anticancer drugs exhibit diverse mechanisms to directly eradicate cancer cells, mainly interfering with processes involved in progression through the cell cycle, for example by inducing DNA damage, inhibiting DNA replication, and disrupting mitosis.[12] Despite the successful development of new compounds with antitumoral activity in the recent years, conventional chemotherapy continues to face several challenges that necessitate further efforts towards the development of new approaches. One major concern associated with chemotherapy is drug resistance. This situation occurs when cancer cells become resistant to an antitumoral agent. In addition to this, decreased absorption

of drugs and drug efflux are the major causes of such conditions. Other disadvantages of using conventional chemotherapeutic methods include complications in dose selection, a decline in selectivity, low penetration through tissues, rapid drug metabolism, and side effects caused by off-target toxicity.[13]

Finally, in the development of a new chemotherapeutic agent, it is insufficient to just pursue high cytotoxic potency, instead, an early evaluation of the compound's pharmacokinetic (PK) profile is equally critical. The PK profile of a compound encompasses the following: absorption, distribution, metabolism, and excretion (ADME). A considerable number of candidates that show promise in preclinical or clinical stages are unsuccessful due to unfavourable ADME characteristics, such as poor bioavailability, rapid clearance, or off-target tissue accumulation. Consequently, in conjunction with the efforts of medicinal chemistry to optimize efficacy, it is crucial to integrate advanced drug-delivery strategies, controlled release systems and targeted therapy approaches, improving the likelihood of clinical success.

1.1.2. Immunotherapy and monoclonal antibodies

The fundamental principle of immunotherapy is that the immune system can be harnessed to cope with advanced neoplastic diseases.[14] The objective of immunotherapy is to enhance or restore the immune system's defences against cancer cells. It represents one of the most recent advancements in cancer treatment, and its combination with conventional approaches has proven to be successful. A range of immunotherapies, including immune checkpoint blockades (ICBs), adoptive cell therapies, cancer vaccines, and cytokine therapies, have been developed to target specific components of the immune system.[15,16] Several of these have been approved by the United States Food and Drug Administration (FDA).[17] As previously stated, although conventional therapies demonstrate high initial response rates, they are limited by short-term responses, treatment resistance, and cancer tissue heterogeneity. Conversely, emerging immunotherapies have been shown to provide a long-term response by activating host antitumor immunity. Analysis of preclinical and clinical data has demonstrated that patients with highly immunogenic or early-stage tumors are more likely to respond positively to immunotherapies. Nevertheless, the response rate to immunotherapies is low, with observations indicating that only 10% to 40% of cancer patients demonstrate a positive response.[17]

Among the most extensively studied elements of cancer immunotherapy are monoclonal antibodies (mAbs), which are designed to specifically bind to antigens expressed on the surface of tumor cells or within the tumor microenvironment.[18] These biologics have the capacity to mediate anti-tumor effects through a variety of mechanisms. Unconjugated mAbs have been shown to interfere directly with oncogenic signalling pathways by blocking ligand-receptor interactions or by inducing receptor internalization and degradation.[19] Furthermore, they have the capacity to trigger immune-mediated mechanisms such as antibody-dependent cellular cytotoxicity (ADCC), in which the fragment crystallizable (Fc) region of the antibody engages Fcγ receptors on effector immune cells, including natural killer (NK) cells and macrophages.[20] This process ultimately results in the destruction of antibody-coated cancer cells. Another significant mechanism is complement-dependent cytotoxicity (CDC), whereby antibody binding activates the complement cascade, leading to lysis of the target cell.[20] Furthermore, mAbs have been shown to facilitate antigen uptake by dendritic cells and promote cross-presentation to T lymphocytes, thereby initiating or amplifying adaptive immune responses. Despite these advantages, the clinical efficacy of mAbs remains limited in many cancer types. Response rates are subject to significant variation and are influenced by a number of factors, including antigen heterogeneity, tumor immune evasion strategies, and individual patient immunogenetics. Tumor cells may downregulate or even completely lose expression of the target antigen, thus rendering antibody-based therapies ineffective over time.[17] Furthermore, solid tumors frequently present a hostile microenvironment, characterised by physical barriers, immunosuppressive cytokines, and regulatory cell populations, all of which can impair antibody penetration and limit immune effector function.[21] These biological and physical obstacles contribute to the modest response rates observed in many clinical settings and highlight the intrinsic limitations of relying solely on the immunostimulatory potential of mAbs.

Nevertheless, the most valuable feature of mAbs is their excellent specificity for tumor-associated antigens, which allows precise targeting of malignant cells while sparing healthy tissues. This distinctive property represents the foundation for pioneering strategies that extend beyond the immediate immunotherapeutic function of antibodies. In particular, mAbs have been successfully repurposed as targeted delivery vehicles for cytotoxic agents, toxins, radionuclides, or immune modulators. This approach has led to the development of antibody-drug conjugates (ADCs), a class of therapeutics that combine the selective targeting capability of antibodies with

the potent cell-killing activity of chemotherapy agents. Consequently, even in cases where mAbs are inadequate as standalone therapeutic agents, their structural and functional properties remain highly valuable for the design of next-generation targeted therapies.

1.1.3. Antibody-drug conjugates

In this context ADCs stand out as promising antitumoral therapeutics and one of best tools in targeted therapy. The approach to targeted chemotherapy was formulated at the beginning of the twentieth century by Paul Ehrlich's concept of the "magic bullet".[22] The principle of this concept aims at avoiding adverse effects: drugs must be guided and released into the tumor sites through association with ligands that are overexpressed or selectively expressed in the tumor. Ehrlich's proposal has been translated into practical applications for therapy with the development of the first conjugated antibodies. In order to become pharmacologically active drugs, mAbs can be linked to either a radioisotope (producing radioimmunoconjugates, RICs), a drug (ADCs) or a protein toxin (producing immunotoxins)[23,24].

An ADC is composed of three main elements: i) a mAb which specifically recognizes and binds an antigen that is overexpress or exclusively expressed by the target cell, ii) a pharmacologically active compound, also referred to as “payload” or “warhead”, iii) a linker, which is a chemical spacer that covalently connects the payload and the mAb (**Figure 3**).[25] Each component is indispensable and plays a key role in the efficacy of an ADC. For this reason, the design process is a complex field, that implies expertise in organic chemistry, biochemistry and medicine.

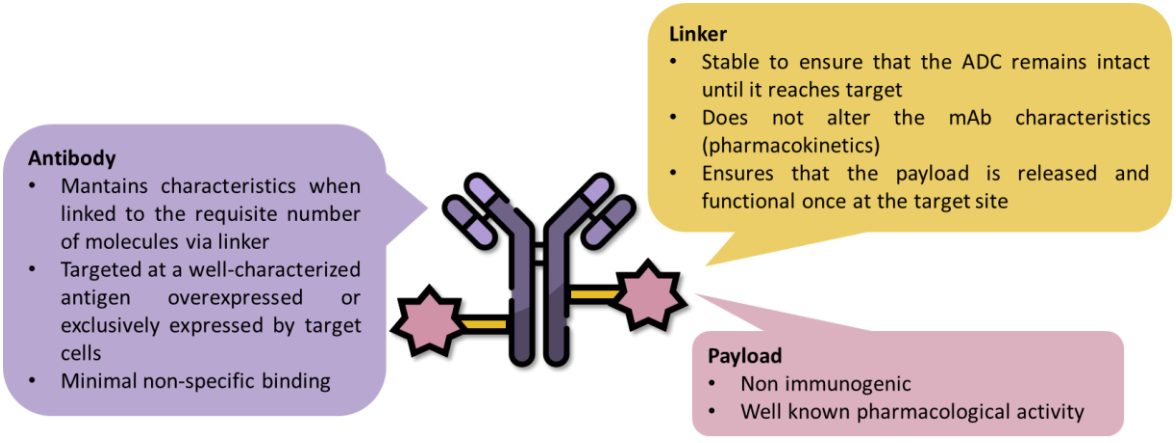

Figure 3. General structure of an ADC.

Indeed, while the mAb must interact selectively with the tumor cells, and the payload must be able to exhibit its pharmacological action once in the designated site, the linker must be properly

designed to ensure stability of the bioconjugate in plasma while also being able to release the payload in its active form once the ADC is internalized in the target cell. A key parameter in the field of ADCs is the "Drug-Antibody Ratio" (DAR), which indicates the number of linker-payload molecules attached on a single mAb.

The general mechanism of action starts with the intravenous administration of the bioconjugate, because of poor oral bioavailability and to avoid proteolytic degradation by digestive enzimes.[26] The ADC remains inactive during blood circulation, until it finds and binds its cellular target. On binding to its target, the ADC-antigen complex is usually internalized via clathrin-mediated endocytosis, forming an early endosome containing the ADC-antigen complex.[27] Early endosomes eventually mature into late endosomes before fusing with lysosomes. Once internalized in the tumor cell, certain conditions, depending on the linker chemical structure and properties, can initiate the cleavage of the linker-payload system thus releasing the payload. The payload is then transported from the lysosome lumen to the cytosol.[27] Within the intracellular environment the drug leads to cellular death (**Figure 4**).

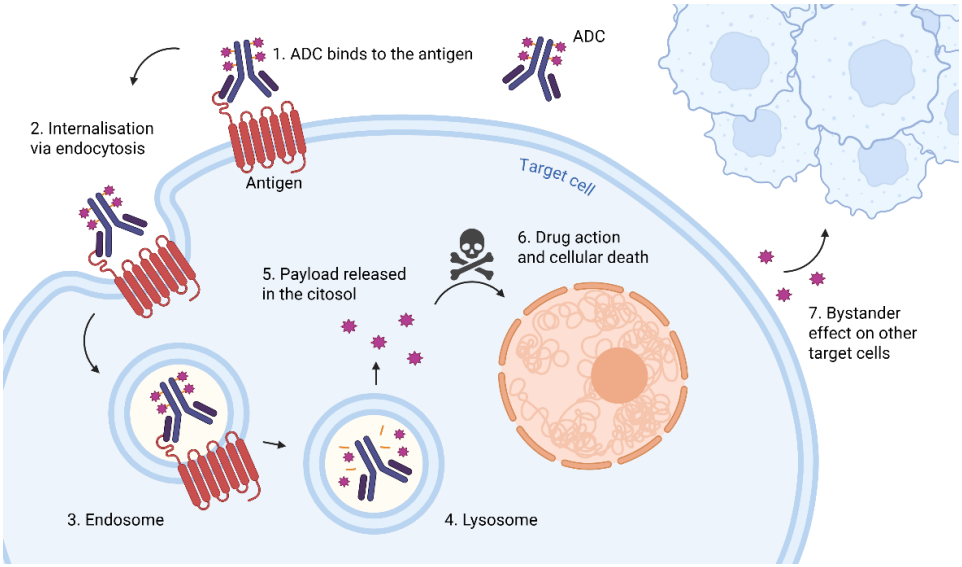

Figure 4. General mechanism of action of ADCs. Created with Biorender.

The therapeutic index (TI), defined as the ratio between the toxic dose and the effective dose of a drug, has always been a critical parameter in drug development. ADCs were initially conceived to enhance this ratio by delivering potent chemotherapeutic agents with heightened selectivity, thereby aiming to mitigate systemic toxicity.[28] ADCs allow to use very potent cytotoxic agents that would otherwise be too toxic for standalone systemic administration. By largely confining

their activity to tumor cells, ADCs facilitate significantly higher local drug concentrations within the tumor microenvironment.[29]

Furthermore, a crucial advantage of the ADC technology is the bystander effect. This phenomenon occurs when the cytotoxic chemotherapeutic agent, once released, can permeate the cell membrane and affect neighboring tumor cells that may not express the specific target antigen. [30] This represents a substantial leap forward in drug design because it directly addresses tumor heterogeneity, a major contributing factor to resistance.[31] Tumors are often a heterogeneous mix of cells, some expressing the target antigen and others not. The bystander effect ensures that even non-expressing cells within the tumor microenvironment are exposed to the cytotoxic drug, leading to more complete tumor eradication and potentially overcoming resistance arising from antigen loss or downregulation. By enabling the killing of "non-conforming" cells, it significantly broadens the therapeutic reach of the ADC within the tumor, leading to a more durable response. Consequently, this enhances the probability of long-term remission in complex tumor environments.

1.1.4. ADCs in the market

Paul Ehrlich's concept of targeted therapy was put into practice in 1958 when methotrexate (MTX) was linked to an antibody targeting leukemia cells.[32] In the following decades, several efforts have been made for the development of ADCs, first employing polyclonal antibodies, that enabled for the first time preclinical efficacy studies in animal models with both noncovalent-linked ADCs and later covalently linked ADCs.[33,34] The first ADCs were produced with murine mAbs, until advances in antibody engeneering allowed the production of humanized mAbs with lower immunogenicity.[35] After several failures in human clinical trials, caused by immunogenicity issues, instability of linkers and low drug potency, a new generation of ADCs has been developed exhibiting encouraging results.

In 2000 the FDA approved the first ADC, Mylotarg® (gemtuzumab ozogamicin), which combines an anti-CD33 antibody with the DNA-targeting agent calicheamicin, for the treatment of acute myeloid leukaemia (AML).[36] Unfortunately it was withdrawn from the market a decade later due to lack of improvement in overall survival and most importantly the occurrence of severe cases of veno-occlusive disease. In 2012, a study showed that dose fractionation, replacing a single dose of 9 mg/m^2 with three doses of 3 mg/m^2, was sufficient to control liver toxicity while

maintaining anti-leukaemic activity.[37] Therefore, Mylotarg was reapproved by the FDA in 2017, both in the first-line setting and in relapsed or refractory CD33-positive AML in adults and children. In 2011, Adcetris® (brentuximab vedotin), a CD30-specific mAb linked to monomethyl auristatin E (MMAE), gained access to the market for the treatment of Hodgkin's (HL) and anaplastic large-cell lymphomas (ALCL).[38,39] Kadcyla® (ado-trastuzumab emtansine, T-DM1) combined for the first time the already approved and widely administered humanized antibody trastuzumab with a potent antimicrotubule cytotoxic agent using a highly stable linker, and was approved for the treatment of HER2-positive breast cancer, being the first ADC approved for the treatment of any solid tumor.[40,41] Following Kadcyla®, a second HER2-targeted ADC, Enhertu® (trastuzumab deruxtecan), also called T-DXd, was approved for metastatic HER2-positive breast and gastric cancer.[42–44] Trastuzumab emtansine and trastuzumab deruxtecan differ in their cytotoxic payloads (a tubulin inhibitor and topoisomerase I inhibitor, respectively).

Following these successes many ADCs have demonstrated impressive activity against treatment-refractory cancers, resulting in approvals in numerous and diverse indications. To date, 17 ADCs have received regulatory approval (**Table 1**) , and hundreds are under clinical trials.

Interest and investments in the development of ADCs have increased significantly. Pharmaceutical companies are investing heavily to expand the range of conditions for which ADCs can be effective. According to a report from late 2023, the global ADC market grew from USD 1.4 billion in 2016 to USD 11.3 billion in 2023, and is projected to reach USD 23.9 billion by 2032.[45]

Table 1. Overview of approved ADCs.

Year	ADC (Trade Name)	Target	Cancer Type
2000	Gemtuzumab ozogamicin (Mylotarg)[a]	CD33	acute myeloid leukemia
2011	Brentuximab vedotin (Adcetris)	CD30	Hodgkin lymphoma and systemic ALCL
2013	Trastuzumab emtansine (Kadcyla)	HER2	metastatic breast cancer
2017	Inotuzumab ozogamicin (Besponsa)	CD22	B-cell precursor acute lymphoblastic leukemia
2018	Moxetumomab pasudotox (Lumoxiti)	CD22	hairy cell leukemia
2019	Polatuzumab vedotin (Polivy)	CD79b	diffuse large B-cell lymphoma
2019	Enfortumab vedotin (Padcev)	Nectin-4	metastatic urothelial carcinoma
2019	Trastuzumab deruxtecan (Enhertu/T-DXd)	HER2	various HER2-positive cancers
2020	Sacituzumab govitecan (Trodelvy)	TROP2	triple-negative breast cancer and urothelial carcinoma
2020	Belantamab mafodotin (Blenrep)	BCMA	multiple myeloma
2020	Cetuximab saratolacan (Akalux)[b]	EGFR	head and neck cancer
2021	Loncastuximab tesirine (Zynlonta)	CD19	large B-cell lymphoma
2021	Disitamab vedotin (Aidixi)	HER2	urothelial/gastric cancers
2021	Tisotumab vedotin (Tivdak)	TF	cervical cancer
2022	Mirvetuximab soravtansine (Elahere)[c]	FRα	ovarian cancer
2024	Sacituzumab tirumotecan (Jiatailai)[d]	TROP2	lung cancer
2025	Datopotamab deruxtecan (Datroway)	TROP2	HR^+, $HER2^-$ breast cancer

[a] Discontinued in 2010, reapproved in 2017.
[b] Approved in Japan.
[c] Discontinued in August 2023 due to commercial considerations.
[d] Approved in China.

1.2. ANTIBODY-DRUG CONJUGATES: COMPONENTS, PROPERTIES, AND CHALLENGES

As mentioned above, ADCs represent the frontier of oncological treatment and targeted therapy. However, they are extraordinarily complicated in nature, and the design and development of an efficacious bioconjugate therefore involves overcoming a series of challenges and requires expertise in several scientific fields, including protein chemistry, organic chemistry, pharmacology and medicine.

1.2.1. Antibodies and antigens

Antibodies, also known as immunoglobulins, are Y-shaped proteins that are secreted by B lymphocytes as part of the adaptive immune response. Each antibody consists of two identical heavy chains (H) and two identical light chains (L), which are held together by disulfide bonds formed by cysteine residues. Each chain is made up of one *N*-terminal variable (v) immunoglobulin domain and one or more *C*-terminal constant (c) Ig domains. Enzymatic processing can break up antibodies into two fragments named Fragment antigen binding (Fab) and Fragment crystallizable (Fc) (**Figure 5**).[46] The paired v-H and v-L domains at the tips of the Y form the antigen-binding site, and it is the hypervariable complementarity-determining regions (CDRs) in these domains that confer high specificity to a corresponding epitope. In contrast, the C domains, which form the Fc region, are highly conserved and mediate various functions, such as recruiting complement or binding Fc receptors on phagocytes. Upon binding to an antigen, an antibody can neutralize pathogens or toxins by blocking key interactions and tagging microbes for clearance by phagocytic cells. This combination of modular structure and high-affinity specificity makes antibodies powerful molecular recognition elements, therefore they are widely used as reagents and therapeutics in diagnostics and biomedical applications. There are five classes of immunoglobulins, IgG, IgM, IgA, IgD, and IgE. These are distinguished by the type of heavy chain found in the molecule. Among these, immunoglobulins G (IgG) are favoured for ADCs because they possess long serum half-life (≈ 21 days in humans), are structurally stable under physiological conditions, have reduced complexity (monomeric structure), and finally have strong safety and efficacy track record.[47]

Human IgGs comprise four subclasses (IgG1, IgG2, IgG3 and IgG4), which differ in their constant domains and hinge regions.[48] Subtle variations between these subclasses affect the solubility and half-life of mAbs as well as their affinity for different Fcγ receptors (FcγRs) expressed on immune effector cells. Most ADCs employ an IgG1, as this subclass offers a balanced combination of

pharmacokinetic and functional properties. Although IgG2 and IgG4 are also employed, for example in gemtuzumab ozogamicin and inotuzumab ozogamicin, IgG1 antibodies demonstrate comparable serum half-lives while exhibiting superior complement activation and Fcγ receptor engagement.[49,50] Conversely, IgG3, are seldom utilized in the development of ADCs, primarily due to relatively short serum half-life, which limits the therapeutic efficacy.[51]

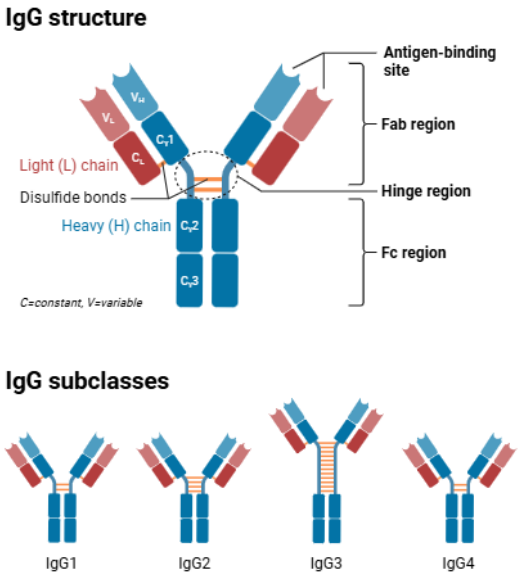

Figure 5. Schematic representation of IgG structure and classification. Created with Biorender.

Given the need for high target specificity, strong binding affinity, and sustained exposure at the tumor site, the selection of antibodies should aim for minimal cross-reactivity with healthy tissues, sub-nanomolar affinity for the target antigen, and a prolonged PK half-life coupled with low immunogenicity.[52] The immunogenic potential of an ADC is a key determinant of its circulatory half-life: antibodies with poor tumor specificity are more likely to be rapidly cleared due to immune recognition, resulting in reduced target exposure and diminished therapeutic efficacy.[53] In the early stages of ADC development, murine monoclonal antibodies were commonly used; however, these frequently elicited the formation of human anti-mouse antibodies (HAMA) within weeks of a single dose, thereby limiting their clinical utility.[54] Consequently, murine antibodies were replaced by chimeric IgGs, and later by humanised IgGs. More recently, the interest has shifted towards the development of ADCs incorporating either humanised or fully human antibodies, which offer enhanced tolerability and reduced immunogenic risk (**Figure 6**).[52]

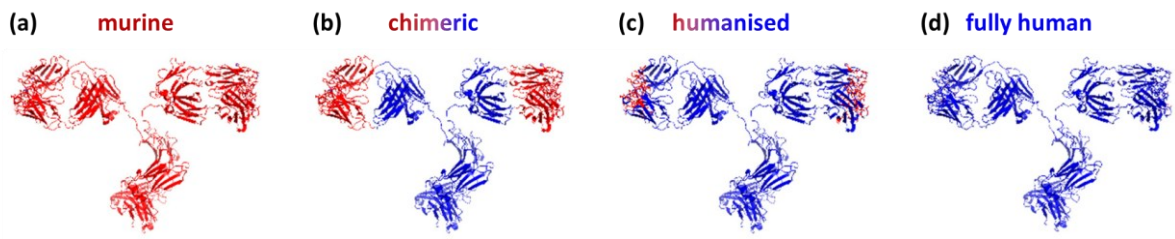

Figure 6. (**a**) murine, (**b**) chimeric, (**c**) humanised, and (**d**) fully human monoclonal antibodies. Red and blue represents mouse and human antibody sequence respectively.[55]

The efficacy of any antibody-based therapy fundamentally depends on the expression of antigens and their subsequent recognition, thus making the selection of antigens a pivotal aspect of ADC design. A well-established guiding principle is the selection of cell-surface proteins that are highly expressed on tumor cells but are largely absent from healthy tissues. The aforementioned selective expression has been demonstrated to broaden the therapeutic window and reduce the likelihood of systemic toxicity.[56] Ideally, ADC targets are uniformly and densely expressed across the tumor cell population; however, absolute homogeneity is not always necessary, as some ADCs are capable of eliciting a bystander killing effect.[57] Target accessibility is another essential consideration: high interstitial pressure within the tumor, in conjunction with endothelial, stromal, and epithelial barriers, has the capacity to restrict ADC penetration, resulting in only a fraction of the administered dose reaching the intended target. From a biological perspective, the selection of an effective ADC target must therefore balance tumor expression density, antigen internalization rates, and the chosen antibody Fc format to optimize delivery and therapeutic impact.

Therapeutic mAbs recognize a variety of tumor-associated antigens, which can be classified into several categories:

- haematopoietic differentiation antigens, often glycoproteins associated with cluster of differentiation (CD) markers, include CD20, CD30, CD33, and CD52;[58,59]
- cell surface differentiation antigens comprise diverse glycoproteins and carbohydrates expressed on both normal and tumor cells;
- growth and differentiation signalling antigens include growth factors and receptors such as CEA[60], EGFR (ERBB1)[61], ERBB2 (HER2)[62], ERBB3[63], MET (HGFR)[64], IGF1R[65], EPHA3[66], TRAILR1 (TNFRSF10A), TRAILR2 (TNFRSF10B), and RANKL (TNFSF11)[67];

- angiogenesis-associated antigens, such as VEGF, VEGFR, integrin αVβ3, and integrin α5β1, support neovascularization within the tumor microenvironment;[68]
- stromal and extracellular matrix antigens, including fibroblast activation protein (FAP) and tenascin, contribute to tumor architecture and survival. [69,70]

Recent research has focused on discovering novel antigens suitable for antibody-based cancer therapies. Serological, genomic, proteomic, and bioinformatic approaches have identified antigens and receptors overexpressed in tumor cells or linked to oncogenic mutations that drive malignancy.[71]

1.2.2. Linkers and spacers

Although the linker may not directly correlate with the overall potency of an ADC, the delivery of the payload to tumor cells, and therefore the therapeutic efficacy of an ADC, ultimately depends on the stability of the linker and its ability to trigger the release of the payload at the correct site.[72] The linker is a critical structural component that governs stability, selectivity, and pharmacological outcome of the conjugate, far from being a simple connection between the cytotoxic payload and the antibody.[73] It must prevent premature drug release in circulation while enabling the efficient, selective liberation of the payload once the ADC has bound to the antigen and has been internalized by the target cell. Additionally, linker design can impact the physicochemical properties of the ADC, influencing its solubility, stability, and biodistribution.

An optimal linker should:

- form a stable covalent bond with the payload via specific functional groups;
- contain reactive moieties for site-selective conjugation to amino acid residues of the antibody;
- remain stable under physiological conditions to ensure plasma circulation without premature drug release, as well as remain stable in buffered aqueous solutions to allow formulations for intravenous administration;
- undergo cleavage only under defined intracellular conditions, enabling controlled payload release at the target site through chemical or enzymatic transformations.

Generally linkers are named and classified according to their release mechanisms (**Figure 7**), the two main classes being that of cleavable linkers and non-cleavable linkers.

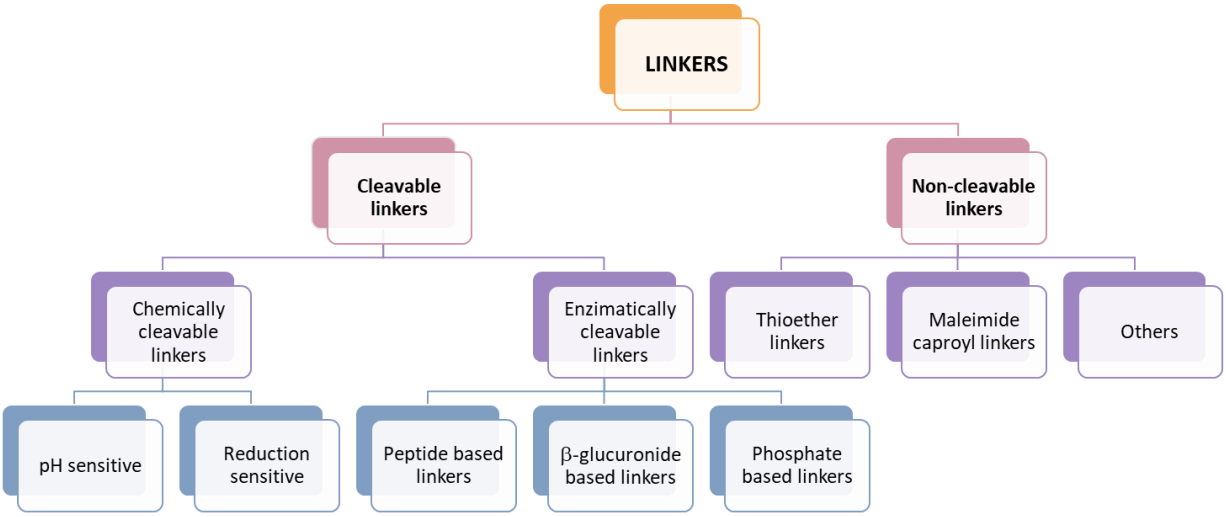

Figure 7. Classification of linkers.

1.2.2.1. Cleavable linkers

Cleavable linkers exploit the differences in conditions between the bloodstream and the cytoplasm within tumor cells. The change in environment once the ADC-antigen complex has been internalized triggers the cleavage of the linker and release of the active payload. Cleavable linkers are divided into two main sub-categories: chemically cleavable linkers and enzimatically cleavable linkers.

1.2.2.1.1. Chemically cleavable linkers

Chemically cleavable linkers are designed to respond to specific chemical stimuli present at the target site, thereby triggering the release of the cytotoxic payload through structural transformations. Common triggers include the acidic pH and reductive environment characteristic of tumor tissues (**Figure 8**).

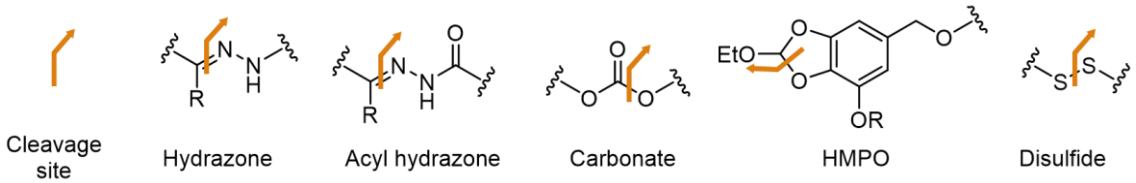

Figure 8. Chemically labile linkers and their cleavage sites.

Rapid metabolism and uncontrolled proliferation in cancer create a hypoxic microenvironment that is enriched in acidic metabolites and reduces the extracellular pH to approximately 5.7-6.9.[74]

Within tumor cells, further proton influx lowers the intracellular and subcellular pH to 5.0-6.0.[75] Acid-sensitive linkers, such as hydrazone[76], acylhydrazone[77] and carbonate[78] linkers, can be easily synthesised and are cleaved selectively under these acidic conditions. Notable examples include the first-generation ADCs gemtuzumab ozogamicin (Mylotarg®) and inotuzumab ozogamicin (Besponsa®), both of which employ an acyl hydrazone linker (**Figure 9**). However, hydrazone and acylhydrazone linkers suffer from limited plasma stability, often releasing the payload prematurely. Their synthesis is also limited to carbonyl or hydrazine derivatives, which restricts their applicability to drugs containing these functional groups.[79]

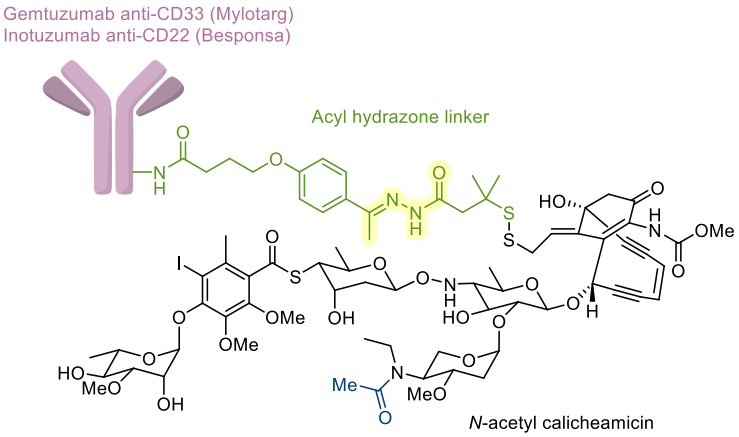

Figure 9. Structure of ADCs Mylotarg® and Besponsa®, containing an acyl hydrazone linker.

In this context, Migliorini and colleagues developed a pH-sensitive linker based on the natural product gallic acid.[80] The 5-(hydroxymethyl)pyrogallol orthoester derivative (HMPO – **Figure 8**) has been shown to remain stable for up to 24 hours at pH 7.4 and 6.6, as well as in plasma. Under acidic conditions (pH 5.5), it releases molecules bound to the hydroxymethyl moiety via a 1,6-elimination mechanism (**Scheme 1**). The linker was non-toxic and was able to successfully conjugate Doxorubicin and Combretastatin A4 to Cetuximab.

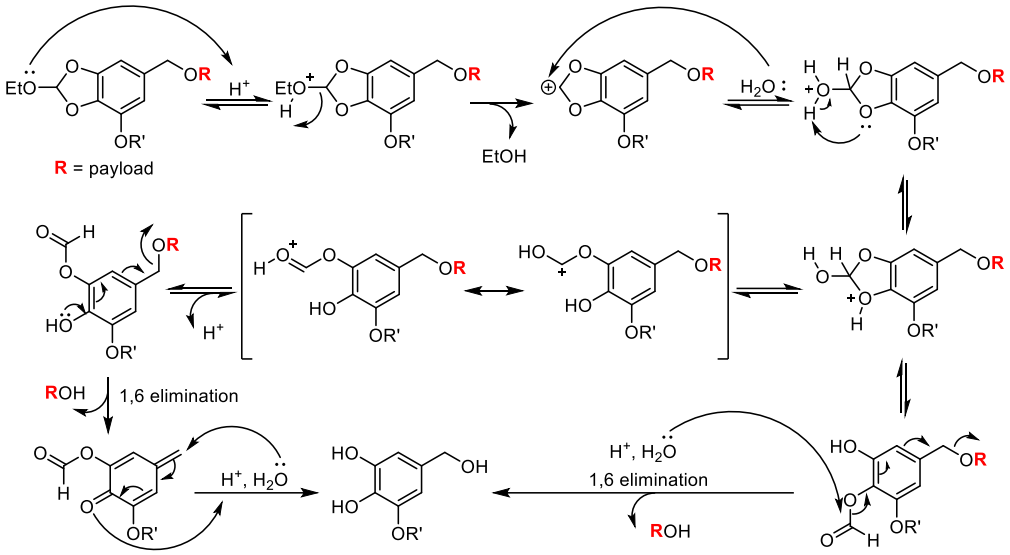

Scheme 1. Proposed mechanism of the HMPO linker.

Regarding linkers that are sensitive to reductive environment, disulfide linkers exploit the higher concentrations of glutathione (GSH) in tumor tissue compared to normal tissue, particularly under hypoxic conditions, to selectively cleave.[81,82] A disulfide linker has many advantages: good biocompatibility, feasable synthesis, high drug-release performance. Their main drawback is instability, which has been partially mitigated by introducing steric hindrance to reduce susceptibility to premature breakdown.[83] As a consequence, ADCs incorporating disulfide linkers often have reduced *in vivo* potency due to faster clearance of prematurely released payloads.[84] An example is Mirvetuximab soravtansine (Elahere®) which incorporates a disulfide linker known as Sulfo-SPDB (1-(2,5-dioxopyrrolidin-1-yl)-oxo-4-(pyridin-2-yldisulfanyl) butane-2-sulfonic acid), which covalently attaches the payload, DM4, a potent anti-tubulin agent, to the mirvetuximab antibody, a chimeric IgG1 monoclonal antibody that targets FRα (**Figure 10**).

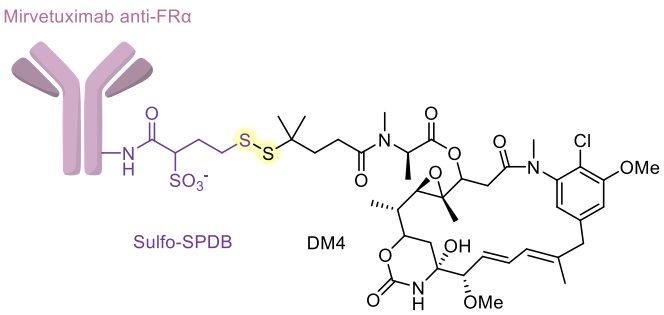

Figure 10. Structure of ADC Elahere®, bearing a disulfide linker.

1.2.2.1.2. Enzimatically cleavable linkers

Compared with other cleavable systems, enzymatically cleavable linkers offer superior plasma stability.[85] They are activated by lysosomal proteases, such as cathepsin B (CatB), which is frequently overexpressed in tumors and is associated with cancer invasiveness and metastasis.[86] Proteases recognize and cleave specific dipeptide sequences (**Figure 11**). This releases the active drug within the lysosomal compartment, preventing premature cleavage in circulation.

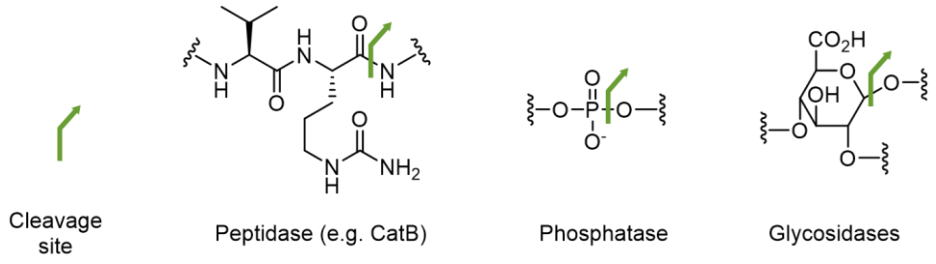

Figure 11. Some enzimatically labile linkers and their cleavage sites.

Among these, the most widely used is the valine-citrulline (Val-Cit) dipeptide linker, combined with the self-immolative *p*-aminobenzyl alcohol (PABA) spacer.[87] Upon proteolytic cleavage, the amide-linked PABA undergoes 1,6-elimination to liberate carbon dioxide and release the drug in its amine form (**Scheme 2**).[88]

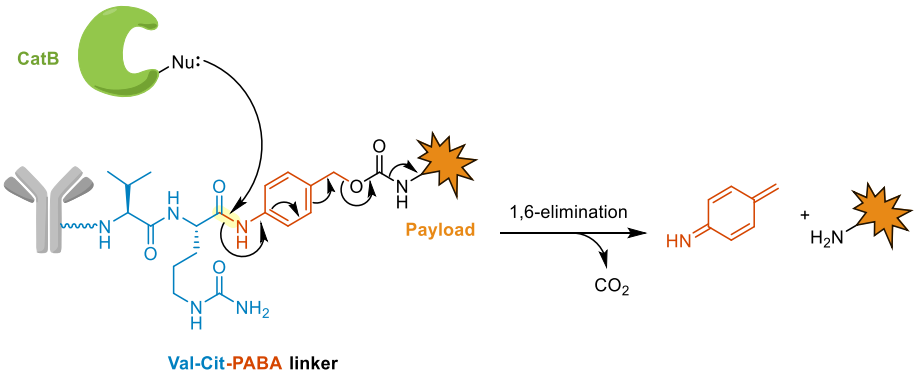

Scheme 2. Mechanism of release of CatB-labile linker Val-Cit-PABA.

Debowchik and coworkers systematically evaluated a library of dipeptide linkers for Doxorubicin release via enzymatic hydrolysis. They reported that Phe-Lys and Val-Lys were cleaved rapidly (with half-lives of 8 and 9 minutes, respectively), while Val-Cit displayed markedly slower cleavage (with a half-life of 240 minutes). Removal of the PABA group reduced the cleavage rate, likely due to steric interference with enzyme binding. Meanwhile, substituting PABA with glycine preserved proteolytic accessibility, but did not allow drug release.[89,90] A separate study

comparing auristatin MMAE conjugates revealed that Val-Cit linkers were over 100-fold more stable in human plasma than hydrazone linkers, with Phe-Lys being significantly less stable than Val-Cit.[91] This enhanced stability under physiological conditions is the reason for the widespread adoption of the Val-Cit-PABA system, as demonstrated by its successful application in Adcetris® and other approved ADCs (**Figure 12**).

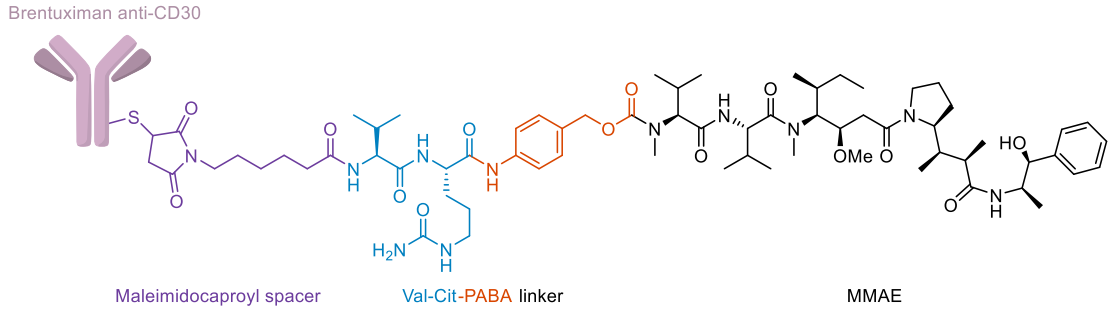

Figure 12. Structure of ADC Adcetris®, bearing a Val-Cit-PABA linker.

Non-peptide cleavable linkers are also being investigated. For istance, the glucuronide linker incorporates a hydrophilic sugar moiety which is specifically cleaved by the lysosomal enzyme β-glucuronidase. Following the enzymatic removal of the sugar from the phenolic backbone, the release of the free drug is triggered by the self-immolation of the PABA spacer (**Scheme 3**).

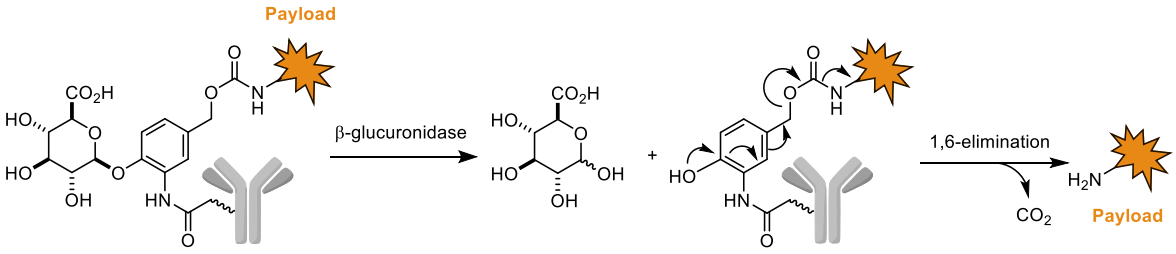

Scheme 3. Mechanism of release of β-glucuronidase-labile linker.

This linker was initially used to conjugate MMAE, MMAF and doxorubicin propyloxazoline to various antibodies.[92] In a comparative study, the aggregation and therapeutic performance of glucuronide- and Val-Cit-PABA-linked ADCs were assessed.[88] Glucuronide-linked conjugates exhibited minimal aggregation (<5%), whereas dipeptide-linked ADCs showed aggregation levels of up to 80%. While the two linker types demonstrated comparable *in vitro* potency, the glucuronide system exhibited superior antitumor efficacy *in vivo*. However, its use was limited due to reduced tolerability compared with Val-Cit-PABA-based ADCs. Finally other functional groups that are responsive to other lysosomial enzymes such as sulfatase[93], glycosidase[94],

phosphatase[95], caspase[96], legumain[97], and non-lysosomal enzymes like fibroblast activation protein have gained attention as potential alternatives[98].

1.2.2.2. Non-cleavable linkers

In the absence of a drug-release trigger, linkers are classified as non-cleavable linkers, since payload release depends on complete degradation of the antibody scaffold within the lysosome following internalization. This mechanism ensures that the cytotoxic drug is only released once the mAb has undergone lysosomal metabolism; otherwise, the efficacy of the bioconjugate is not granted. The primary advantage of non-cleavable linkers is their enhanced plasma stability compared to the majority of cleavable systems.[99] Despite the limited bystander effect, their capacity to resist premature cleavage outside target cells can enhance the precision of drug-delivery, thereby minimising off-target toxicities.[100]

Among the most widely utilised metabolically-sensitive linkers are those which contain a succinimide-thioether moiety, generated via a Michael addition between thiols and maleimides (**Figure 13**). Payload release is believed to proceed through a retro-Michael reaction within lysosomes, potentially combined with proteolytic degradation of the antibody, which may facilitate linker rearrangement and subsequent drug release.[101]

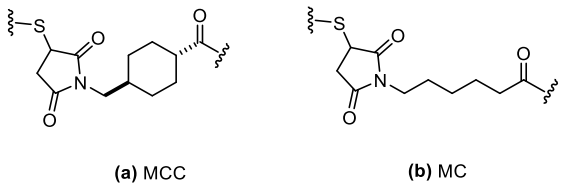

Figure 13. Most commonly used non-cleavable linkers. **a)** MCC, **b)** MC.

Despite the fact that the precise mechanism remains to be fully elucidated, this approach has been clinically validated. For instance, Kadcyla® utilizes a thioether linker comprising *N*-maleimidomethylcyclohexane-1-carboxylate (MCC), wherein the cyclohexane ring provides steric hindrance, therefore enhancing linker stability (**Figure 14**). Another commonly used non-cleavable linker is the maleimidocaproyl (MC) linker, incorporated in Adcetris® (in combination with a Val-Cit cleavable linker, see **Figure 12** above), as well as in Polivy® and Padcev®.

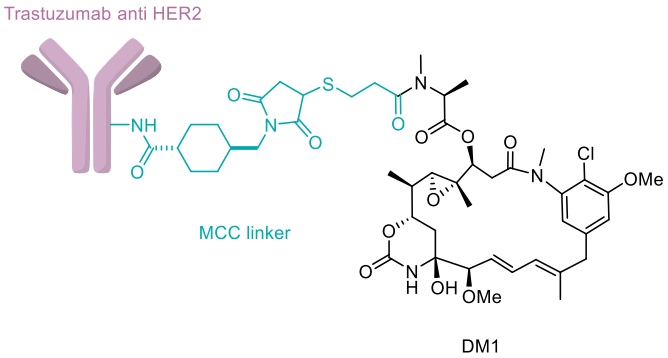

Figure 14. Structure of ADC Kadcyla®, bearing a non-cleavable linker.

1.2.2.3. Spacers

Spacers can be considered as structural connectors, bridgning the core components of an ADC: the bioconjugation moiety, the linker and the payload. Advances in ADC technology have led to increased attention on spacers design, as they can significantly impact the hydrophilicity of the conjugate, the efficiency of drug release, and consequently the therapeutic efficacy of the ADC.[102]

Most payloads in ADCs are highly hydrophobic, including widely utilized compounds such as MMAE and exatecan. This intrinsic hydrophobicity poses a significant challenge in the development of ADCs, as it can promote aggregation, compromise PK[103], and complicate both manufacturing and storage.[104] A well-established strategy to address this issue is the incorporation of hydrophilic spacers, such as polyethylene glycol (PEG), a polymer made of repeating units of ethylene oxide. PEG has found extensive application in the field of linker design, becoming to-date the gold standard for improving physicochemical properties of therapeutic agents. This is primarily due to its advantageous safety profile, chemical stability, and capacity to enhance solubility.[105] However, PEG presents several limitations, such as a non-biodegradable backbone and cases of hypersensitivity or accelerated blood clearance.[106,107] For this reason, a range of alternative spacer technologies have been investigated, including sulfamate[108], sulfamide[109], glutamic acid[110], fleximer[111], and polysarcosine[112] (PSAR) (**Figure 15**).

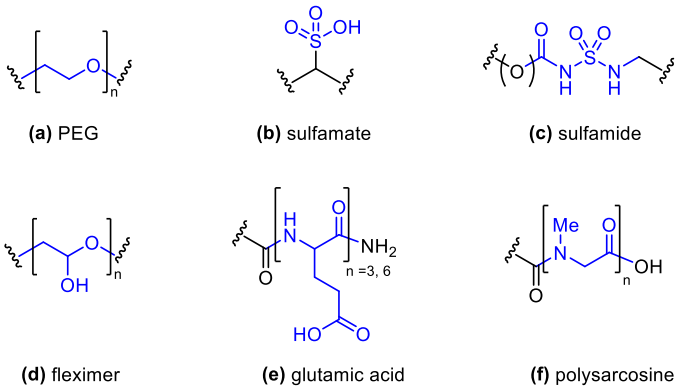

Figure 15. Spacers to enhance the hydrophilicity of linker. **a)** PEG, **b)** sulfamate, **c)** sulfamide, **d)** fleximer, **e)** glutamic acid, and **f)** polysarcosine.

Polysarcosine (**Figure 15f**), also known as poly(*N*-methylglycine), is a biocompatible and biodegradable polymer that is derived from the naturally occurring amino acid sarcosine. Despite it being underexplored in the field of ADCs, PSAR has been successfully applied in nanoscale drug delivery systems[113], as an antifouling polymer for surface modification[114], and in fluorophore-conjugates for imaging.[115] More recently, PSAR has been investigated for therapeutic protein conjugation, where it was shown to provide protease resistance and extend circulation half-life.[116] Viricel and colleagues have demonstrated the potential of polysarcosine as a hydrophobicity-masking entity in ADCs.[117] This has enabled the development of high drug-load conjugates with improved physicochemical properties, favourable PK profiles, and enhanced antitumor activity. It is important to note that this approach has proven to be particularly effective for ADCs incorporating very hydrophobic payloads that would otherwise display high aggregation propensity.

Self-immolative spacers play a pivotal role in the controlled release of ADCs. Functioning as dynamic chemical bridges between the linker and the payload, they are designed to undergo spontaneous, sequential fragmentation once the linker is cleaved, thereby ensuring traceless drug release. The covalent bond between the spacer and the payload must break cleanly, so that the cytotoxic agent is liberated in its native form, without residual chemical groups that could compromise drug activity or induce undesired immune responses.[118] Two major self-immolative mechanisms are commonly employed. In the first, the process of linker activation initiates an electronic cascade, which proceeds through the formation of a quinone or azaquinone methide intermediate. This ultimately results in the release of the drug. In the second, the disassembly of the spacer occurs via intramolecular cyclization, producing heterocyclic by-products such as

imidazolidinone, oxazolidinone, or 1,3-oxathiolan-2-one rings. In both cases, the process is initiated by the generation of nucleophilic functional groups (hydroxy, amino, or thiol moieties) that are either conjugated with or located in proximity to a leaving group. The reactivity of the former initiates a self-immolation cascade, leading to the efficient and selective release of the unmodified payload.[119]

Self-Immolation by 1,4-, 1,6-, or 1,8-Elimination

Self-immolative spacers are designed to disassemble via electronic cascades and are typically based on aromatic scaffolds bearing hydroxy[120,121], amino[122,123], or thiol groups[124]. In their protected (or masked) state, these groups are not nucleophilic enough to trigger electronic delocalization in the non-activated precursor. However, upon the occurrence of an external stimulus, intrinsic nucleophilicity is restored, thereby initiating a self-immolation cascade and releasing the active payload in one or several steps. This process is entropically favoured and is often accompanied by the formation of stable by-products, such as CO_2 in the case of carbonate- or carbamate-linked systems, rendering the reaction both spontaneous and irreversible.

The majority of reported examples rely on 1,4- (**Scheme 4a**) or 1,6-elimination mechanisms (**Scheme 4b**), although 1,8-elimination (**Scheme 4c**) has been demonstrated in specific scaffolds such as *p*-amino(or hydroxy)cinnamyl alcohol and coumarinyl alcohol spacers.[125] Among these, PABA is by far the most widely applied. PABA undergoes a 1,6-elimination process to generate quinone methide (QM) intermediates, to release the drug in its unmodified form.[126] Its effectiveness and reliability have led to its incorporation in five FDA-approved ADCs, most often in combination with the dipeptide Val-Cit linker. PABA is typically attached to the payload through carbonate or carbamate linkages, which are engineered to cleave cleanly upon spacer breakdown, ensuring traceless drug release.

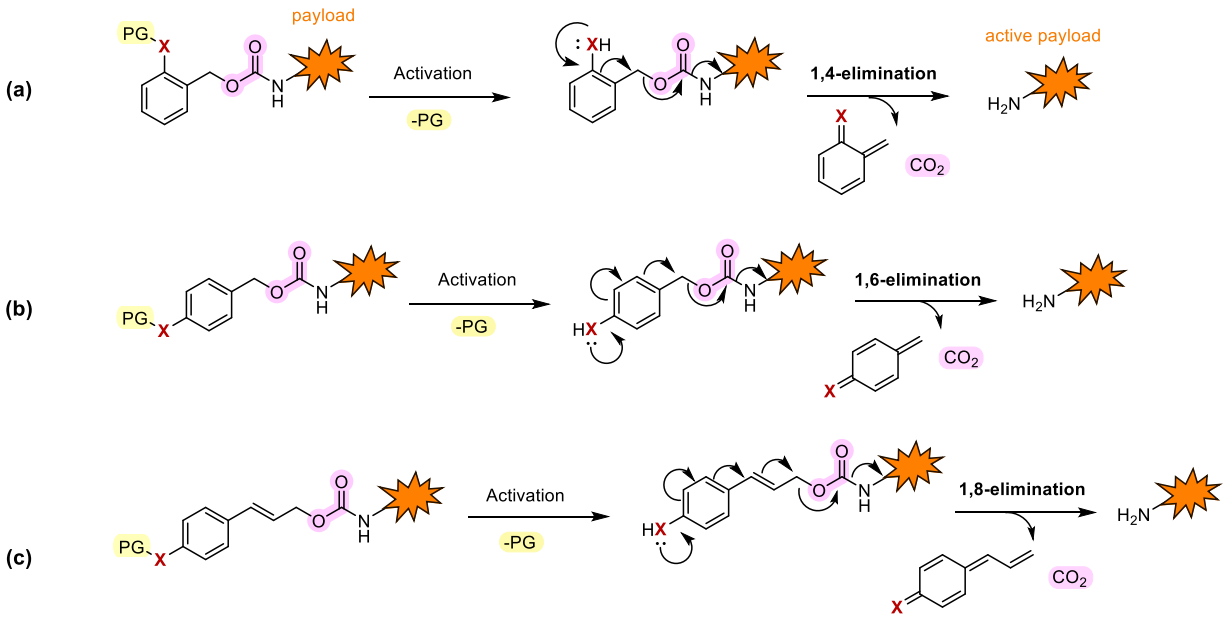

Scheme 4. Mechanisms of self-immolation via electronic cascade. PG = protecting group; X = O, NH, S. **a)** 1,6-elimination (e.g. PABA), **b)** 1,4-elimination, **c)** 1,8-elimination.

Self-Immolation by cyclization

Self-immolative spacers that disassemble through cyclization often employ linkers based on alkyl chains, such as mercaptoethanol (**Scheme 5a**) and ethylenediaminecarbamate (**Scheme 5b**), or ortho-substituted aromatic scaffolds (**Scheme 5c**).[127–129] Upon activation, these systems undergo intramolecular nucleophilic attack, typically on a carbonyl group or an electrophilic aliphatic carbon.[130] Cyclization may occur either directly after activation or via a preliminary elimination step.[131] As with electronic cascade mechanisms, the process is entropically favoured and further driven by the formation of thermodynamically stable cyclic products, most commonly 5- or 6-membered rings.

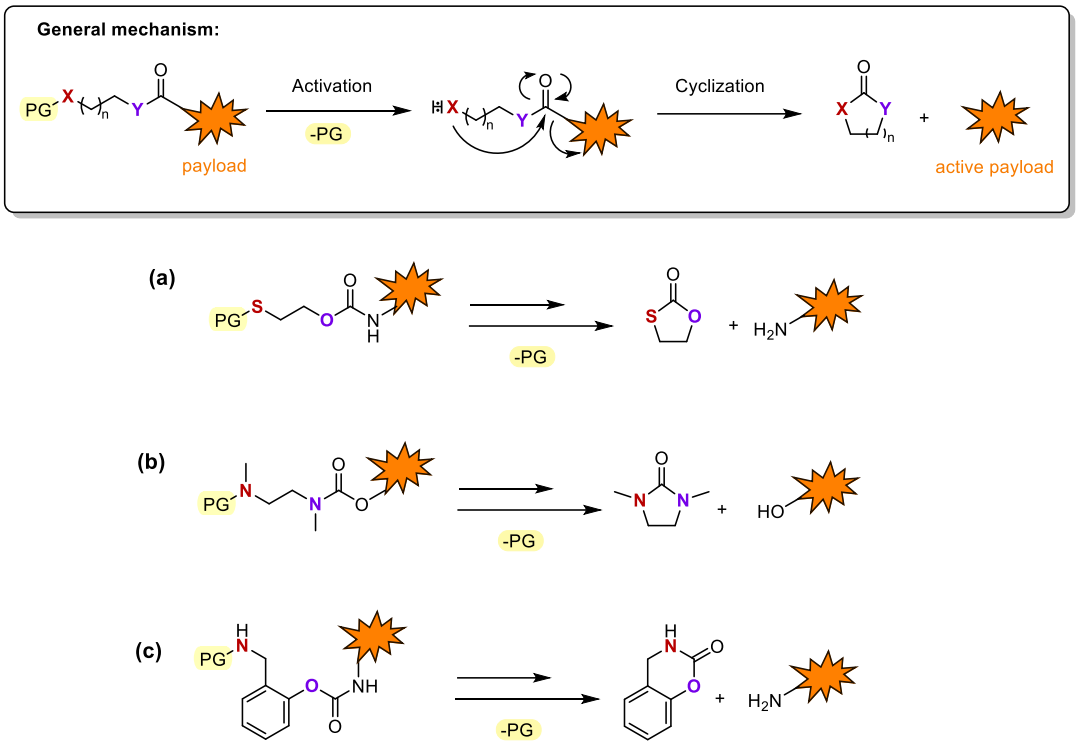

Scheme 5. Mechanism of self-immolation via cyclization. PG = protecting group; X = O, NR^1, S; Y = O, NR^2, CH_2 **a)** mercaptoethanol, **b)** ethylenediamine-carbamate, **c)** *ortho*-substituted aromatic spacer.

1.2.2.4. Polarity

The overall polarity of the linker exerts a significant influence on the PK, potency, DAR, and therapeutic efficacy of an ADC.[132] It is important to note that, since most commonly used linkers and payloads are inherently hydrophobic, ADCs typically achieve drug loads of about 3-4 molecules per antibody. Attempts to increase DAR are often motivated by the need to compensate for low antigen density on tumor cells. However, such efforts frequently lead to detrimental effects, including increased aggregation[88,133], accelerated systemic clearance[134], or reduced antigen-binding affinity[134]. To overcome this, hydrophilic substituents can be incorporated into the linker, thereby enabling the generation of ADCs with higher DARs, up to 9, without notable aggregation or loss of binding affinity.[135] It was demonstrated that these higher-load ADCs exhibited increased potency in antigen-positive cells in comparison with standard ADCs that possessed DARs of 3-4. Furthermore, conjugates bearing polar linkers demonstrated enhanced activity against multidrug-resistant cell lines expressing P-glycoprotein (Pgp).[136] This phenomenon can be attributed to the inherent preference of Pgp transporters for hydrophobic molecules. Subsequent to lysosomal degradation, the residual polar linker present on the released drug diminishes Pgp-mediated efflux.

This strategy is conceptually aligned with the use of aforementioned hydrophilic spacers such as PEG, polysarcosine, or glutamic acid derivatives. In these cases, the tuning of polarity at the level of the linker or spacer allows for higher drug loading while minimizing aggregation, thus improving PK. In essence, polarity modulation demonstrates the necessity of integrating linker design, spacer engineering, and payload chemistry as a cohesive system. The fine-tuning of each component is essential for ensuring the stability, selectivity, and therapeutic efficacy of the ADC.

1.2.3. Payloads

Besides its activity, the fundamental criterium for selecting an ideal payload is the presence of functional groups suitable for bioconjugation. Many highly potent pharmaceuticals do not possess such suitable connection sites, and a chemical modification required for their introduction can compromise biological activity. Furthermore, if the conjugated drug is not ultimately released in its free, active form, its cytotoxic potency may be reduced. Once attached, the payload should be stable in blood circulation, reaching the cytosol intact, after internalization, and processing. In this context, the linker plays a dual role as both a connector and a protective group.

Other key parameters that define an optimal payload are solubility, conjugation compatibility, and stability.[137] Lipophilic drugs have a high degree membrane permeation, thereby increasing their likelihood of escaping the lysosome following release. However, candidate payloads must also be sufficiently soluble to allow efficient conjugation in aqueous media, as organic solvents can denature the antibody. Poorly soluble drugs can be modified by incorporating hydrophilic linkers.[138]

Early ADCs were designed to deliver conventional chemotherapics with well-established anticancer activity, such as methotrexate[139], doxorubicin[140], or vinca alkaloids.[141] However, these conjugates did not prove to have superior efficacy compared to the free cytotoxic drugs frequently requiring very high dosing, thus undermining the goal of reducing systemic toxicities.[142] This realization led to the development of ADCs incorporating ultrapotent compounds, including auristatins, calicheamicins, maytansinoids, and camptothecin analogues, which exert activity at sub-nanomolar concentrations.[143,144] However, it is important to highlight that advances in bioconjugation technologies have encouraged research to shift focus from

classical cytotoxic payloads to non-cytotoxic agents with alternative pharmacological activities. Additionally, there has been an exploration of ADCs for non-oncological indications.

Nevertheless, to date, all clinically approved ADCs employ payloads from two primary classes (**Table 2**). The first group of these agents comprises microtubule inhibitors, which disrupt mitosis. Examples of this group include auristatin analogues and maytansinoids.[91] The second consists of DNA-targeting agents, such as calicheamicin analogues, which bind the minor groove of DNA and induce double-strand breaks leading to apoptosis.[77]

Table 2. Most commonly used payloads.

TYPE	PAYLOADS/EXAMPLES
Payloads inhibiting tubulin polymerization	
Maytansinoids	DM1, DM4
Auristatins	MMAE, MMAF
DNA damaging payloads	
Double Strand Break agents	Calicheamicin
Topoisomerase I enzymes	Camptothecins (topotecan, SN-38, belotecan)
Topoisomerase II inhibitors	Anthracyclines (doxorubicin, epirubicin, daunorubicin, idarubicin)
Crosslinkers	Pyrrolobenzodiazepines (PBDs)
Alkylating agents	Duocarmycin, Indolinobenzodiazepine (IGNs)

1.2.3.1. Payloads inhibiting tubulin polymerization

Maytansinoids

DM1 (mertansine or emtansine) and DM4 (ravtansine or soravtansine), are semisynthetic derivatives of maytansine, a natural benzoansamacrolide originally isolated from plants belonging to the *Maytenus genus* (**Figure 16**).[145] These compounds bind to tubulin and inhibit microtubule assembly, thereby blocking cell proliferation during mitosis.[146] Maytansine itself was found to be too toxic for direct clinical use, however its derivatives have proved to offer excellent stability and sufficient aqueous solubility, thus being suitable as payloads for the development of ADCs.[147] Notable examples include Kadcyla® (T-DM1), which employs a non-cleavable MCC linker, and lorvotuzumab mertansine, which uses a cleavable linker.

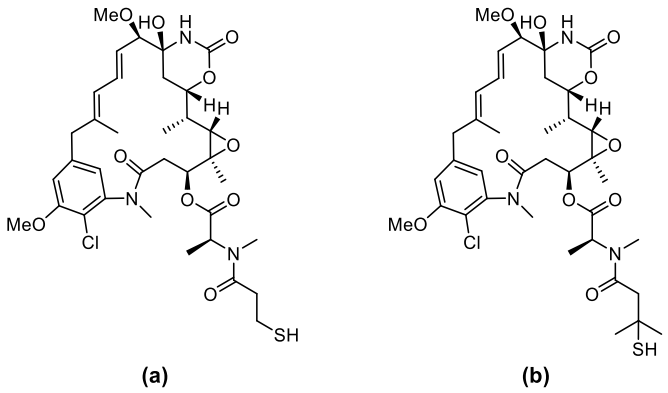

Figure 16. Structure of maytansinoids **a)** DM1, **b)** DM4.

Auristatins

Monomethyl auristatin E (MMAE, **Figure 17a**) and monomethyl auristatin F (MMAF, **Figure 17b**), are fully synthetic analogues of dolastatin-10, a highly potent antimitotic peptide isolated from the sea hare *Dolabella auricularia*.[39] However, due to its extreme systemic toxicity, dolastatin-10 itself is not suitable for therapeutic use. Nevertheless, its derivatives, MMAE and MMAF, retain nanomolar potency while displaying improved solubility, stability under physiological conditions, and chemical compatibility with linker technologies. It has been established that both act as microtubule destabilizers, thereby preventing tubulin polymerization and inducing G2/M cell cycle arrest.[148] Clinically, Adcetris® and Polivy® exploit MMAE as their cytotoxic warhead for the treatment of lymphomas.

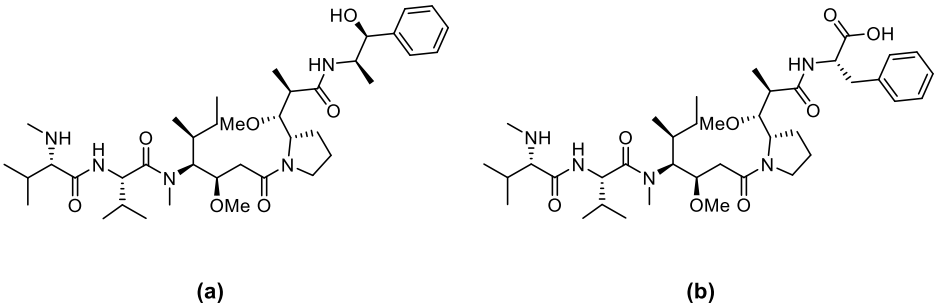

Figure 17. Structure of auristatins **a)** MMAE, **b)** MMAF.

1.2.3.2. DNA damaging payloads

Double-strand break agents

Calicheamicins represent a group of highly potent enedyine antibiotics that were first isolated from *Micromonospora echinospora*. These compounds bind to the DNA minor groove, inducing double-strand cleavage in a site-specific manner through a radical-mediated mechanism.[149] The semisynthetic derivative *N*-acetyl calicheamicin (**Figure 18**) has been incorporated into two approved ADCs: Mylotarg® and Besponsa®. A major limitation of calicheamicins resides in their extreme hydrophobicity, which restricts the DAR that can be achieved before protein aggregation compromises product stability.[150]

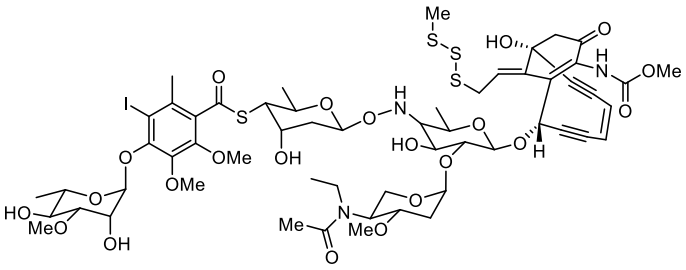

Figure 18. Structure of *N*-acetyl calicheamicin.

Topoisomerase I enzymes

Camptothecins, including topotecan, irinotecan, and belotecan, were originally derived from the bark of *Camptotheca acuminata*. These agents inhibit DNA topoisomerase I by stabilizing the cleavable complex, thereby preventing DNA re-ligation and ultimately leading to lethal strand breaks.[151] Among them, SN-38 (**Figure 19**), the active metabolite of irinotecan, is approximately 1000-fold more potent than its parent compound. However, it suffers from poor solubility and unacceptable systemic toxicity when administered directly. Conjugation to antibodies addresses these drawbacks: the ADCs anti-CEACAM5-SN38 (labetuzumab govitecan) and Trodelvy® both

deliver SN-38 with high homogeneity (DAR ≈ 8) and improved aqueous solubility, providing a clinically viable strategy to exploit this otherwise intractable payload.[152]

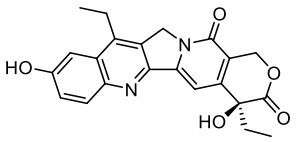

Figure 19. Structure of SN-38.

Topoisomerase II inhibitors

Anthracyclines, including doxorubicin, daunorubicin, epirubicin, and idarubicin, which are isolated from *Streptomyces* species, function through intercalation into DNA, thereby inhibiting topoisomerase II and inducing double-strand breaks (**Figure 20**).[153] The structural diversity exhibited by this class of compounds is reflected in their distinct pharmacological profiles. Epirubicin, for instance, demonstrates prolonged half-life, while the lipophilic idarubicin exhibits enhanced intracellular uptake. Doxorubicin, a clinically established anticancer drug, has a relatively low potency compared to the other classes of payloads, however it display few advantages as an ADC payload: high hydrophilicity, low cost, well-established pharmacodynamics and the presence of multiple functional groups that facilitate linker attachment.[154]

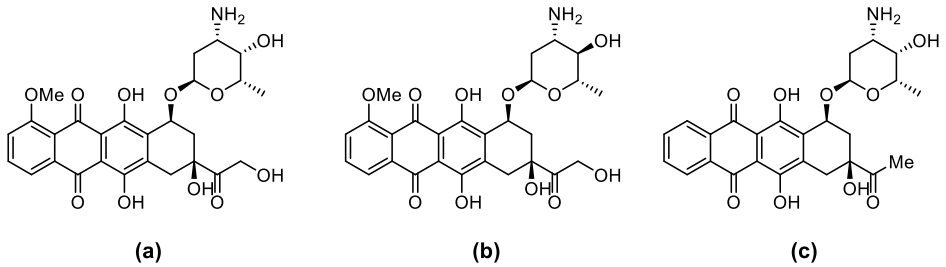

Figure 20. Structures of anthracyclines. **a)** Doxorubicin, **b)** Epirubicin, **c)** Idarubicin.

Crosslinkers

Pyrrolobenzodiazepines (PBDs) are naturally derived DNA-binding agents that covalently interact with the minor groove of DNA in a sequence-specific manner, producing interstrand crosslinks that impede replication and cell division.[155] This mechanism minimizes the emergence of resistance and endows PBDs with picomolar potency against a wide range of tumor cell lines. PDB dimers SGD-1882 (**Figure 21a**) and SG-3199 (**Figure 21b**) are the most commonly used for the development of ADCs. The ADC SGN-CD33A (vadastuximab talirine) utilises a PBD dimer payload. Dimerization strategies, which yield symmetrical or asymmetrical structures, enable

efficient crosslinking by tethering two guanine residues on opposing DNA strands. Beyond PBDs, indolinobenzodiazepine pseudodimers (IGNs) are under development; structural optimisation to a monoimine form has been shown to preserve cytotoxic potency while reducing off-target DNA crosslinking and toxicity.[156]

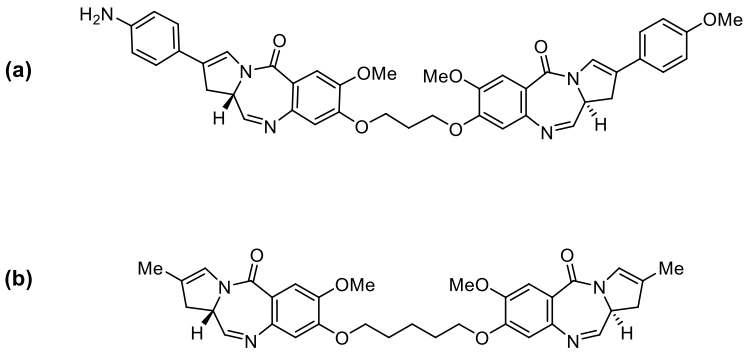

Figure 21. Structures of PBDs. **a)** SGD-1882, **b)** SG-3199.

Alkylating agents

Duocarmycins, which are derived from *Streptomyces* species, are minor groove-binding alkylating agents (**Figure 22a**). These agents irreversibly alkylate the N3 position of adenine in duplex DNA. The extreme potency and ability to retain activity against multidrug-resistant (MDR) tumor models renders them an attractive option as ADC payloads. For instance, the HER2-targeting ADC SYD983 incorporates a duocarmycin derivative as its warhead.[157] Similarly, IGN dimers (**Figure 22b**) based on indolinobenzodiazepines act through irreversible alkylation, representing an additional class of promising payloads with tunable potency and selectivity.[156]

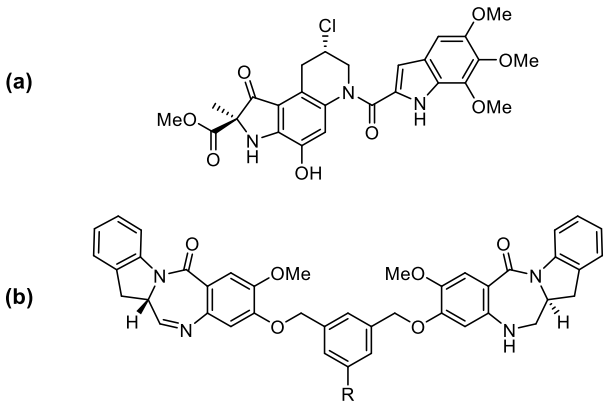

Figure 22. Structures of two alkylating agents. **a)** Duocarmycin C1, **b)** General structure of IGNs.

1.2.3.3. Recent advancements in ADCs charged with non-cytotoxic payloads

With only a few exceptions, represented by topoisomerase inhibitors, the dominant paradigm in ADC research has been that therapeutic efficacy requires conjugation to an extremely potent cytotoxic payload. This principle has driven the development of the majority of clinically approved ADCs to date. Nevertheless, the intrinsic cytotoxicity of these agents poses considerable limitations.[158] From a manufacturing perspective, the extreme potency of the payloads necessitates stringent containment measures during production to ensure operator and environmental safety, thus complicating large-scale development.[159] In order to overcome these challenges, research has expanded its efforts for the design of non-cytotoxic ADCs, in which antibodies are conjugated to payloads with alternative mechanisms of action. These next-generation ADCs are being explored not only for oncology but also for a variety of non-cancer therapeutic areas, representing a significant shift in the field.

1.2.3.3.1. Epigenetic modulators

Epigenetic aberrations have been demonstrated to play a crucial role in the onset and progression of multiple diseases, arising from the gain or loss of function in epigenetic regulatory proteins.[160] Among these, histone deacetylases (HDACs) have emerged as valuable therapeutic targets, since aberrant deacetylation events contribute to a number of pathologies, including neurological disorders, inflammatory conditions, viral and protozoal infections, cardiovascular pathologies, and cancer.

In 2018, Cini and coworkers developed new ADCs charged with ST7612AA1, a novel thiol-based HDAC inhibitor capable of slowing down both *in vitro* and *in vivo* growth of several tumors, including Ras-mutant colon carcinoma, non-small cell lung cancer, ovarian cancer, triple-negative breast cancer (TNBC), acute myeloid leukemia, and diffuse large B-cell lymphoma.[161] Beyond its antitumor activity, ST7612AA1 was shown to modulate the NF-κB pathway, epithelial-mesenchymal transition (EMT), and transcripts involved in immune regulation and other key pathogenic processes, suggesting a potential application in the management of inflammatory diseases.[162]

Since the active form of ST7612AA1 contains a thiol functional group, two alternative conjugation strategies were explored:

- a MC-like non-cleavable linker, comprising a maleimide group and a thiol group (**Figure 23a**);
- a cathepsin B-sensitive Val-Cit dipeptide with a PABA self-immolative spacer (**Figure 23b**).

The linkers were coupled through stable amide bonds to lysine residues of the EGFR-specific mAb cetuximab (Ctx). The resulting HDAC inhibitor-antibody conjugates preserved EGFR recognition, displayed efficient internalization in tumor cells, and induced a significant increase in acetylation of histones H3, H4, and α-tubulin. In animal models of human solid tumors, these conjugates demonstrated strong antitumor efficacy without the systemic toxicities commonly associated with traditional cytotoxic ADCs.

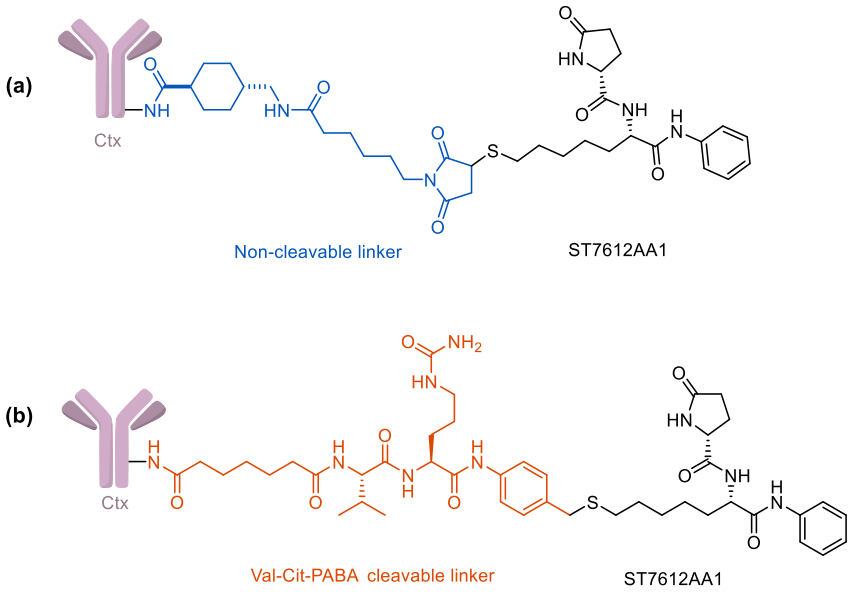

Figure 23. Structures of two ADCs charged with the novel HDAC inhibitor ST7612AA1. **a)** DAR = 8 (±1), **b)** DAR = 6 (±0.5).[161]

In a follow-up study, the same group reported the successful conjugation of two additional HDAC inhibitors, SAHA (Vorinostat) and Dacinostat.[163] The corresponding ADCs demonstrated the capacity to inhibit HDAC in a variety of tumor cell lines, effectively impeding the proliferation of lung adenocarcinoma cells. These type of conjugates also provided a strategy to overcome the poor pharmacokinetic properties of hydroxamic acids.[164,165] Significantly, the work demonstrated the feasibility of employing unconventional functional groups as conjugation handles, expanding beyond conventional amines, alcohols, and phenols. In particular, conjugates were successfully

prepared using a non-cleavable thioether-maleimide linker (**Figure 24a-b**) as well as a cathepsin B-sensitive Val-Cit linker (**Figure 24c**).

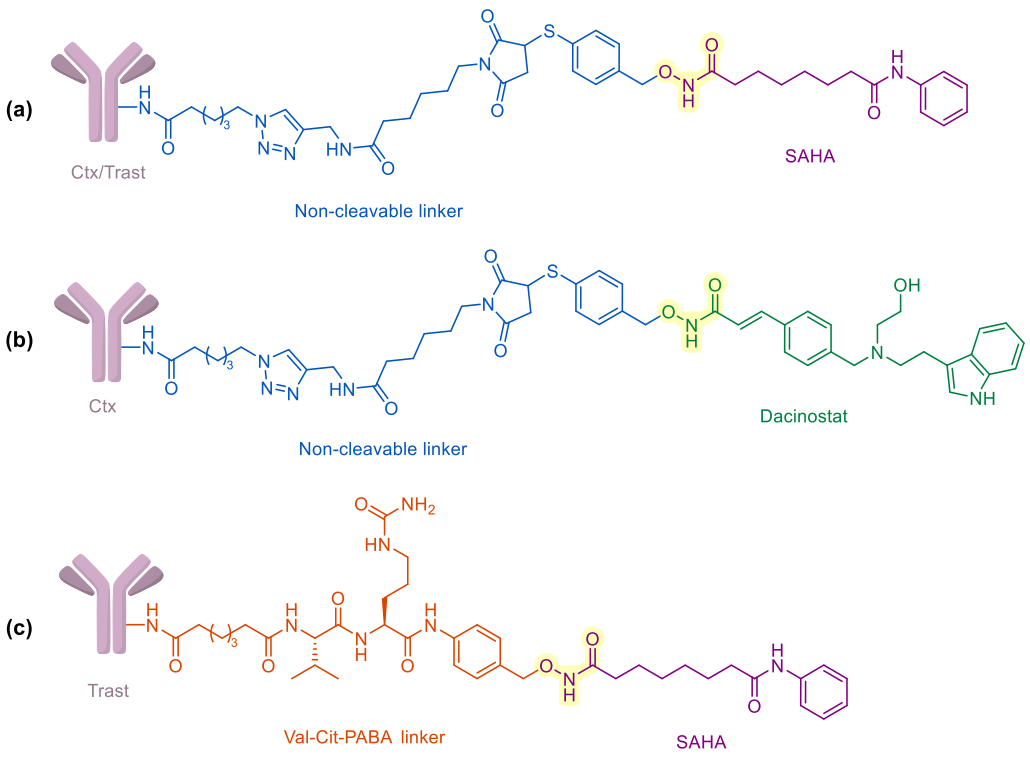

Figure 24. Structures of two ADCs charged with HDAC inhibitors SAHA and Dacinostat. **a)** DAR(Ctx) = 4 (±0.5), DAR(Trast) = 5 (±0.5), **b)** DAR = 3 (±0.5), **c)** DAR = 6 (±0.5).[163]

1.2.3.3.2. Immune-stimulating antibody-drug conjugates (iADCs/ISACs)

The clinical success of ADCs has prompted the development of a related class of therapeutics called "immune-stimulating antibody conjugates" (ISACs, also referred to as iADCs). ISACs consist of an antibody directed against a tumor-associated antigen, which is conjugated to an immunostimulatory payload (**Figure 25**).[166] The immunostimulatory payload can be composed of agonists of Toll-like receptors (TLRs)[167] or the stimulator of interferon genes (STING) pathway.[168] Although TLR agonists are recognised as potent activators of the innate immune system, their systemic administration is limited by severe toxicity.[169] ISACs overcome this limitation by exploiting the antibody-mediated targeted delivery of immunostimulatory molecules directly into the tumor microenvironment. Once internalized, ISACs induce a localized influx of pro-inflammatory cytokines, leading to dendritic cell activation and ultimately promoting a robust antitumor T-cell response. It has been demonstrated in preclinical models that ISACs can induce enduring immunological memory against tumors.[170]

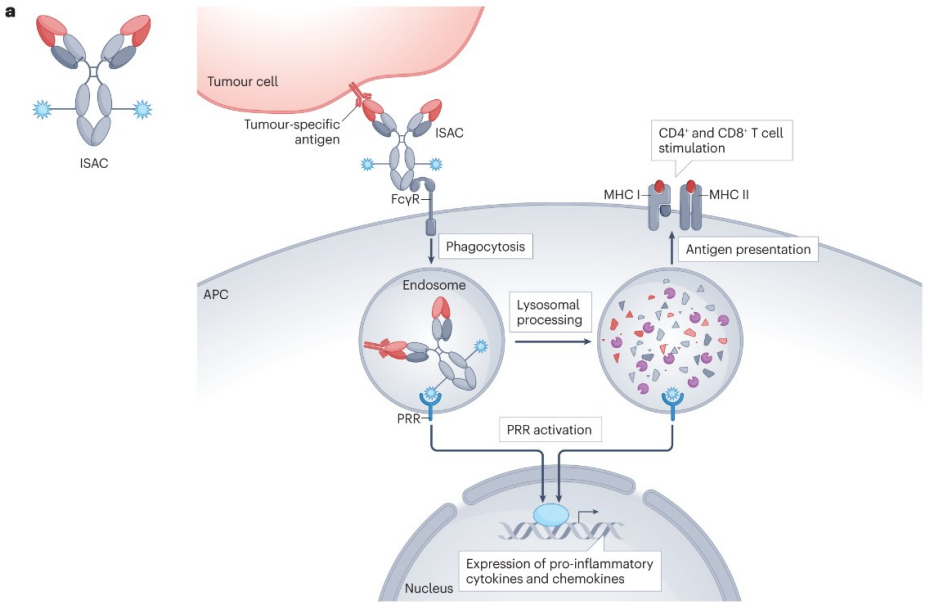

Figure 25. General mechanism of action of immune-stimulating antibody conjugates.[171]

Presently, no ISACs have received FDA approval, reflecting the early stage of their clinical development. However, the concept has attracted significant interest, particularly in the context of immune synergy, which envisions combining ISACs with immune checkpoint inhibitors to achieve enhanced therapeutic efficacy. Preliminary studies indicate that this combined approach may enhance the effectiveness of antitumor responses over time, thereby establishing ISACs as a promising new frontier in the field of ADCs.

1.2.3.3.3. Payloads for non-oncology indications

Beyond oncology, there is growing recognition of the potential of ADCs in the treatment of different diseases. Historically, a significant number of drug candidates failed the preclinical or clinical stages of development. This failure was attributed to a lack of target selectivity, resulting in a poor therapeutic index. The ADC strategy provides a significant opportunity to re-evaluate such molecules, particularly by enhancing their selectivity and minimizing systemic toxicity.[172]

<u>Anti-inflammatory ADCs</u>

Synthetic glucocorticoids, such as dexamethasone, are widely used for their potent anti-inflammatory activity.[173] However, the chronic use of these medications is limited by the occurrence of serious adverse effects, including bone mobilization, muscle wasting, immunosuppression, and metabolic dysregulation.[173] In order to retain their efficacy while minimizing systemic toxicity, a biodegradable anti-CD163 antibody-dexamethasone conjugate

was developed.[174] CD163 is a glucocorticoid-regulated surface protein expressed by monocytes and macrophages, with key roles in the clearance of debris, immune modulation, and pathogen recognition.[175] Its restricted expression at inflammatory sites makes it an attractive target for tissue-specific delivery. The CD163-dexamethasone ADC preserved high binding affinity post-conjugation, a reduction in TNF-α secretion in lipopolysaccharide-stimulated macrophages, and *in vivo* efficacy in mice. It is interesting to note that, compared to free dexamethasone, the ADC was able to attenuate systemic adverse effects such as thymic lymphocyte apoptosis, weight loss, and cortisol suppression.

Immunosuppressive ADCs

Analogous strategies have been employed in the development of non-hormonal immunosuppressants. Dasatinib, a tyrosine kinase inhibitor originally developed for oncology, is an oral drug applied in the treatment of chronic myelogenous leukemia and certain forms of acute lymphoblastic leukemia.[176,177] It has significant immunosuppressive potential but suffers from severe systemic side effects (e.g., neutropenia, myelosuppression).[178] To harness its activity more safely, researchers designed a dasatinib ADC targeting CXCR4, a receptor which is highly expressed on T and B cells and monocytes.[179] This approach restricted drug delivery to immune cells, thereby reducing off-target effects and broadening the therapeutic window.

Antibody-antibiotic conjugates (AACs)

Beyond the field of immunology, the technology of ADCs has been adapted for the treatment of intracellular bacterial infections. An antibody-antibiotic conjugate (AAC) targeting *Staphylococcus aureus* was recently developed.[180,181] This AAC contains a protease-sensitive linker cleaved by the phagolysosome, thereby releasing the antibiotic precisely in the infection sites. In preclinical models, the AAC demonstrated superiority to vancomycin in the treatment of bacteremia. A cathepsin-cleavable linker was also employed to tether a rifamycin derivative (rifalogue) to an anti-wall teichoic acid (WTA) antibody, achieving potent intracellular bactericidal activity. It is noteworthy that rifalogue retained activity in acidic environment and accumulated inside infected cells, while rifampicin conjugates demonstrated poor efficacy under the same conditions.

Together, these advancements underscore the versatility of ADC technology as a delivery platform that extends significantly beyond the domain of oncology. This underscores the

potential for therapeutic applications in immunology, infectious diseases, and chronic inflammatory disorders.

1.2.4. Bioconjugation strategies

In ADC manufacturing, bioconjugation is defined as the reaction that links the linker-payload system to functional groups of amino acid residues on the antibody. Typically, accessible residues on the antibody surface undergo a controlled reaction with a reactive handle installed on the linker. The majority of ADCs are based on IgG1 scaffolds, which are ~150 kDa biomolecules that provide multiple native conjugation sites and can also be engineered to introduce additional reactive positions. Conventional conjugation strategies generally exploit nucleophilic residues, while advanced approaches use genetic engineering to introduce electrophilic groups such as aldehydes or ketones. In all cases, conjugation chemistry must selectively target reactive sites without compromising the antibody's structural integrity.[85]

Depending on the method, the reaction often generates a heterogeneous mixture of ADCs with variable DARs and conjugation sites. A broad DAR distribution has been demonstrated to reduce efficacy and complicate pharmacological behaviour. While higher DAR values have been shown to increase potency, they are also associated with increased aggregation, faster clearance, and premature payload release in circulation.[182] The employment of hydrophilic and sufficiently stable linkers is a crucial and effective measure for the mitigation of these risks. Achieving an optimal DAR, typically ranging from 2 to 8, with a controlled distribution is imperative to optimize efficacy while ensuring tolerability and minimising off-target toxicity.

1.2.4.1. Bioconjugation through native residues

1.2.4.1.1. Bioconjugation through lysines

Lysine is a nucleophilic amino acid with an ε-amino side chain (pKa ≈ 10.5), which is predominantly protonated under physiological conditions. Due to the high prevalence of lysine in proteins, with approximately 80 lysine residues present in IgG molecules, lysine has historically been the most conventional and straightforward target for bioconjugation.[182] However, it presents significant challenges: controlling chemoselectivity and regioselectivity is difficult, and conjugation typically yields highly heterogeneous ADC products.

The most established reagents for lysine modification are *N*-hydroxysuccinimide (NHS) esters.[183] These activated acyl species are reactive, commercially available, and capable of forming amide bonds efficiently at a pH range of 7.0-9.0 and in a relatively short time frame (**Scheme 6**). The development of the first generation of clinically approved ADCs, including trastuzumab emtansine, gemtuzumab ozogamicin, and inotuzumab ozogamicin, was enabled by NHS ester chemistry.

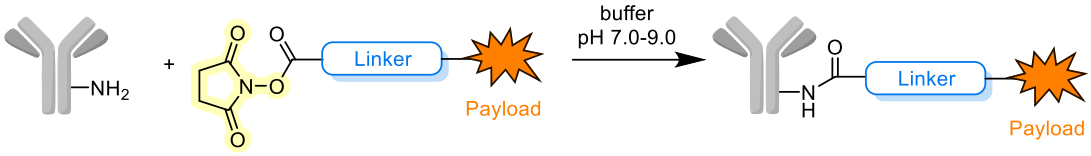

Scheme 6. Bioconjugation to lysine -NH_2 using NHS-ester (yellow) activation.

Nevertheless, NHS ester-based conjugation produces heterogeneous mixtures, as demonstrated by Kadcyla® (trastuzumab-DM1), which contains a distribution of species with DAR values ranging from 0-8, corresponding to ~40 possible lysine modification sites.[184] Further disadvantages are associated with hydrolysis of the reactive ester and off-target reactions with other nucleophilic residues, such as histidine, serine, threonine, and tyrosine.[185,186] A range of alternative reagents, including sulfonyl halides[187,188], iminoboronates[189], diazonium salts[190], aldehydes[191] and isothiocyanates[192], have been the focus of investigation in order to enhance chemoselectivity (**Scheme 7**). However, their application in the context of antibody modification remains restricted.

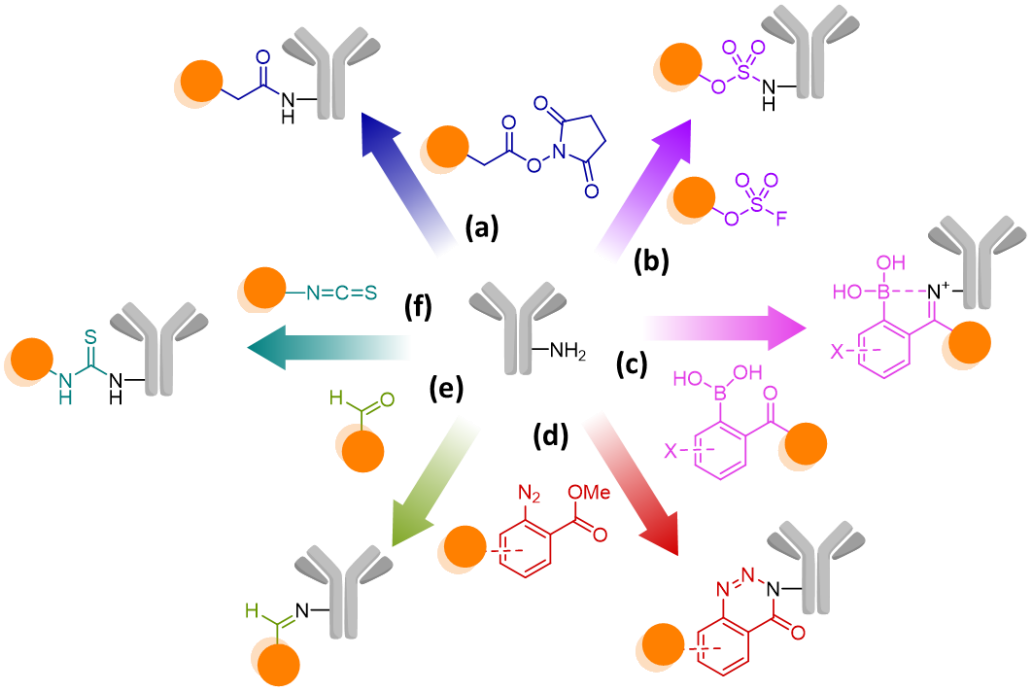

Scheme 7. Conventional lysine bioconjugation reagents: **(a)** NHS esters, **(b)** sulfonyl fluorides, **(c)** iminoboronates, **(d)** diazonium salts, **(e)** aldehydes, **(f)** isothiocyanates. Linker-payload in orange.

Recent advances have introduced new strategies for lysine-selective bioconjugation. In 2021, the Yao group reported an azaphilone-based reagent that reacts selectively with primary amines in proteins under mild conditions, generating only water as a by-product (**Scheme 8a**).[193] The resulting conjugates demonstrated satisfactory serum stability for a period of up to seven days. In a more recent development in 2024, Teng and colleagues have pioneered the development of biocompatible click reagents that utilize alkynone β-trifluoroborates as electrophiles (**Scheme 8b**).[194] Competition experiments between benzylamine and benzyl mercaptan demonstrated excellent chemoselectivity for amines (82% yield) over thiols (trace), thus highlighting the potential of these boron-containing reagents for lysine-based ADC bioconjugation. The same group has also developed β-silyl alkynoate-based methodology for amide bond formation (**Scheme 8c**). In the same year, Allimuthu and coworkers introduced isotonic anhydrides as a novel lysine-selective reagent for amide bond formation (**Scheme 8d**), further expanding the chemical toolbox for next-generation ADC design.[195]

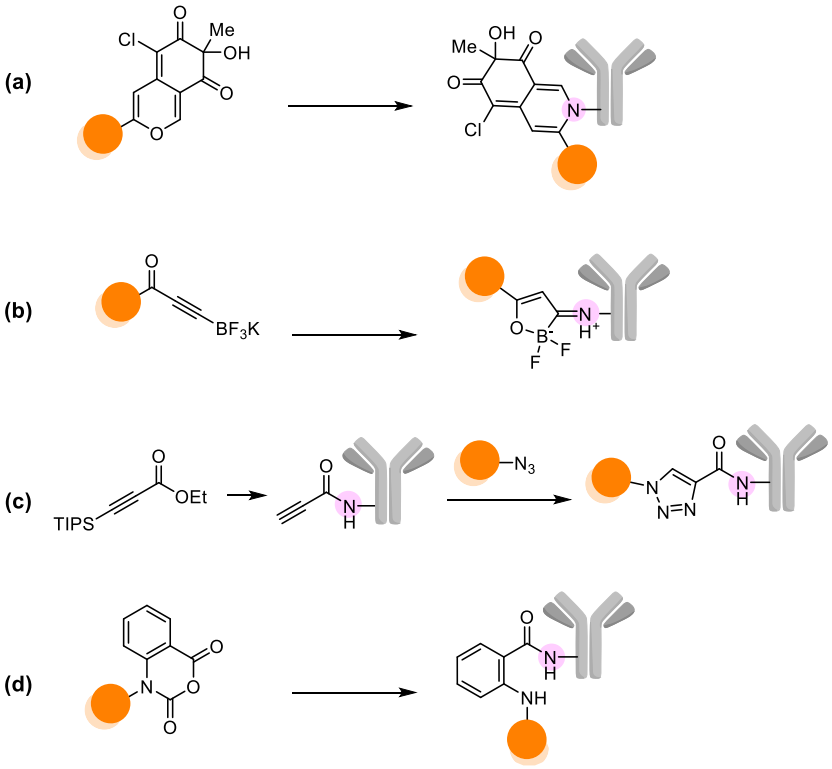

Scheme 8. Recent innovative lysine bioconjugation reagents: **(a)** azaphilone-based reagent, **(b)** alkynone β-trifluoroborates reagent, **(c)** β-silyl alkynoate reagent, **(d)** isotonic anhydrides reagent. Linker-payload in orange.

1.2.4.1.2. Bioconjugation through cysteines

Cysteine is the second most exploited amino acid residue for ADC bioconjugation. In IgG1 antibodies, cysteines are engaged in disulfide bonds, with four inter-chain disulfides, two connecting heavy and light chains and two connecting the heavy chains in the hinge region, maintaining the structural integrity of the antibody, and an additional twelve intra-chain disulfides which stabilize the antibody domains.[196] Reduction under mild conditions, employing reagents such as Dithiothreitol (DTT) or Tris(2-Carboxyethyl)phosphine (TCEP), selectively cleaves inter-chain disulfides while preserving intra-chain bonds.[197] This process generates free thiol groups suitable for conjugation. This controlled reduction makes cysteine conjugation particularly attractive in comparison to lysine conjugation, as it typically yields more homogeneous ADC preparations, together with easier characterization and quality control. However, it is important to note that partial reduction may result in the dissociation of the light chain, which could potentially compromise antigen binding and cross-linking capacity, processes that are critical for efficient internalization.[51]

Free thiols generated from cysteine residues can undergo various types of functionalization, including Michael additions, α-halo carbonyl alkylations, and disulfide re-bridging. This strategy was employed for the development of FDA-approved ADCs, including Adcetris® and trastuzumab deruxtecan (T-DXd). Among available reagents, maleimides (**Scheme 9a**) have emerged as the most widely used. However, the resulting thiosuccinimide bond is susceptible to retro-Michael reactions, leading to payload deconjugation and premature drug release from the antibody.[198] In order to address this instability, a number of strategies have been devised. For instance, Lyon and coworkers introduced a self-stabilizing maleimide-diaminopropionic acid (DPR - **Scheme 9b**) linker that promotes intramolecular catalysis of thiosuccinimide hydrolysis, thereby preventing retro-Michael elimination and improving conjugate stability.[199] Furthermore, Christie and coworkers demonstrated that *N*-aryl maleimides exhibit substantially lower deconjugation rates compared to *N*-alkyl derivatives.[200] This finding was later applied to PBD-based ADCs.[201] In addition, alternative cysteine-reactive chemistries have been developed to overcome the liabilities associated with maleimide chemistry. For instance, allenamides (**Scheme 9c**) enable rapid and irreversible conjugation under aqueous conditions[202]; 2-sulfonylpyrimidines (**Scheme 9d**) allow mild yet highly selective thiol functionalization[203]; pentafluorobenzene proved to be a versatile handle for selective functionalization of cysetine via nucleophilic aromatic substitution (**Scheme 9e**)[204]; and more recently, silicon-containing thiol-specific reagents have been reported with superior resistance to retro-reactions.

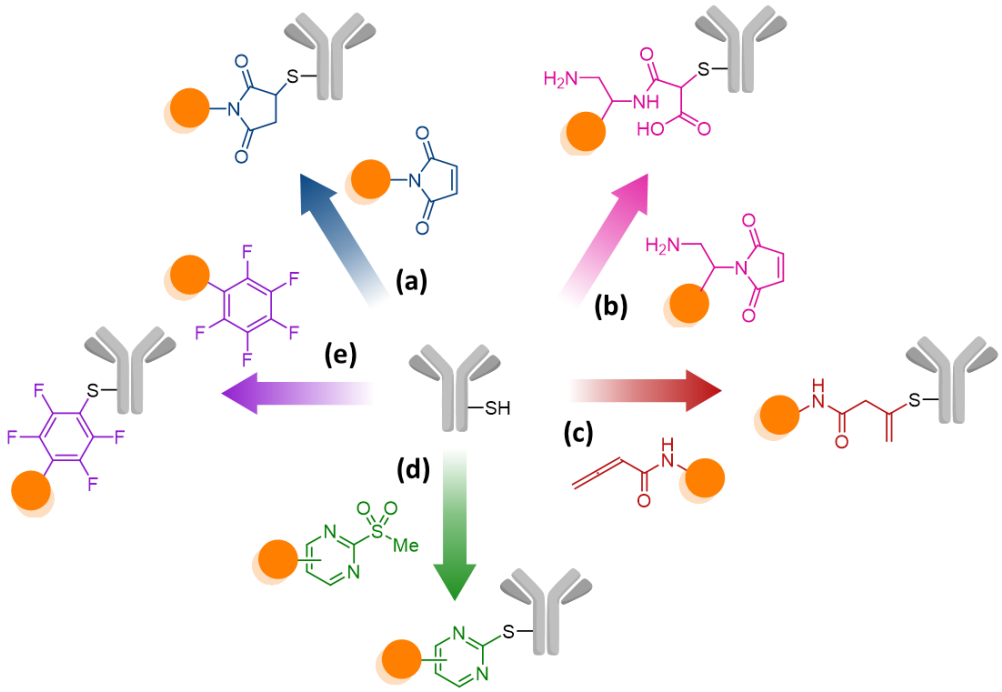

Scheme 9. Some cysteine bioconjugation reagents: **a)** maleimide, **b)** self-hydrolizing maleimide, **c)** allenamide, **d)** 2-sulfonylpyrimidine, **e)** pentafluorobenzene. Linker-payload in orange.

Despite these advances, conjugation to naturally occurring cysteine residues still generates heterogeneous ADC populations, potentially affecting pharmacokinetics and stability.[205,206] In order to address this issue, a range of site-specific approaches has been developed.

Another method to obtain homogeneous products is by fully reducing four pairs of disulfide bonds and conjugating with linker-payloads, utilizing disulfide re-bridging technology. Disulfide re-bridging involves dual thiol-reacting linkers to simultaneously bind to a pair of cysteines. Payloads can be straightly introduced through re-bridging disulfide bonds or connected via bioorthogonal reactions after introducing a highly reactive trigger. This method maintains the antibody's morphology and controls the reaction site, with the DAR of the products adjustable to approximately 4, 8, or 16 by varying the amounts of payloads on the linkers. Instead of stochastic coupling, disulfide re-bridging involves the reaction with cysteine-selective cross-linking reagents, such as bis-alkylating bis-sulfones, (**Scheme 10a**) dibromomaleimide (**Scheme 10b**) and dibromopyridazinediones (**Scheme 10c**).[207–209] In comparison with conventional heterogeneous ADCs, these site-specific conjugates exhibit enhanced homogeneity, reduced off-target toxicity, and improved therapeutic efficacy *in vivo*.[210,211] Consequently, the development of cysteine-based site-specific conjugation strategies remains a primary focus in the optimisation of next-generation ADCs.

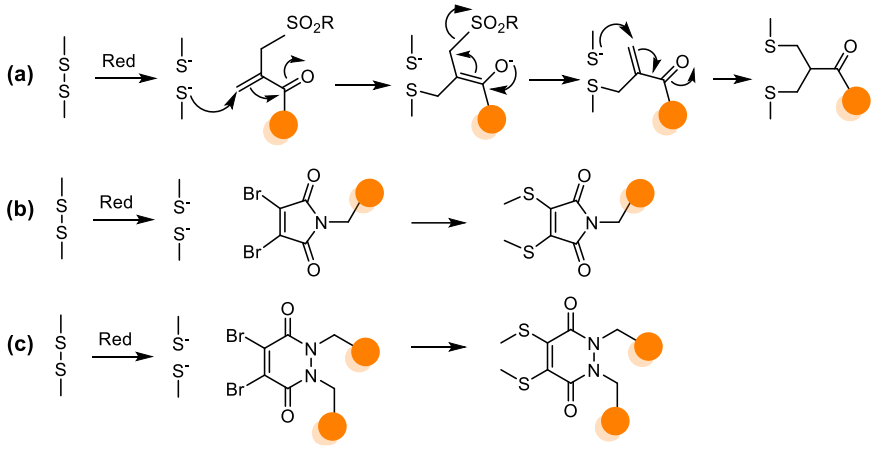

Scheme 10. Disulfide bond rebridging: **(a)** Bis-alkylating bis-sulfones, **(b)** Dibromomaleimides, **(c)** Dibromopiridazinediones. Linker-payload in orange.

1.2.4.2. Other strategies of bioconjugation

The shift towards homogeneous ADC design has driven the emergence of bioorthogonal approaches that exploit reactive functionalities beyond thiols and amines, greatly expanding the diversity of conjugation strategies. Recent advances have enabled the generation of homogeneous ADCs with precise control over the DAR, thereby improving stability, PK, and therapeutic efficacy.

Insertion or mutation of cysteine residues

A successful approach is the insertion of engineered cysteine residues into antibodies. This preserves the integrity of native disulfide bonds while generating well-defined attachment sites for conjugation. This strategy guarantees a uniform DAR while preserving antibody stability *in vivo*, on the condition that the introduced cysteines do not hinder antibody folding or antigen recognition. A prominent example is the development of THIOMAB antibodies, in which cysteine substitutions are introduced at carefully selected positions.[212] Further development of this concept was pursued by Sadowsky and colleagues, who combined THIOMABs with recombinant XTEN peptide technology, thereby generating THIOMAB XTEN-drug conjugates.[213] The amino acid sequence known as XTEN, which is characterized by its pseudo-repetitive nature, was engineered to incorporate up to nine cysteine-based conjugation sites. This innovation produced highly homogeneous ADCs with DAR values reaching 18. Remarkably, TXCs demonstrated superior *in vitro* anti-tumor activity compared to conventional low-DAR ADCs, and improved delivery efficiency both in cancer models and against *Staphylococcus aureus*.

Insertion of unnatural amino acids

A significant area of research in the field of ADC technology is the genetic incorporation of noncanonical amino acids (ncAAs) into antibodies. Beyond cysteine substitution, other residues, including selenocysteine and *p*-acetylphenylalanine (pAcF), have been explored as unique conjugation handles. Selenocysteine, which contains selenium in its side chain, displays enhanced nucleophilicity compared to cysteine, especially toward electrophiles such as maleimides under acidic conditions.[214] This property has been exploited for dual-conjugation strategies, combining selenocysteine- and cysteine-based chemistries to generate multi-drug ADCs with potential applications in overcoming drug resistance.[215]

The employment of genetic code expansion technology facilitates the incorporation of ncAAs, allowing the introduction of bioorthogonal functional groups (e.g., azides, alkynes) into antibodies.[50] This requires engineered aminoacyl-tRNA synthetases/tRNAs to recognize nonsense codons and directing the incorporation of ncAAs during the process of translation.[216] For instance, in an anti-CXCR4 antibody, pAcF incorporation facilitated conjugation of auristatin through a non-cleavable hydrophilic linker, resulting in a homogeneous ADC (DAR = 2) with >95% conjugation efficiency.[217]

Glycan modification

Another promising strategy exploits the conserved N-linked glycosylation site at asparagine 297 in the CH2 domain of IgG antibodies. This glycan site can be selectively modified to provide a handle for site-specific drug conjugation. It is important to note that glycan engineering does not interfere with antigen recognition and Fc-mediated functions.[218] One-pot conjugation methodologies have been developed, yielding homogeneous ADCs with defined DARs ranging from 2 to 12, thereby providing both flexibility and structural diversity.[219]

Enzymatic conjugation

Enzymes represent powerful tools for site-specific conjugation, offering high selectivity under mild conditions. A number of biocatalysts have been adapted for the development of ADCs. These include transpeptidases, formylglycine-generating enzymes, and microbial transglutaminases.[220] Sortase A (SrtA) is capable of recognizing the LPXTG motif that has been engineered into antibodies, and it catalyses the cleavage process between threonine and glycine residues. The resulting acyl-enzyme intermediate is resolved by nucleophilic attack from an oligoglycine-containing linker, producing a new peptide bond.[221] As demonstrated, the Sortase-

mediated antibody conjugation (SMAC) technology preserves antigen-binding affinity after modification.[221] Nevertheless, the low catalytic efficiency of SrtA remains a issue, necessitating either elevated enzyme concentrations or extended reaction times. Microbial transglutaminase (MTGase) catalyzes the formation of amide bonds between the γ-carboxamide group of glutamine and primary amines.[222] In the context of antibodies, MTGase has been shown to target Gln295 on the heavy chain, thereby facilitating site-specific modification. For instance, the conjugation of MMAE via MTGase-mediated modification, followed by strain-promoted azide-alkyne cycloaddition (SPAAC), produced trastuzumab-MMAE ADCs with a DAR of 2, which displayed potent *in vitro* cytotoxic activity.[223]

1.2.4.3. Click chemistry for the synthesis of ADCs

The term "click chemistry", first defined by Kolb, Finn, and Sharpless in 2001 [224], refers to a class of reactions that are characterized by their modularity, high yield, stereospecificity, and the production of predominantly benign by-products under conditions that are mild, oxygen- and water-tolerant. The combination of these features with the availability of simple starting materials and straightforward product isolation has resulted in the widespread application of click reactions across diverse scientific fields, including materials science, drug discovery and bioconjugation.[225]

In the context of bioconjugation, click reactions offer several notable advantages, including high efficiency, mild and aqueous-compatible conditions, stereoselectivity, and straightforward purification. However, for a click reaction to be suitable for biological applications, it must also be bioorthogonal and proceed with minimal interference from endogenous functional groups. In the field of ADC development, a variety of click-based strategies have been employed, including copper-catalyzed azide-alkyne cycloaddition (CuAAC - **Figure 26a**), strain-promoted azide-alkyne cycloaddition (SPAAC - **Figure 26b**), hydrazino-iso-Pictet-Spengler ligation (HIPS - **Figure 26c**), and inverse electron-demand Diels-Alder (IEDDA - **Figure 26d**) reactions.

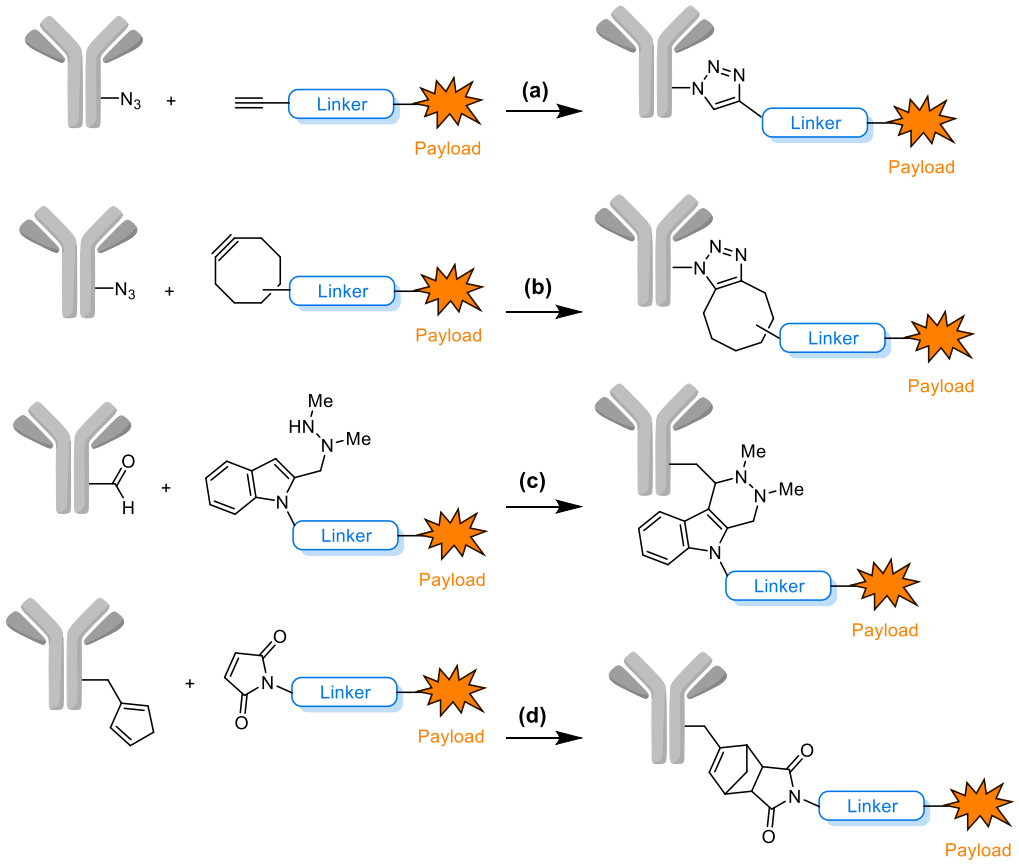

Figure 26. Click chemistry reactions in the synthesis of antibody-drug conjugates: **(a)** copper-catalyzed azide-alkyne [3+2] cycloaddition; **(b)** strain-promoted [3+2] azide-alkyne cycloaddition reaction; **(c)** hydrazino-iso-Pictet-Spengler ligation; **(d)** Diels-Alder reaction.

CuAAC was the first reaction formally recognized as a "click" transformation. The development of this methodology by Tornoe, Christensen, and Meldal for the synthesis of 1,2,3-triazoles has since resulted in its establishment as a core principle of organic synthesis.[226] Its utility is wide-ranging, covering peptide and protein modification, nucleic acid and polymer chemistry, nanostructure synthesis, and bioconjugation.[227] Azides and alkynes exhibit a low degree of reactivity towards biological compounds due to their weak acid-base properties. Consequently, they are predominantly inactive towards reactions that occur within living cells. In the CuAAC reaction, copper(I) ions activates terminal alkynes, resulting in the selective and rapid formation of triazoles (**Scheme 10-1a**). Despite its high yields and specificity, the CuAAC reaction has limited *in vivo* applications due to copper-induced toxicity, primarily from the generation of reactive oxygen species.[228]

To overcome the limitations of Cu(I) toxicity, the Bertozzi group pioneered SPAAC, a catalyst-free alternative that exploits the release of ring strain in cycloalkynes. When subjected to reaction

with azides, strained cycloalkynes undergo [3+2] cycloaddition to yield triazoles with sp^2-hybridized carbons (**Scheme 11-1b**). Despite its comparatively reduced speed in comparison to CuAAC, SPAAC is biocompatible and therefore highly attractive for *in vivo* applications.[229]

Significant efforts have been directed towards accelerating SPAAC by structural modification of cycloalkynes, given the recognized influence of reactivity, lipophilicity, and steric properties on the reaction rate.[230] This has resulted in the development of more reactive scaffolds, including dibenzoannulated cyclooctyne (DIBO, **Scheme 11-2a**), dibenzocyclooctyne amine (DBCO, **Scheme 11-2b**), aza-dibenzocyclooctyne (DIBAC, **Scheme 11-2c**), and bicyclononyne (BCN, **Scheme 11-2d**).[231–233] The increased ring strain in these derivatives, often arising from additional sp-hybridized carbons, dramatically enhances the kinetics of the reaction.[230] SPAAC combines fast kinetics, high selectivity, and bioorthogonality with superior safety in comparison to CuAAC. Consequently, it has become one of the most widely applied click reactions in the design and synthesis of homogeneous ADCs.

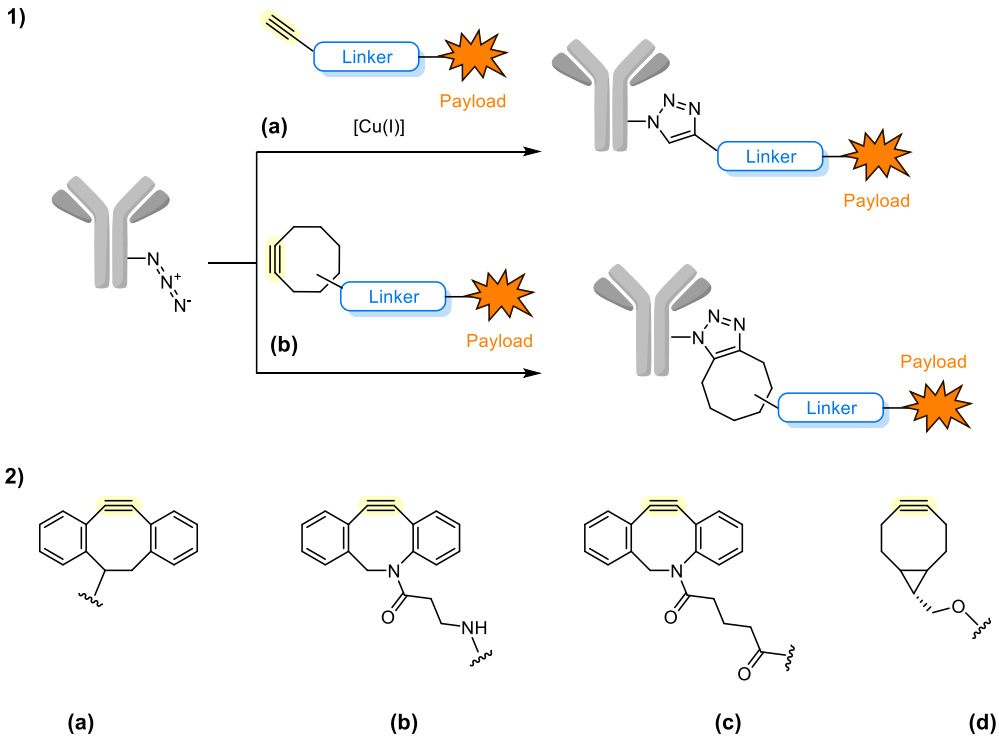

Scheme 11. 1a) Copper-catalyzed azide-alkyne [3+2] cycloaddition, **1b)** Strain-promoted [3+2] azide-alkyne cycloaddition, **2)** The cycloalkynes used for SPAAC: **a)** DIBO, **b)** DBCO, **c)** DIBAC, **d)** BCN.

1.2.5. ADME and pharmacological considerations in ADC development

The design of each component of an ADC has a significant influence on the ADME properties of the bioconjugate. The stability of the linker-payload system, the distribution of the compound within tissues, and the PK of the drug have been demonstrated to have a substantial impact on both the effectiveness and the safety of the pharmaceutical agent. The exposure-response relationship is a fundamental determinant of the therapeutic index (TI).[234]

A key example is Mylotarg® (gemtuzumab ozogamicin), which was initially approved in 2000 for the treatment of acute myeloid leukaemia. In light of the safety concerns pertaining to linker instability, the ADC was withdrawn in 2010. Following a re-evaluation of exposure-response relationships, an adjustment of dosing, and the implementation of new scheduling, Mylotarg® was successfully re-approved by the FDA in 2017 for patients diagnosed with CD33-positive AML. The analysis of the ADME properties of ADCs is a complex process, since each component, antibody, linker, and payload, contributes to the overall profile (**Table 3**).

Table 3. ADME Characterization approaches for ADCs and their constituents.

Species	ADME Information
Antibody	• Determine PK-dose relationship *in vivo* • Characterize target affinity/specificity *in vitro*, target expression/turnover *in vivo*, unintended or off-target binding *in vitro* and *in vivo*

ADC	• Linker component
	  ○ Characterize linker stability and kinetics of catabolism *in vitro* and *in vivo* across species
	  ○ Evaluate nature of the released species (active payload and its catabolites)
	• Conjugation site
	  ○ Evaluate influence of conjugation site on linker stability *in vitro* and *in vivo*
	  ○ Determine the effect of conjugation site on PK
	• DAR
	  ○ Determine in vivo PK and disposition with heterogeneous and homogeneous DAR species

Payload	• Metabolite identification, characterize drug-drug interaction (DDI) potential (CYP inhibition, induction and reaction phenotypes) • P-gp substrate or inhibitor • Characterize non P-gp transporters • Plasma protein binding

The antibody determines the slow clearance, long half-life, and limited tissue distribution typical of these modalities. Furthermore, its PKs have been shown to be influenced by target antigen expression, turnover, Fc receptor interactions, and isotype. The presence of anti-drug antibodies (ADA) can potentially reduce ADC's half-life.[235,236] The linker and payload must be considered equally important, since factors such as linker composition, conjugation site, and DAR have been demonstrated to affect clearance, stability, and aggregation. In addition, high DAR species tend to clear more rapidly due to increased hydrophobicity.[237] Conversely, the introduction of hydrophilic linkers has been shown to improve exposure in anti-CD70 and anti-HER2 ADCs.[84] Linker stability is a pivotal factor in ensuring safety, as the optimal ADC is designed to release its payload exclusively in the target tissue.[238] However, due to the prolonged half-life of the antibody, linkers are perpetually subjected to protease attack within the systemic circulation. The evaluation of stability can be conducted *in vitro* through plasma incubation or *in vivo* by monitoring payload release and DAR shifts.

The site of conjugation also plays a significant role in PK and disposition.[239,240] The employment of site-specific engineering strategies (e.g. engineered cysteines, unnatural amino acids, and chemical tags such as selenocysteine or aldehyde groups) allows DAR control and potencially enhancing the therapeutic index.[241] The biodistribution of ADCs is generally comparable to that of antibodies, with predominant accumulation in the liver, kidneys, lungs, and skin.[242,243] However, distribution varies depending on antigen binding and physicochemical properties.[244] The clearance of ADCs is achieved through two distinct mechanisms: target-mediated drug disposition (TMDD), wherein ADC-antigen complexes are trafficked to lysosomes for degradation and payload release, and nonspecific pinocytosis, which can result in degradation or FcRn-mediated recycling.[245] Following release, the unconjugated payload is distributed extensively, similarly to a conventional small molecule drug, and its elimination is contingent on hepatic and renal function. For instance, in the case of brentuximab vedotin, the MMAE payload is primarily excreted in feces (~72%) with the remainder excreted in urine.[246] Furthermore, resistance to ADCs has emerged as a significant challenge. The genesis of this phenomenon may be attributed to a number of factors, including downregulation or mutation of the target antigen, increased activity of drug efflux transporters that expel the payload, or alterations in intracellular trafficking that impair linker cleavage and payload release.[247] These mechanisms underscore the intricate interplay between antibody, linker, and payload properties, and the necessity of carefully balancing each element to achieve both efficacy and safety in next-generation ADC design.

1.2.6. Non-internalizing ADCs

The clinical success of FDA-approved ADCs, all of which rely on internalizing monoclonal antibodies, reinforced the notion that efficient internalization was mandatory for therapeutic activity. Nevertheless, this strategy is not without its limitations:

- it depends on the expression of internalizing antigens, which are not uniformly distributed across tumors;
- antibodies are large molecules, with limited tumor penetration due to slow diffusion;
- the phenomenon of the "antigen barrier" effect, in which antibodies bind to cells at the tumor periphery in proximity to blood vessels, impedes penetration into deeper regions[248];
- tumor resistance can arise through changes in internalization, antigen recycling, trafficking, or lysosomal degradation.[249,250]

In light of these constraints, the strict requirement for internalization has been contested. Interestingly, some anti-lymphoma ADCs have demonstrated efficacy in mouse models, even when targeting poorly internalized antigens such as CD20, CD21, and CD22.[251,252] A particularly promising approach, is Cancer Stromal Targeting (CAST), which exploits the fact that many solid tumors display blood coagulation and fibrin deposition in the stroma.[253] Antibodies directed against fibrin or collagen IV were conjugated to cytotoxins, thereby generating non-internalising ADCs that demonstrated potent activity in preclinical models.[254]

In the pursuit of synthesizing a non-internalizing ADC, the design strategy shifts from intracellular to extracellular drug release (**Figure 27**). The key point is the employment of labile linkers (e.g., protease-cleavable dipeptides, reducible disulfides), that do not require internalization for the release of the payload to occur, taking advantage of the distinct enzymatic and redox environment of tumors compared with normal tissues. Following release, payloads diffuse through the tumor microenvironment, thereby enhancing bystander killing and achieving deeper penetration than antibody-driven delivery alone. This non-internalizing mechanism of action has been demonstrated to broaden the spectrum of ADC targets by relaxing the stringent requirements for high antigen internalization.[255] There are several notable antigen targets, including CD20, CD21, CD72, TAG72, CEACAM5, and NKA27, as well as extracellular or secreted proteins, such as Gal3BP, LRG1 and MMP9.[248] Beyond antigens, attention has also been directed

towards tumor-specific stromal and vascular components, including collagen, fibrin, fibronectin, and tenascin-C.

Collectively, these advances indicate that non-internalizing ADCs may offer a complementary and potentially broader-spectrum anticancer strategy, particularly for solid tumors with rich stromal components and limited internalizing antigen expression.

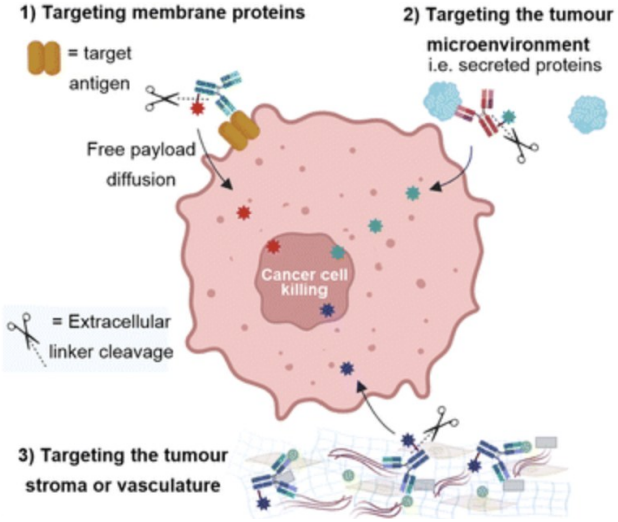

Figure 27. Mechanisms of action of non-internalizing ADC. [248]

1.2.7. Characterization of ADCs

Once an ADC has been synthesized, the bioconjugate need to be purified. This is necessary to remove excess reactants, organic co-solvents, additives and reaction by-products. Classical protein purification methods may be performed either independently or sequentially. Such methods include membrane filtration, gel filtration with desalting resins, size-exclusion chromatography (SEC) to eliminate aggregates, dialysis, or tangential flow filtration (TFF) using membranes with a suitable molecular weight cut-off.[256] As a final step, an additional buffer exchange process may be required to preserve the ADC in the correct buffer. Once purified, the ADC needs to be properly characterized, determining the DAR. A variety of analytical approaches, depending on the specific payload employed, are available, including UV-visible spectroscopy, hydrophobic interaction chromatography (HIC), and liquid chromatography coupled to mass spectrometry (LC-MS). Additionally, it is important to highlight that each of the components involved in the design and synthesis of ADCs influence the stability, the PK, and the pharmacodynamics of the final product.[257] Consequently, significant efforts have been dedicated to the assessment of the physicochemical characteristics of ADCs. Nevertheless, there are currently no standardized guidelines that directly correlate a specific property to a given

outcome. Analytical techniques commonly employed primarily aim at determining the DAR and dispersity, although complementary strategies are also being investigated. For instance, dynamic light scattering (DLS) can provide information on aggregation,[258] differential scanning calorimetry can highlight changes in higher-order protein structure,[259] matrix-assisted laser desorption/ionization (MALDI) can be applied to determine DAR,[260] and immunoassays can detect disrupted binding of the Fc region.

UV/Vis

Among the available techniques, UV/Vis spectroscopy is the most frequently reported for determining DAR. This approach is based on the Lambert-Beer law and relies on the comparison of the IgG's absorbance at 280 nm with that of the drug molecule. Simultaneous equations enable the calculation of the molar ratio.[261,262] The method has been employed to evaluate ADCs conjugated with a variety of payloads, including DM1, methotrexate, calicheamicin analogues and auristatins.[237,263] However, potential contributions of other sample components must be taken into account when evaluating the observed absorption at 280 nm, as well as the possible variations in extinction coefficients that may be attributable to the utilization of diverse buffer systems.[260,264] Furthermore, UV/Vis spectroscopy provides an average DAR across the entire sample, unless orthogonal analytical methods are applied to resolve the bioconjugate composition.

Chromatography

Chromatography is also widely applied in ADC characterization, since the conjugation process often generates heterogeneous mixtures differing in the number and site of payload attachment. Orthogonal techniques are therefore valuable for resolving these distinct profiles. HIC is particularly useful for separating species based on their different hydrophobicity, thereby allowing the determination of the DAR distribution, while Capillary Electrophoresis (CE) is effectively employed to resolve charge variants and positional isomers of native ADCs.[265–267] Although SEC is primarily used as a purification method, it can also offer insights into ADC variants when aggregation is suspected. However, the hydrophobicity of the payload can occasionally result in nonspecific interactions with the stationary phase. Furthermore, the conjugation of small drug molecules may not induce a sufficiently large shift in hydrodynamic radius to be detected by SEC.[268] Conjugation has been demonstrated to influence the electrostatic properties of antibodies. As a consequence, charge-based separation methods, such as CE, ion-exchange

chromatography or isoelectric focusing, have been shown to be informative, as these methods can detect alterations to the isoelectric point caused by lysine conjugation.[269] However, these approaches are less applicable when the ADC mixture is highly heterogeneous and displays only small isoelectric point differences. Site-specific conjugates, such as those obtained through unnatural amino acids or glycoengineering, can be efficiently analysed using reverse-phase high-performance liquid chromatography (HPLC) with C18 columns.[270] Conversely, direct characterization of intact cysteine-linked ADCs is more challenging: disruption of inter-chain disulfide bonds under denaturing conditions can lead to instability due to incomplete covalent linkage between subunits. In such cases, it is possible to separate and characterize heavy and light chains individually.[271] It has been demonstrated that HIC is particularly advantageous for intact ADCs since it employs pH-neutral, non-denaturing salt gradients, and is especially suited to relatively homogeneous conjugates, such as those obtained through inter-chain disulfide linkage or site-specific methods.[265] When coupled with orthogonal techniques, such as UV/Vis or mass spectrometry, chromatographic separation greatly enhances the information obtained. For instance, Hamblett and coworkers demonstrated that HIC-UV/Vis analysis could resolve and identify individual antibody species bearing from zero up to eight molecules of vc-MMAE.[237]

Mass Spectrometry

Mass spectrometry has become an increasingly important tool for ADC characterization, due to advances in ionization techniques such as MALDI and electrospray ionization (ESI).[257] These techniques allow the analysis of large biomolecules over wide mass ranges when used in conjunction with time of flight (TOF) or quadrupole detectors.[272] Although the acquisition of mass spectra is relatively straightforward, it is important to remove salts and excipients that interfere with ionization. Desalting is often facilitated by coupling MS with liquid chromatography.[273] Deglycosylation with enzymes such as PNGase is also a common practice in order to simplify analysis. MALDI-TOF MS has been shown to detect the mass shift between the unconjugated antibody and the conjugated ADC, thus providing evidence of conjugation and an estimate of the average DAR.[85] However, the instrument's mass accuracy is inadequate for distinguishing between individual DAR species. Conversely, ESI-MS generates multiple charged "envelopes" that, upon deconvolution, reveal distinct species corresponding to different DAR values.[274]

1.3. HEDGEHOG SIGNALLING PATHWAY

Until recently, the majority of ADCs approved by the FDA relied on highly potent cytotoxins as payloads. However, it is actually known that is not mandatory to charge the mAb with extremely cytotoxic agents to achieve effective ADCs. This paradigm shift led to a broadening of the spectrum of available payloads and cellular targets.

In this context, the Hedgehog (Hh) signalling pathway has recently gained significant attention due to its involvement in a wide range of human cancers. During embryonic development, Hh signalling regulates proliferation and differentiation in a time- and position-dependent manner, ensuring that developing tissues acquire the correct size, cellular composition, vascularization, and innervation.[275] The pivotal function of Hh signalling during development is evident from the severe consequences of its disruption, exemplified by holoprosencephaly observed in *Sonic Hedgehog* (SHh) mutants, a birth defect that can result as a consequence of insufficient Hh signalling. [276] It relates to a failure of the brain to properly separate into two halves and in its extreme form can be associated with cyclopia, the presence of a single centrally located eye. In adult organisms, Hh activity is markedly reduced compared to embryonic and neonatal stages. Furthermore, it is restricted to a few tissues, including neural stem cells in the CNS, as well as the gut epithelium . This finding does not imply that the Hh pathway is without essential function in the adult. Beyond the process of embryogenesis, Hh signalling also plays important roles in the processes of stem cells renewal, tissue repair, and overall regeneration.[277] Consequently, it is not surprising that a pathway regulating both proliferation and differentiation, once mutated or aberrantly activated, can contribute to tumorigenesis or accelerate tumor growth. The Hh pathway is of particular relevance in two malignancies where therapeutic needs remain unmet: basal cell carcinoma (BCC), the most common cancer in the Western world, and medulloblastoma, a childhood tumor with historically poor prognosis.[278] Furthermore, germline mutations that promote aberrant activation of the Hh pathway have been associated with an increased incidence of cancers in specific tissues, such as brain, skin, skeletal muscle, liver, and colon in humans and mice, as well as bladder cancer in mice.[277] Further studies have demonstrated that antagonizing Hh signalling, through pharmacological inhibitors, ligand-blocking antibodies, or overexpression of inhibitory pathway components, confirms the persistent requirement for pathway activity in sustaining the growth of other malignancies, including small-cell lung cancer and carcinomas of the oesophagus, stomach, pancreas, biliary

tract, and prostate. The diversity of tissues in which Hh pathway-dependent tumors arise mirrors the broad range of organs in which this pathway plays a critical role in stem cells renewal.

1.3.1. Mechanisms of Hh signal transduction

Hh proteins are secreted signalling molecules first discovered in *Drosophilae Melanogaster* together with many components of their transduction machinery.[279] These proteins are highly hydrophobic and, upon secretion, are capable of diffusing through tissues to generate gradients that are fundamental to embryonic development.[275] Despite the significant differences between *Drosophilae* and vertebrates, the underlying signalling mechanisms are remarkably well conserved. In humans, three homologues have been identified with distinct spatial and temporal distribution patterns: *Sonic hedgehog* (SHh), *Indian hedgehog* (IHh), and *Desert hedgehog* (DHh). In mammals, Hh signalling can be initiated through two distinct mechanisms: canonical ligand-dependent signalling and non-canonical, ligand-independent mechanisms that act downstream of Smoothened (SMO).[280]

Canonical Hh signalling (**Figure 28**) begins when the Hh glycoprotein binds to and inactivates the 12-transmembrane receptor Patched1 (PTCH1).[281] In the absence of Hh ligand, the function of PTCH1 is to suppress the activity of Smoothened (SMO), a GPCR-like protein.[282] This, in turn, allows SMO to accumulate at the primary cilium (PC), where it becomes activated and initiates the downstream cascade. The activation of SMO has been demonstrated to promote the nuclear translocation of GLI family transcription factors, which in turn drive the expression of target genes.

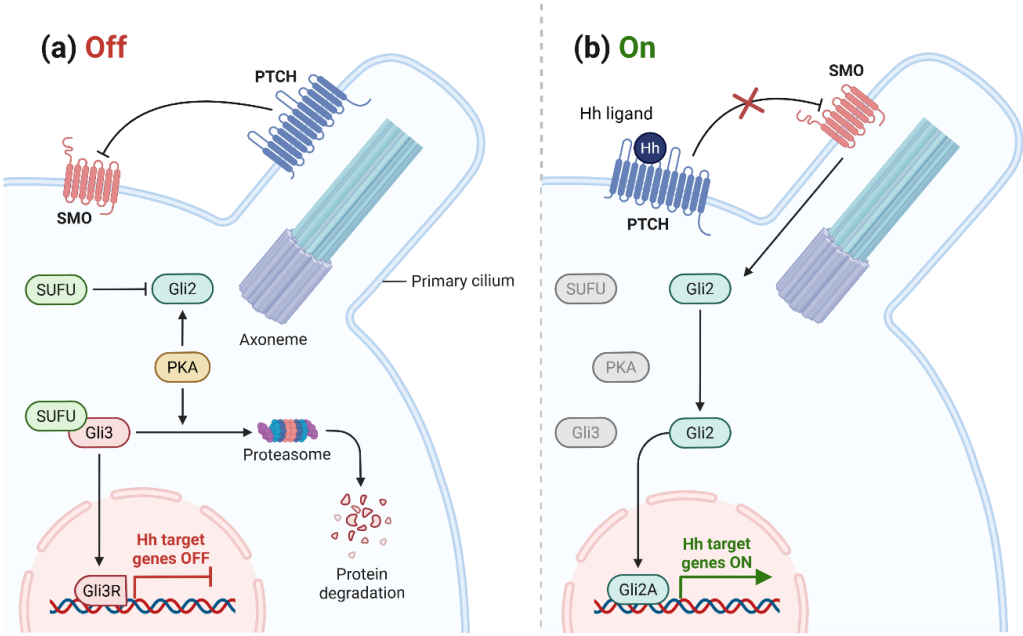

Figure 28. A schematic of the vertebrate Hh signalling pathway **a)** in the absence or **b)** presence of Hh ligands. Created with Biorender.

The GLI transcription factors are central effectors of the pathway. Three GLI proteins (GLI1, GLI2 and GLI3) are zinc-finger transcription factors that are expressed in vertebrates, in overlapping and partially redundant domains. GLI1, initially characterised as an amplified oncogene in malignant glioma, functions as a transcriptional activator.[283] The function of GLI2 is predominantly as a transcriptional activator, whilst that of GLI3 is principally as a repressor.[284] The equilibrium between the activator (GLI-A) and repressor (GLI-R) forms of these proteins is pivotal in determining the outcome of signalling.[285]

Another significant regulator is Suppressor of Fused (SuFu), a negative regulator of GLI activity.[286] In the absence of Hh ligand, SuFu binds GLI proteins in the cytoplasm, thereby preventing their nuclear translocation and maintaining pathway repression.[287] The retention of GLI proteins by SuFu can result in the processing of these proteins into truncated repressor forms following the process of phosphorylation by kinases such as GSK3β, CK1, and PKA.[284] This process leads to the partial degradation of the proteins via the proteasome.[288] Activation of Hh signalling results in SuFu hyperphosphorylation, leading to the release of GLI proteins and their subsequent penetration of the nucleus, where they initiate transcription.[289] A number of kinases have been demonstrated to regulate this process at various levels, including PKA, PKC, CK1, MEK1, GSK3, PI3K, and DYRK1.[290–292]

In addition to phosphorylation, post-translational modifications, including ubiquitination and acetylation, have been shown to further refine the activity of Gli. Ubiquitination, first characterised in *Drosophilae* and later confirmed in vertebrates, leads to the degradation or proteolytic cleavage of Gli proteins.[293] Furthermore, acetylation has been demonstrated to modulate GLI function: The acetylation of GLI1 and GLI2 at lysines 518 and 757, respectively, represents an inhibitory modification that is reversed by HDAC1.[294] The process of HDAC1-mediated deacetylation promotes transcriptional activation of the pathway. Conversely, the degradation of HDAC1 through the action of an E3 ubiquitin ligase complex results in the termination of the signal, thus ensuring a positive autoregulatory loop in the presence of Hh ligand.[294] Genetic alterations in negative regulators of the pathway provide evidence of its oncogenic potential. Mutations in the PTCH1 and SuFu genes, for instance, have been associated with tumorigenesis.[295] As demonstrated by knockout mouse models, SuFu loss alone has been shown to be sufficient to activate Hh signalling independently of receptor input.[296] However, the development of tumors also requires the loss of a second tumor suppressor gene, such as p53.[297] This illustrates how aberrant activation of canonical SHh signalling contributes to the molecular basis of cancer.

Additionally, "non-canonical" Hedgehog signalling activations are known. These processes can be categorized into two distinct types: type I, which functions downstream of SMO to regulate intracellular calcium flux and actin cytoskeleton dynamics, and type II, which operates independently of SMO, promoting cell proliferation and survival.[298] Over the past decade, most studies on non-canonical Hh signalling have emerged within the field of tumor biology. Nevertheless, the precise mechanisms remain to be elucidated. Initially, it was hypothesised that canonical signalling required SMO entry into the PC, whereas exclusion from the PC redirected signalling towards non-canonical pathways.[299] However, recent studies have demonstrated that non-canonical signaling can also occur in a PC-dependent manner, for instance by promoting SMO-mediated calcium signalling and subsequent α-tubulin acetylation in mouse embryonic fibroblasts.[300] Recent findings suggest that non-canonical signalling may have a detrimental effect on osteoblast differentiation and bone formation. [301] Despite the insights afforded by these observations, the molecular determinants that govern the selection between canonical and non-canonical routes remain largely unresolved.

1.3.2. Hh pathway in osteogenesis and bone metabolism

The Hh signalling pathway is a fundamental regulator of bone development, remodelling, and homeostasis. Its influence extends to multiple cell types and processes, orchestrating the formation, maintenance, and repair of skeletal tissues. In endochondral ossification, the process by which most long bones develop, IHh is the predominant ligand.[302] IHh functions to coordinate the engagement of mesenchymal stem cells (MSCs) and regulate chondrocyte proliferation and maturation, which are critical for forming the cartilage template that is later replaced by bone.[303] SHh, another key ligand, plays an important role in intramembranous ossification, responsible for the formation of flat bones such as those in the skull, and also in the crucial processes of bone fracture repair. SHh achieves this by driving the differentiation of MSCs towards the osteogenic lineage.[304] The regulatory reach of the Hh pathway is not limited to bone formation. It also participates in the complex process of bone remodelling by influencing both osteoblasts (bone-forming cells) and osteoclasts (bone-resorbing cells).[305] In essence, the Hh pathway has a complex role, coordinating multiple cellular activities to ensure proper skeletal development and to mediate repair in adult organisms.

The function of the Hh pathway in osteogenesis is complex and exhibits a stage-specific duality. While the activation of Hh signalling is a vital initial step for promoting early osteoblast differentiation and proliferation, its role is not one of continuous, uninhibited activation. The process of terminal maturation into bone-forming osteocytes requires a precise decrease in Hh activity.[306,307] This sophisticated function of the Hh pathway in bone homeostasis is a critical consideration for therapeutic strategies. It implies that simply activating the pathway indefinitely is not the goal for promoting bone formation. Instead, successful interventions must act more like a rheostat, providing a precisely timed and localized signal that promotes early differentiation while avoiding the negative consequences of prolonged activation in mature cells.

The successful repair and regeneration of bone tissue are not solely dependent on the formation of new bone matrix. These processes are inherently linked to the development of a functional vascular network to supply oxygen and nutrients. SHh is identified as a master molecule that synergistically links osteogenesis and angiogenesis, a dual function that holds immense therapeutic potential. SHh acts as an upstream regulator for some of the most prominent angiogenic growth factors, including Vascular Endothelial Growth Factor (VEGF) and angiopoietins.[308] By inducing the expression of these factors in interstitial mesenchymal cells,

SHh stimulates angiogenesis through paracrine mechanisms.[308] Beyond this indirect, paracrine effect, SHh also acts as a direct mediator for endothelial cell activation and tube formation via Gli-independent pathways. Its influence on vascularization is further enhanced by its ability to promote vessel stabilization. Shh contributes to the recruitment of mural cells and supports the proliferation of smooth muscle cells (SMCs), leading to the wrapping of new microvessels with a stabilizing cellular sheath.[309] This coordination of both new vessel formation and their stabilization is a significant advantage over therapeutic approaches that focus on a single aspect, such as using only VEGF, which often results in unstable vessels. The ability of a single molecule or pathway agonist to simultaneously orchestrate bone formation and its vital vascular supply mirrors the body's natural healing mechanisms. This dual role presents a much more complete and powerful strategy for regenerative medicine applications and provides a compelling rationale for the search for small molecules that can modulate this pathway.

Motivated by the significant therapeutic potential of activating the Hh signalling pathway in regenerative medicine, our research group focused its attention on the development of novel small-molecule agonists of SMO. A pharmacophoric model derived from the chemical structures of two well-established canonical SMO agonists, SAG and purmorphamine was developed.[310] This computational model served as a blueprint for a virtual screening process of a large chemical library. The screening of commercial compound libraries led to the identification of a new quinolinecarboxamide derivative, **GSA-10** (**Figure 29**), whose chemical structure was found to fit the pharmacophoric model well, possessing two hydrogen bond acceptor groups and four hydrophobic regions, thus providing a strong foundation for its further characterization as a potential SMO agonist.

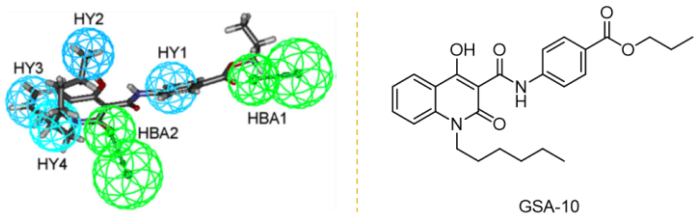

Figure 29. Proposed pharmacophoric model for **GSA-10** and chemical structure of **GSA-10**.

GSA-10 demonstrated an approximate half-maximal effective concentration (EC_{50}) of 1.2 µM, which is comparable to that of purmorphamine (EC_{50}~0.8 µM) but less potent than SAG (EC_{50} ~0.13 µM). However, a notable finding was that the maximal response achieved by **GSA-10** was significantly higher than that of SAG, representing only about 75% of the maximal response of

GSA-10. This is a crucial pharmacological difference, as it indicates that while SAG is more potent (as it requires a lower concentration to produce a response), **GSA-10** is ultimately more efficacious in promoting osteogenesis at its saturating dose. This distinction makes **GSA-10** a more powerful inducer of the osteogenic response. **GSA-10** functions involving a fundamentally different, non-canonical mechanism of action compared to conventional SMO agonists. This molecule does not exhibit several of the established hallmarks of Hh pathway activation. First, it does not compete for the classic Bodipy-cyclopamine (BC) binding site on the SMO receptor, suggesting it targets a novel and distinct active site. This is further supported by the observation that its osteogenic effects are not inhibited by cyclopamine, unlike other SMO agonists, but are blocked by a panel of other antagonists, such as SANT-1.

GSA-10 scaffold was employed for the design and synthesis of a new class of quinolone derivatives.[311] Modifications to the ester moiety were a critical determinant. Replacing the propyl ester with a carboxylic acid group, as in compound **1** (**Figure 30a**), resulted in a substantial two-fold improvement in activity, yielding an EC_{50} of 0.6 µM. This suggests a preference for a free carboxylic acid group in the binding site. Conversely, converting the ester to an amide or an ether led to a dramatic loss of activity. Lastly, decorating the condensed phenyl ring generally did not improve activity, with one notable exception. The 6,7-dimethoxy substitution in compound **2** (**Figure 30b**) yielded a remarkable submicromolar EC_{50} of 0.36 µM, making it approximately three times more potent than **GSA-10** and on par with the reference agonist SAG. This finding suggests that specific, targeted modifications to this ring can significantly enhance the molecule's osteogenic potential. This studies successfully elucidated key structure-activity relationships (SARs), leading to the identification of optimized compounds with enhanced osteoinductive activity. Together, these achievements highlight the potential of developing targeted small molecules as therapeutic agents to promote bone regeneration through the controlled activation of the Hedgehog signaling pathway.

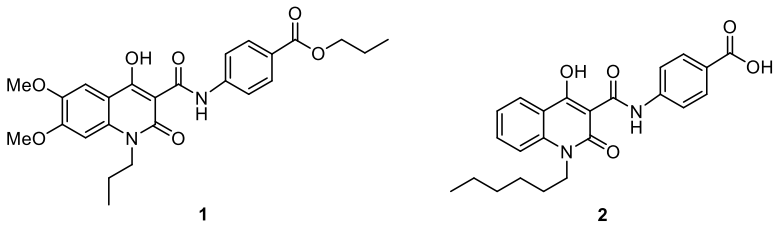

Figure 30. Chemical structure of Hh agonists **1** and **2**.

1.3.3. Hh pathway mutations and cancer

The correlation between Hh pathway activity and cancer was first documented with the identification of heterozygous mutations in PTCH as the underlying genetic cause of Gorlin's syndrome.[312] Patients with this syndrome develop numerous BCCs throughout their lifetime and are also predisposed to other malignancies, most notably medulloblastoma, which originates from cerebellar granule neuron progenitor cells, and rhabdomyosarcoma, a tumor of muscle tissue.[313] Following studies revealed that the majority of BCCs manifest hyperactivation of the Hh pathway, as evidenced by increased mRNA levels of the Hh target genes GLI1 and PTCH1 in tumor cells.[314] In such cases, inactivating mutations of PTCH1 are most frequently observed, although activating mutations of SMO are detected in approximately 10% of BCCs.[315] Furthermore, more than one-third of human medulloblastomas exhibit aberrant Hh signalling, frequently associated with PTCH1 mutations and, less frequently, with SuFu mutations.[316] In all these scenarios, deregulated Hh pathway activity is believed to drive excessive cell proliferation, ultimately leading to tumor formation. Experimental evidence from mouse models has largely confirmed these observations. The overexpression of GLI1[317], GLI2[318] or constitutively active SMO[315] in the skin of otherwise normal mice demonstrated to produce lesions that closely resemble BCCs in both their histological features and the expression of phenotypic markers. Furthermore, mice heterozygous for PTCH1 mutations, which are considered a murine model of Gorlin's syndrome, display increased body size, a higher incidence of spontaneously arising medulloblastomas, and greater susceptibility to UV-induced BCCs. [319] This closely reflects the phenotype observed in human patients. Furthermore, mice carrying heterozygous loss-of-function mutations in SuFu develop skin abnormalities similar to those seen in Gorlin's syndrome.[296]

As previously discussed, the Hh pathway plays a dual role, being essential for both cancer growth and tissue regeneration through its influence on stem cell renewal. These apparently divergent processes, cancer and tissue repair, may in fact be mechanistically connected. Increased cancer risk has been demonstrated to be strongly associated with chronic exposure to harmful agents such as alcohol, tobacco smoke, and organic chemicals[320,321], with persistent infections such as *Helicobacter pylori* and other pathogens[322], and with inflammatory conditions including sclerosing cholangitis and inflammatory bowel disease[323], all of which share the common feature of prolonged tissue damage. Acute injury is typically followed by an increase in stem cell pools and a transient activation of the Hh pathway.[324] However, in the context of chronic injury, the repeated damage to tissue prevents complete regeneration, resulting in continued pathway

activation and an expansion of progenitor cell populations (**Figure 31**). The continuous Hh signalling and proliferative activity mirrors the persistent activation seen in cancer cells. These findings provide support for the hypothesis that the development of tumors may represent a pathological extension of an otherwise physiological repair process. In this model, genetic or epigenetic alterations prevent the return of stem or progenitor cells to quiescence once regeneration is complete, effectively trapping them in a state of continuous self-renewal and thereby initiating tumorigenesis.

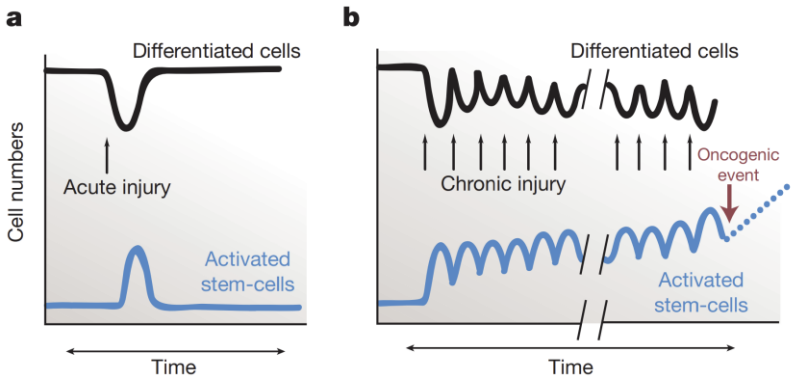

Figure 31. a) Acute injury produces an increase in the pool of activated stem cells. Upon completion, the number of activated stem cells returns to baseline. **b)** Chronic injury also causes expansion in the pool of activated stem cells, but because of repeated injury the pool size does not return to baseline. As a result, the total number of activated stem cells is greatly increased over time, increasing the probability that an oncogenic event will trap a stem cell in the activated state.[325]

In accordance with this hypothesis, the Bmi-1 gene, which is required for the renewal of haematopoietic stem cells, has also been demonstrated to be essential for the propagation of leukaemia in transplantation experiments.[326] Furthermore, the expression of Bmi-1 and nestin, both markers of stem cell renewal[327], is dependent on Hh pathway activity in Hh-driven tumors.[328,329] It is hypothesized that multiple genetic or epigenetic modifications are required to sustain this aberrant state, not only locking stem cells into continuous self-renewal, but also enabling their autonomous proliferation, thus bypassing the regulatory signals that typically sustain their identity. Collectively, these observations demonstrate the critical involvement of the Hh pathway in oncogenesis and highlight its relevance as a therapeutic target. Pharmacological antagonists of Hh signalling have already produced encouraging results, particularly in the treatment of BCC, medulloblastoma, and several solid tumors in preclinical studies.

1.3.4. Inhibiting Smoothened

SMO is a member of the G protein-coupled receptor (GPCR) superfamily, specifically belonging to class F, also known as the Frizzled family.[330] Unlike most GPCRs, SMO is characterised by an extended carboxyl-terminal (*C*-terminal) domain, which is indispensable for Hh-dependent signalling.[331] This domain contains four conserved clusters of basic amino acids within a region bearing six serine/threonine phosphorylation sites. In *Drosophilae*, the SMO receptor is present as a constitutive multimer due to interactions between its *N*-terminal regions.[332] Upon binding of Hh ligand to PTCH, a process of phosphorylation of the *C*-tail occurs, resulting in a reduction of the overall positive charge of the basic clusters and enabling the *C*-tails to interact more closely.[332] Despite the significant differencies in the amino acid sequence of SMO between *Drosophilae* and mammals, the structural features that regulate self-association, the phosphorylation motifs, and the conformational shifts induced by phosphorylation are well conserved.[298] Following these modifications, in *Drosophilae* SMO translocates to the plasma membrane, whereas in mammalian cells it is specifically directed to the membrane of the PC, which is strictly required for Hh signalling in vertebrates.[333]

Similarly to other GPCRs, SMO is presumed to function through ligand binding at its extracellular domain.[334] Despite extensive research, a conclusive physiological ligand remains to be identified. Moreover, studies on PTCH suggest that its inhibitory effect on SMO is not mediated by direct stoichiometric interaction, but rather through a catalytic mechanism in which PTCH regulates intracellular concentrations of small-molecule modulators of SMO.[335] Nevertheless, given its pivotal role in transmitting the Hh signal, SMO has become the primary therapeutic target for pathway inhibition. Pharmacological blockade of SMO has been demonstrated to prevent the downstream activation of GLI transcription factors, thereby ultimately suppressing the transcription of genes that promote tumor growth and progression.

<u>Cyclopamine</u>

Cyclopamine, a steroidal alkaloid first isolated from *Veratrum Californicum*, commonly known as corn lily, was the first compound identified to strongly interact with SMO and suppress Hh signalling (**Figure 32a**).[336] During the 1950s, cases of lambs born with cyclopia, a rare malformation characterized by a single median eye, were reported in Idaho. Following years of investigation, researchers were able to identify the underlying cause to be the ingestion of corn lily by pregnant female sheep.[337] It was not until several decades later that the connection

between this teratogenic effect and the Hh pathway was elucidated. Through experimental studies, the phenomenon of cyclopia was successfully replicated by silencing the SHh gene. This finding served to establish a crucial link between the genetic evidence and the observations that had been made forty years earlier. In 1998, the initial reports indicated that cyclopamine possessed the capability to impede SHh signal transduction.[338] By the year 2000, the potential applications of cyclopamine in the field of oncology had come to attention, with evidence of its activity against multiple tumor types.[339] Since then, cyclopamine has been widely recognized in both its capacities as a molecular probe for the investigation of Hh biology and as a candidate therapeutic agent in conditions driven by aberrant Hh signalling. Preclinical studies confirmed its ability to suppress tumor growth in a broad variety of malignancies, including glioma, melanoma, colorectal, pancreatic, prostate, and small-cell lung cancers, as well as medulloblastoma.[324,328,335,340–342] Despite its extensive use as a Hh pathway inhibitor in cell-based and murine models, the clinical translation of cyclopamine has been hindered by its poor solubility and relatively low potency.[324,328,342] Furthermore, the presence of a Lewis acid or conditions of pH < 2 determinate the opening of E ring, providing the analogue Veratramine (**Figure 32b**). Veratramine can cause hemolysis by its non-specific cytotoxic activity.[343]

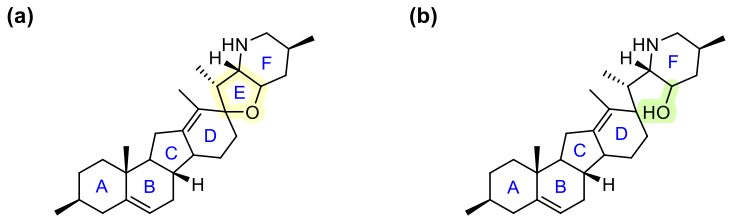

Figure 32. Structure of **a)** Cyclopamine, and its analogue **b)** Veratramine.

Vismodegib (GDC-0449)

In January 2012, vismodegib (**Figure 33**) became the first Hh pathway inhibitor approved by the FDA, following encouraging outcomes from early phase I and II trials that demonstrated its efficacy in BCC.[344] Since then, the drug has been extensively evaluated in a variety of advanced malignancies.[345,346] Vismodegib exerts its function through binding to SMO, thereby blocking downstream signalling within the Hh cascade. The most significant examination of its clinical activity and safety was conducted in the international, open-label STEVIE trial, which enrolled 1215 patients with either locally advanced or metastatic BCC across 36 countries.[347] The study documented objective response rates of 68.5% for locally advanced disease and 36.9% for

metastatic cases. Nevertheless, adverse events were significant, with serious complications occurring in 289 patients (23.8%) and 46 deaths (3.8%) being reported.

One unresolved issue concerns the potential association between vismodegib treatment and an increased incidence of cutaneous squamous cell carcinoma (SCC). A case-control analysis indicated an eightfold rise in SCC occurrence among vismodegib-treated patients[348], whereas another study failed to confirm this correlation.[349] In light of the conflicting findings, it is recommended that patients undergo regular dermatological monitoring during their therapy. Another critical challenge is the development of acquired resistance: approximately 21% of patients experienced tumor regrowth during continuous vismodegib administration, with a mean detection time of 56.4 weeks based on clinical evaluation.[350]

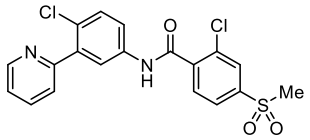

Figure 33. Structure of vismodegib.

Sonidegib (LDE-225)

Sonidegib (**Figure 34**) is a small-molecule inhibitor that directly targets SMO, thereby preventing Hh pathway activation, and is currently approved for the management of advanced BCC.[351] In clinical phase I evaluation, this compound exhibited a satisfactory safety profile in patients with advanced solid tumors, whilst concomitantly demonstrating antitumor activity, not only in advanced BCC, but also in relapsed medulloblastoma.[352] The results of a subsequent phase II trial demonstrated that the daily administration of 800 mg did not yield superior efficacy in comparison with 200 mg, while it was associated with a significantly higher incidence of grade 3/4 adverse events (64.0% vs 43.0%). In view of the ineradicable nature of BCC, median overall survival (OS) had not been attained even after 30 months of treatment. It is estimated that the two-year OS rates for patients receiving 200 mg daily were 93.2% in cases of locally advanced disease and 69.3% in cases of metastatic BCC, although complete responses remained infrequent.[353] When compared with vismodegib, sonidegib appears to have a similar overall response rate (ORR) in cases of locally advanced BCC (57% vs 69%), but the complete response rate was markedly lower (3% vs 31%). In the context of metastatic disease, vismodegib demonstrated a substantial advantage, exhibiting an ORR that was 2.7 times higher than that observed with sonidegib (39% vs 15%).[354] The spectrum of adverse events was found to be

comparable between the two agents, although gastrointestinal toxicity occurred with greater frequency in patients treated with sonidegib. Furthermore, cross-resistance has been observed, with patients with advanced BCC who had failed vismodegib therapy demonstrating cross-resistance to sonidegib as well.[355] Beyond its approved indication, sonidegib is currently being investigated both as monotherapy and in combination regimens for a range of solid and haematological malignancies.[351]

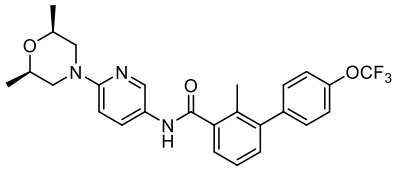

Figure 34. Structure of sonidegib.

Saridegib (IPI-926)

Saridegib (**Figure 35**), a semisynthetic analog of cyclopamine, has been proved to be a potent and selective inhibitor of SMO. The antitumor activity of the substance has been demonstrated in a range of studies conducted *in vitro* and *in vivo*, including research into ovarian cancer, medulloblastoma and head and neck tumors.[356] Notably, experiments in a genetically engineered mouse model of pancreatic cancer revealed that saridegib reduces tumor-associated stroma while simultaneously increasing intratumoral vessel density.[357] This stromal depletion enhances the delivery of co-administered systemic chemotherapy, ultimately resulting in reduced tumor size and prolonged survival in treated mice. A multicentre phase I clinical trial was conducted, in which saridegib was tested in combination with FOLFIRINOX, a chemotherapy regimen made up of four drugs (folinic acid, 5-fluorouracil, irinotecan and oxaliplatin).[358] The treatment yielded an objective response rate of 67%. Despite these encouraging findings, the trial was terminated prematurely following the results of a separate phase II study, in which the combination of saridegib with gemcitabine produced adverse outcomes. Nevertheless, clinical trials are ongoing to assess the efficacy of saridegib in the treatment of BCC, chondrosarcoma, and metastatic pancreatic cancer.[351]

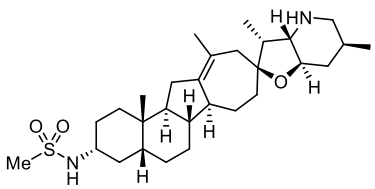

Figure 35. Structure of saridegib.

Itraconazole

Itraconazole (**Figure 36**) is a synthetic antifungal agent belonging to the triazole class. It has been approved for the treatment of several fungal infections, including aspergillosis, sporotrichosis, blastomycosis, systemic candidiasis, and paracoccidioidomycosis.[359] Beyond its antifungal applications, itraconazole has demonstrated pharmacological activities of oncological relevance, including anti-angiogenic effects, inhibition of the Hh pathway, induction of autophagy, and cell cycle arrest.[360] Its mechanism of action on the Hh pathway involves blocking the ciliary accumulation of SMO, a process that differs from that of cyclopamine and other SMO inhibitors. Clinical studies have been conducted to investigate its potential in oncology. In an open-label phase II trial conducted on 29 patients diagnosed with BCC, itraconazole demonstrated a 45% reduction in cell proliferation, a 65% decrease in Hh pathway activity, and a 24% reduction in tumor area.[361] A further phase II randomised trial investigated the use of itraconazole in patients with metastatic castration-resistant prostate cancer. Amongst the 46 participants, 29 received a high-dose of itraconazole (600 mg/day), whilst 17 received a low-dose (200 mg/day). At 24 weeks, progression-free survival (PFS) was 48% in the high-dose group and 11.8% in the low-dose group, with median PFS of 11.9 and 35.9 weeks, respectively.[362] Further retrospective analyses have indicated a survival benefit of itraconazole in patients with refractory cancers, including ovarian clear cell carcinoma, triple-negative breast cancer, pancreatic cancer, and biliary tract malignancies.[363–366]

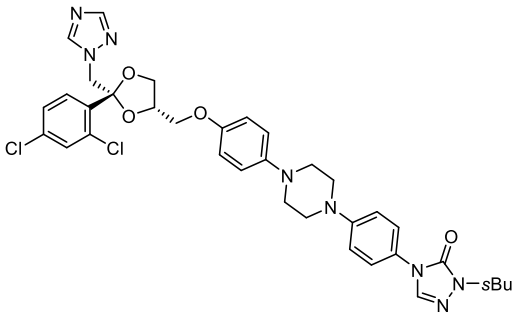

Figure 36. Structure of itraconazole.

1.3.4.1. SMO drug resistance

The development of SMO inhibitors has provided substantial therapeutic benefits in the treatment of cancer. Nevertheless, the emergence of drug resistance remains a considerable obstacle. One of the principal resistance mechanisms involves mutations in SMO, as demonstrated by genomic analyses of resistant tumors, particularly within its drug-binding pocket, which result in a reduction or complete loss of inhibitor binding.[367] For instance, a significant proportion of patients diagnosed with BCC initially exhibit a positive response to vismodegib, yet over time, resistance frequently develops. Yauch and coworkers identified the SMO^{D473H} mutation in a medulloblastoma patient, thereby inducing resistance to vismodegib.[368] As another example, Buonamici and colleagues reported that although sonidegib initially induced tumor regression in medulloblastoma models, resistance soon developed through SMO mutations that restored Hh pathway activity.[369]

In addition to SMO mutations, cancer cells have the capacity to exploit alternative signalling pathways to bypass Hh inhibition. In other malignancies, such as metastatic colorectal cancer, non-canonical GLI1 activation via RAS/RAF or PI3K/AKT pathways renders SMO inhibition ineffective, explaining the lack of response to vismodegib.[370] Unexpectedly, activation of the phosphatidylinositol 3-kinase (PI3K) pathway has also been identified as a mechanism of resistance. Combination therapy involving PI3K inhibitors and sonidegib has been demonstrated to significantly delay the emergence of resistance.[369] Consequently, novel therapeutic strategies are being explored, including the design of drugs targeting downstream components of the Hh pathway (e.g., GLI transcription factors) and rational combinations of SMO inhibitors with agents blocking alternative pathways such as PI3K or MEK inhibitors. These approaches offer a potential solution to the issue of resistance and enhance the durability of the response.

As described above, further limitation of Hh inhibitors is associated with their adverse effects and off-target toxicities. Consequently, the development of agents that exhibit an optimal balance between efficacy and tolerability remains paramount. Innovative drug delivery systems, including nanoparticles and targeted drug conjugates, offer a promising route to optimize tumor targeting while minimizing systemic toxicity.

1.3.4.2. MRT compounds

Over the past decade, our research group has developed a consistent body of work on Hh pathway inhibition through novel SMO and GLI antagonists, combining structural pharmacology, mechanistic exploration in melanoma, and preclinical validation in cancer models. The initial work focused on virtual screening of commercial compound libraries against a SMO antagonist pharmacophore, identifying MRT-10 (**3**, **Table 4**), an acylthiourea with antagonist activity in various Hh assays (half maximal inhibitory concentration, IC_{50} = 0.65 µM for blocking differentiation of multipotent mesenchymal C3H10T1/2 cells into AP-positive osteoblasts)[371]. Subsequent optimisation processes led to a family of acylthiourea, acylurea, and acylguanidine derivatives, including MRT-83 (**4**, **Table 4**).[372] This acylguanidine displayed antagonist activity comparable to that of GDC-0449.[373] To better understand the interaction of MRT compounds with the receptor SMO, available X-ray crystal structures of human SMO in complex with various antagonists, including LY2940680, SANT-1, cyclopamine, and Anta XV, were evaluated in combination with targeted mutagenesis experiments.[374] The investigation identified two major categories of seven-transmembrane (7TM)-directed antagonists: type I ligands, which bind predominantly at the extracellular loop (ECL) region, such as LY2940680 (**Figure 37a**), cyclopamine, Anta XV, and type II ligands, which extend more deeply into the 7TM cavity, as exemplified by SANT-1 (**Figure 37b**).[330,375] These findings gave rise to the hypothesis that a third class of antagonists could be developed, characterised by the ability to engage both regions simultaneously.

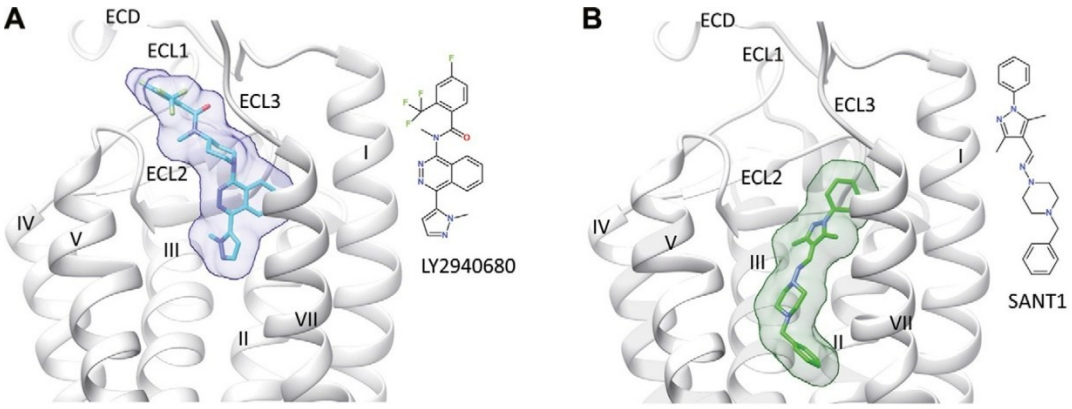

Figure 37. X-ray structures (PDB accession codes 4JKV and 4N4W, respectively) of hSMO binding different antagonists, **a)** LY2940680; **b)** SANT-1, to the transmembrane domain (white ribbons). The bound ligand is indicated by sticks and rendered by a transparent surface. The inset illustrates the structure of each ligand.[374]

Compound **4** was able to inhibit BC binding to HEK-hSMO cells, suggesting that it engages residues within site 1. Although reproducible docking of **4** into cleft-closed hSMO structures proved unsuccessful, the cleft-open conformation (4N4W, with SANT-1 bound) readily accommodated **4**, consistent with observations of structure-activity relationships.[373] It is noteworthy that docking indicated that the deepest portion of the cavity (site 2) remained unoccupied, suggesting that elongation of the biaryl moiety may yield analogues with superior potency.

Pursuing this rationale, derivatives of **4** with extended biaryl moieties were synthesized (**Table 4**), evaluating their activity in blocking SMO-mediated differentiation of mesenchymal progenitors into osteoblasts induced by the SMO agonists SAG and GSA-10).[376] Among the five analogues generated, MRT-92 (**6**, **Table 4**) exhibited the most striking profile, with the ability to block SAG-induced differentiation of C3H10T1/2 cells at an IC_{50} of 5.6 nM. In contrast, **6** demonstrated significantly weaker antagonism against GSA-10, with an IC_{50} of 1000nM. The results indicated that **6** is a low-affinity antagonist of SMO-GSA-10, but a highly potent and selective blocker of SMO-SAG signalling in C3H10T1/2 cells. It was demonstrated that other acylguanidine and thioacylurea derivatives exhibited comparable micromolar inhibition of SMO-GSA-10. However, these derivatives were found to be less effective than **6** against SMO-SAG-driven responses.[374]

Table 4. Structures and IC_{50} values for vismodegib, MRT-83 and derivatives on SAG and GSA-10 -induced differentiation of C3H10T1/2 cells.[374]

Compound	*Structure*	*IC_{50} (μM)*	
		Smo^{SAG}	*Smo^{GSA-10}*
Vismodegib	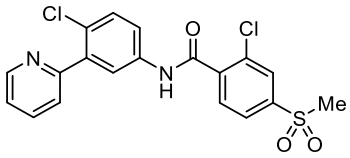	0.011± 0.002	-
3 (MRT-10)	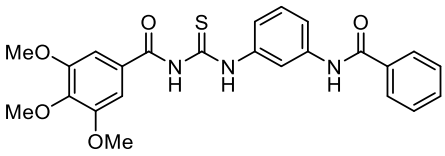	-	-
4 (MRT-83)	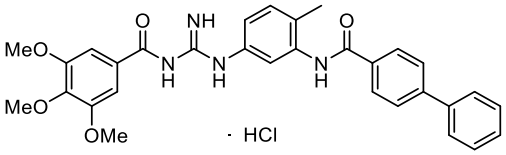	0.011 ± 0.003	0.038 ± 0.007
5 (MRT-91)	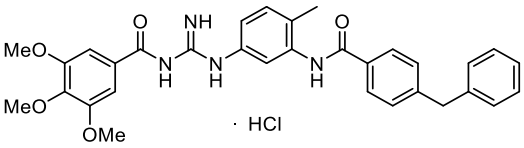	0.22 ± 0.02	2.6 ± 1.4
6 (MRT-92)	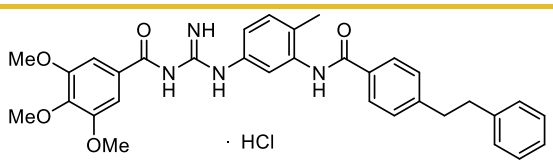	0.006 ± 0.001	1.0 ± 0.05
7 (MRT-93)	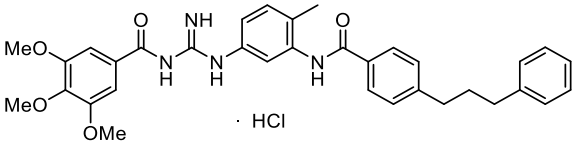	0.039 ± 0.009	1.4 ± 0.4
8 (MRT-94)	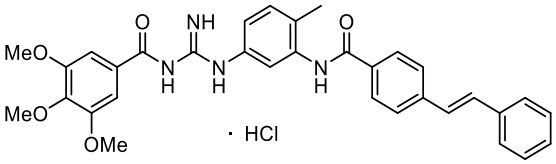	0.015 ± 0.004	0.7 ± 0.1
9 (MRT-95)	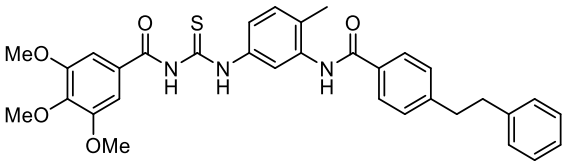	0.033 ± 0.006	1.5 ± 0.4

Further pharmacological characterization revealed that **6** acts as a competitive antagonist of SAG: increasing SAG concentrations shifted the inhibition curve of **6** progressively to the right, with up to a 60-fold increase in IC_{50} (**Figure 38a-c**). These findings confirmed that **6** shares a binding site with SAG. Its functional activity was validated in a range of cell-based assays, where compound **6** consistently demonstrated potency comparable to, and in many cases greater than, established SMO antagonists.

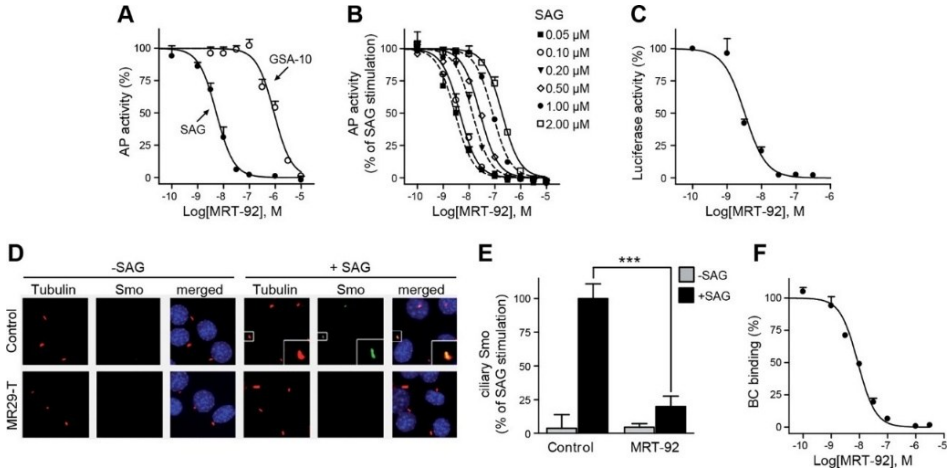

Figure 38. Characterization of **6** in biological assays. **a-c)** Activity of **6** on SAG (0.1mM) or GSA-10 (1 mM) induced differentiation of C3H10T1/2; **d, e)** NIH3T3 cells untreated or treated with SAG (1 mM) alone or in the presence of **6** (0.3 mM) were stained with antibodies against endogenous Smo (green), acetylated tubulin (red), and DAPI (blue); **f)** Inhibition of BC (5 nM) binding to HEK-hSMO cells in presence of increasing concentrations of **6** was visualized using fluorescence microscopy in a representative field.[374]

Mechanistic studies have provided further elucidation on the mode of action of compound **6**. In cell models, **6** effectively prevented the ciliary translocation of SMO triggered by SAG stimulation (**Figure 38d-e**). Docking simulations predicted that **6** occupies the entire 7TM cavity, from the upper ECL to the cytoplasmic-proximal region, thereby exhibiting features of both type I and type II antagonists (**Figure 39a**). The compound was shown to establish three principal anchoring interactions:

- aromatic and hydrophobic contacts between the trimethoxyphenyl group and the upper ECD/ECL3;
- a hydrogen-bonding network involving the central acylguanidine and amide moieties with polar residues in the extracellular region of the cavity;
- extensive hydrophobic and aromatic interactions within the narrow, deep portion of the cavity.

The results of the mutagenesis experiments confirmed the involvement of residues from both subpockets (**Figure 39b**). It is of particular significance that this dual-site engagement confers activity against the clinically significant SMO^{D473H} mutation, a well-known mechanism of resistance to vismodegib and sonidegib, as demonstrated by preserved radioligand binding and inhibitory potency.

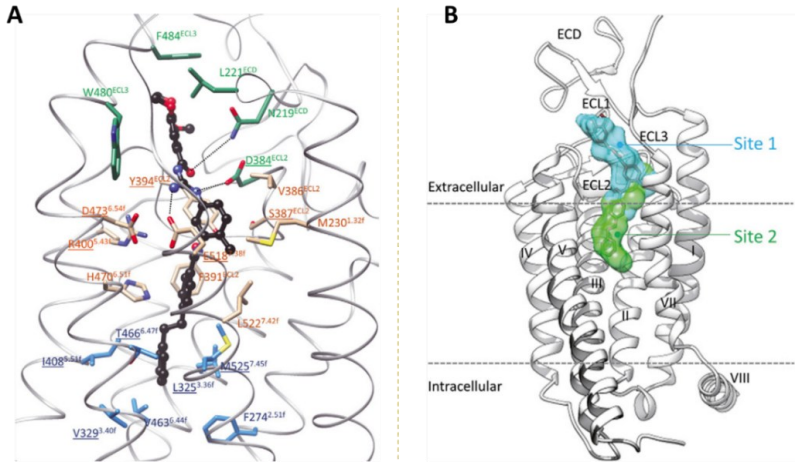

Figure 39. a) Close-up of the proposed binding mode of **6** to hSMO. The ligand is displayed in ball and sticks using the following color coding: carbon, black; nitrogen, blue, oxygen, red. SMO side chains (carbon atoms) are colored according to their contribution to bind only LY2940680 (green), only SANT-1 (cyan), or both antagonists (tan). **b)** Schematic representation of **6** binding to hSMO. Site 1 (cyan) is occupied by the agonists (SAG) and antagonists (LY2940680; Anta XV, cyclopamine, GDC-0449), whereas site 2 (green) is only used by the antagonist SANT-1. Compound **6** occupies both sites simultaneously.[374]

On the basis of these structural and pharmacological findings, compound **6** was investigated in melanoma models.[377] This demonstrated that SMO antagonism exerts profound effects on tumor cell viability and plasticity. It was demonstrated that compound **6** inhibits GLI1 expression and reduces melanoma cell proliferation in a dose-dependent manner (**Figure 40a**). Mechanistic investigations revealed that **6** induced replication stress and DNA damage, activating the ATR/CHK1 checkpoint pathway, leading to G_2/M arrest, multipolar spindle formation, and ultimately mitotic catastrophe (**Figure 40b**). It is noteworthy that the impact of these agent was not limited to bulk tumor cells; it also impeded the growth of melanoma stem-like cell populations by reducing sphere formation, self-renewal potential, and expression of stemness markers.

(a)

Cell lines	Compound 6 IC_{50} (nM)
A375	299 ± 0.05
SSM2c	393 ± 0.1
MeWo	608 ± 0.05

(b)

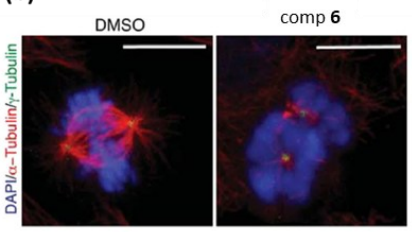

Figure 40. a) IC_{50} values for each cell line. **b)** Representative confocal microscopy images of A375 cells counted as normal mitosis (DMSO) or mitotic catastrophe after treatment with compound **6**.[377]

In vivo, systemic administration of compound **6** led to a substantial reduction in A375 xenograft growth without any effect on body weight (**Figure 41**). Furthermore, analysis of tumor samples from treated mice revealed a significant decrease in GLI1 levels. Experiments involving RNA interference (RNAi) to silence SMO abrogated these effects, thereby establishing the target specificity. Collectively, these findings expanded the relevance of SMO inhibition from developmental models to aggressive solid tumors, while highlighting the capacity of **6** to target both proliferating tumor cells and therapy-resistant stem-like compartments.

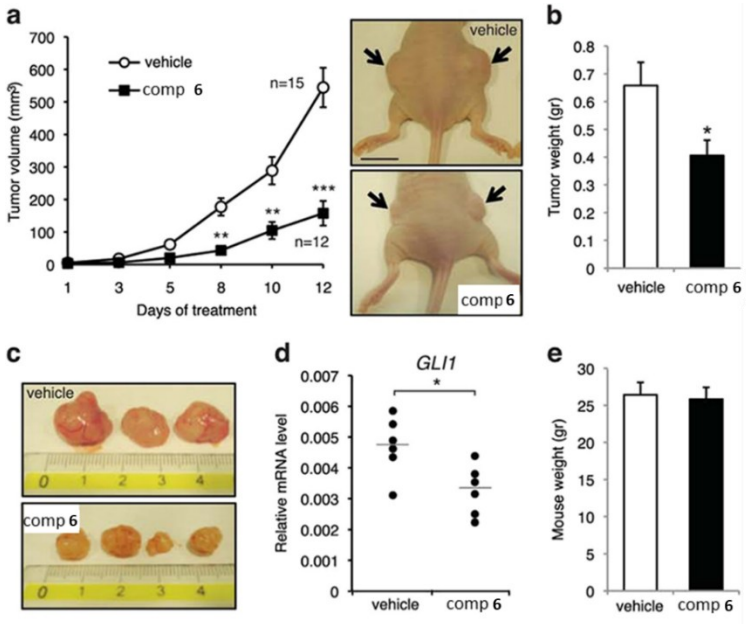

Figure 41. a) *In vivo* tumor growth of A375 melanoma cells subcutaneously injected into athymic nude mice. Animals were treated at tumor appearance with vehicle or compound **6** (15 mg/kg). After 12 days of treatment, mice were sacrificed. Scale bar = 10 mm; **b)** Tumor weight in mice treated with vehicle or compound **6**; **c)** Representative tumor size in mice treated with vehicle or compound **6**; **d)** qPCR of GLI1 mRNA in melanoma xenografts in mice treated with vehicle or compound **6**; **e)** Mice body weight at the end of the treatment.[377]

The translational potential of this chemical class was subsequently tested in Hh-dependent colorectal cancer, where pathway activity contributes to tumor maintenance and progression.[378] Compound **6** again emerged as the most promising candidate, combining potent inhibition of GLI1 transcription with favourable drug-like characteristics, including absence of P-glycoprotein interaction, acceptable permeability in Caco-2 assays, and high selectivity across a 45-kinase panel. *In vivo*, oral administration of compound **5** (200 mg/kg, 5 days/week for two weeks) resulted in a significant 48% reduction in LS180 xenograft tumor volume without any weight loss or overt toxicity, while also downregulating Hh pathway markers in tumor tissues.

In vitro ADME parameters, and *in vivo* metabolism and PK of compound **6** were also investigated.[378] Compound **6** displays a favorable interaction profile in terms of P-glycoprotein and intestinal absorption. In the P-gp ATPase assay, it showed no detectable interaction with the transporter, indicating that it is unlikely to be either a substrate or an inhibitor of P-gp, which minimizes the risk of efflux-related poor bioavailability or drug-drug interactions. Consistently, in the Caco-2 permeability assay, its influx/efflux (I/E) ratio was close to 1, further suggesting passive diffusion across intestinal epithelium without significant transporter involvement and a low risk of compromised oral absorption. Regarding CYP450 interactions, compound **6** interfered with CYP1A2, CYP3A4, CYP2C9, and CYP2C19 activities, but not CYP2D6. The interference was variable and not always concentration-dependent, which indicates that metabolic interactions with certain CYP isoforms may occur and should be considered in drug-drug interaction assessments. In terms of metabolic stability, compound **6** showed moderate metabolic degradation in murine plasma at 37 °C. In mouse hepatocytes, it exhibited a relatively high intrinsic clearance (CL_{int} = 756 mL/min/kg) and a short half-life of about 8 minutes, suggesting rapid metabolism in the liver. The *in vivo* PK profile in mice following a single oral dose of 200 mg/kg showed that compound **6** was quantifiable in plasma up to 24 hours, with a distinct absorption profile characterized by multiple peaks, the highest observed at 4 hours post-dose. Its plasma elimination half-life was approximately 2.5 hours. However, it exhibited a higher apparent clearance (CL/F = 1460 mL/h/kg) compared to other analogues tested, which translated into lower systemic exposure overall.[378]

1.3.5. Inhibiting GLI

As discussed above, SMO is the primary target of Hh pathway inhibition. However, SMO inhibitors are ineffective in controlling tumors that rely on the non-canonical activation of the zinc-finger transcription factors GLI1 and GLI2.

Furthermore, the direct targeting of GLI proteins through the employment of small molecules emerges as a promising strategy to overcome the drug resistance that is often associated with SMO mutations. Despite this potential, only a limited number of GLI inhibitors have been identified (**Figure 42**), and none possess the PK profile required for clinical development, largely due to poor metabolic stability, low aqueous solubility, and high hydrophobicity.

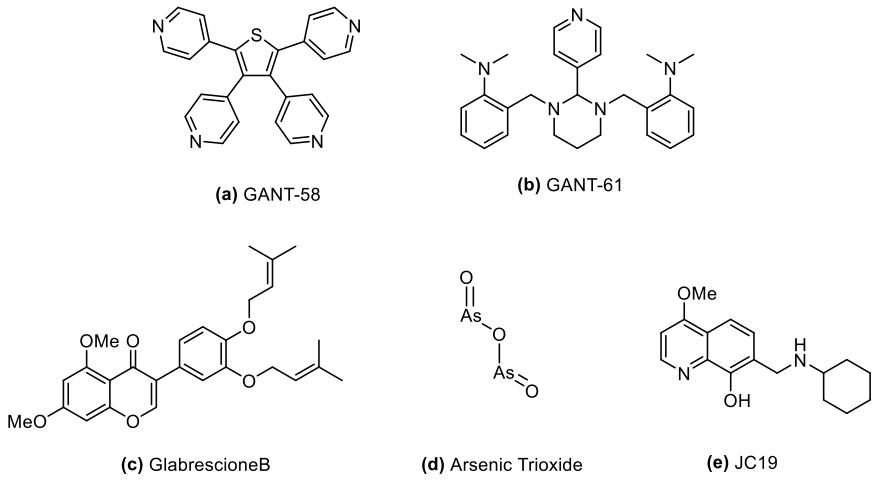

Figure 42. Structures of GLI inhibitors. **a)** GANT-58; **b)** GANT-61; **c)** GlaB; **d)** ATO; **e)** JC19.

GANTs

GLI antagonists, known as GANTs, were first identified at the National Cancer Institute in a GLI-luciferase reporter assay performed in HEK293 cells.[289] These compounds have been shown to interfere with the nuclear translocation of GLI, thereby preventing its binding to DNA. It has been demonstrated that both GANT-58 (**Figure 42a**) and GANT-61 (**Figure 42b**) inhibit GLI-mediated gene activation; however, GANT-61 is more specific for GLI proteins and has proved to be more effective in reducing the DNA-binding activity of GLI1 and GLI2. Several studies have demonstrated that GANT-61 exerts its antineoplastic effects by inhibiting GLI1 and GLI2 in various cancer cell lines, including those derived from rhabdomyosarcoma, osteosarcoma, neuroblastoma, and ovarian cancer.[379–381] In a mouse xenograft model of human prostate cancer, GANT-61 reduced tumor growth and proliferation and strongly downregulated PTCH1 mRNA expression. Despite these encouraging findings, both GANT-61 and GANT-58 exhibit suboptimal

drug-like properties. GANT-61 is only moderately potent, with micromolar IC_{50} values, and undergoes rapid hydrolysis under physiological conditions, producing an inactive aldehyde and an active diamine metabolite.[382] This instability, when combined with its low aqueous solubility, has thus far precluded its advancement, and no clinical trials have been initiated. GANT-58 is less potent than GANT-61. Furthermore, the extreme lipophilicity of GANT-58 results in very poor solubility and low bioavailability. Indeed, *in vivo* studies demonstrated that unformulated GANT-58 was essentially inactive, and therapeutic effects were only observed when it was encapsulated in polymeric nanoparticles.[383]

Glabrescione B (GlaB)

GlaB (**Figure 42c**), a natural isoflavone that displays selective antagonism against GLI1, also exhibits significant limitations. It is evident that GlaB, in its native state, is highly insoluble in water, unstable in plasma, and exhibits low oral bioavailability. In order to address these issues, recent preclinical studies have formulated GlaB in self-assembling mPEG-cholane micelles, thereby improving its solubility and stability.[384] In this form, GlaB demonstrated high drug loading capacity, extended circulation time, and minimal off-target toxicity. It was found that micelle-encapsulated GlaB was able to successfully permeate the blood-brain barrier, thereby significantly suppressing Hh-driven medulloblastoma growth in murine models. These results confirm the potential of GlaB as a GLI inhibitor but also underline that unmodified GlaB is not suitable for clinical use due to its poor bioavailability.

Arsenic Trioxide (ATO)

ATO (**Figure 42d**), an FDA-approved pharmaceutical agent, has been shown to directly inhibit the GLI1 and GLI2 transcription factors, and is clinically used in the treatment of acute promyelocytic leukaemia (APL).[385] This compound has been shown to bind GLI1 and GLI2, thereby blocking their activity and reducing the expression of Hh target genes.[386] It has also been demonstrated that this process reduces GLI2 stability, thereby preventing its accumulation in the primary cilium following Hh activation.[387] In preclinical models, ATO increased apoptosis, reduced tumor cell growth, and downregulated Hh target genes across a wide spectrum of malignancies, including osteosarcoma, APL, malignant pleural mesothelioma, rhabdomyosarcoma, prostate cancer, colon cancer, and pancreatic cancer stem cells. Noteworthy, ATO demonstrated the ability to target both tumor epithelial cells and tumor-initiating cells, thus highlighting its therapeutic relevance.[388] However, the systemic administration of ATO is associated with significant

drawbacks. The compound exhibits extensive tissue distribution and is cleared slowly, leading to prolonged exposure even at low doses.[389] From a clinical perspective, this results in significant toxicities, including leukocytosis, QT-interval prolongation, elevation of hepatic enzymes, and the potentially fatal "differentiation syndrome" observed in APL therapy.[389] Furthermore, ATO is a simple inorganic compound with limited aqueous solubility, and the higher doses required to inhibit solid tumors cannot be tolerated in patients.[390] These PK and toxicological issues have restricted the use of ATO, limiting its applicability as a GLI inhibitor in solid tumors.

1.3.5.1. JC19

Alongside the development of MRTs SMO inhibitors, significant effort have been directed by our research group towards the identification of compounds that efficiently target GLI transcription factors. Starting from known GLI1 inhibitors GlaB and vismione E (**Figure 43a**), a pharmacophore-based virtual screening approach was applied to databases of commercially available molecules in order to identify novel GLI1 modulators.[391] The resulting five-feature pharmacophore (**Figure 43b**) consisted of two hydrophobic groups, two hydrogen bond acceptors, and one aromatic ring, which corresponded to the two terminal methyl groups of the *m*-prenyl side chain of GlaB and the 7-prenyl group of vismione E, the oxygen atoms at positions 4 and 5 of GlaB and positions 8 and 9 of vismione E, as well as the condensed phenyl ring of GlaB and the central phenyl ring of vismione E, respectively. This screening process led to the identification of negative GLI1 modulators belonging to the thiophene, pyrazolo-pyrimidine, and quinoline derivative classes, that populated databases of commercially available compounds.[391]

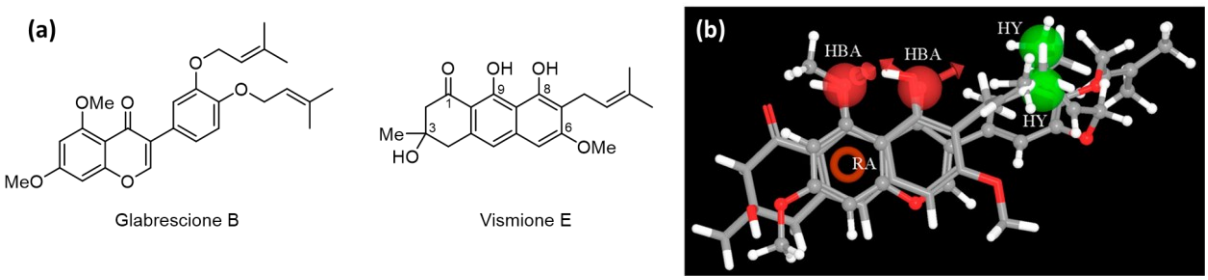

Figure 43. a) Chemical structure of GlaB and vismione E used to generate the pharmacophore model for GLI1 inhibitors; **b)** Graphical representation of the five-feature pharmacophoric model for compounds affecting GLI1 protein level. Green spheres are hydrophobic regions (HY); red spheres are hydrogen bond acceptor groups (HBA); the red ring is an aromatic ring feature (RA).[391]

Among these hits, compound **10** (**Figure 44**), a commercially available quinoline, was prioritised and used as the starting point for the synthesis of a focused library. This library was designed to improve the biological profile and establish SARs.[392] 8-hydroxyquinoline derivatives revealed several significant data. Antiproliferative activity appeared to be only modestly dependent on substituents and substitution patterns on the phenyl ring of the C7 benzyl moiety, with IC_{50} values in the low micromolar or submicromolar range. Conversely, the capacity to modulate GLI1 protein levels was found to be profoundly influenced by these characteristics: unsubstituted compounds or those bearing small substituents such as Cl or Me exhibited a minimal or no effect on GLI1 levels. However, the C7 benzyl moiety was not indispensable for activity, and a simple 5-chloroquinolyl-8-ol (**11** - **Figure 44**) proved inactive. On this basis, 8-hydroxyquinoline SST0776 (**12** - **Figure 44**) and oxazino-quinoline SST0794 (**13** - **Figure 44**) were prioritised for further evaluation as GLI inhibitors.

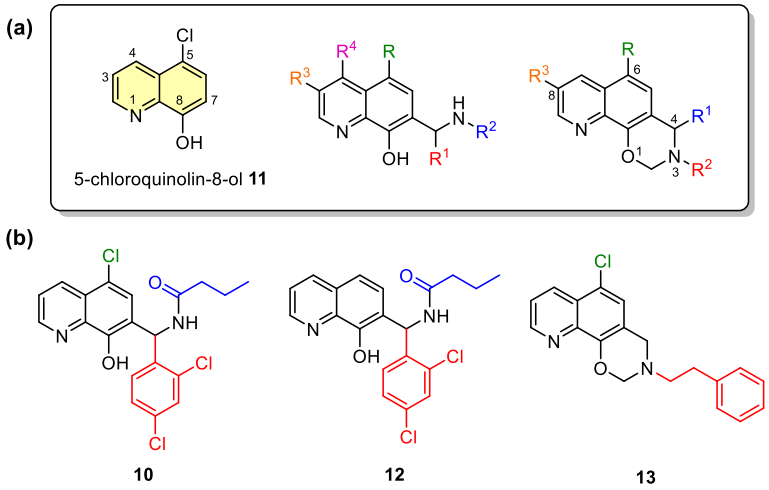

Figure 44. a) General chemical structures of 5-chloroquinolyl-8-ol **11,** and quinoline derivatives; **b)** Structures of compounds **10**, SST0776 **12**, and SST0794 **13**.

Subsequently, a classical hit-to-lead optimization strategy was pursued, reducing scaffold complexity in **13** and removing the chiral center of **12**. This ultimately resulted in the identification of compound JC19 (**14** - **Figure 45**).[393] It is noteworthy that **12**, **13** and **14** exhibited superior activity in comparison to the established GLI inhibitors GANT61 and GlaB. It was demonstrated that all three quinolines were capable of downregulating GLI1 and GLI2 protein levels in a dose-dependent manner in NIH3T3 cells. Furthermore, it was established that **14** was able to reduce both proteins by approximately 80% at 0.5 µM.

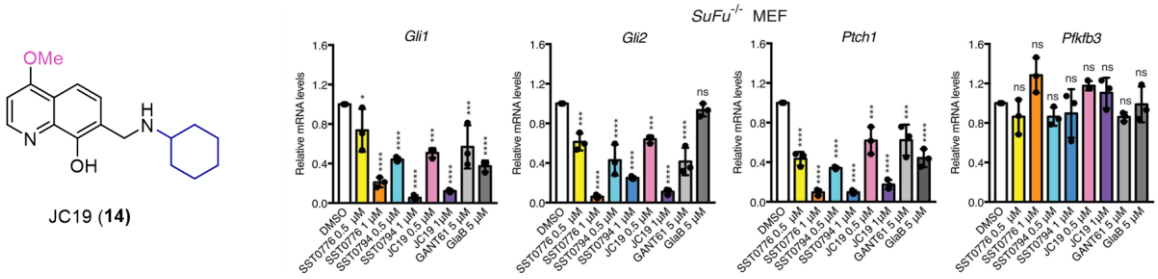

Figure 45. Structure of compound **14** and qPCR of GLI1, GLI2, PTCH1, and Pfkfb3 in SuFu$^{-/-}$ MEFs treated with SST0776, SST0794, and JC19 at 0.5 and 1 µM, or GANT61 and GlaB at 5 µM for 48 h, with cells treated with DMSO equated to 1.[393]

Mechanistic investigations revealed that these quinolines impaired GLI-mediated transcription by disrupting the binding of GLI1 and GLI2 to DNA, as demonstrated by reduced occupancy on the PTCH1 promoter. Furthermore, mithramycin treatment fully abolished their effects on PTCH1 mRNA reduction, supporting a direct role in DNA binding inhibition. Consequently, strong suppression of Hh target gene expression was evident across a wide range of cancer cell lines. The treatment of commercial melanoma cells (A375, MeWo, SK-Mel-5), primary melanoma cells (SSM2c, Me-53), glioblastoma (U87-MG), medulloblastoma (DAOY), breast cancer (MCF7), and intrahepatic cholangiocarcinoma (HuCCT1, CCLP1) over a period of 72 hours resulted in a dose-dependent decrease in cell growth, with IC_{50} values ranging from 0.1 to 1.6 µM. Electrophoretic mobility shift assays (EMSA) and DNA pull-down experiments demonstrated that **14** disrupted GLI1/DNA complex formation. The results of molecular docking studies further corroborated these findings, predicting **14** interaction with GLI1 residues located in zinc fingers ZF4 and ZF5. Site-directed mutagenesis was employed to confirm the involvement of H351, a residue in ZF4 that coordinates zinc, in **14** binding. By targeting the interaction of GLI1 and GLI2 with DNA, **14** effectively inhibited both canonical PTCH/SMO-dependent and non-canonical Hh activation, suppressing oncogenic hyperactivation of the pathway. Evidence from genetic silencing and CRISPR/Cas9 knockout experiments reinforced the specificity of these quinolines: the ablation of GLI1 or GLI2 strongly reduced the effects of the compounds on cell proliferation and Hh target gene expression. This specificity was further confirmed by the absence of effects on the catalytic activity of 77 protein kinases linked to Hh signalling or known to modulate GLI transcription factors via post-translational modifications. Preliminary ADME profiling identified quinoline **14** as the most suitable lead candidate (**Table 5**). In contrast to compounds **12** and **13**, **14** exhibited notable aqueous solubility.

Table 5. ADME parameters of compounds **12**, **13** and **14**.[393]

Cmpd	Aqueous Solubility (µg/mL)		Plasma Stability (%)	PAMPA (10^{-6}cm/sec) (%MR)	Metabolic Stability U(%) ± SD
	H_2O MilliQ	Buffer Solution			
12	0.52 (logS = -5.87)	-	> 98	12.16 (9.59)	98.30 ± 0.07
13	2.95 (logS = -5.04)	-	> 98	15.35 (21.57)	95.69 ± 0.35
14	813.62 (logS = -2.56)	741.23 (logS = -2.59)	> 98	12.98 (17.28)	99.35 ± 0.09

PK studies of **14** revealed a short half-life and high clearance after a single intraperitoneal dose (**Table 6**). However, repeated administration twice daily for 12 days achieved a dose-dependent inhibition of tumor growth, with a 70% reduction in tumor volume at 25 mg/kg. Importantly, no systemic toxicity was observed, and no hepatic accumulation occurred.

Table 6. PK parameter of compound **14.**[393]

Parameters	Unit	15/mg/kg	25 mg/kg
$t_{1/2}$	h	6.479	4.353
T_{max}	h	0.083	0.083
C_{max}	µg/mL	0.890	1.570
$AUC_{0\text{-}24h}$	µg/mL*h	0.548	1.228
$AUC_{0\text{-}inf}$	µg/mL*h	0.586	1.324
$MRT_{o\text{-}inf}$	h	5.004	5.983
V_Z/F	(mg/kg)/(µg/mL)	239.142	118.518
Cl/F	(mg/kg)/(µg/mL)/h	25.583	18.869

In vivo treatment resulted in a dose-dependent reduction in GLI1 mRNA levels in melanoma xenografts, thereby confirming GLI1 downregulation as a biomarker of response (**Figure 46**). In conclusion, the hit-to-lead design and synthesis of the quinoline derivative **14**, alongside the biological characterisation of three potent quinolines, identified **14** as a highly active GLI1/GLI2 inhibitor. The activity of the compound under investigation extends to both canonical and non-canonical Hh activation, and it effectively counteracts pathway hyperactivation. In addition, it demonstrates favourable solubility, strong *in vivo* efficacy, and a promising safety profile.

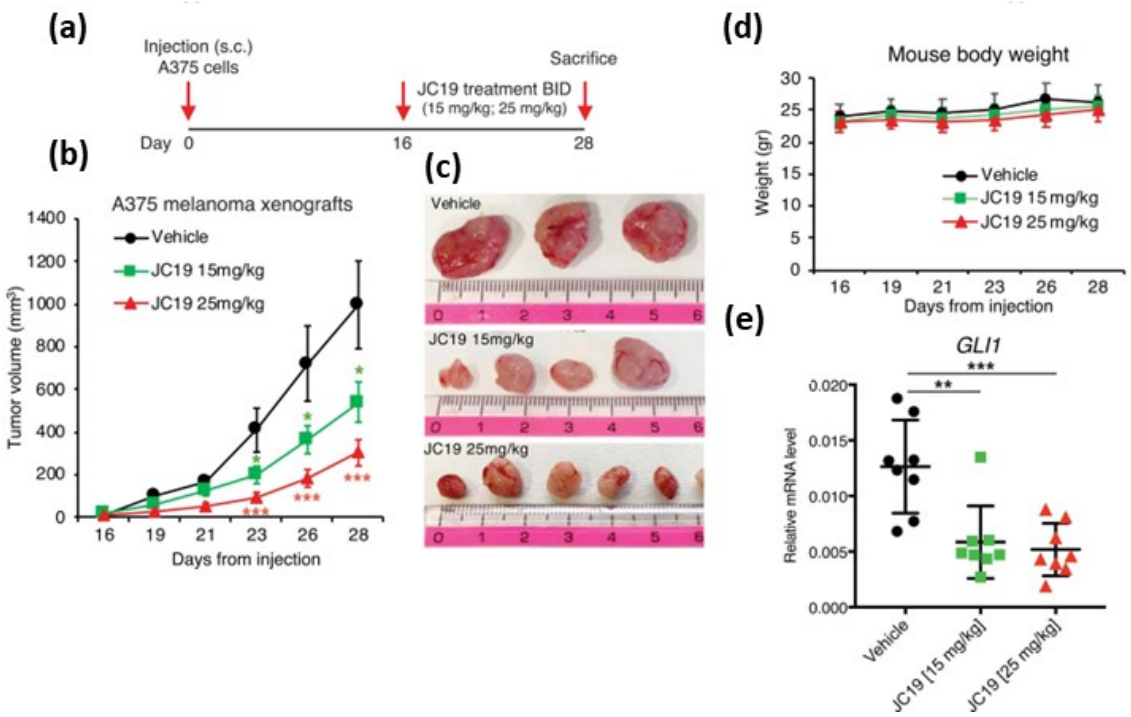

Figure 46. a) Experiment timeline of the *in vivo* treatment; **b)** *In vivo* growth of A375 melanoma cells subcutaneously injected in athymic nude mice; **c)** Representative images of tumors at the sacrifice; **d)** Mice body weight during treatment; **e)** qPCR of GLI*1* in melanoma xenografts treated with vehicle, JC19 15 mg/kg or 25 mg/kg for 72 h. [393]

Furthermore, a recent work by our research group revealed its ability to overcome 5-Fluorouracil (5-FU) chemoresistance in colorectal cancer (CRC) by targeting a newly identified GLI1-PHGDH positive feedback loop.[394] The study found that combining JC19 with 5-FU produced a strong synergistic effect, particularly in CRC models that overexpress PHGDH, significantly enhancing the tumor cells' sensitivity to the chemotherapy. This combination therapy was validated *in vivo* using mouse xenografts, where the JC19/5-FU regimen proved superior to monotherapy in inhibiting tumor growth, reducing cell proliferation, and downregulating the expression of PHGDH and survival proteins like c-Myc. This research thus validates targeting the PHGDH-HH axis with JC19 as a promising strategy to combat 5-FU drug resistance.

1.4. PROTIDE TECHNOLOGY

Nucleoside analogues (NAs) are a crucial class of drugs used to treat cancer and viral infections.[395] To exert their therapeutic effect, NAs must enter the cell and undergo sequential phosphorylation by host kinases to their active triphosphorylated form. However, this activation pathway has several limitations. The first phosphorylation is often inefficient due to structural differences between the NA and natural nucleosides. Furthermore, NAs are typically polar molecules, which results in poor intestinal permeability, low oral bioavailability, and inefficient passive diffusion across cell membranes.[396]

The ProTide technology, developed by McGuigan, Mehellou, Balzarini, and co-workers, was designed to overcome these issues.[397] This prodrug strategy "masks" the first phosphate group of the NA monophosphate with an amino acid moiety and an aryl ester. This neutral, more lipophilic construct allows the ProTide to efficiently cross the cell membrane via passive diffusion. Once inside, the masks are enzymatically cleaved to release the nucleoside monophosphate directly. This approach bypasses the problematic first phosphorylation step, allowing for rapid conversion to the active triphosphate metabolite, which can then inhibit intracellular enzymes or be incorporated into nucleic acid chains to terminate elongation and promote apoptosis.[398]

The intracellular activation cascade begins with the cleavage of the amino acid's ester group by an intracellular esterase, such as Cathepsin A, which generates a free carboxylate (**Scheme 12**). This carboxylate then performs a nucleophilic attack on the central phosphorus atom, displacing the aryl group and forming a highly unstable five-membered anhydride intermediate. This ring is rapidly opened by a water molecule (attacking either the carbonyl carbon or the phosphorus atom) to generate a phosphoramidate metabolite. The final step is the cleavage of this metabolite's P–N bond by the phosphoramidase HINT1 (histidine triad nucleotide binding protein 1), releasing the active nucleoside monophosphate. [398,399] ADCs charged with ProTide-based scaffolds have never been reported, and the combination of ProTide activation pathway and the selectivity of the monoclonal antibody could allow to overcome the limitations of nucleoside analogues and phosphorylated drugs in general, avoiding off-target effects.

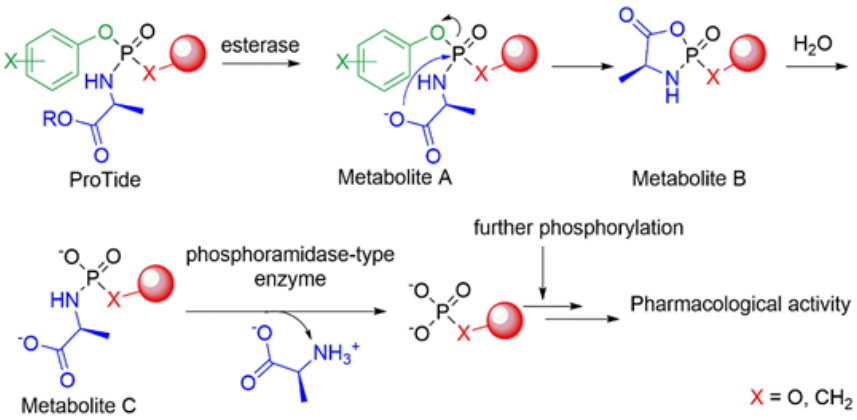

Scheme 12. General mechanism of the ProTide activation.

1.5. AIM OF THIS RESEARCH WORK

The continuous search for more selective and tolerable cancer treatments has positioned ADCs at the forefront of pharmaceutical innovation. This therapeutic technology, which harnesses the specificity of mAbs to deliver a pharmacological agent directly to the tumor site, is evolving beyond the use of only highly potent cytotoxic payloads, opening the door to a broader spectrum of therapeutic mechanisms. In this context, attention has shifted towards targeting key oncogenic signalling pathways, such as the Hedgehog signalling pathway, whose aberrant activation contributes to the progression of various malignancies and makes it a critical therapeutic target. Our research group has successfully developed several Hh pathway modulators, including the potent SMO inhibitors such as compound **6** and the GLI inhibitor **14**. Compound **6** is particularly promising because of its sub-nanomolar activity in different tumor cell lines and a unique dual-site binding mechanism that mantains its efficacy in mutant strains commonly observed with vismodegib. However, its full therapeutic potential is constrained by a suboptimal PK profile, leading to rapid systemic clearance, thereby limiting its clinical utility. Consequently, the conjugation of **6** to a selective mAb through an ADC strategy represents a rational and necessary approach to circumvent these liabilities. Bioconjugation is expected to enable targeted delivery, increase plasma half-life, and enhance its local concentration at the tumor site.

Building on this rationale, the objectives of this research work aim to advance both the Hh inhibitors development and the ADC technology platform:

1. to enhance the therapeutic potential of our in-house developed Hh pathway inhibitors by integrating them into the ADC platform.

2. to systematically explore and optimize novel bioconjugation methodologies, applying these advancements not only to the Hh inhibitors but also to various linker-payload systems, directed at different cellular targets.

3. To better understand the dual role of the Hh pathway by continuing the study of the agonist activity of previously developed compounds (GSA-10, compound **1**, and compound **2**) and evaluating their osteogenic capabilities in new, relevant cell models, thus exploring the potential of these compounds in regenerative medicine.

1.5.1. Synthesis of new ADCs charged with Hh inhibitors

The primary objective of this research is the design, synthesis, and comprehensive characterization of novel ADCs utilizing our Hh pathway inhibitors such as **6** and **14**, as the payloads (**Figure 47**). This effort is driven by the need to overcome the PK limitations of the free compound through a targeted delivery approach. The synthetic strategy involves several critical steps: first, the chemical modification of the Hh inhibitor to introduce a suitable linker-attachment handle without compromising its intrinsic pharmacological activity. Second, the careful selection and synthesis of a cleavable and non-cleavable linker system, a decisive factor affecting the stability of the ADC in circulation and efficient payload release within the tumor microenvironment or lysosome. Finally, the bioconjugation of the activated linker-payload moiety to a selected mAb. The resulting ADCs will be characterized for their DAR and subjected to *in vitro* and *in vivo* studies to evaluate their stability, targeted cytotoxicity, mechanism of action, and therapeutic index compared to the unconjugated inhibitor. This project aims to validate the hypothesis that the ADC format can "rescue" potent inhibitors with suboptimal PK profiles, thereby unlocking their full therapeutic potential in oncology.

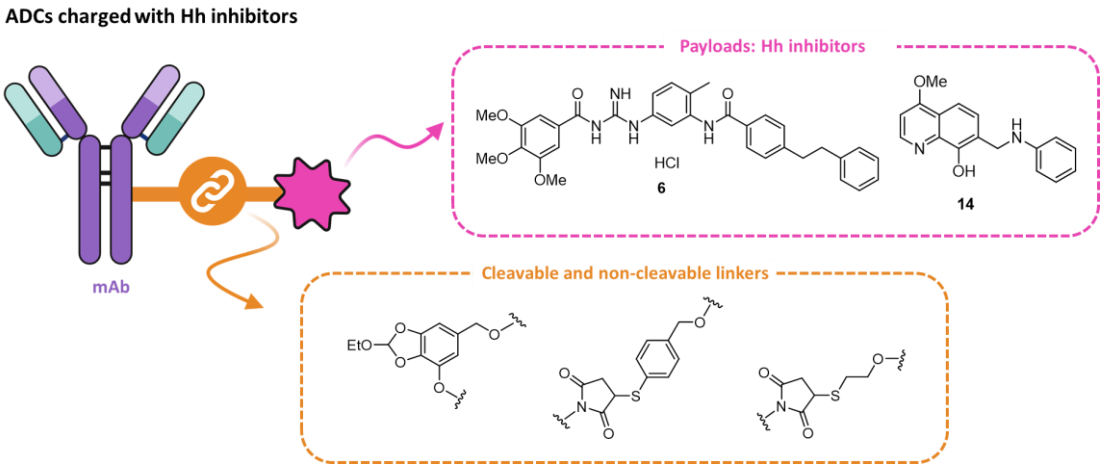

Figure 47. Graphical representation of the proposed ADCs charged with Hh antagonists.

1.5.2. Exploration and development of bioconjugation methodologies

Parallel to the specific synthesis of the Hh-inhibitor ADCs, a core aim of this work is the exploration and advancement of general bioconjugation methodologies. This objective implies the employment chemoselective ligation strategies (e.g., click chemistry, strained alkyne cycloadditions, or bioorthogonal reactions), innovative linker-payload systems and implementation of robust analysis techniques (**Figure 48**).

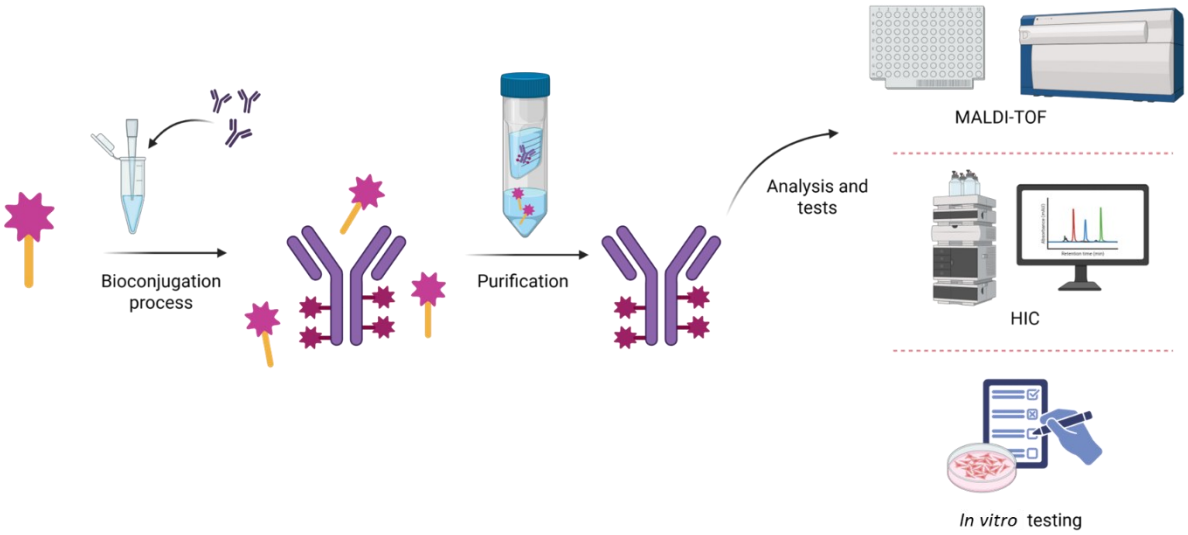

Figure 48. General steps for the development of an ADC. Created with Biorender.

1.5.3. Synthesis and evaluation of Hh agonists for osteogenic applications

Finally, leveraging our research group's established expertise in Hh pathway modulation, a distinct yet related objective is the continuation and expansion of studies focusing on the agonist activity of selected small molecules. The Hh pathway is not solely implicated in cancer; its controlled activation plays a crucial and fundamental role in tissue homeostasis, notably in bone morphogenesis, repair, and regeneration. Specifically, compounds such as GSA-10, compound **1**, and compound **2**, previously developed as dual Hh pathway modulators, have shown promise for their agonist activity on the pathway. This objective will focus on: carrying out an efficient synthesis of these agonists, followed by the in-depth biological evaluation of their osteogenic capacity (**Figure 49**). New cellular models of bone differentiation will be employed (e.g., mesenchymal stem cells or specific osteoblast lines) to precisely quantify their ability to induce differentiation markers (e.g., Alkaline Phosphatase, collagen synthesis) and promote bone formation *in vitro*. This line of investigation seeks to evaluate the group's chemical library for applications in regenerative medicine, providing a valuable diversification of the research beyond oncology.

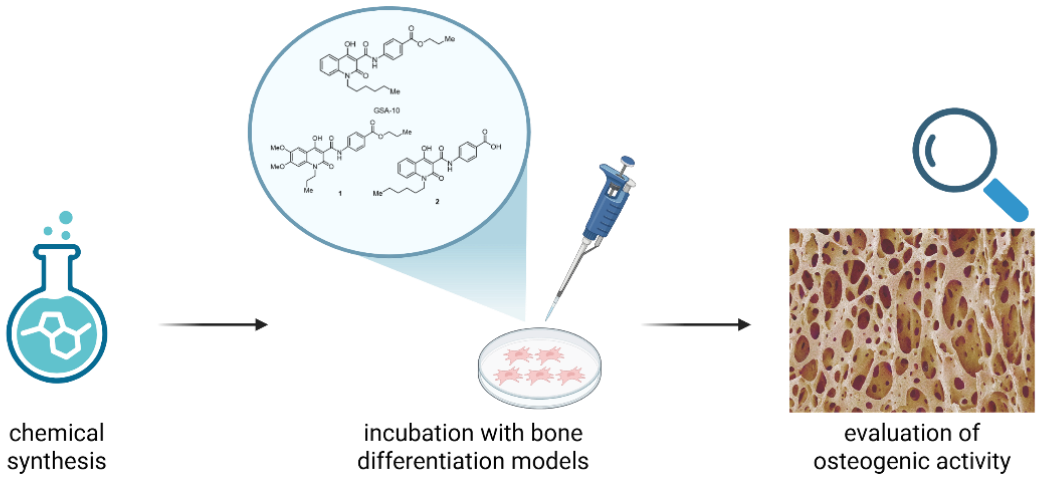

Figure 49. General steps for the synthesis and evaluation of Hh agonists.

CHAPTER 2. RESULTS AND DISCUSSION

2.1. SYNTHESIS OF NEW ADCs CHARGED WITH Hh INHIBITORS

2.1.1. Design of ADCs for the first bioconjugation strategy

For the bioconjugation of Hh inhibitors, two different linkers were selected, both allowing the bioconjugation with Lys residues of Cetuximab (**Figure 50**): i) A non-cleavable linker inspired by conventional MCC and MC linkers combined with a self-immolative spacer (**Figure 50a**); ii) The HMPO linker, a cleavable system previously developed by our research group (**Figure 50b**).[80]

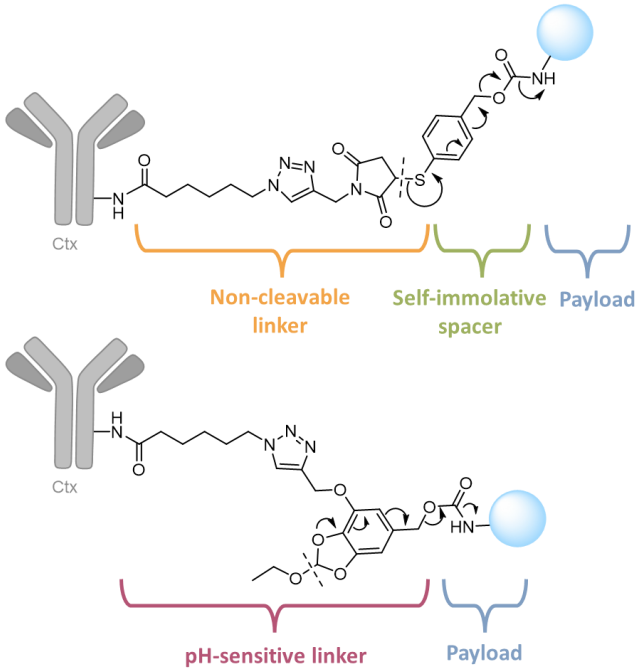

Figure 50. General structure of the proposed ADCs using two different linkers, **a)** non-cleavable linker, **b)** HMPO linker.

2.1.1.1. Definition of connection sites for the introduction of linkers

Our initial efforts for the synthesis of ADCs charged with in-house developed Hh inhibitors were primarily focused on the potent SMO inhibitor compound **6** (**Figure 51a**). A fundamental requirement in ADC design is that the payload must bear a functional handle suitable for linker connection, and for the release of the payload in its active form. Since the core structure of **6** lacked such a moiety, the original synthetic route was strategically modified to incorporate a self-

immolative PABA-like spacer containing an anilinic group onto the guanidine moiety. As a possible alternative to the introduction of a spacer to make the acylguanidine **6** accessible to the insertion of a linker, a modification of its structure was proposed. The only functionality that could be modified without affecting its inhibitory activity toward SMO was the trimethoxybenzyl moiety. An analogue of **6**, compound **15**, was developed for this purpose (**Figure 51**). As already indicated by previously reported SAR analysis of this class of compounds[373], the replacement of a -OMe group with an -OH moiety in *para* position did not impact in the activity (*in vitro* assay: **6**: A375 IC_{50} = 0.299 ± 0.05 µM, BT474 IC_{50} = 1.0 ± 0.1 µM; **15**: A375 IC_{50} = 1.06 ± 0.6 µM, BT474 IC_{50} = 0.5 ± 0.1 µM).

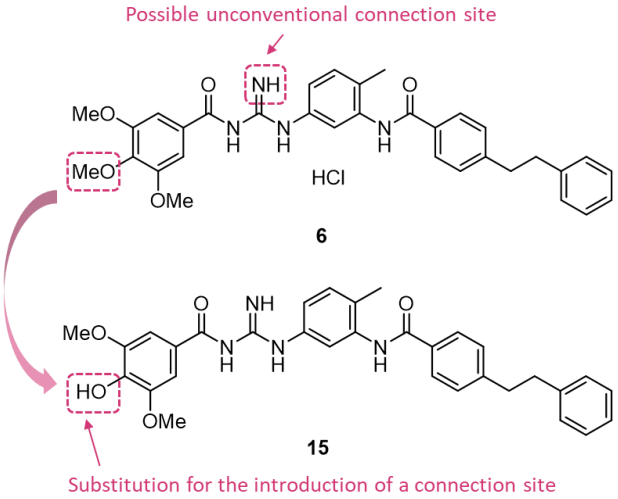

Figure 51. Structure of compound **6** and its analogue **15**.

Our synthetic approach for the functionalization of compound **6** and the introduction of a linker, was guided by the retrosynthetic analysis shown in **Scheme 13**. We first envisioned disconnecting the linker-payload system **16** at its triazole moiety, a cleavage that reveals alkyne **17** and azide **18** as the primary precursors. Intermediate **17** was further simplified: a retrosynthetic cleavage of its carbamate group suggests it could be assembled from linker **19** and the functionalized payload **20**. Payload **20** was retrosynthetically cleaved at its thiourea moiety to provide synthons **21** and **22**. Compound **21** could be obtained from acyl chloride **23** and aniline **24**. Finally, fragment **24** was traced back to the simple starting materials, aniline **25** and carboxylic acid **26**, via disconnection of its central amide bond.

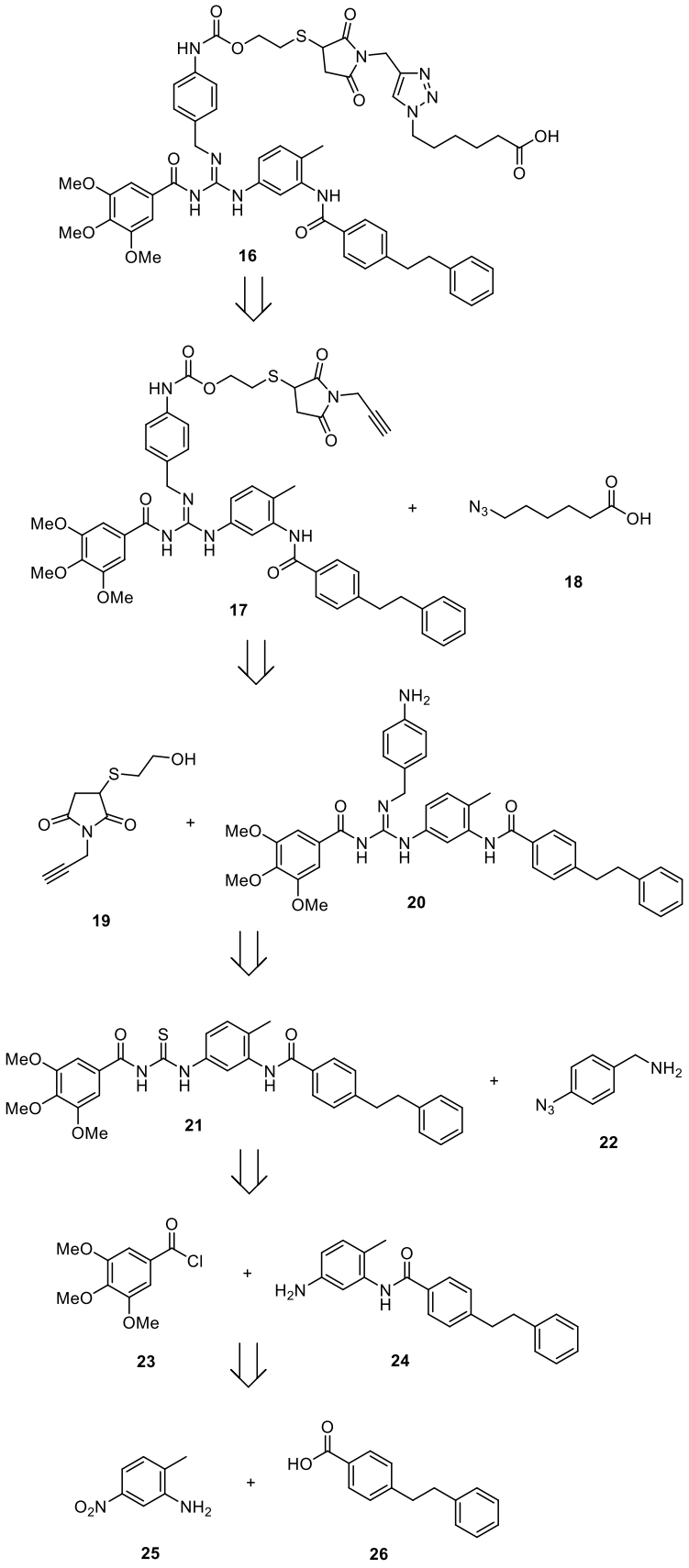

Scheme 13. Retrosynthetic scheme for the preparation of linker-payload system **16**.

Phosphonium salt **28** was prepared in 91% yield by treating benzyl bromide **27** with triphenylphosphine. The resulting salt was subjected to a Wittig reaction with benzaldehyde in the presence of Lithium bis(trimethylsilyl)amide (LiHDMS) to yield the intermediate **29** in 99% yield. The alkene moiety was subsequently reduced with H_2 in presence of Pd/C to obtain compound **26** (83% yield). The carboxylic acid was activated to the corresponding chloride **30** by treatment with thionyl chloride, enabling the formation of an amide bond with aniline **25**, yielding compound **31** (80% yield). The reduction of the nitro group to amine with H_2 in presence of Pd/C furnished compound **24** in 99% yield. This amine was finally treated with commercially available acyl chloride **23** and ammonium thiocyanate to successfully provide the target acylthiourea intermediate **21** in 73% yield (**Scheme 14**).

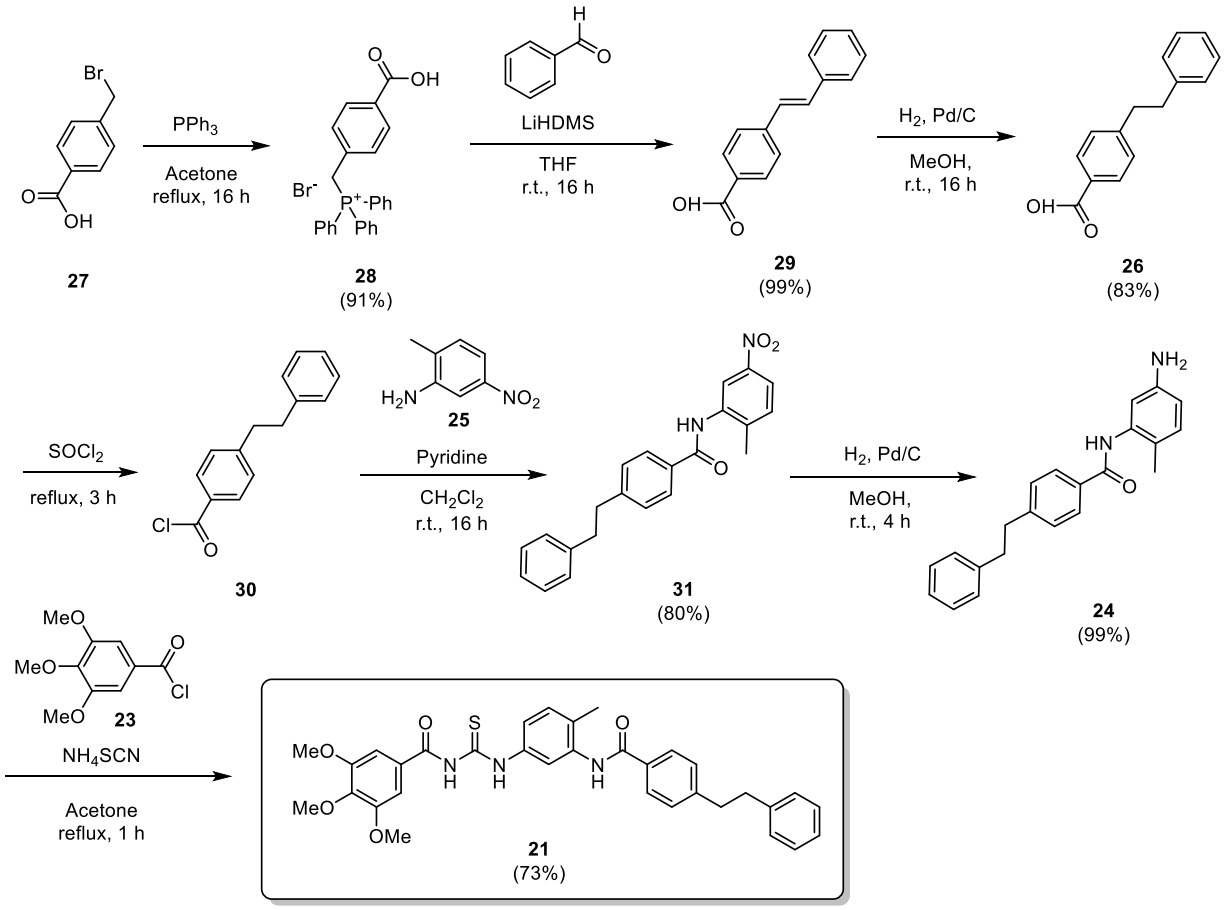

Scheme 14. Synthesis of intermediate **21**.

Meanwhile, the spacer **22** was prepared starting from PABA. The synthesis required the formation of the corresponding diazonium salt using $NaNO_2$, followed by a substitution by NaN_3 providing the azide intermediate **32** in 98% yield (**Scheme 15**). Subsequently, the benzylic alcohol moiety was converted into the corresponding bromide **33** (85% yield) by treatment with PBr_3.

The amine **22** was obtained through a Gabriel reaction: the phthalimide intermediate **34** was obtained in 95% yield and hydrolyzed by treatment with hydrazine, yielding the required benzylamine **22** in 81% yield. The crucial introduction of the spacer onto the payload was then performed by reacting the acylthiourea intermediate **21** with the benzylamine **22** in the presence of $HgCl_2$. This step successfully provided the desired alkylated guanidine, compound **35**, in excellent 91% yield. Finally, the azide group was reduced by treatment with trimethylphosphine, furnishing the final functionalized payload **20** in 60% yield (**Scheme 15**). This successful synthetic sequence allowed us to functionalize an unconventional moiety (the guanidine nitrogen) of the SMO inhibitor, thereby making it suitable for the subsequent connection with properly designed linkers.

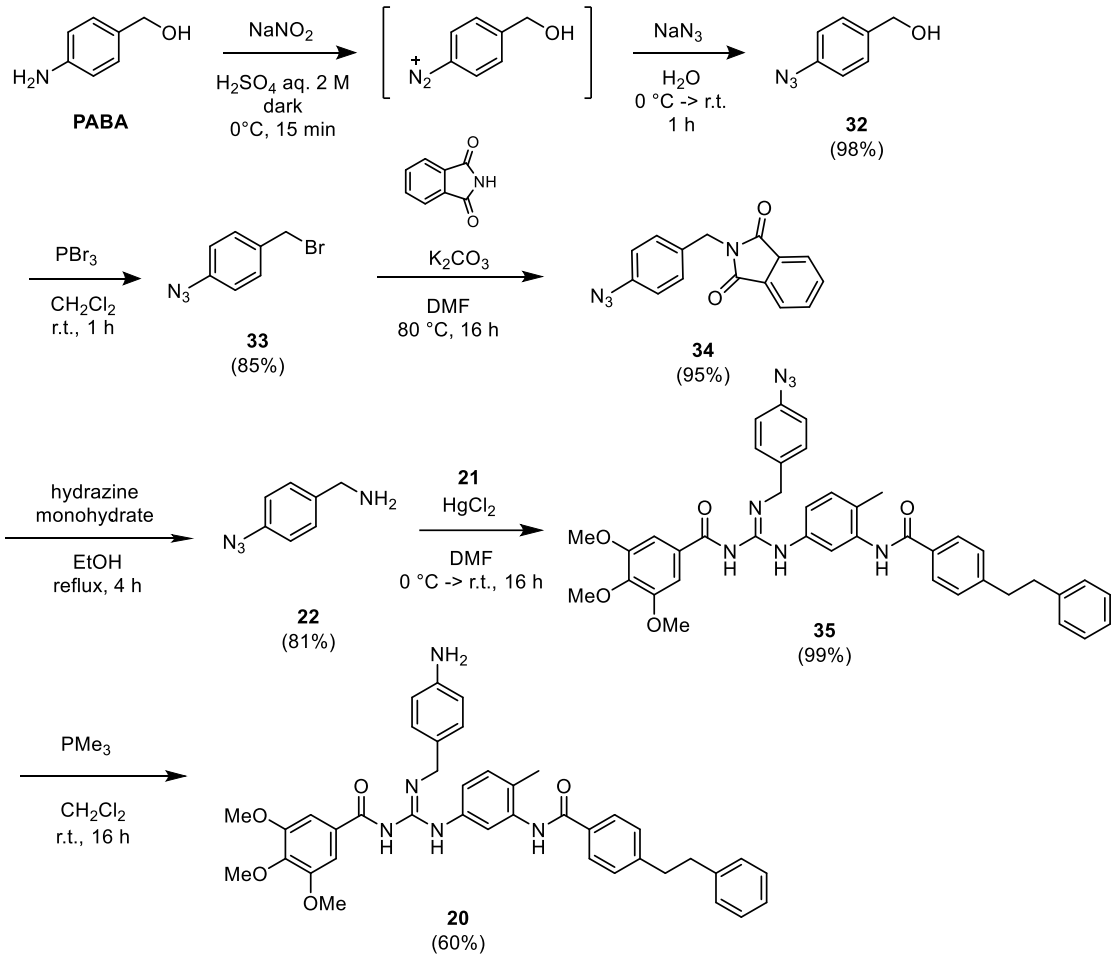

Scheme 15. Synthesis of compound **20**.

2.1.1.2. Connection of compound 20 with a non-cleavable linker

The non-cleavable linker was prepared by reacting maleic anhydride with propargyl amine and acetic anhydride. The desired compound **36** was obtained in 60% yield (**Scheme 16**). Subsequently, the Michael addition of 2-mercaptoethanol provided the intermediate non-cleavable linker **19** in 78% yield. Notably, the 2-mercaptoethanol moiety functions as a self-immolative spacer within the ADC structure, releasing the payload through a cyclization rearrangement once the non-cleavable linker is effectively cleaved *in vivo*.

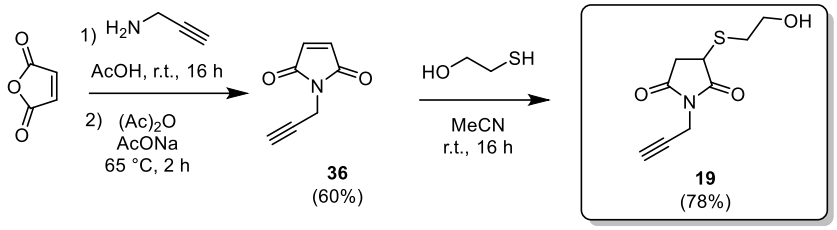

Scheme 16. Preparation of linker **19**.

For the introduction of the payload, the alcohol **19** was activated by treatment with *p*-nitrophenyl chloroformate, converting it into the more reactive carbonate intermediate **37** (**Scheme 17**). This intermediate was treated with **20**, successfully obtaining the linker-payload system **17** in 32% yield over the two steps. As a final step, the introduction of a carboxylic acid group onto the linker was required to enable amide bond formation with the lysine residues of the mAb. A CuAAC reaction was carried out with alkyne **17** and the azido-acid **18**. The final compound, **16**, was successfully synthesized and isolated.

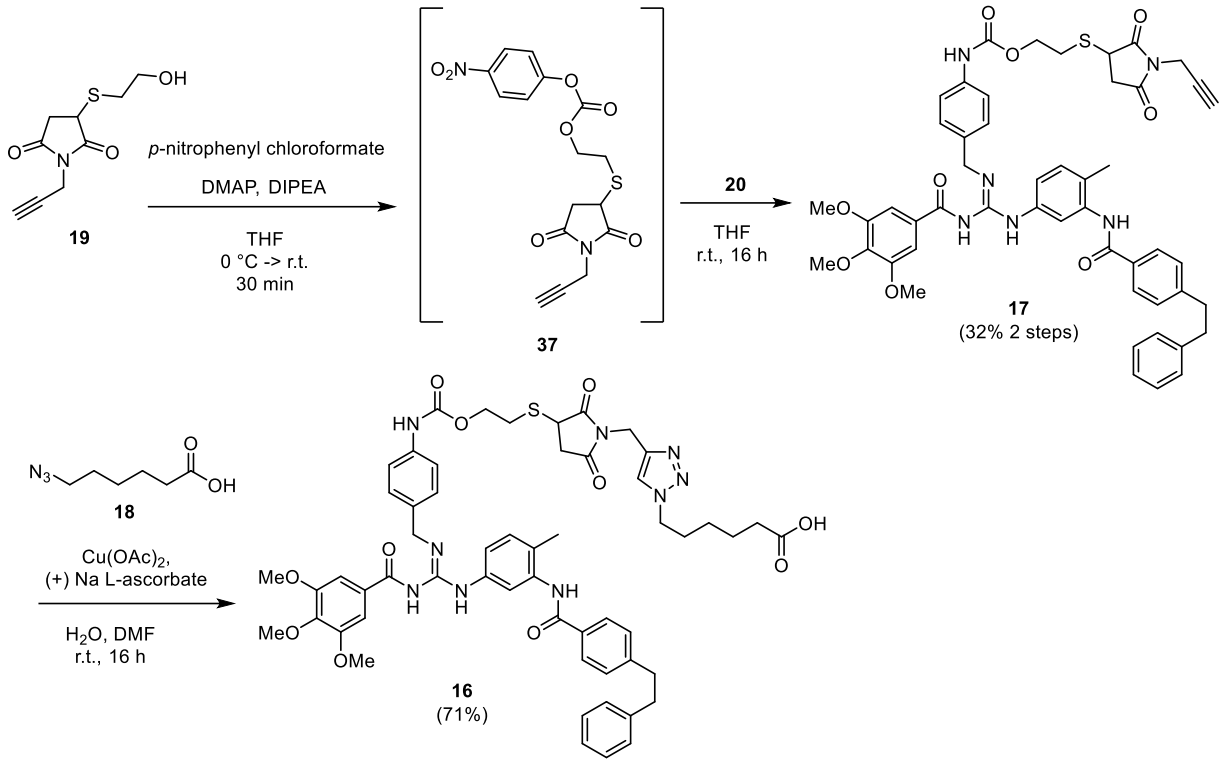

Scheme 17. Synthesis of the linker-payload system **16**.

2.1.1.3. Connection of compound 15 with a non-cleavable linker

A similar non-cleavable linker was applied for the preparation of a linker-payload system charged with **15**. The non-cleavable linker was prepared by Michael addition of 4-mercaptobenzyl alcohol onto the intermediate **36**, successfully yielding the linker-spacer system **38** in 84% yield. The benzyl alcohol moiety of **38** was subsequently converted into the corresponding, highly unstable bromide **39** by treatment with PBr_3. This reactive intermediate **39** was immediately alkylated by **15** under alkaline conditions, affording the desired product **40** in 45% yield. Finally, the terminal alkyne moiety of the system was functionalized by a CuAAC reaction with the azide **18**, thereby providing the final linker-payload system **41** ready for bioconjugation (**Scheme 18**).

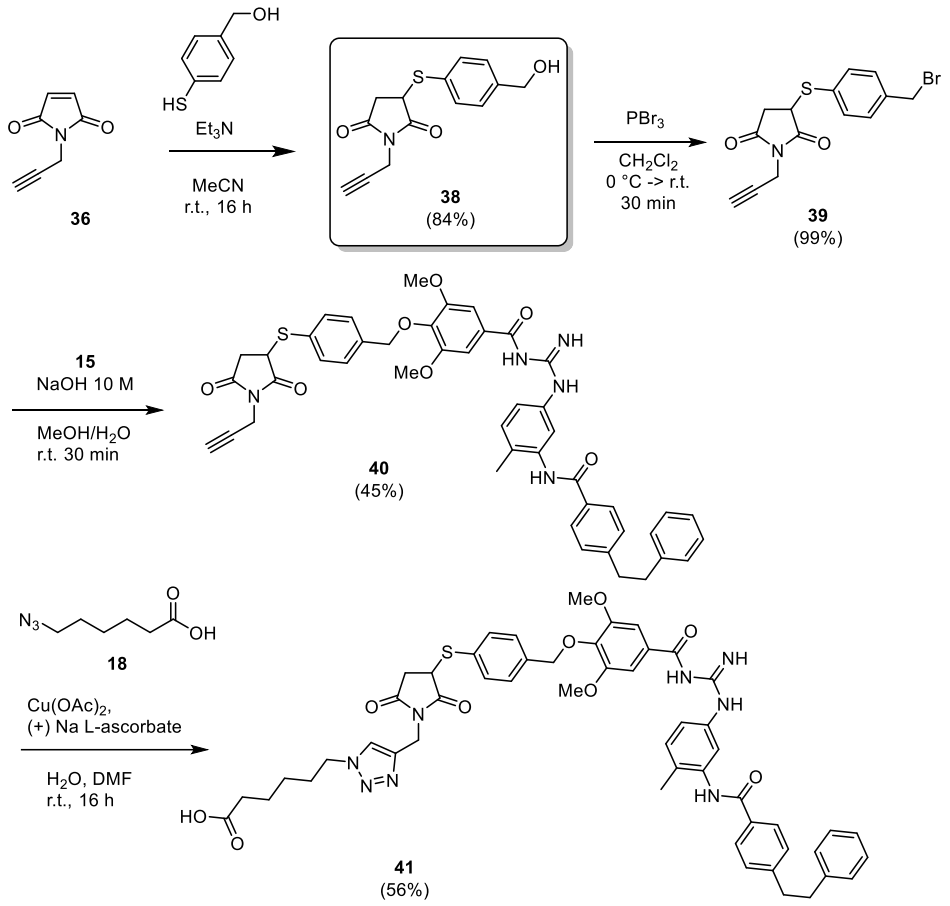

Scheme 18. Synthesis of the linker-payload system **41**.

2.1.1.4. Connection of compound 15 with a cleavable linker

A third linker-payload system, composed of compound **15** and the pH-sensitive HMPO linker, was also successfully synthesized. The preparation of the HMPO linker followed the previously optimized procedure developed.[400] A cyclization reaction of ethyl gallate with triethyl orthoformate in the presence of the acidic resin Amberlyst 15, provided the intermediate **42** in excellent 95% yield (**Scheme 19**). Subsequently, the free phenol moiety was subjected to an alkylation reaction using propargyl bromide, yielding compound **43** with 88% yield. Finally, the reduction of the ester moiety in the presence of $LiAlH_4$, furnished alcohol **44** in 95% yield.

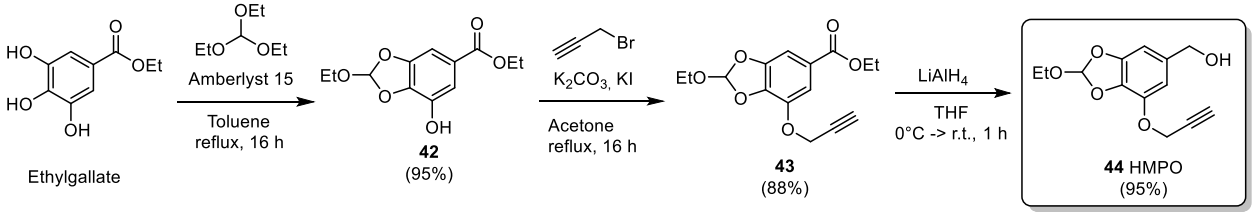

Scheme 19. Synthesis of the pH-sensitive linker **44**.

For the introduction of the payload, the benzyl alcohol moiety of **44** was converted into the corresponding chloride **45** by treatment with $SOCl_2$. Given the acidic lability of the orthoester structure within the HMPO linker, the chlorinating step required careful control: the chlorinating agent was added dropwise at 0 °C, and the pH was maintained alkaline adding Et_3N to prevent decomposition. Subsequently, the functionalized payload **15** was introduced via an alkylation reaction on its phenol moiety, in the presence of NaOH. The resulting intermediate **46**, was successfully isolated in 76% yield. This intermediate was then subjected to the final functionalization step: a CuAAC reaction with the azide **18**, which provided the desired, complete linker-payload system **47** in a 48% yield (**Scheme 20**).

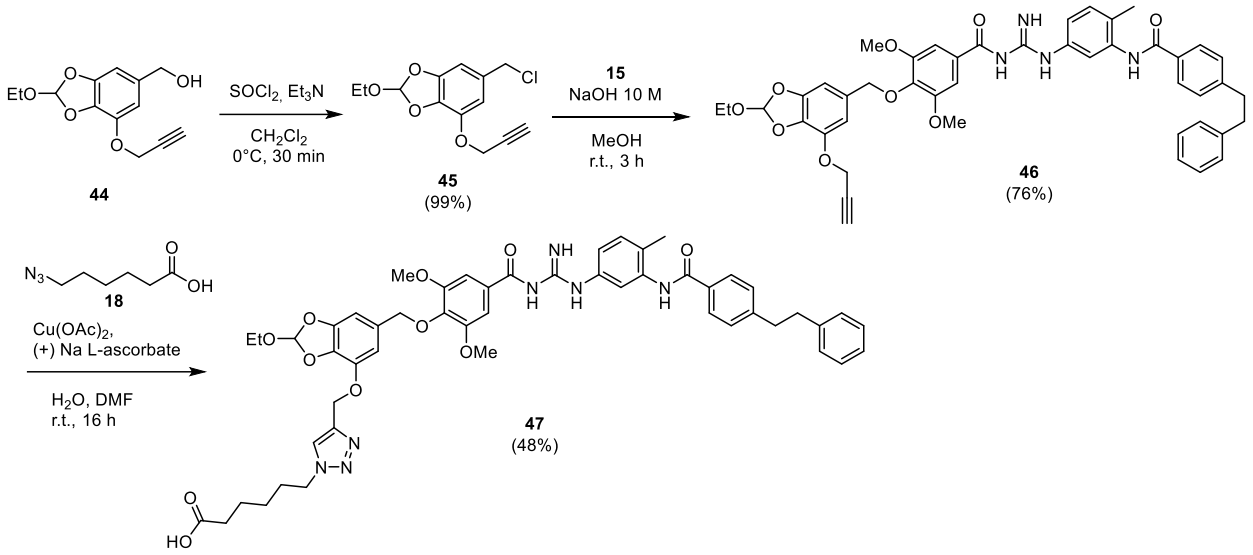

Scheme 20. Synthesis of the linker-payload system **47**.

2.1.1.5. Bioconjugation reaction via amide coupling on Lys residues

Having successfully synthesized three distinct linker-payload systems charged with the Hh inhibitor **6** and its derivative **15**, the bioconjugation reactions were performed. The mAb selected for this process was Cetuximab (Ctx). Ctx is selective for the EGFR antigen, which is frequently overexpressed across multiple tumors, including those that are Hh-pathway dependent. Furthermore, Ctx was selected due to its established clinical safety profile, known pharmacology, and ready availability.[401] The bioconjugation proceeded in a two-step sequence. First, the carboxylic acid moiety present on the linker-payload system was converted into the activated sulpho-*N*-hydroxysuccinimide (S-NHS) ester intermediate using S-NHS and 1-Ethyl-3- (3-dimethylaminopropyl)carbodiimide hydrochloride (EDC·HCl) as the coupling reagents. Second, the resulting activated linker-payload was added to a solution of Ctx in PBS buffer (pH 7.4) and

stirred at room temperature (r.t.) for 1 hour (**Scheme 21**). The resulting mixture was then purified by ultrafiltration, using a 10 kDa cutoff membrane. This final purification step was essential to efficiently remove the excess of unreacted linker-payload and residual reagents, thereby isolating the final ADCs **48-50**.

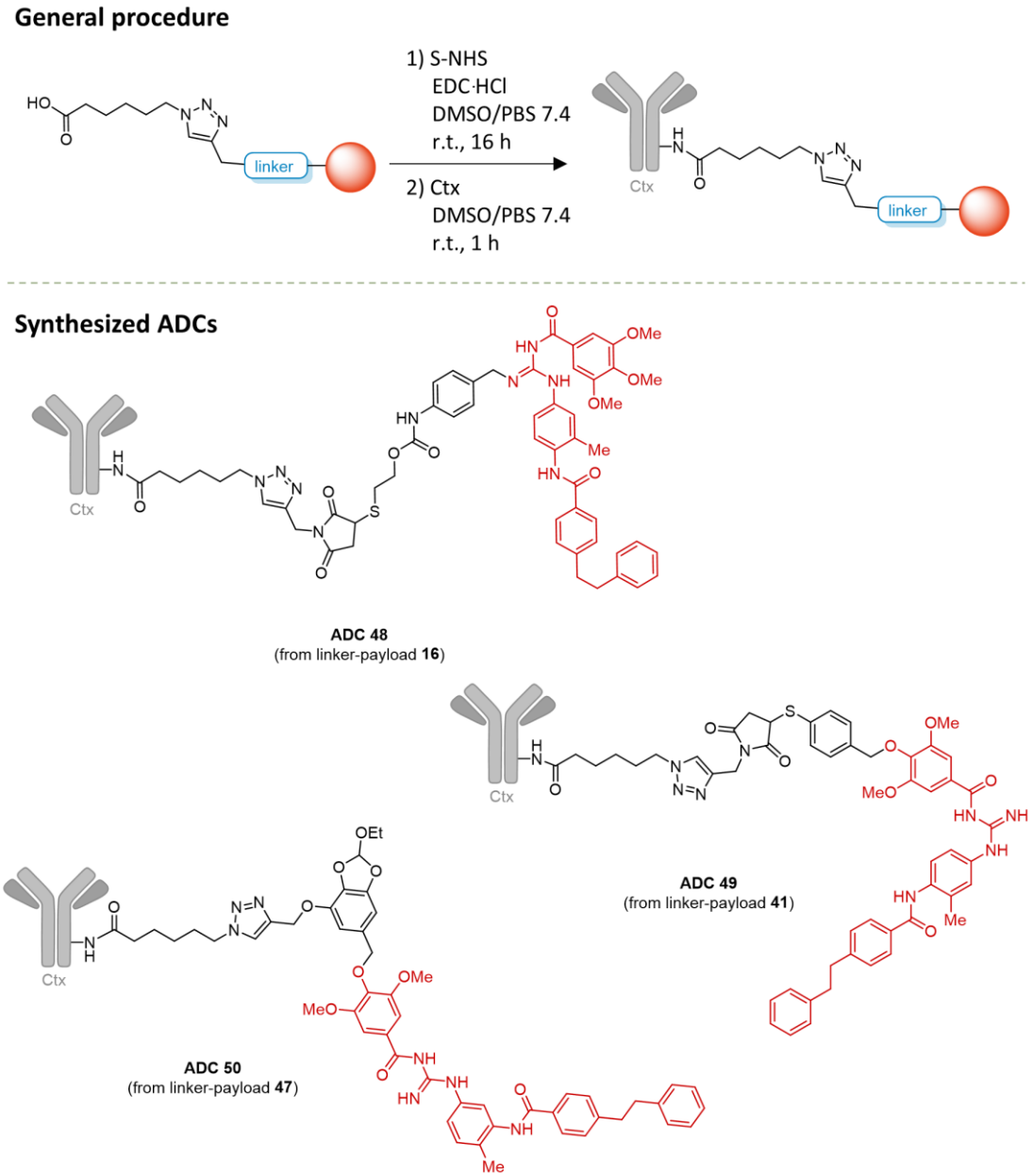

Scheme 21. Synthesis of ADCs **48**-**50**. Payload in red.

The DAR values for the obtained bioconjugates were determined via MALDI-TOF analysis using the formula:

$$\frac{MW_{ADC} - MW_{mAb}}{MW_{linker-payload}}$$

All three ADCs **48**–**50** exhibited satisfactory mean DAR values (**Table 7**). However, the absolute numerical DAR value alone is insufficient to define the overall quality profile of an ADC. The ideal scenario involves a homogeneous distribution of the payload across the antibody molecules. In the case of ADCs **48–50**, a significant heterogeneous distribution of the DAR was observed from the MALDI analysis, a factor that could potentially compromise the PK profile of the bioconjugate *in vivo*.

Table 7. DAR values for ADCs **48-50**.

ADC	*Linker-payload*	***DAR***
48	16	**2.30**
49	41	**3.40**
50	47	**1.90**

Providing additional confirmation of this challenge, a substantial loss of protein material was concurrently noted when monitoring the mAb concentration throughout the bioconjugation process. This loss is likely correlated with aggregation phenomena and subsequent precipitation of the ADCs, a common side effect of non-selective conjugation that further underscores the need for more controlled, site-specific methodologies.

2.1.2. Second bioconjugation strategy

With the aim to obtain more homogenous bioconjugate and DAR distribution, a second bioconjugation strategy was investigated. To achieve a more tunable and homogenous loading of the linker-payload systems over the mAb, a prefunctionalization of the mAb with a spacer bearing a dibenzocyclooctyne (DBCO) moiety was approached. This strategic modification allows for two critical improvements: i) It enables the intermediate step to be precisely monitored, thereby limiting the distribution of the DAR, ii) It exploits the high chemoselectivity of the Cu-free SPAAC reaction to introduce the linker-payload system in a subsequent, highly efficient step (**Figure 52**). This process necessitated the development of new linker scaffolds, appropriately designed to incorporate an azide moiety suitable for the click reaction. For this second strategy GLI inhibitor **14** was also investigated as a payload.

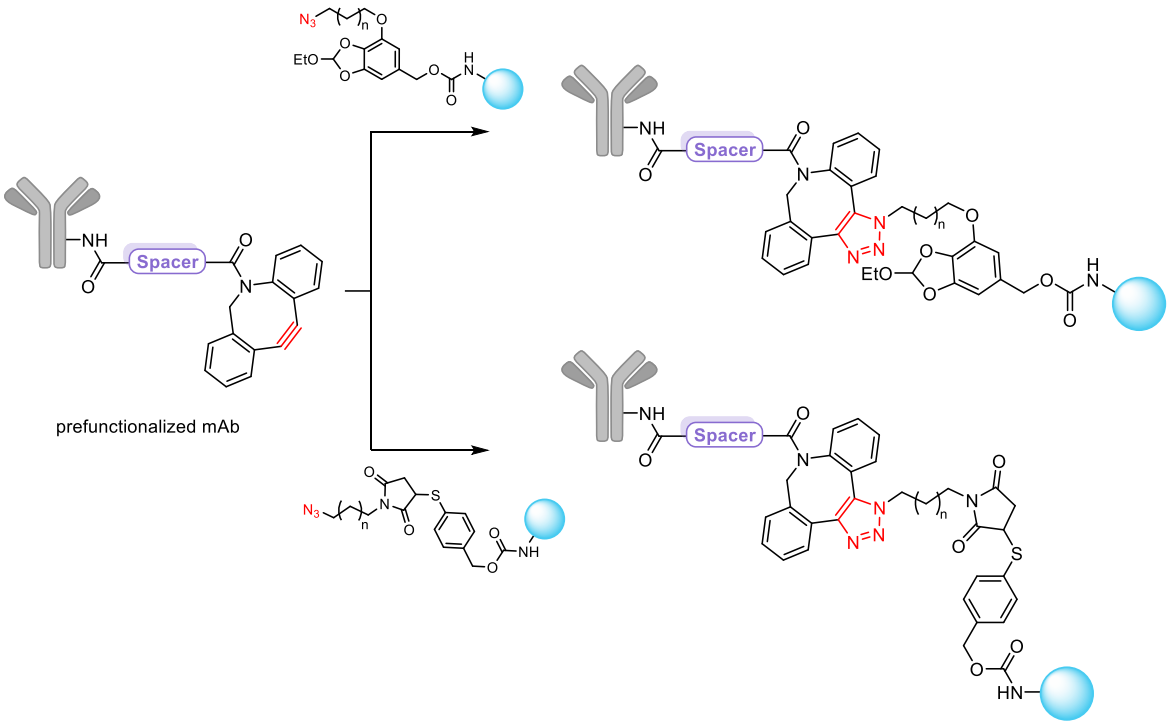

Figure 52. General structure of the proposed ADCs. Payload in light blue.

2.1.2.1. Synthesis of clickable non-cleavable linkers

Several synthetic protocols were attempted for the preparation of a non-cleavable linker bearing the necessary azide moiety. The initial strategy involved the chlorination of maleimidohexanoic acid using $SOCl_2$, followed by an amide coupling with *N*-Boc-ethylenediamine, which successfully furnished intermediate **51** in 60% yield. The subsequent step required the removal of the *tert*-butyl carbamate (Boc) protecting group by treatment with trifluoroacetic acid (TFA), providing compound **52** and a second amide coupling with the activated NHS-ester **53**. However, this step resulted in a very low yield of compound **54** due to the significant formation of uncharacterized by-products.

Despite the poor outcome of the last step, the Michael addition of the 2-mercaptoethanol spacer on **54** was investigated. Initial attempts suggested the reaction was not occurring, as the starting material was completely recovered. However, monitoring the reaction overtime (**Table 8**) revealed that the addition occurred very quickly (within minutes). Critically, the addition product **55** was rapidly subjected to a Retro-Michael reaction, fully restoring the starting material (**Scheme 22**). Because of high instability of **55** a different synthetic approach was investigated.

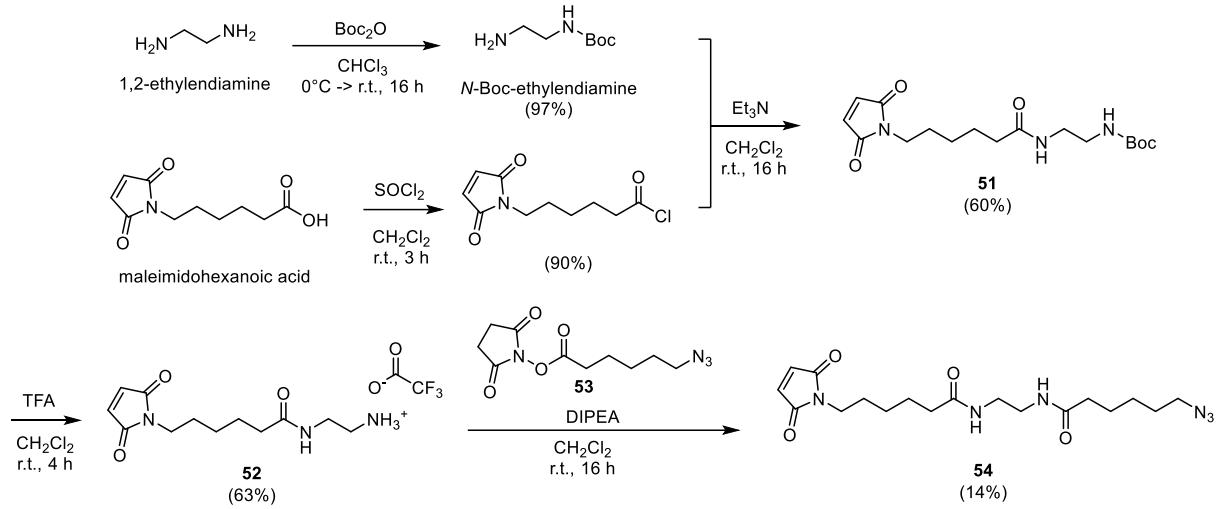

Scheme 22. First synthetic route for the synthesis of the clickable non-cleavable linker.

Table 8. Michael addition reaction and monitoring over time.

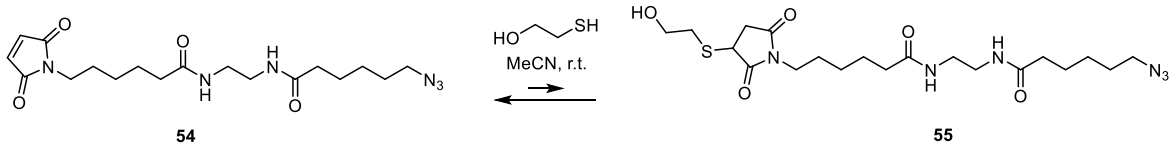

Time (min)	Ratio 54 : 55[a]
2	45 : 55
5	20 : 80
10	85 : 15
15	100 : 0

[a]Reaction procedure: **54** (1 equiv), dry MeCN (0.5 M), 2-mercaptoethanol (1.1 equiv). Reaction stirred at r.t. and checked *via* HPLC-MS.

Reacting maleic anhydride with 5-aminopentan-1-ol and acetic anhydride in acetic acid at reflux temperature, compound **56** was obtained in good yield (**Scheme 23**). The acetyl ester of **56**, was hydrolyzed by treatment with HCl to furnish the target alcohol **57** in 69% yield. The isolated compound **57** was converted to the corresponding bromide **58** and then treated with NaN_3. The expected compound **59** was not obtained even heating at 100 °C. Treating **57** in Appel's conditions, with PPh_3, NaN_3, tetrabutylammonium iodide (TBAI), and tetrabromomethane no better results were obtained.

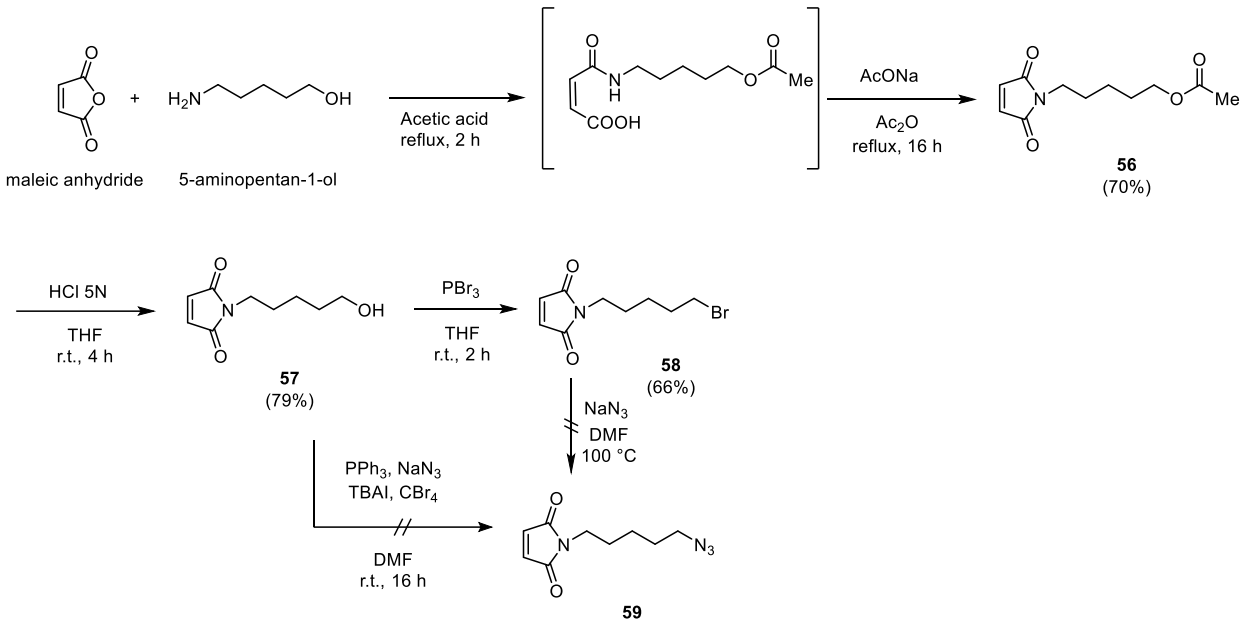

Scheme 23. Second attempt for the synthesis of the clickable non-cleavable linker.

Finally, the azide was directly introduced on maleimidohexanoic acid, using Propylphosphonic anhydride (T3P) and azide **22**. T3P was chosen as a convenient coupling agent due to its compatibility with less hazardous solvents like ethyl acetate (EtOAc), its non-flammability and non-toxicity, and the easy removal of its side product (propylphosphonic acid) via simple aqueous workup.[402] This reaction afforded the desired product (**60**) in acceptable 46% yield (**Scheme 24**). Crucially, on this new scaffold, the Michael addition with 2-mercaptoethanol and 4-mercaptobenzylalcohol gave excellent results, providing the stable linkers **61** and **62** in optimal yields (respectively 82 and 76%), thereby confirming that the new **60** structure successfully circumvented the stability issues encountered in the previous approaches .

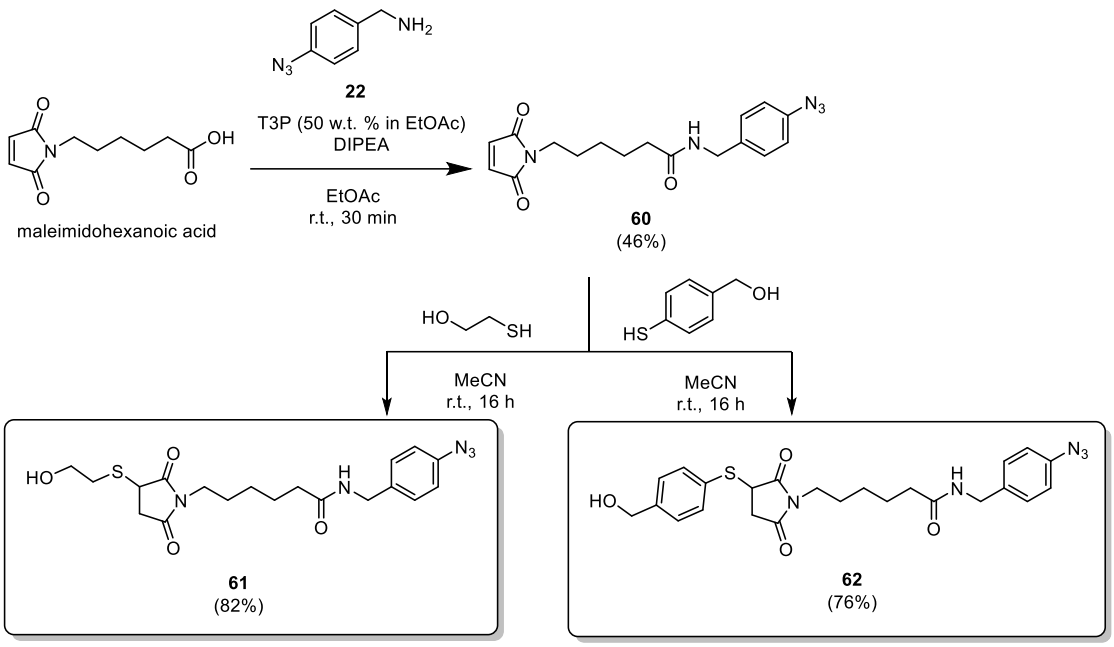

Scheme 24. Successful synthesis of non-cleavable linkers **61** and **62**.

2.1.2.2. Connection of non-cleavable linkers with payloads 15 and 20.

For the synthesis of the first clickable linker-payload system, the hydroxyl moiety of the non-cleavable linker **61** was initially activated by treatment with *p*-nitrophenyl chloroformate, thereby converting it into the more reactive carbonate intermediate **63** (**Scheme 25**). Prior attempts to isolate the carbonate **63** were unsuccessful due to its high instability. Consequently, the reaction crude was immediately subjected, without further purification, to the coupling reaction with the payload **20** to form the carbamate moiety via the aniline group (**Scheme 23**). The desired linker-payload system **64** was successfully obtained in low 20% yield. This modest yield was attributed to the numerous purification steps required to isolate the final product as pure compound.

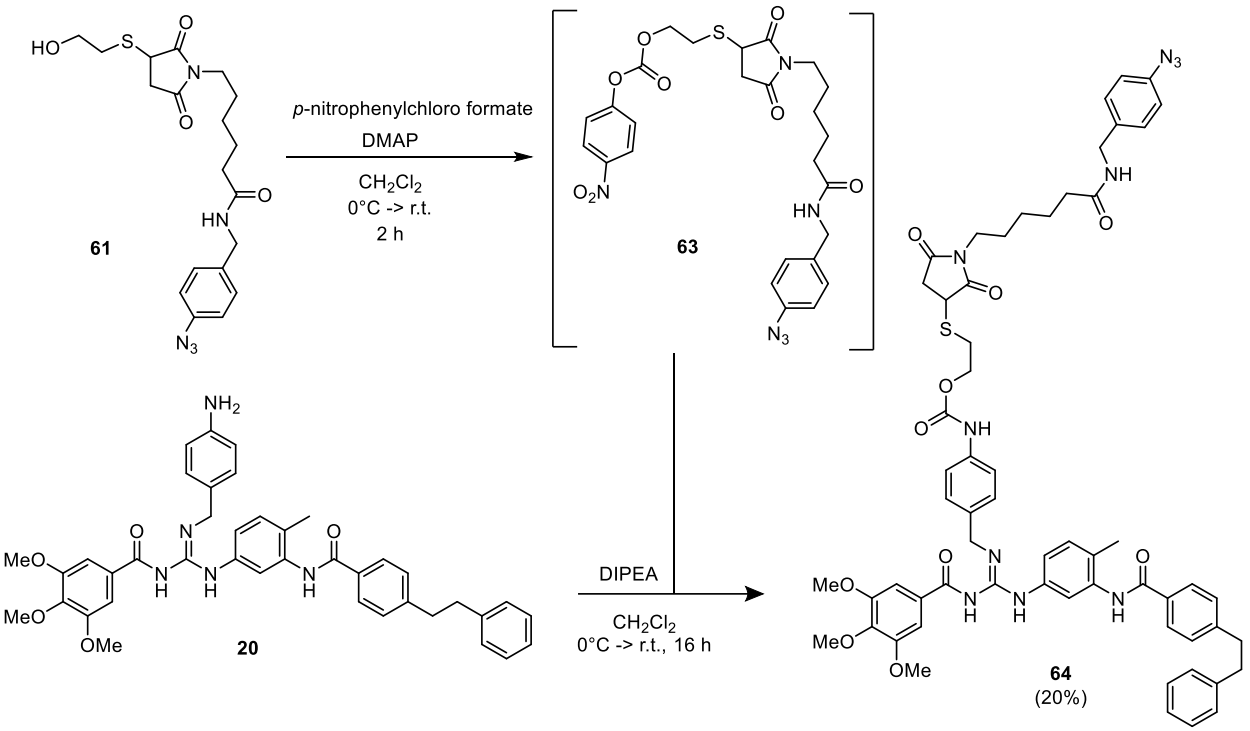

Scheme 25. Synthesis of linker-payload system **64.**

A second clickable linker-payload system, composed of the non-cleavable linker **62** and the payload **15**, was then prepared. This synthesis involved the initial chlorination of the hydroxyl moiety of **62** by treatment with $SOCl_2$, which furnished the intermediate **65**. Intermediate **65** was highly reactive and was utilized immediately without further purification. It was subsequently reacted with compound **15** in the presence of *N*,*N*-Diisopropylethylamine (DIPEA) in dichloromethane (**Scheme 26**). This alkylation reaction proceeded very slowly, requiring reflux temperature to initiate the conversion of the starting material. Furthermore, even after 4 days, a portion of the unreacted starting material remained. Nevertheless, the desired product **66** was successfully isolated and purified in 20% yield via preparative thin-layer chromatography, a method necessary due to the complexity of the reaction mixture.

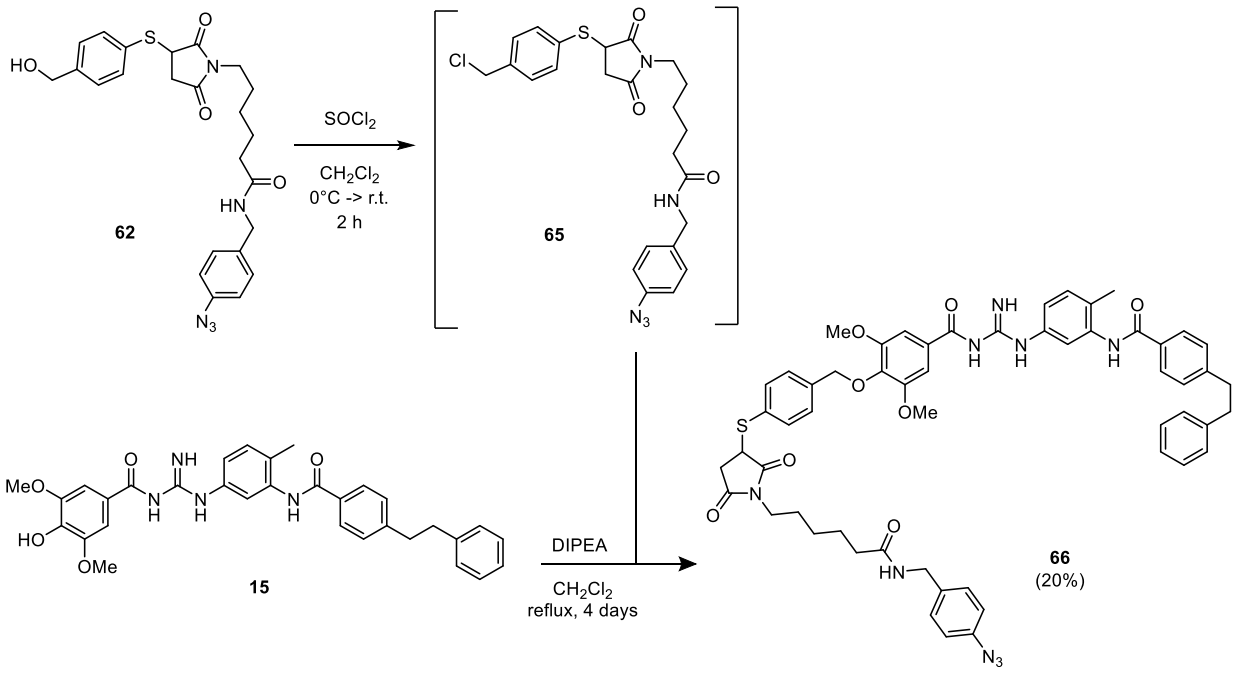

Scheme 26. Synthesis of linker-payload system **66.**

2.1.2.3. Connection of non-cleavable linker with GLI inhibitor 14

For the synthesis of linker-payload systems charged with the GLI inhibitor **14**, it was not necessary to introduce an additional handle for the linker, unlike the previous cases. This simplification was possible because compound **14** already possesses a secondary amine group that could be directly exploited as a connection site for carbamate formation. Payload **14** was first synthesized according to the reported procedure. [393] Similar to the reaction sequence described in **Scheme 25**, the non-cleavable linker **61** was converted *in situ* into the reactive carbonate intermediate **63**. This intermediate was immediately treated with **14** and DIPEA, successfully isolating the desired product **67**, in sufficient 45% yield (**Scheme 27**).

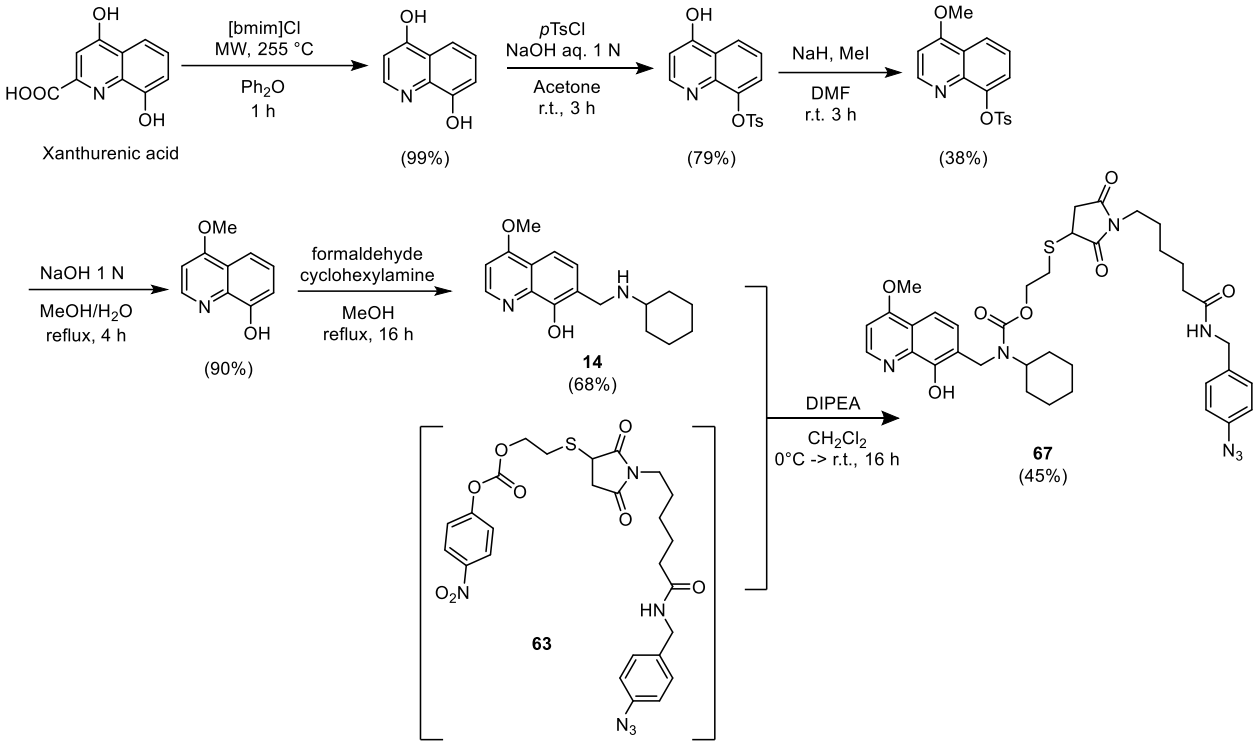

Scheme 27. Synthesis of payload **14** and linker-payload system **67.**

2.1.2.4. Synthesis of a clickable cleavable linker

The synthesis of the pH-sensitive HMPO linker containing an azide moiety, was also explored. Compared to the synthesis of the non-azide linker **44** (see **Scheme 19**), two key steps needed to be modified: i) Instead of alkylating the phenol with propargyl bromide, a Mitsunobu reaction was carried out to introduce the azido-alcohol **68**, which successfully provided the intermediate **69** in excellent 95% yield, ii) The final reduction of the ester was not possible with previously applied $LiAlH_4$, as the reduction of the azide into the corresponding primary amine occured. Instead, the milder reducing agent Diisobutylaluminum hydride (DIBALH) successfully provided the desired benzyl alcohol **70** in 70% yield (**Scheme 28**).

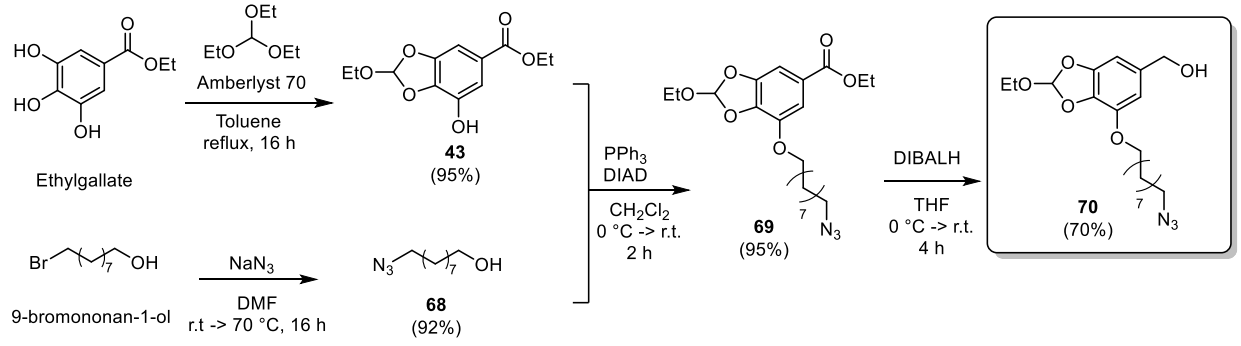

Scheme 28. Synthesis of pH-sensitive linker **70**.

2.1.2.5. Connection of the cleavable linker 70 with payloads 14, 15 and 20

For the connection of compound **20** with the pH-sensitive linker **70**, the initial approach consisted of activating the benzyl alcohol moiety of **70** to the corresponding reactive carbonate intermediate **71** by treatment with *p*-nitrophenyl chloroformate. As previously observed, the high instability of this intermediate required to directly treat **71**, without purification, with **20** (**Scheme 29**). However, in the presence of DIPEA the desired product was not observed, while the formation of the activated species **71** was confirmed by MS. Attempts of carrying out the reaction at higher temperatures led to the degradation of the starting materials.

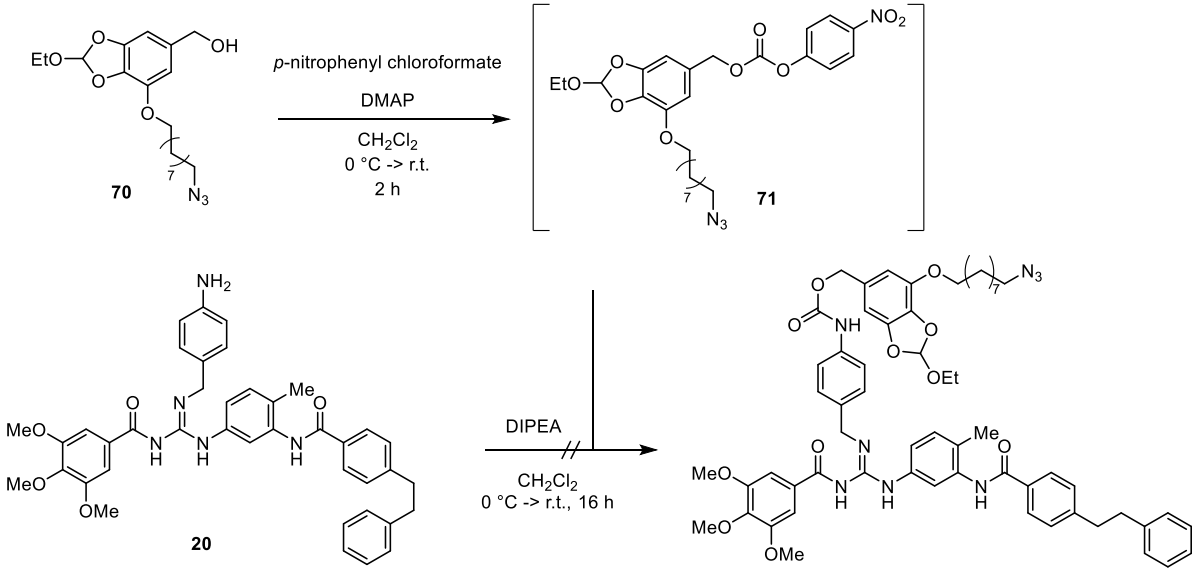

Scheme 29. Failed attempt for the introduction of linker **70** on compound **20**.

Consequently, direct connection of the aniline to the benzyl carbon of the linker, avoiding the formation of the carbamate was investigated. The corresponding chloride **72** was prepared by treating **70** with *p*-toluenesulphonyl chloride (TsCl). The proposed mechanism for this unusual chlorination reaction was elucidated to involve the initial formation of the tosylated intermediate **73**. This intermediate then readily cleaves to the resonance-stabilized carbocation intermediate **74** (due to the influence of electron-donating groups), which is finally attacked by a chloride anion (Cl^-) to yield the desired chlorinated compound (**Scheme 30**).[403]

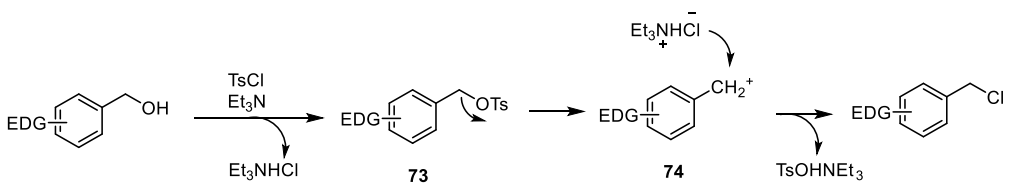

Scheme 30. Proposed mechanism for the chlorination of compound **70** with TsCl.

This intermediate was successfully purified by flash chromatography and isolated in 85% yield. The final coupling reaction between **72** and payload **20** in the presence of DIPEA afforded the desired linker-payload system, **75**, in 24% yield (**Scheme 31**).

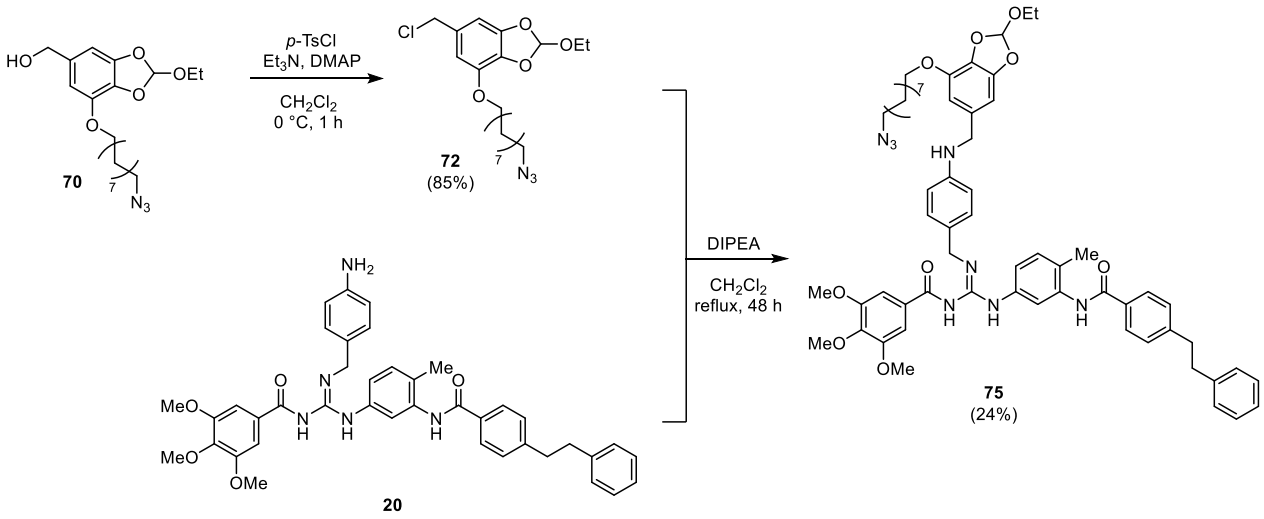

Scheme 31. Synthesis of compound **75**.

The same successful protocol was subsequently utilized to introduce linker **70** onto the phenolic payload **15**. The reaction involved treating the chloride intermediate **72** with the phenolic moiety of **15** in the presence of DIPEA. This alkylation provided the desired linker-payload system **76** in 33% yield (**Scheme 32**).

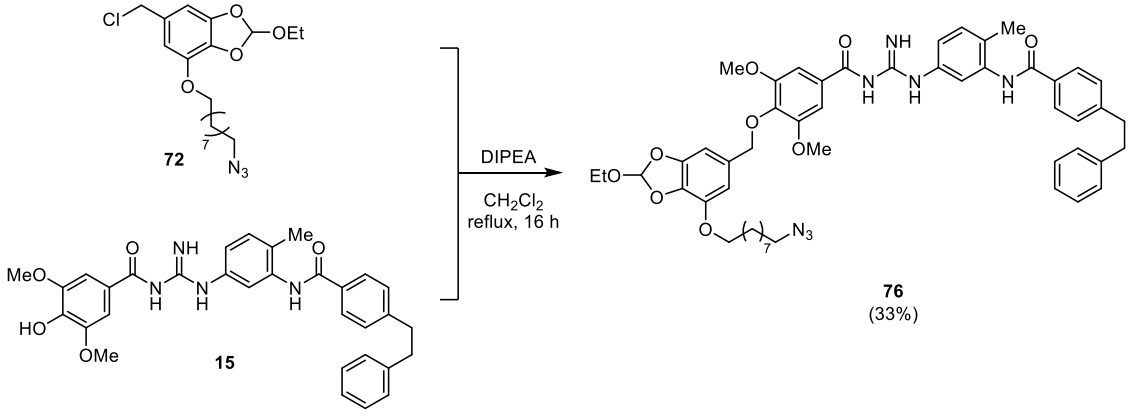

Scheme 32. Synthesis of compound **76**.

For the synthesis of the final linker-payload system, composed by the pH-sensitive linker **70** and the GLI inhibitor **14**, the *in situ* formation of a carbamate moiety was investigated once again. The activated carbonate **71** was prepared and subsequently treated with **14** in the presence of DIPEA. In this instance, the reaction successfully afforded the desired linker-payload product **77** in 34% yield (**Scheme 33**).

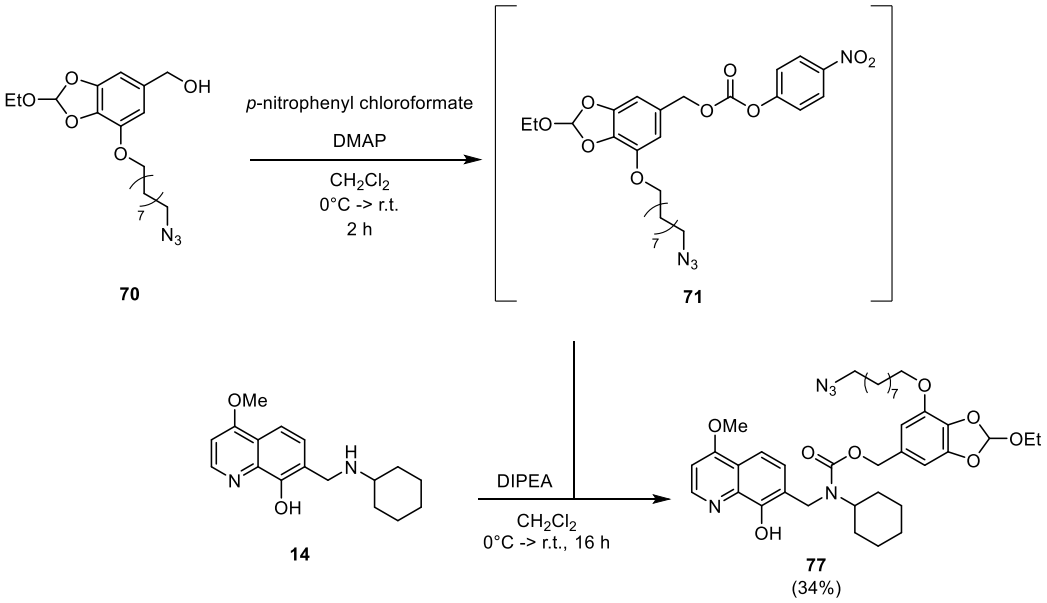

Scheme 33. Synthesis of compound **77**.

2.1.2.6. mAb prefunctionalization and bioconjugation via click reactions

To carry out the bioconjugation of the clickable linker-payload systems, the development of specifically designed spacers was required. We decided to explore the prefunctionalization of the mAb not only on lysine residues but also on cysteines by preparing two distinct spacers. Both spacers (**78** and **79**) were synthesized starting from maleimidohexanoic acid (**Scheme 34**). For the synthesis of spacer **78** maleimidohexanoic acid was first activated as the NHS-ester **80** (94% yield), followed by an amide coupling, providing the intermediate **81** in 32% yield. A Michael addition of DBCO-amine on **81** afforded spacer **78** (70% yield). This spacer is specifically designed for the prefunctionalization of lysine amine residues via amide bond formation with the carboxylic acid moiety. Spacer **79** was prepared in a good 85% yield in a single step coupling maleimidohexanoic acid and DBCO-amine in the presence of EDC, HOBt and Et_3N. This final spacer has a reactive maleimide moiety and is therefore suitable for direct bioconjugation to the cysteines on the mAb via Michael addition.

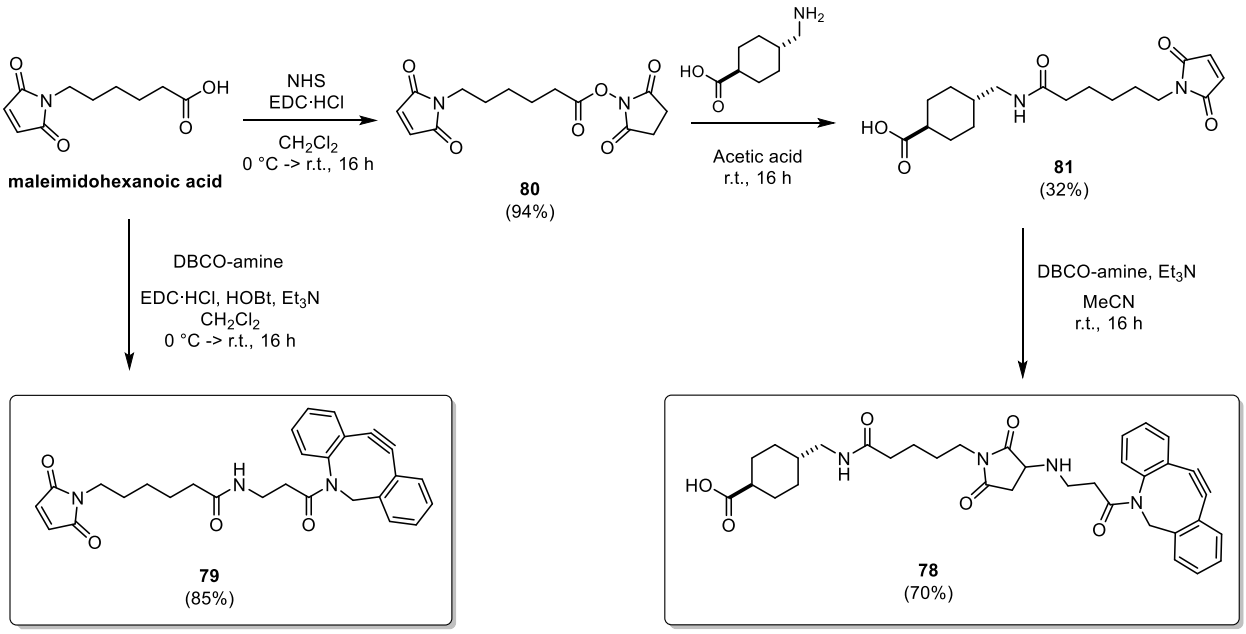

Scheme 34. Synthesis of spacers **78** and **79**.

Once synthesized the clickable spacers, the prefunctionalization conditions were optimized. For spacer **78**, the carboxylic acid was *in situ* activated using S-NHS and EDC·HCl and then added to a solution of Ctx in PBS (pH 7.4) (**Figure 53a**). The bioconjugation product **83** was clearly detectable in MALDI-TOF spectra, showing an average DAR (calculated on the *mono-charge* (*m/z*=MW/1), *di-charge* (*m/z*=MW/2), and *tri-charge* (*m/z*=MW/3) peaks) equal to 5.14 (**Figure 53b**). Notably, no loss of protein material and no precipitation were observed during the prefunctionalization process.

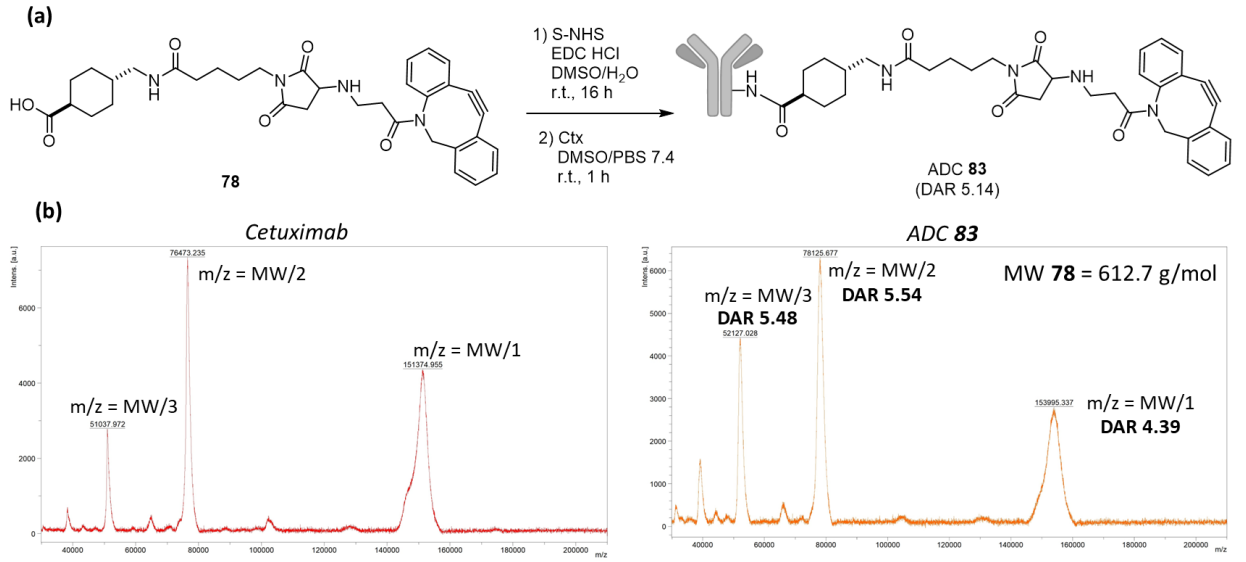

Figure 53. **a)** Prefunctionalization reaction of Ctx with spacer **78**, **b)** MALDI-TOF analysis of unconjugated Ctx (red) and ADC **83** (orange).

For spacer **79**, the mAb Bevacizumab, an anti-VGFR IgG, was firstly reduced by treatment with TCEP to obtain free thiol moieties (**Figure 54a**). It was then immediately incubated with a solution of **79** and analyzed by MALDI-TOF. In this case as well, no precipitation was observed and the prefunctionalization was successfully achieved, as observed from the functionalization of the heavy chain, light chain and half mAb (**Figure 54b**).

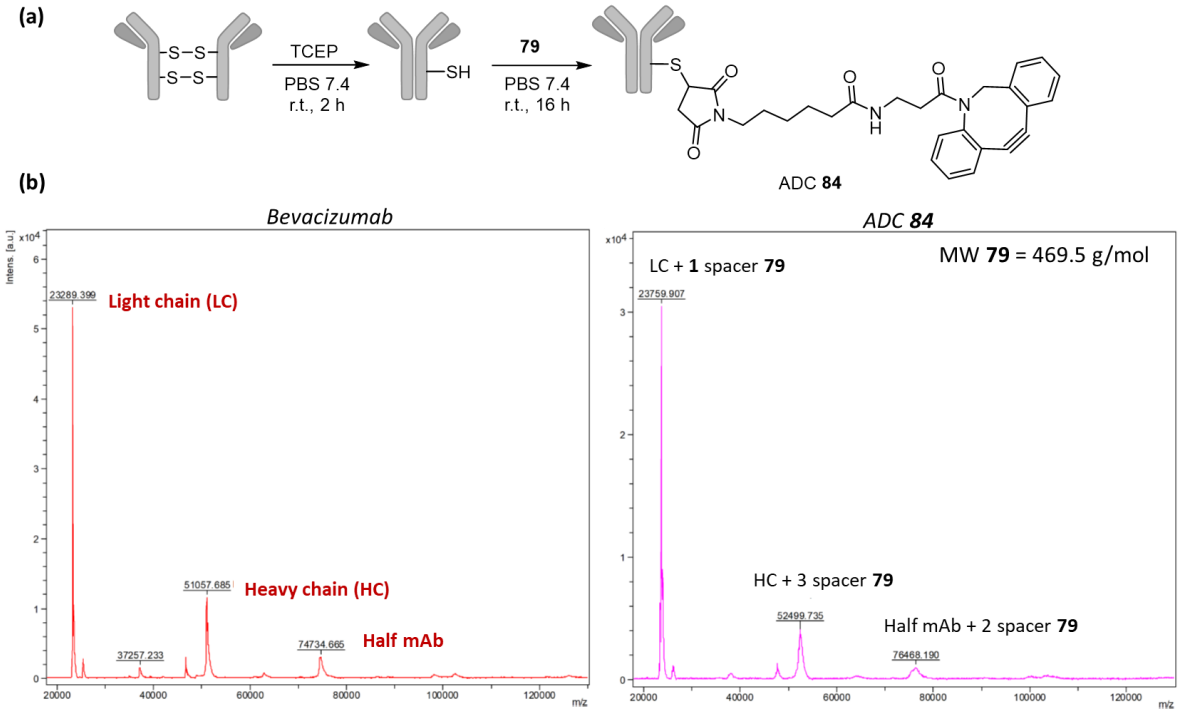

Figure 54. **a)** Prefunctionalization reaction of Bevacizumab with spacer **79**, **b)** MALDI-TOF analysis of reduced mAb (red) and ADC **84** (pink).

Following the successful prefunctionalization of the mAbs with spacers **78** and **79**, the SPAAC click reactions with the synthesized linker-payload systems were carried out by adding the linker-payload solution in DMSO to the solution of the prefunctionalized mAb in PBS (pH 7.4) and stirring the resulting mixture for 16 hours at 4 °C. Unfortunately, the bioconjugation reactions were not successful: MS spectra presented no significant mass variation compared to the DBCO-functionalized ADCs **83** and **84**, indicating a failure of the click reaction. Simultaneously, visible precipitation was observed during the bioconjugation process, and the concentration of the mAb significantly decreased. We hypothesized that the lipophilicity of the linker-payload systems was a crucial parameter affecting the outcome of the bioconjugation. As highlighted by a recent work from our research group, the LogP of the linker-payload system, the descriptor that estimates lipophilicity of a molecule by measuring its solubility in nonpolar solvents versus water, can directly impact the success of the bioconjugation by generating undesired aggregates.[404]

Therefore, LogP values were predicted[405] for each prepared compound demonstrating to be too high (6.9 – 12.6) to be compatible with aqueous bioconjugation conditions (**Figure 55**). This high lipophilicity is responsible for the aggregation and precipitation, preventing both the effective mixing of reagents and the successful completion of the SPAAC reaction.

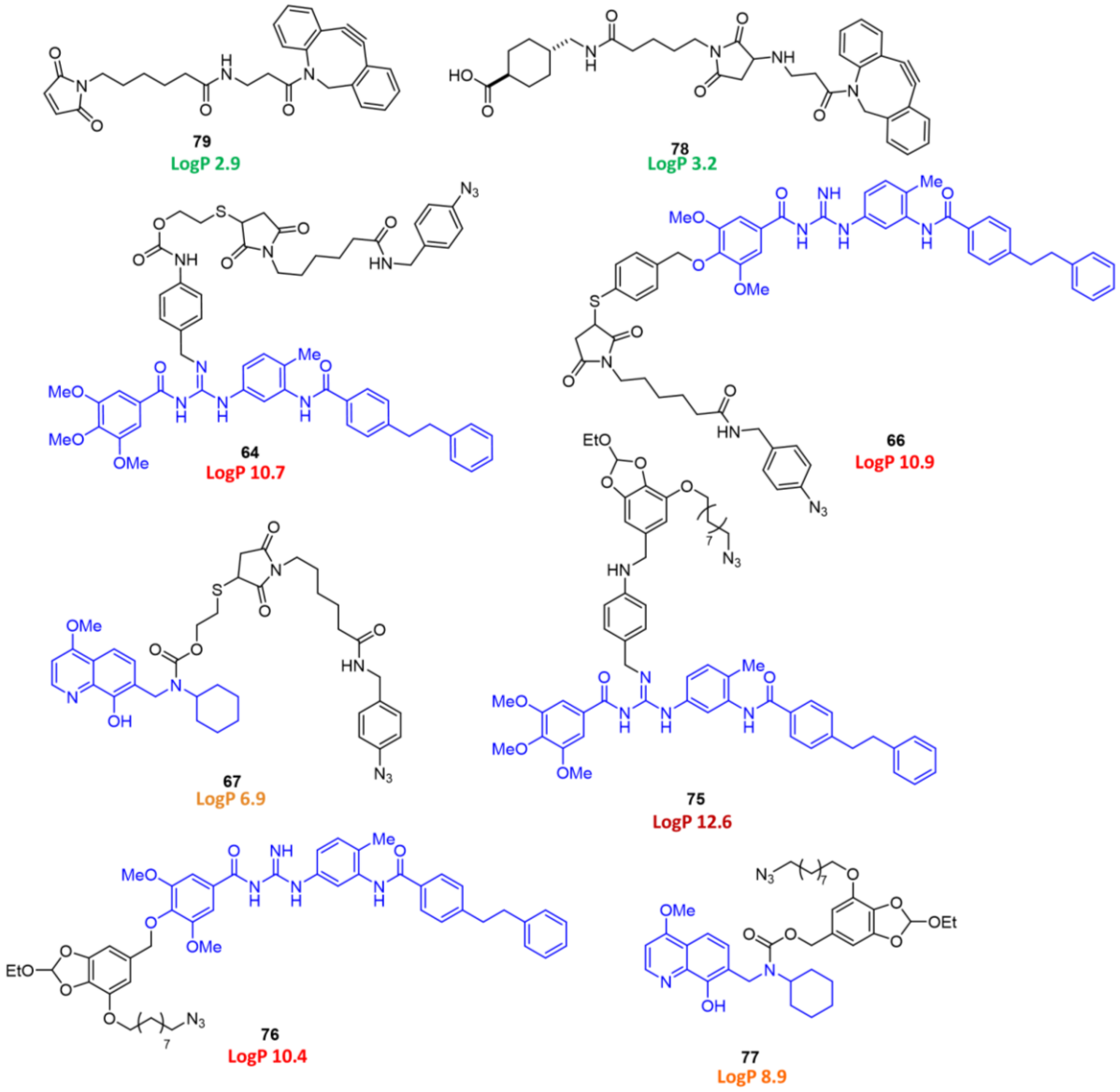

Figure 55. Structures of spacers, clickable linker-payload systems (payload in blue) and predicted LogP values.

2.1.3. Design of a new spacer for enhanced hydrophilicity

The results obtained from the initial two bioconjugation strategies revealed two major, interconnected challenges that must be overcome to synthesize expected ADCs. The first challenge is the DAR distribution, which must be as homogeneous as possible to mitigate potential PK issues *in vivo*. The second, and more critical challenge is the direct correlation between the linker-payload lipophilicity and the aggregation in aqueous media. While the first bioconjugation attempts (targeting lysines) successfully yielded the bioconjugates, the wide DAR distribution and the partial precipitation required to plan a different approach. Although the second strategy (based on SPAAC click chemistry) failed, it allowed us to successfully explore the reactivity of both lysine and cysteine residues on the mAbs and, most significantly, to identify the LogP parameter as a crucial property to be considered in the design of the linker-payload systems. To overcome these issues, we decided to focus on the bioconjugation to cysteine residues. This approach is inherently superior for DAR control, as IgG antibodies contain only four inter-chain disulfide bonds, a number far smaller than the eighty available lysine residues, thus enabling a more controlled and defined DAR distribution. Furthermore, instead of developing and synthesizing entirely new linker-payload systems, a third clickable spacer was designed to be applied to the previously synthesized payloads (**Scheme 35**). This new spacer integrates three main characteristics aimed at addressing the identified challenges:

- a DBCO moiety for the SPAAC click reaction, allowing for the stable introduction of the linker-payload prior to the final bioconjugation;
- a reactive moiety specifically designed for conjugation with the cysteine thiols of the mAb;
- a chain of polysarcosine (PSAR, logP ≈ -6 depending on the lenght of the chain), a highly hydrophilic polymer, to significantly increase the solubility of the entire linker-payload system in aqueous media, thereby mitigating aggregation and precipitation phenomena.

For the bioconjugation to the cysteine residues, the pentafluorobenzene functionality was chosen over the conventional maleimide group, in order to reduce the instability issues caused by the reversible retro-Michael reaction that can occur *in vivo*. In contrast, the pentafluorobenzene moiety reacts with available thiols via an irreversible S_NAr (Nucleophilic Aromatic Substitution) mechanism[204]. This reaction provides a stable thioether covalent bond, which securely links the linker-payload system to the mAb.

Scheme 35 shows the retrosynthetic strategy developed for our spacer. Starting from compounds **88-93**, we first envisioned disconnecting the triazole, revealing spacer **87**, which can be obtained from two subsequent amide coupling reactions of PSAR chain **85**, with DBCO-amine on the carboxylic moiety, and a pentafluorophenyl moiety on the amine.

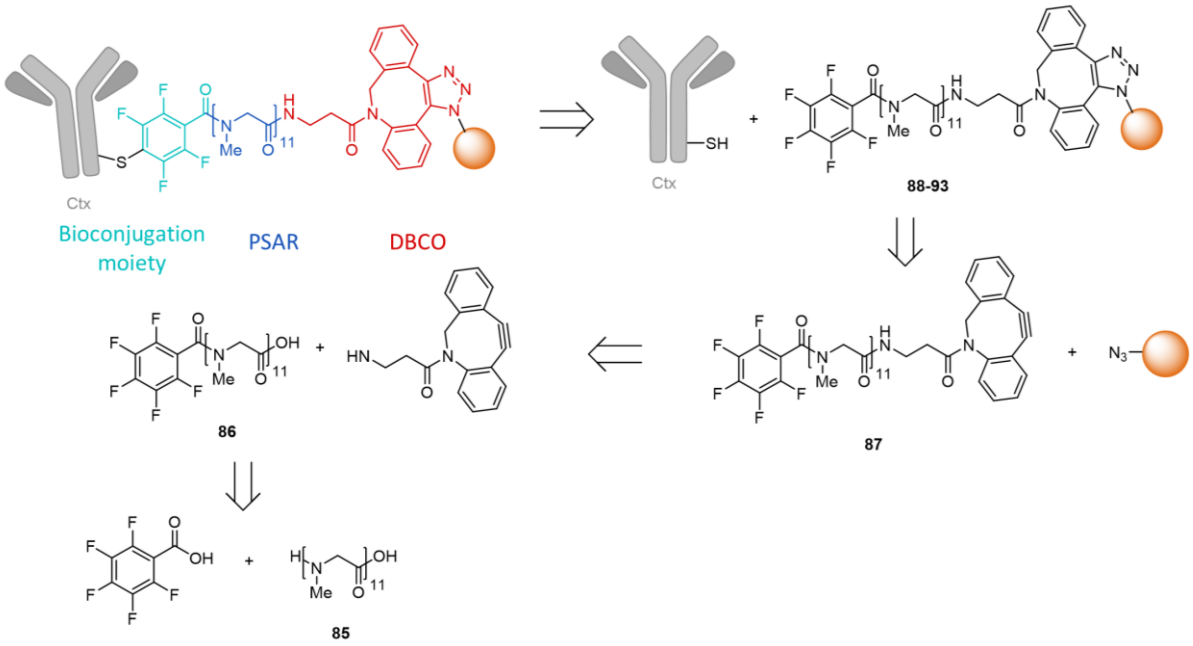

Scheme 35. Retrosynthetic scheme for the synthesis of ADCs via cysteine bioconjugation, using spacer **87** for enhanced hydrophilicity. Linker-payload system in orange.

Prior to the synthesis, the LogP values of the final PSAR-functionalized linker-payload systems (**88-93**) were predicted[405] (**Table 9**), and all demonstrated a significant improvement in hydrophilicity compared to the original clickable linker-payload systems alone, directly confirming that the PSAR chain could successfully mitigate the aggregation issues.

Table 9. LogP values of final compounds **88-93** compared to those of the clickable linker-payload systems (**64**, **66**, **67**, **75**-**77**).

Compound	*Clickable linker-payload precursor (LogP)*	*LogP*
88	**64** (10.7)	8.1
89	**67** (6.9)	4.3
90	**77** (8.9)	6.6
91	**76** (10.4)	8.6
92	**66** (10.9)	7.9
93	**75** (12.6)	10.3

2.1.3.1. Synthesis of spacer 87

For the preparation of the designed spacer, a solid-phase peptide synthesis (SPPS) approach was investigated to obtain an oligo-sarcosine chain containing eleven monomers. A polystyrene based resin, functionalized with 2-chlorotrityl chloride (CTC) was selected as the solid support. The synthesis involved the standard iterative cycle: i) deprotecting the amine moiety by removing the fluorenylmethoxycarbonyl (Fmoc) group with piperidine in DMF, followed by ii) the amide coupling of an additional sarcosine monomer or dimer. These steps were repeated until the desired chain length was achieved, yielding the polymer **85** (**Scheme 36a**). The loading of the resin was assessed by Fmoc cleavage test (absorbance measurement at 301 nm) and the following steps were evaluated using two methods: by cleaving the PSAR charged from a small portion of the resin analyzing by LC-MS and by a colorimetric chloranil based assay for secondary amines (**Scheme 36b**).[406]

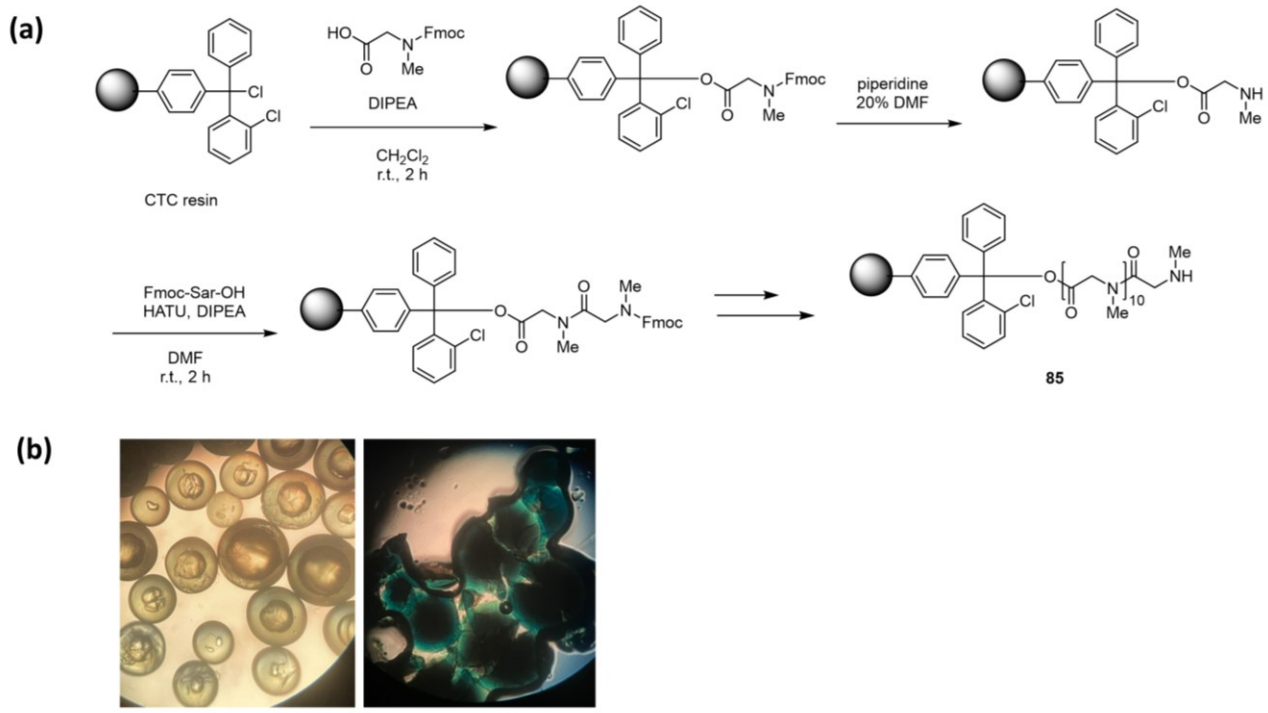

Scheme 36 a) Solid-phase peptide synthesis procedure for the preparation of PSAR polymer **85**, **b)** colorimetric assay for the detection of protected (left) or free (right) secondary amines.

Following the successful synthesis of the PSAR chain, the immobilized polymer **85** was treated with 2,3,4,5,6-pentafluorobenzoic acid in amide coupling conditions using EDC, HOBt and DIPEA (**Scheme 37a**). Finally, the cleavage from the resin was carried out by treatment with a solution of 20% 1,1,1,3,3,3-Hexafluoro-2-propanol (HFIP) and 2% triisopropyl silane in CH_2Cl_2, providing intermediate **86**, which was isolated by precipitation with diethyl ether and centrifugation. The formation of the desired product was confirmed by LC-MS analysis, which clearly revealed the expected peak at 992 *m/z*, corresponding to the $[M-H]^-$ species (**Scheme 37b**). Finally intermediate **86** was treated with DBCO-amine, DIPEA and HATU, to provide spacer **87**, which was purified via preparative HPLC. Spacer **87** formation was again confirmed by LC-MS, which displayed a single peak with 1252 *m/z*, corresponding to $[M+H]^+$ (**Scheme 37c**).

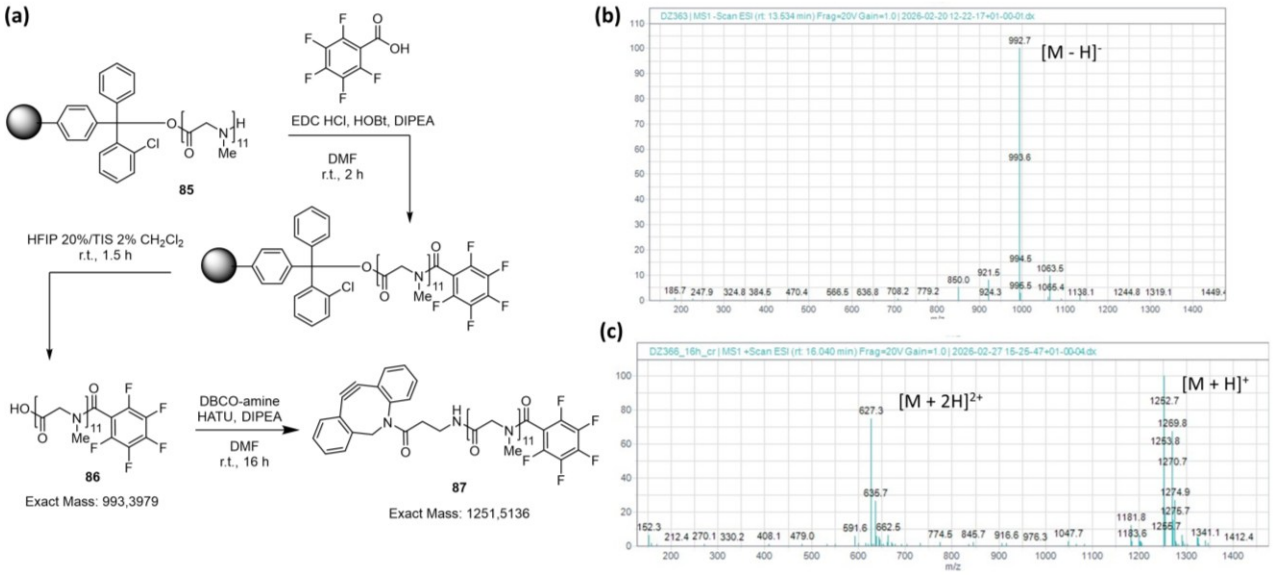

Scheme 37 a) Synthesis of spacer **87**, **b)** MS analysis of **86**, **c)** MS analysis of **87**.

2.1.3.2. Synthesis of linker-payload systems with spacer 87

Compound **87** was subjected to SPAAC click reactions with the six previously synthesized azide-bearing linker-payload systems (**64**, **66**, **67**, **75**, **76** and **77**). The click reactions were performed and analyzed directly via MS (**Scheme 38**), confirming the successful formation of the desired products for 4 out of the 6 systems (**64**, **67**, **76** and **77**), obtaining compounds **88-91** (**Table 10**). However, compounds **66** and **75** were recovered and no reaction was observed.

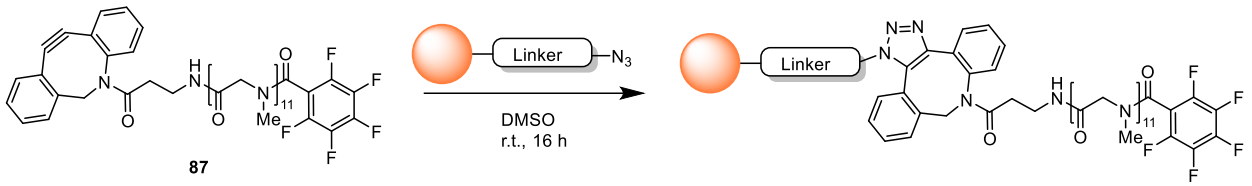

Scheme 38. General procedure for the SPAAC click reaction carried out with spacer **87**.

Table 10. Structure of linker-payload-N_3 systems and outcome of click reaction.

Linker-payload-N_3	Product of the click with 87 (MW)	Outcome
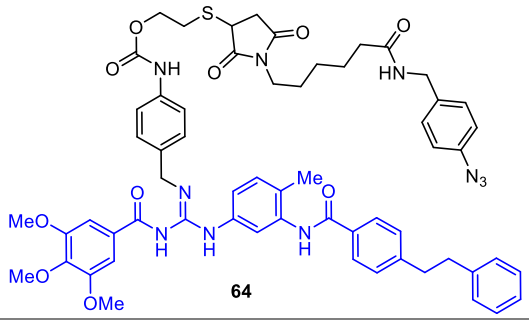 **64**	**88** (2369.5 g/moL)	Confirmed by MS analysis
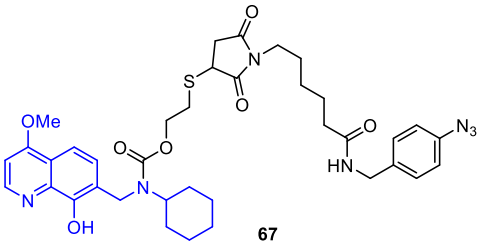 **67**	**89** (1984.1 g/moL)	Confirmed by MS analysis
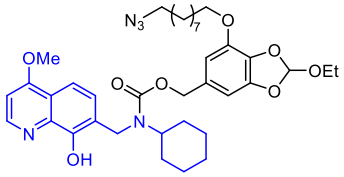 **77**	**90** (1944.1 g/moL)	Confirmed by MS analysis
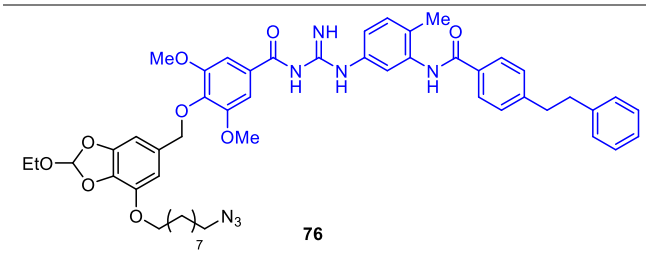 **76**	**91** (2166.3 g/moL)	Confirmed by MS analysis
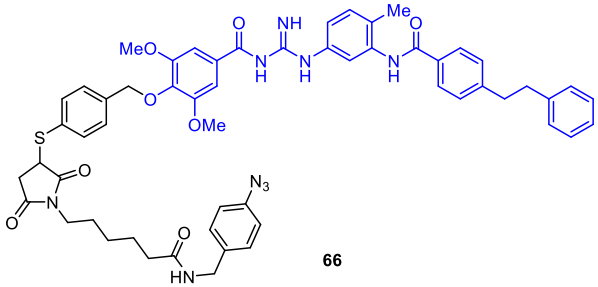 **66**	**92** (2268.5 g/moL)	No reaction
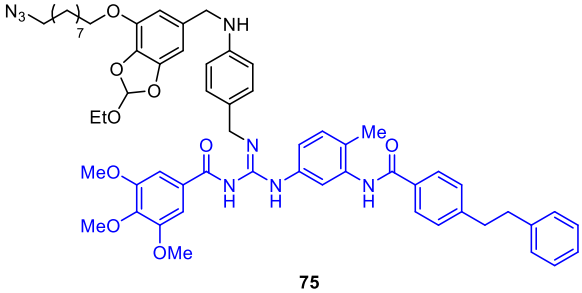 **75**	**93** (2285.5 g/moL)	No reaction

2.1.3.3. Bioconjugation to Cys residues

To carry out the bioconjugation of the PSAR-functionalized linker-payload systems **88-91**, Ctx was reduced with TCEP in TRIS buffer (pH 8) and directly treated with compounds **88-91** (**Scheme 39**). Notably, during the bioconjugation process, no precipitation was observed. This outcome validated the rationale of the third approach proving an increased hydrophilicity of the linker-payload systems thanks to the introduction of the PSAR chain.

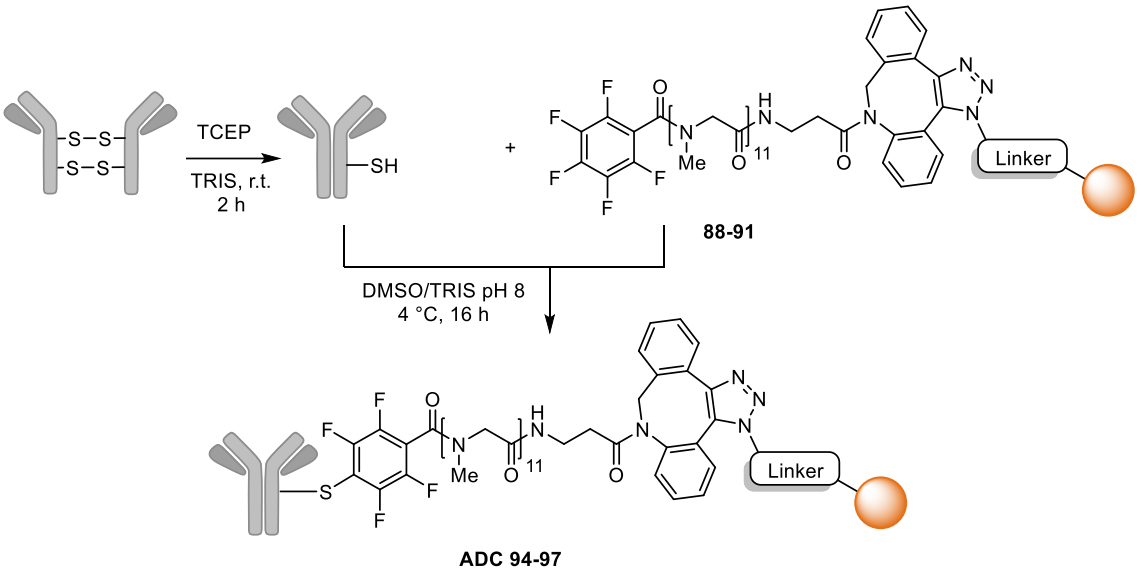

Scheme 39 Synthesis of ADCs **94-97**.

The final bioconjugates **94-97** were purified by ultrafiltration and analyzed by HIC. The HIC chromatograms were compared to the one of the starting Ctx and commercial ADC Adcetris®. All four chromatograms confirmed the successful formation of the bioconjugated species, that showed a longer retention time (**Figure 56**).

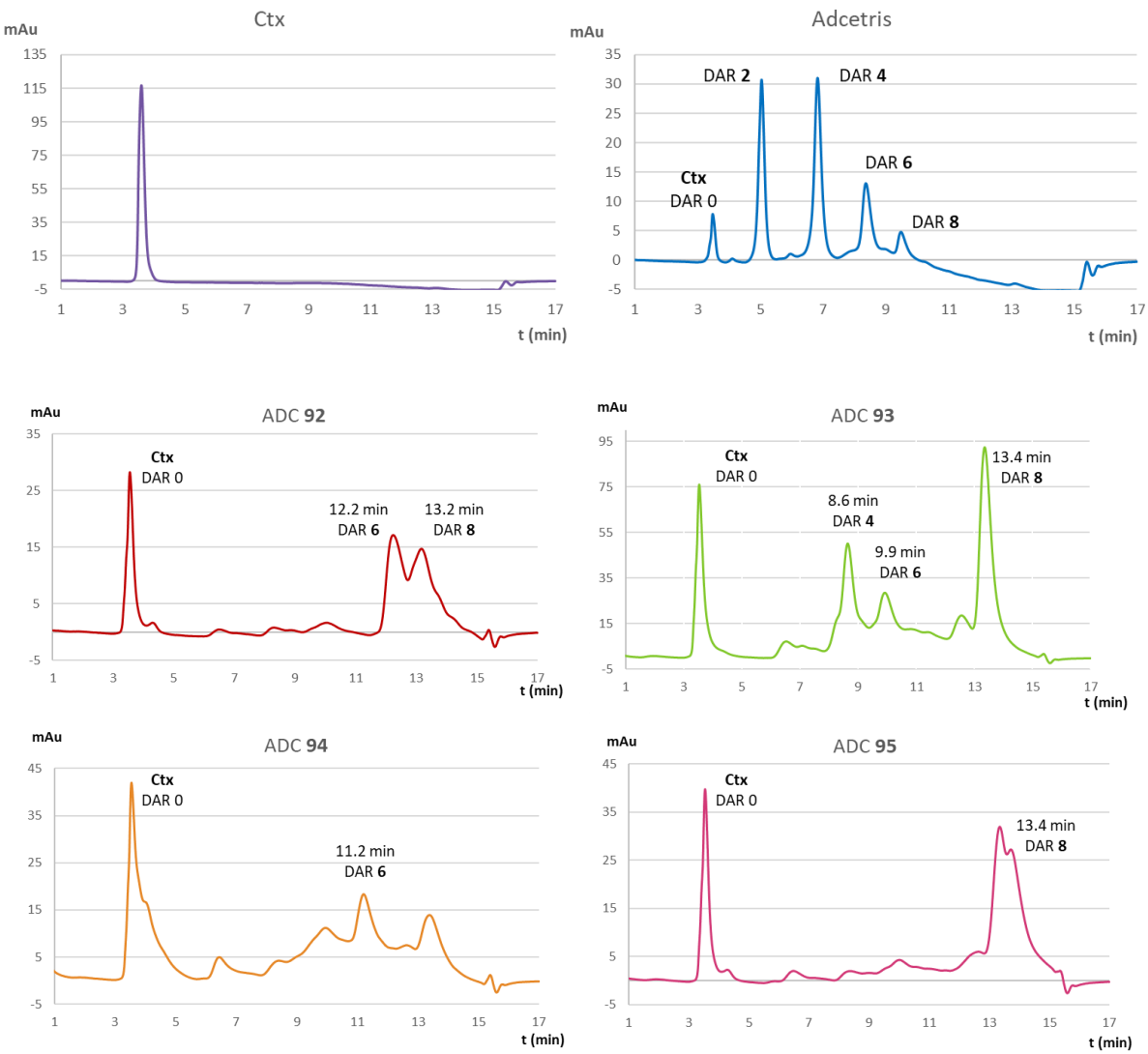

Figure 56. HIC spectra of ADCs **94-97**.

This shift in retention time was expected as a measurable increase in hydrophobicity occured by charging the payload. These results confirmed the covalent linkage between the linker-payload systems and the Cys residues of Ctx. While the determination of the definitive DAR values requires further dedicated MS analysis, an initial DAR was hypothesized by comparing the HIC chromatograms of our ADCs with those of commercially available ADCs, such as Adcetris®. The resulting average DAR values, which necessarily take into account the residual presence of unconjugated mAb, are summarized in **Table 11**.

Table 11. Analysis of the HIC chromatograms with areas of the peaks and DAR calculation.

ADC	*Time (min)*	*Area %*	*DAR*	Average DAR
94	3.547	39.664	0	**4.17**
	12.230	32.887	6	
	13.179	27.449	8	
95	3.536	26.810	0	**4.79**
	8.643	22.258	4	
	9.917	8.805	6	
	13.357	42.127	8	
96	3.540	70.034	0	**1.80**
	11.208	29.966	6	
97	3.538	29.759	0	**5.62**
	13.355	70.241	8	

Beyond the chromatographic validation, additional confirmation of successful conjugation was provided by the extracted absorbance spectra of the detected HIC peaks. The clearest example is demonstrated by ADC **95**: the peaks corresponding to the proposed DAR 4, 6, and 8 all displayed the characteristic protein absorption profile (consistent with unconjugated Ctx). Crucially, they also exhibited a distinct absorption peak at 240 nm, which is specifically related to the absorption of the linker-payload system. This 240 nm absorption progressively increased with the assumed increase in DAR, unequivocally proving that these peaks are derived from species covalently composed of both the protein and the linker-payload system (**Figure 57**). Other peaks that did not display this same behaviour were considered as impurities.

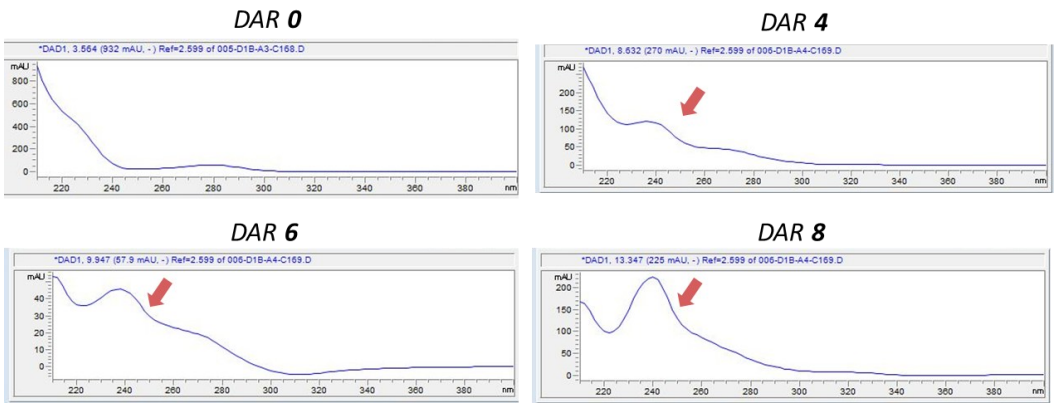

Figure 57. Absorption spectra extracted from the HIC of ADC **95,** with visible peak at 240 nm rising with increasing DAR.

In conclusion, by focusing on cysteine conjugation for superior DAR control and implementing a novel polysarcosine spacer to enhance hydrophilicity and manage the LogP, we achieved the desired outcome. The final PSAR-functionalized linker-payload systems effectively circumvented the aggregation issues, and HIC analysis confirmed the successful formation of four distinct ADCs (**93-97**) with favorable, defined DAR distributions. However, it is important to note that the full characterization of these novel ADCs is still ongoing to define all critical physicochemical parameters, such as confirming the final DAR values.

2.1.3.4. Preliminary biological evaluation of ADCs 95 and 96

Following the successful preparation of four new ADCs charged with in-house developed Hh inhibitors, a preliminary biological evaluation was carried out on the two bioconjugates charged with payload JC19, ADCs **95** and **96**, in collaboration with Dr. Barbara Stecca at Istituto per lo Studio, la Prevenzione e la Rete Oncologica (ISPRO) in Florence.

Biological activity of ADC **95** and ADC **96** was evaluated on melanoma cell lines. Aberrant HH activation is involved in melanoma as several melanoma cell lines express high level of SMO, GLI1, GLI2 and PTCH1. In particular SK-MEL-5 cells were selected because of the high EGFR levels. The antiproliferative activity was investigated in a dose dependent manner compared to Ctx alone, unconjugated **89** and **90** and **JC19** as a positive control. SK-MEL-5 cells were treated at different concentrations for 72 h. As shown in **Figure 58**, ADCs **95** and **96** reduced viability and proliferation, with IC_{50} values in the nanomolar range, while the single components Ctx, **JC19** and unconjugated **89** and **90** had no effect compared to untreated cells.

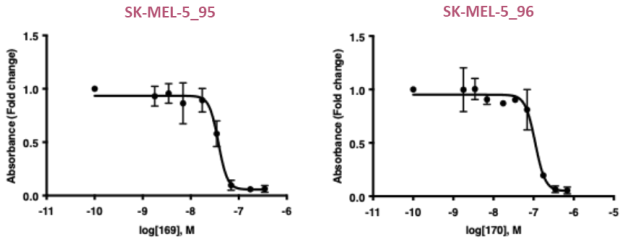

SK-MEL-5	IC_{50} (nM)
89	766,6
ADC 95	**37,58**
JC19	1150
Ctx	ND

SK-MEL-5	IC_{50} (nM)
90	1420
ADC 96	**109,7**
JC19	1150
Ctx	ND

Figure 58 Cell viability assay on SK-MEL-5 melanoma cells treated with ADCs **95**, **96** and controls.

To verify whether an increase in apoptosis induced the antiproliferative effect, an AnnexinV/7-AAD double staining assay with subsequent cytofluorimetric analysis was performed. Treatment with **95** and **96** in SK-MEL-5 cells resulted in an increase of early and late apoptosis (**Figure 59**).

Again, Ctx, JC19 and unconjugated linker-payload systems showed no effects, confirming that the obtained ADCs exerts a significant pro-apoptotic effect on melanoma cell lines.

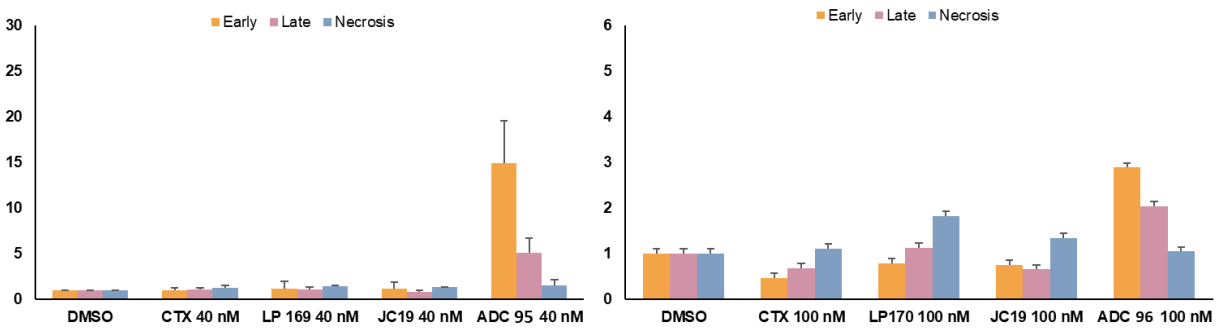

Figure 59 Cytofluorimetric analysis of cell apoptosis on SK-MEL-5 melanoma cells treated with ADCs **95**, **96** and controls.

2.2. EXPLORATION AND DEVELOPMENT OF BIOCONJUGATION METHODOLOGIES

2.2.1. Natural products as payload for ADCs: Cyclopamine linked to Cetuximab for Hedgehog pathway inhibition

As described in paragraph 1.3.4, Cyclopamine is a well-known steroidal alkaloid and natural product inhibitor of the Hh signaling pathway. Despite its pivotal role in discovering the Hh pathway, cyclopamine has never achieved clinical viability due to significant liabilities, including poor solubility, PK issues, and adverse off-target effects. This work aimed to overcome these critical limitations by developing ADCs charged with cyclopamine to investigate whether the incorporation of this natural product into an ADC system could enhance its anticancer activity, circumventing some of the PK limitations observed to date.

2.2.1.1. Bioconjugation of linker-payload systems charged with cyclopamine

Two distinct linker-payload systems were designed and synthesized: compound **98**, featuring an acid-cleavable HMPO orthoester linker, and compound **99**, based on a non-cleavable scaffold (**Figure 60**). The initial bioconjugation approach chosen for both compounds consisted of the in situ activation of the carboxylic acid moiety present on the linkers as NHS-esters. This activation was intended to promote the formation of an amide bond with the lysine residues of the anti-EGFR monoclonal antibody, Ctx.

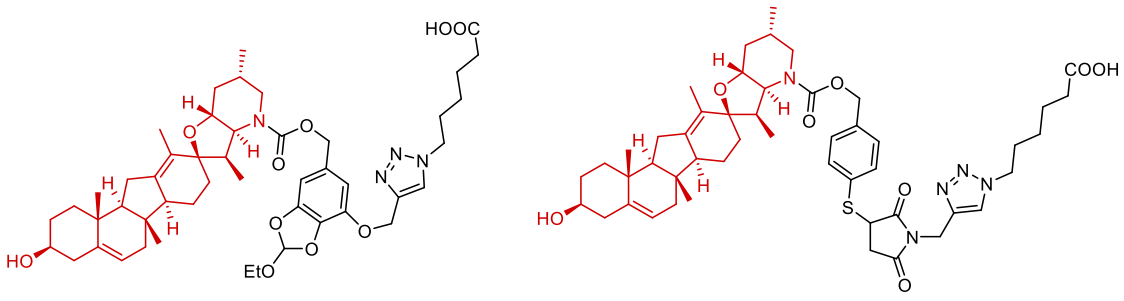

Figure 60. Structures of cyclopamine-based linker-payload **98** and **99**. Payload in red.

Compound **98** was treated with S-NHS and EDC in a DMSO/EPPS mixture, followed by the addition of a freshly prepared stock solution of Ctx in EPPS at pH 8.0 (**Scheme 40**). This process successfully provided the desired ADC **100** with an average DAR of 1.90, as indicated by MALDI-MS analysis (**Figure 61**).

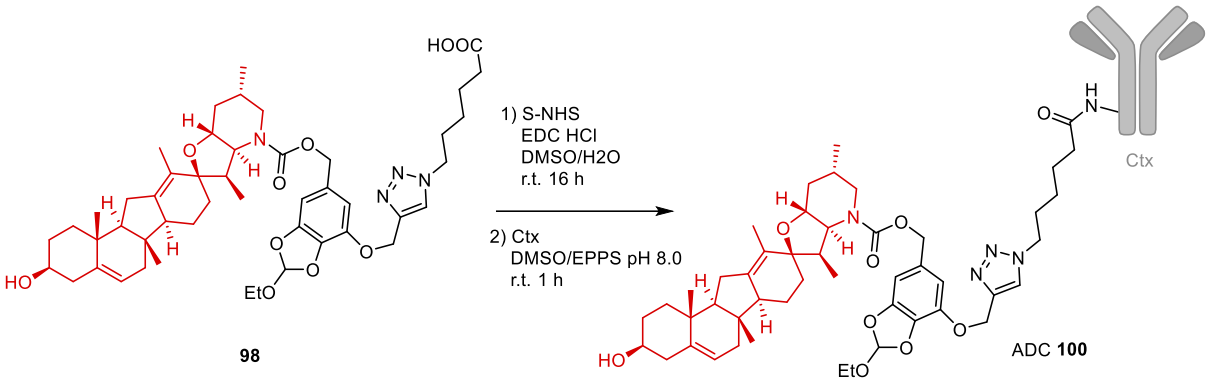

Scheme 40. Synthesis of ADC **100**.

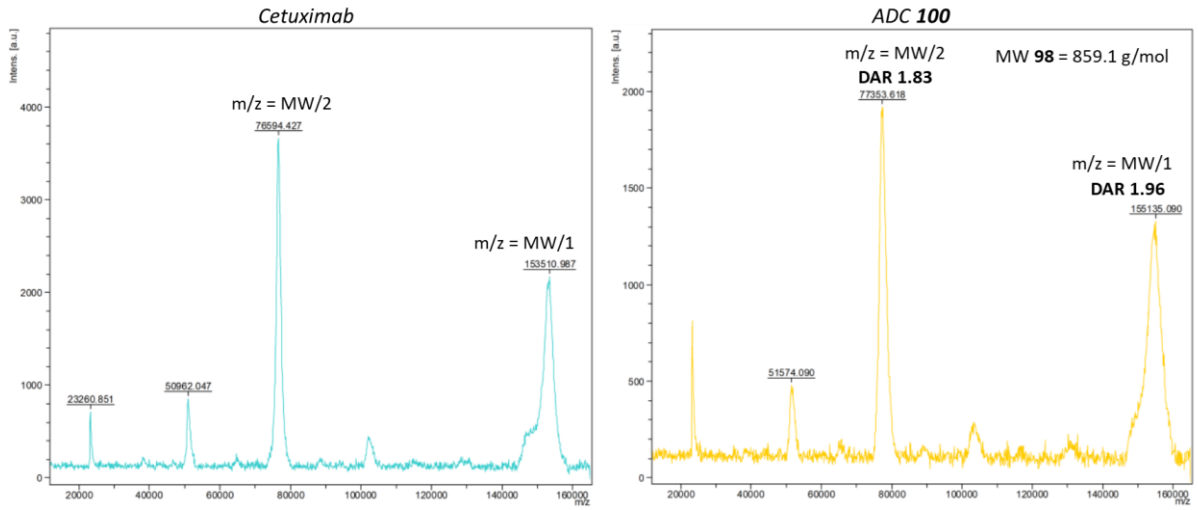

Figure 61. MALDI spectra of unconjugated Ctx (left) and ADC **100**(right).

However, employing the same protocol on substrate **99,** the bioconjugation with Ctx was unsuccessful. Even changing the activation and bioconjugation conditions, it was impossible to obtain the expected bioconjugate.

The different behavior observed between compound **98** and **99** during the bioconjugation suggested that the different lipophilicity of the two linker-payload systems could affect the bioconjugation outcomes. To overcome the issues related to the bioconjugation of **99**, a completely different approach was explored, involving the prefunctionalization of Ctx and the subsequent exploitation of the SPAAC click reaction, as already investigated for the MRT derivatives. The NHS-activated carboxylate **101** was treated with DBCO-amine yielding the DBCO-functionalized amide **102** in a 58% isolated yield (**Scheme 41**). Ctx was prefunctionalized by incubation with the NHS ester of 14-azido-3,6,9,12-tetraoxatetradecanoic acid (**103**) in PBS (pH 7.4). Prefunctionalized Ctx (**Ctx-N_3**) was obtained with DAR equal to 1.80 (**Figure 62**). Finally, the

bioorthogonal click reaction was performed reacting **Ctx-N_3** in PBS (pH 7.4) with a DMSO solution of the DBCO-amide **102**. This successful SPAAC step provided the desired ADC **104**, charged with cyclopamine, with a final DAR equal to 1.0 (**Figure 62**).

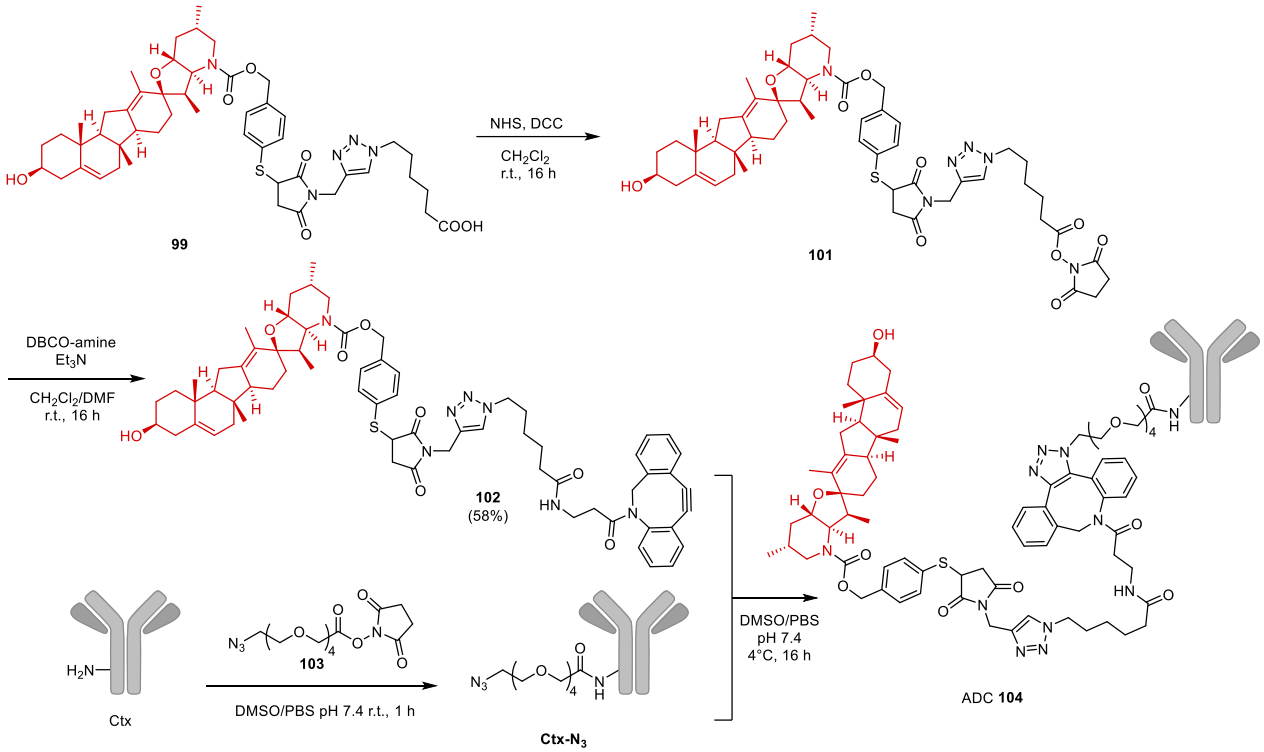

Scheme 41. Synthesis of ADC **104**.

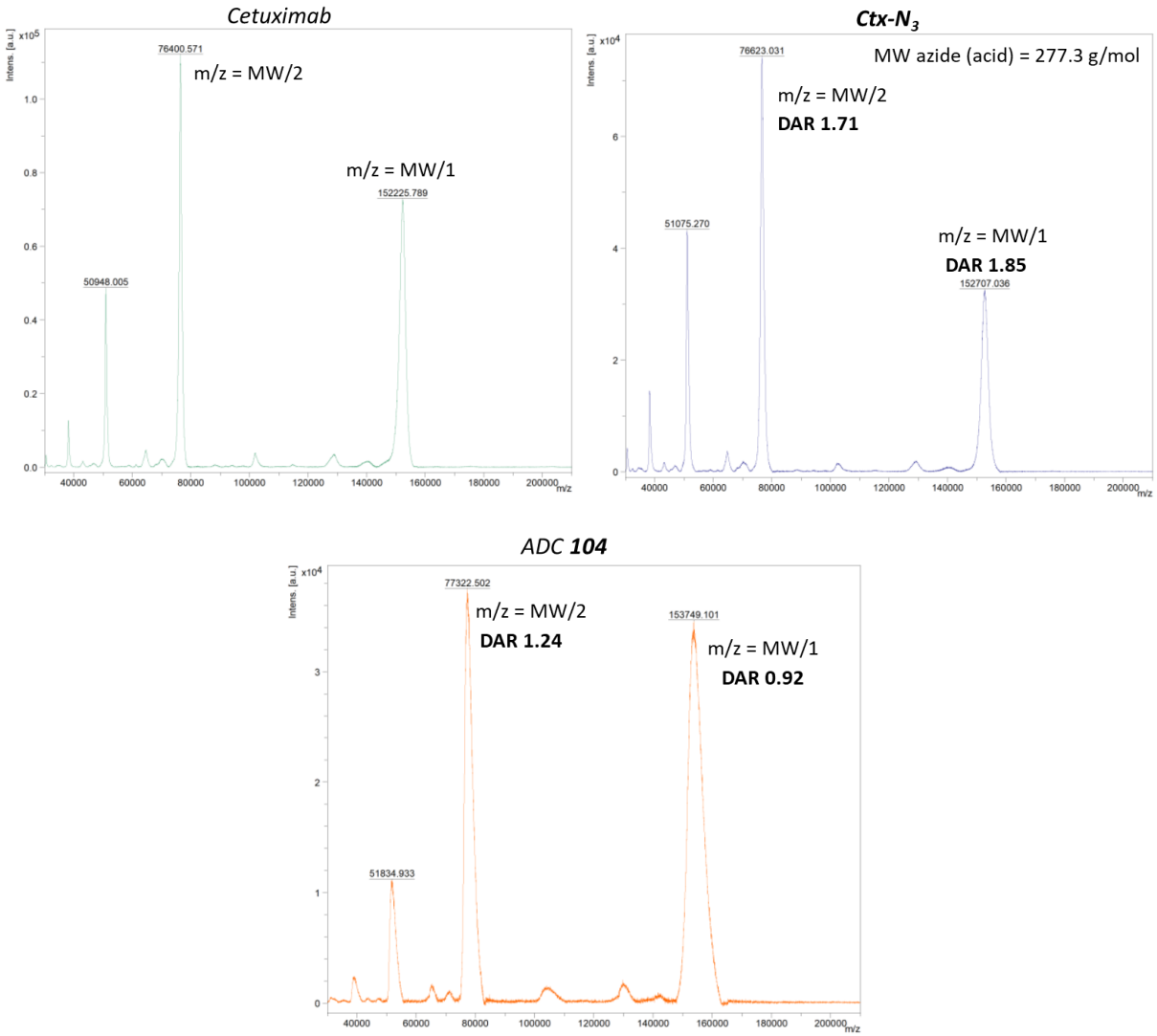

Figure 62. MALDI spectra of unconjugated Ctx, prefunctionalized **Ctx-N_3** and ADC **104**.

2.2.1.2. Preliminary biological evaluation of ADCs 100 and 102

The biological activity of ADCs **100** and **104** was evaluated in collaboration with Istituto per lo Studio, la Prevenzione e la Rete Oncologica (ISPRO) in Florence. Assays were performed on the A375 and SK-MEL-5 melanoma cell lines, both of which were selected due to their confirmed high expression of the EGFR antigen. Treatment with both ADCs resulted in a significant reduction in cell viability and proliferation, where the control groups, including the unconjugated Ctx, free Cyclopamine, and the unconjugated linker-payloads (**98** and **99**), had no effect compared to untreated cells. To confirm that the observed efficacy was indeed mediated by SMO inhibition and targeted delivery, Western blot analysis on A375 cells was performed. This confirmed that both ADCs successfully inhibited the key effectors of both signaling cascades: GLI1 and GLI2 (Hedgehog pathway) and p-EGFR (Tyr11739) and pERK1/2 (EGFR cascade). Additionally, ADC **100**

displayed a potent pro-apoptotic effect. Cell internalization of ADC **100** was evaluated, confirming the specific interaction with EGFR and subsequent internalization necessary for drug release. Finally, HPLC studies provided complementary data, validating that cyclopamine remains stable at pH 5.5, the acidic condition under which it is hypothesized to be released from the HMPO linker within the endolysosomal compartment.[407]

2.2.2. Synthesis of ProTide-enabled ADCs

The clinical application of numerous phosphate and phosphonate drugs is significantly limited by their negative charge, resulting in poor membrane permeability and reduced therapeutic efficacy.[395,396] Furthermore, drugs like Nucleoside Analogues (NAs) necessitate intracellular activation via phosphorylation, a metabolic process frequently compromised by the downregulation of key activating enzymes in drug-resistant tumor cells.[408] To circumvent these challenges, the ProTide technology was developed. The aim of this work is the first integration of ProTide technology with ADCs, establishing a novel platform for the targeted delivery of active, phosphorylated therapeutics. The core of this strategy lies in a specially designed ProTide linker that exploits the established enzymatic activation pathway (involving esterase and phosphoramidase cleavage) to release the active monophosphorylated drug directly inside the target cell (**Scheme 42**). Gemcitabine, a widely used nucleoside analogue, was selected as the model drug and was conjugated non-selectively to the lysine residues of Trastuzumab (an mAb targeting the HER2 receptor). This synthetic approach aimed to combine the high potency and metabolic advantage inherent to the ProTide system with the superior specificity and targeted internalization properties of the antibody, ultimately leading to enhanced therapeutic efficacy and reduced systemic toxicity.

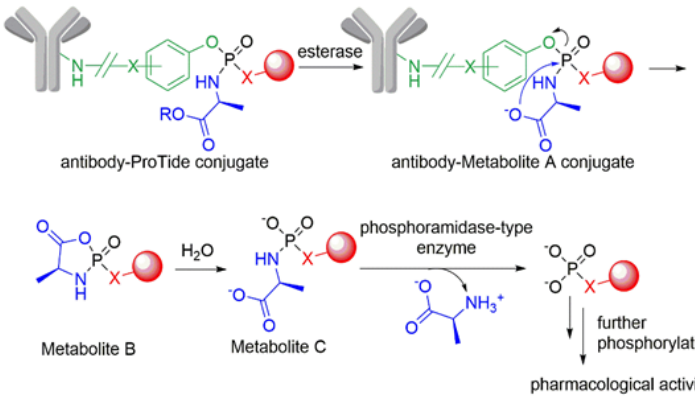

Scheme 42. Proposed release mechanism of phosphorylated nucleosides from antibody-ProTide conjugates.

2.2.2.1. Bioconjugation of ProTide systems charged with Gemcitabine

For the realization of the ADCs, two Gemcitabine-ProTide scaffolds, compounds **105** and **106**, were synthesized, each properly functionalized for bioconjugation to the lysine residues of Trastuzumab via stable amide bond formation. Compounds **105** and **106** were initially converted to the corresponding NHS-esters and subsequently reacted with Trastuzumab in a DMSO/PBS pH 7.4 mixture. The conjugation successfully afforded the expected ADCs (**107** and **108**, **Scheme 43**). The final bioconjugates were purified via dialysis. The DAR was determined by MALDI analysis, yielding an average DAR of 4.63 for ADC **107** and 3.84 for ADC **108** (**Figure 63**). Furthermore, an additional confirmation of the conjugation success was provided by UHPLC-MS analysis performed after extensive DTT-mediated disulfide reduction, with results highly consistent with the initial MALDI data.

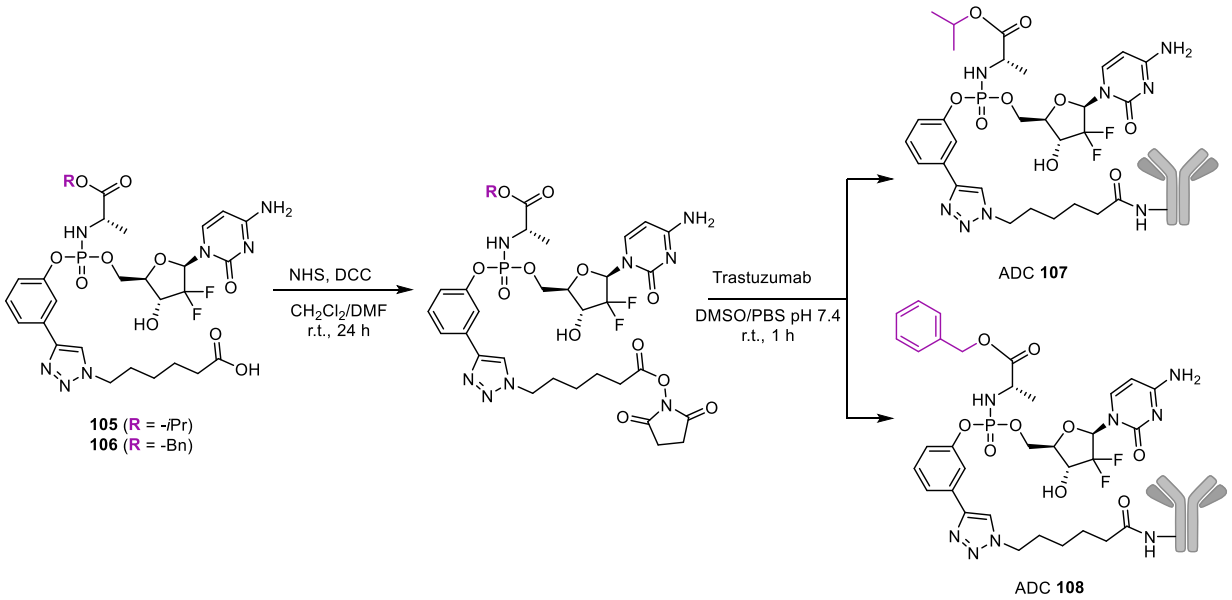

Scheme 43. Synthesis of ADCs **107** and **108**.

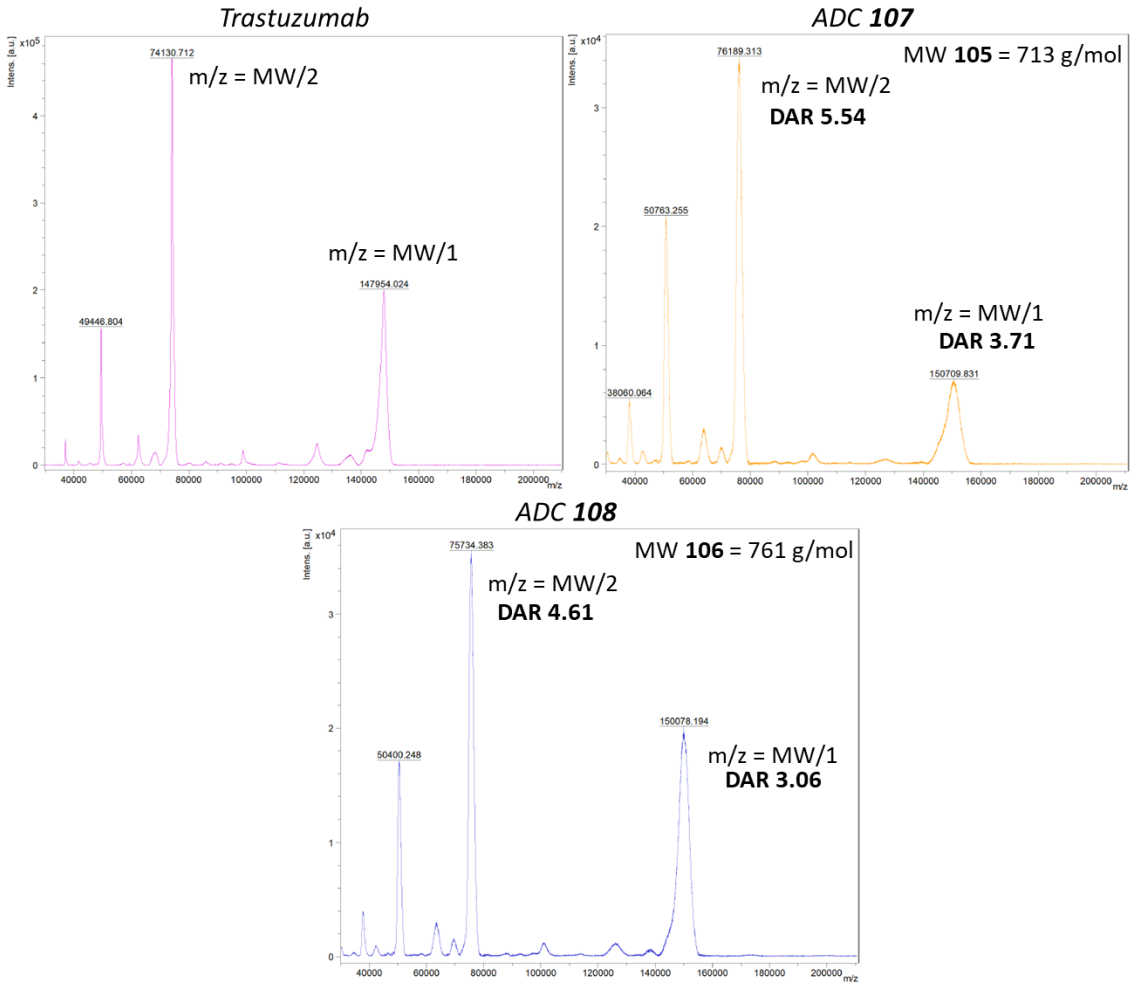

Figure 63. MALDI spectra of unconjugated Trastuzumab, ADC **107** and ADC **108**.

2.2.2.2. Preliminary biological evaluation of ADCs 107 and 108

To validate the crucial hypothesis that the enzymatic activation pathway of the ProTide system remains functional even after conjugation to the antibody, the *in vitro* metabolism of ADCs **107** and **108** was investigated. The ADCs were incubated with Carboxypeptidase Y (a functional analogue of lysosomal Cathepsin A), and the resulting formation of the active metabolite, Metabolite C (monophosphorylated Gemcitabine), was quantified over time using UHPLC/MRM-MS. The results confirmed a clear time-dependent release of Metabolite C from both ADCs, verifying that the enzymatic cleavage pathway is fully preserved post-conjugation. Furthermore, internalization of ADCs **107** and **108** into tumor cells was assessed by immunofluorescence on SKBR3 (human breast carcinoma) and MIA PaCa-2 (human pancreatic adenocarcinoma) cell lines. The data confirmed that the ErbB2 receptors were internalized following binding to the ADCs at a rate equal to that of the unconjugated Trastuzumab, demonstrating that conjugation did not compromise the crucial targeting mechanism. Finally, the two conjugates exhibited a superior

antiproliferative effect compared to the unconjugated Gemcitabine ProTide, thus confirming the enhanced therapeutic potential and successful targeted delivery achieved by these novel ProTide-enabled ADCs.[409]

2.2.3. Synthesis of ADCs charged with ERK inhibitors

The emergence of drug resistance in tumors, driven by cellular heterogeneity and the immunosuppressive Tumor Microenvironment (TME), is a critical clinical obstacle. M2-like Tumor-Associated Macrophages (TAMs), a key TME component, are known to facilitate both metastasis and drug resistance.[410] To overcome this, a promising strategy is to develop a targeted delivery system that simultaneously addresses both tumor cell malignancy and the cell-cell interactions within the TME. The Colony-Stimulating Factor 1 Receptor (CSF-1R) is an ideal dual therapeutic target, as it is expressed on both tumor cells and TAMs. For cancers like Malignant Mesothelioma (MM), tumorigenesis and resistance are dependent on Extracellular Signal-Regulated Kinases (ERK), which modulate inflammation, proliferation, and stem-like phenotypes.[411] Interestingly, one of the signalling pathways downstream of CSF-1R is ERK5, which is required for MM tumorigenesis and drug resistance. All these observations identify ERK5 as a potential target for innovative cancer treatment, although selective and effective targeting of ERK5 pathway remains elusive. The aim of this project is to use the ADC strategy, to produce an anti-CSF-1R-conjugated ERK5 inhibitor, XMD8-92, to suppress both TAMs renewal and mesothelioma cells growth, for dual-action therapy.

2.2.3.1. Bioconjugation of XMD8-92 to anti-CD115 antibody

For the synthesis of the proposed ADC the linker-payload system **109** has been synthesized, introducing on the ERK5 inhibitor XMD8-92 a non-cleavable linker suitable for the bioconjugation to the lysine residues of an anti-CD115 mAb. Compound **109** has a carboxylic moiety already activated as a NHS-ester that could be directly incubated with a solution of mAb in PBS (pH 8) at r.t. for 1 hour, providing the desired ADC **110** (**Scheme 44**). MALDI analysis of **110** confirmed the formation of the expected bioconjugate with an average DAR equal to 7.55 (**Figure 64**).

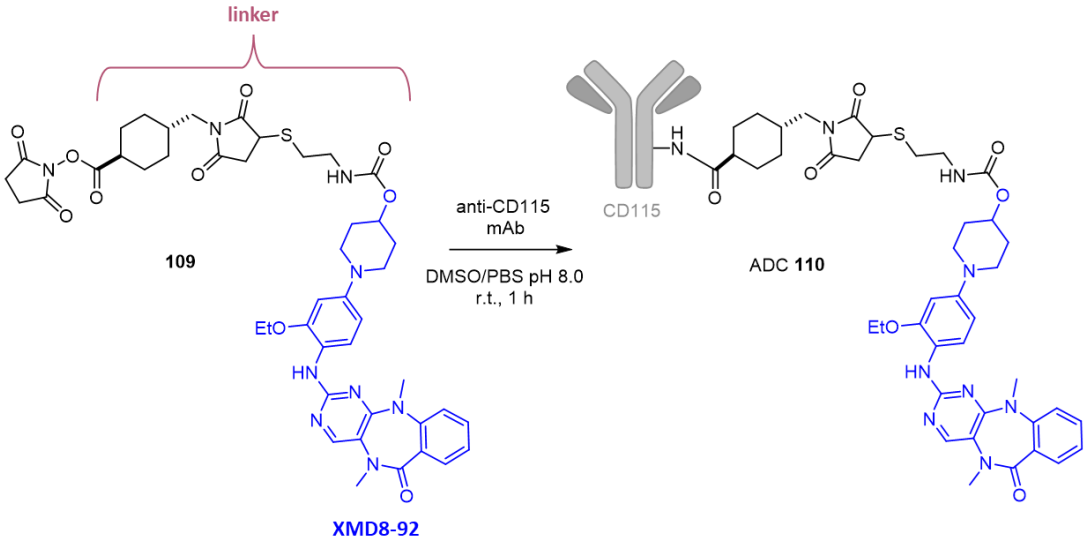

Scheme 44. Synthesis of ADC **110**.

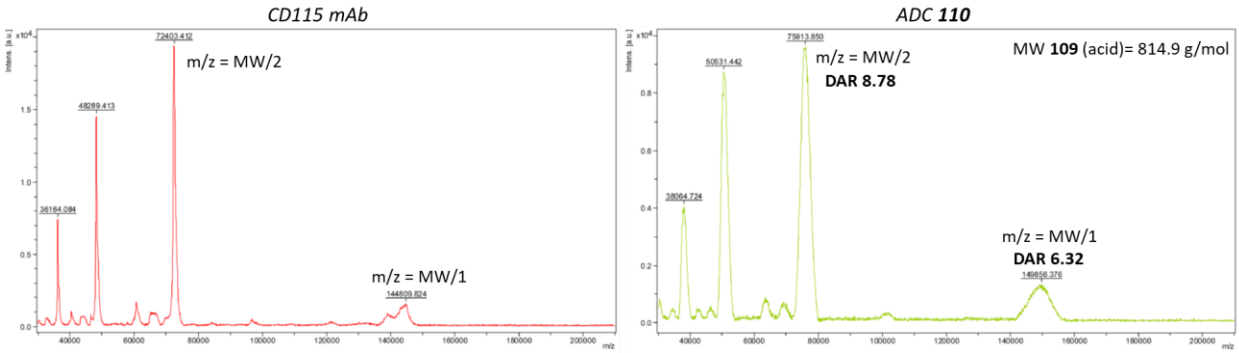

Figure 64. MALDI spectra of unconjugated mAb (left) and ADC **110** (right).

Additionally, a second ADC, **111**, was synthesized exploiting SPAAC click reaction. This process required two main steps. First, the linker-payload **109** was reacted with DBCO-amine to obtain the amide **112**. Simultaneously, the mAb was prefunctionalized by introducing the azide moiety onto the antibody's lysines, yielding the **CD115-N_3** bioconjugate. This initial bioconjugate was analyzed to have a DAR of 6.19. In the final step, a solution of the linker-payload **112** was added to the **CD115-N_3** bioconjugate, resulting in the ADC **111** (**Scheme 45**). MALDI analysis of ADC **111** confirmed the final product had a DAR of 3.81 (**Figure 65**).

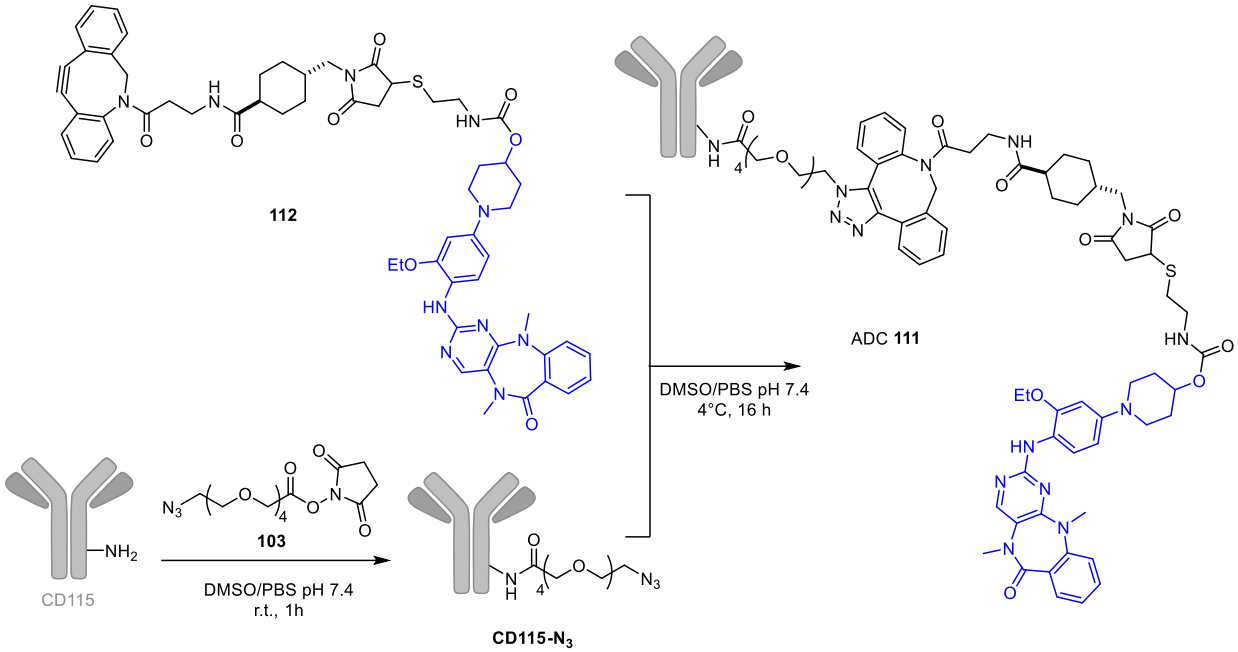

Scheme 45. Synthesis of ADC **111**.

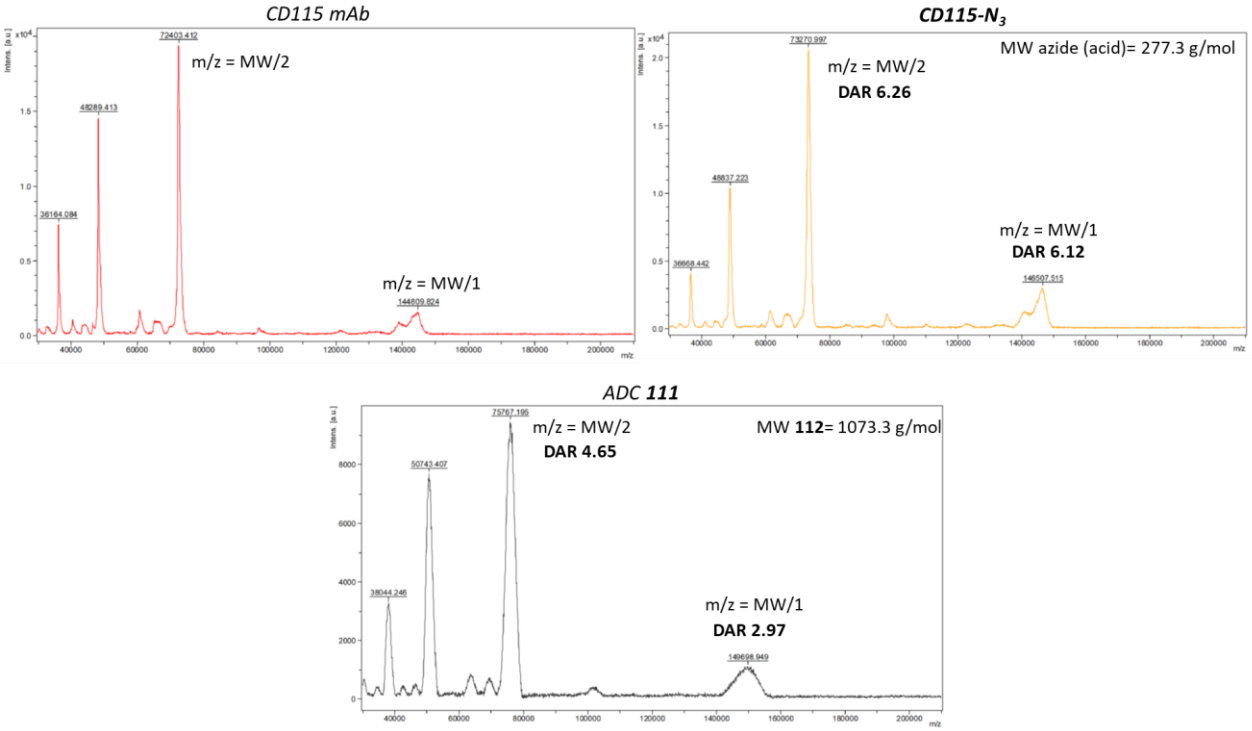

Figure 65. MALDI spectra of unconjugated mAb, **CD115-N_3** and ADC **111**.

2.2.3.2. Preliminary biological evaluation of ADC 111

Preliminary biological data provided encouraging results. The dual-targeting ADCs **110** and **111** exhibited superior anti-proliferative effects in MM (AB1) cells and tumor-associated macrophages TAMs compared to single-agent controls, with the higher DAR formulation proving most effective. ADCs successfully suppressed AB1 cell growth in colony assays, blocked G1/S progression, and significantly reduced TAM proliferation. Mechanistic studies confirmed the binding of ADCs to CSF-1R, its subsequent internalization and lysosomal processing in macrophages, and the release of XMD8-92. Crucially, treatment with the synthesized ADCs directly resulted in the inhibition of phosphorylated ERK5 (pERK5) in TAMs, validating its mechanism.

2.3. SYNTHESIS AND EVALUATION OF Hh AGONISTS FOR OSTEOGENIC APPLICATIONS

While Hh pathway inhibition is primarily known for its application in anticancer therapy, its activation holds significant potential for tissue regeneration and repair following severe injury. Small molecules that positively modulate the SMO receptor are proposed as therapeutic tools to stimulate tissue function, restore compromised repair mechanisms, and enhance engineered tissue implantation, given their ability to promote stem cell differentiation. Their notable osteoinductive activity, specifically the ability to increase bone mass, positions SMO agonists as attractive candidates for treating bone diseases like osteopenia and osteoporosis. Despite this potential, the scope of positive SMO modulators explored for regenerative medicine remains limited. To address this gap, our research group successfully developed and synthesized a novel class of quinolones that act as SMO agonists. Preliminary biological data confirmed their hypothesized osteoinductive activity, suggesting these compounds are potent novel osteogenic agents for multipotent mesenchymal cells and are of therapeutic interest for bone-related diseases. Building on these results, the aim of this project is to synthesize and biologically test these Hh agonists to rigorously evaluate their osteogenic ability on Mesenchymal Stem Cells (MSCs) and three-dimensional systems. This models, composed of multipotent progenitor cells capable of differentiating into osteoblasts, chondrocytes, and adipocytes, could provide crucial insight into the employment of these agonists as a promising tool in musculoskeletal therapies.

2.3.1. Synthesis of Hh agonists

As described in paragraph 1.3.2, GSA-10, compound **1**, and compound **2** were identified as the most promising Hh agonists, leading us to focus our investigation on their synthesis. **GSA-10** and compound **2** shared the initial synthetic steps: the formation of the 3-carboxyquinolone core was achieved by reacting aniline **113** with triethyl methanetricarboxylate under microwave (MW) irradiation, affording intermediate **114** in 65% yield (**Scheme 46**). For **GSA-10**, **114** was treated with aniline **115**, again under MW irradiation, providing the final product, **GSA-10**, in good 70% yield. For the synthesis of compound **2**, **114** was treated with *tert*-butyl 4-aminobenzoate obtaining **116** in 65% yield. Finally, the ester moiety of **116** was hydrolyzed with TFA to afford the corresponding acid, **2**, in excellent 92% yield (**Scheme 46)**.

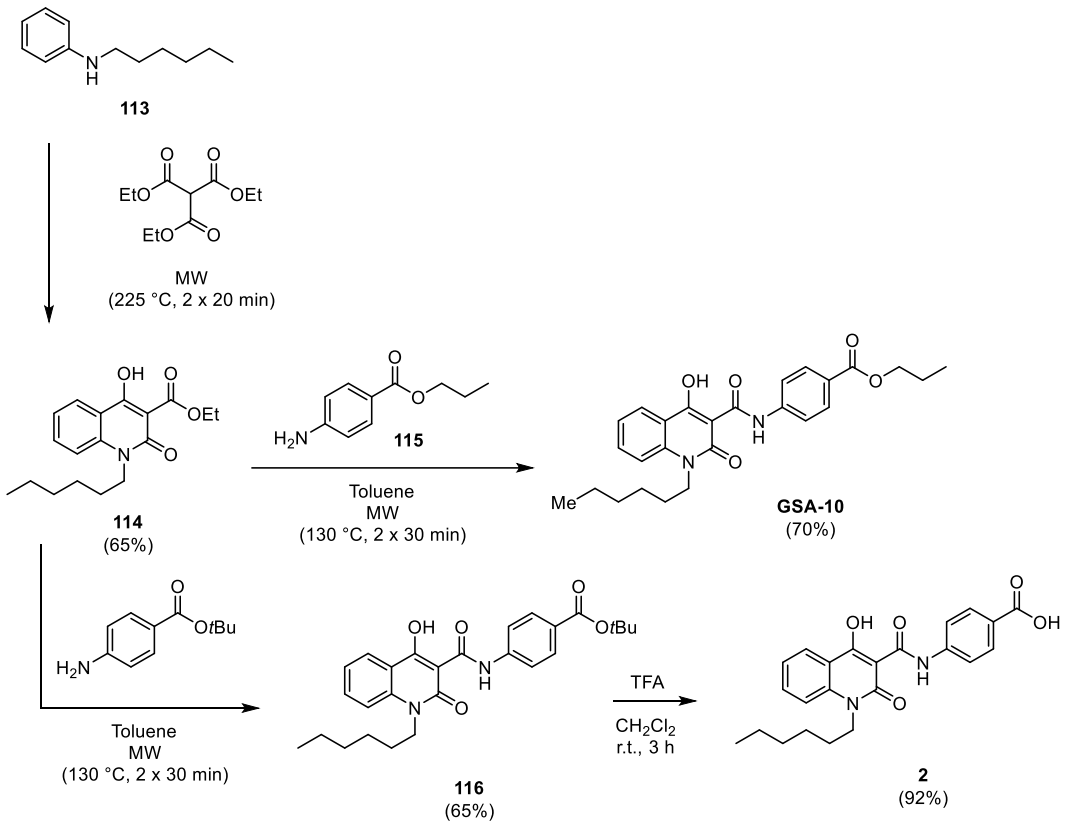

Scheme 46. Preparation of **GSA-10** and compound **2**.

For the synthesis of **1** the carboxylic acid **117** was converted into the corresponding ethyl ester in Fisher's conditions, affording **118** in excellent 92% yield (**Scheme 47**). The nitro group was reduced with $Pd(OH)_2/C$ and H_2, and the aniline obtained was directly treated with propionaldehyde under the same reductive conditions, forming **119** in 58% yield. The newly formed amine group of **119** was then functionalized by treatment with ethyl 3-chloro-3-oxopropanoate, providing the amide intermediate **120** in good 78% yield. An intramolecular cyclization was subsequently achieved by treating compound **120** with NaH, affording the quinolone **121** in 78% yield. Finally, **121** was treated with aniline **122** under MW irradiation, obtaining the desired product **1** in 48% yield.

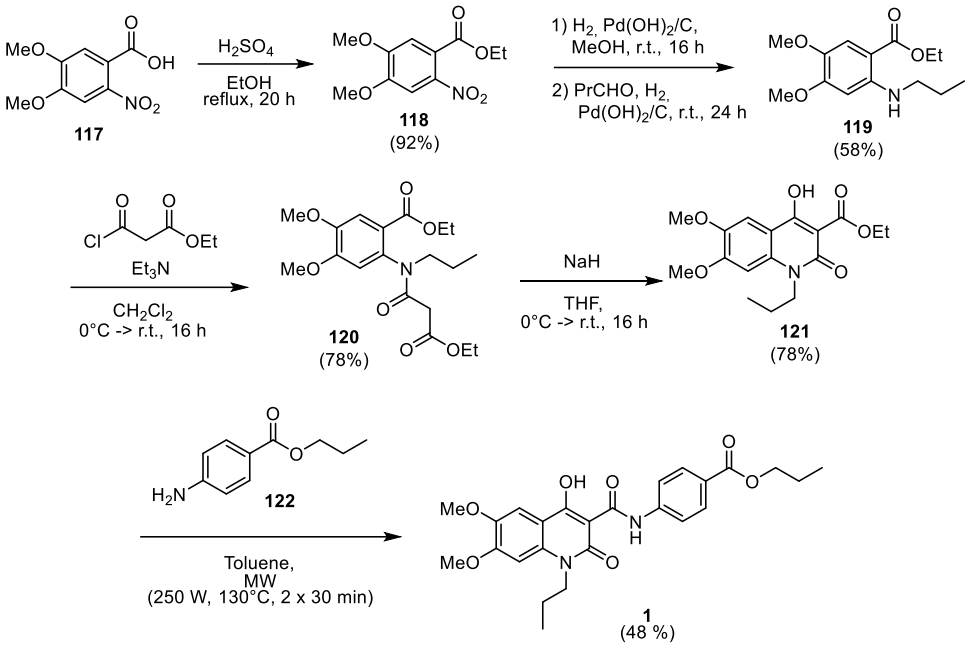

Scheme 47. Preparation of compound **1**.

2.3.2. Evaluation of compounds GSA-10, 1 and 2 on MSCs

Following the successful synthesis of the target Hh agonists, **GSA-10**, compound **1**, and compound **2**, their osteogenic potential was evaluated using bone marrow-derived MSCs (BM-MSCs). The investigation focused on determining whether SMO receptor activation enhances osteoblast differentiation and subsequent calcium deposition *in vitro*. All assays were performed in collaboration with Prof. Renieri's research group at the University Hospital of Siena.

MSCs Isolation and characterization

BM-MSCs were isolated from three human donors (Orthopedic Unit, University Hospital of Siena) after informed consent. Cells were expanded to passage 3 (P3) and characterized prior to differentiation experiments. MSC identity was confirmed via immunofluorescence staining for the characteristic positive cell-surface markers CD73, CD90, and CD105, as mandated by the International Society for Cell Therapy (ISCT). Phalloidin staining was used to visualize actin filaments, and DAPI stained cell nuclei. The confirmed co-expression of these markers, alongside a typical fibroblast-like morphology, ensured that the isolated population was free from hematopoietic or fibroblastic contamination (**Figure 66**).

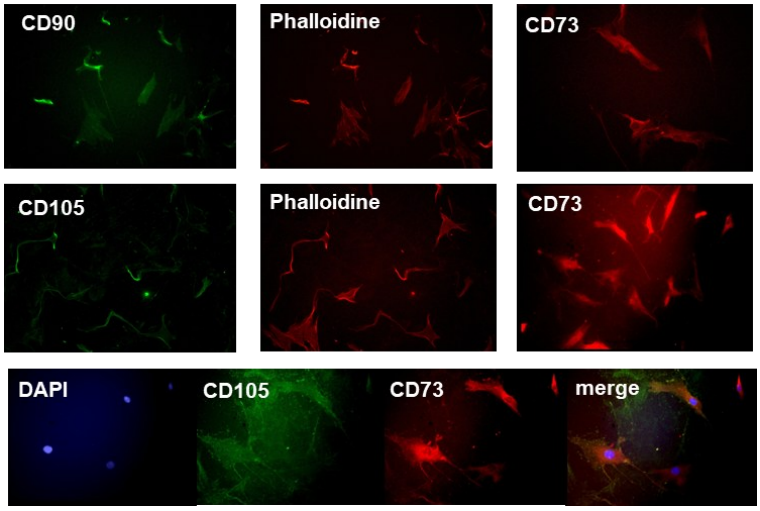

Figure 66. MSCs characterization via immunofluorescence staining to detect cell-surface markers, according to ISCT.

Validation of osteogenic differentiation model

To validate the cellular model, MSCs were subjected to standard osteogenic differentiation medium for up to 35 days. Successful differentiation was confirmed by Alizarin Red S (ARS) staining, which selectively binds to calcium salts deposited in the extracellular matrix. Quantitative ARS analysis measured time-dependent mineralization, showing substantial calcium deposition between days 21 and 35, confirming the efficacy of the differentiation medium and the suitability of the model (**Figure 67**).

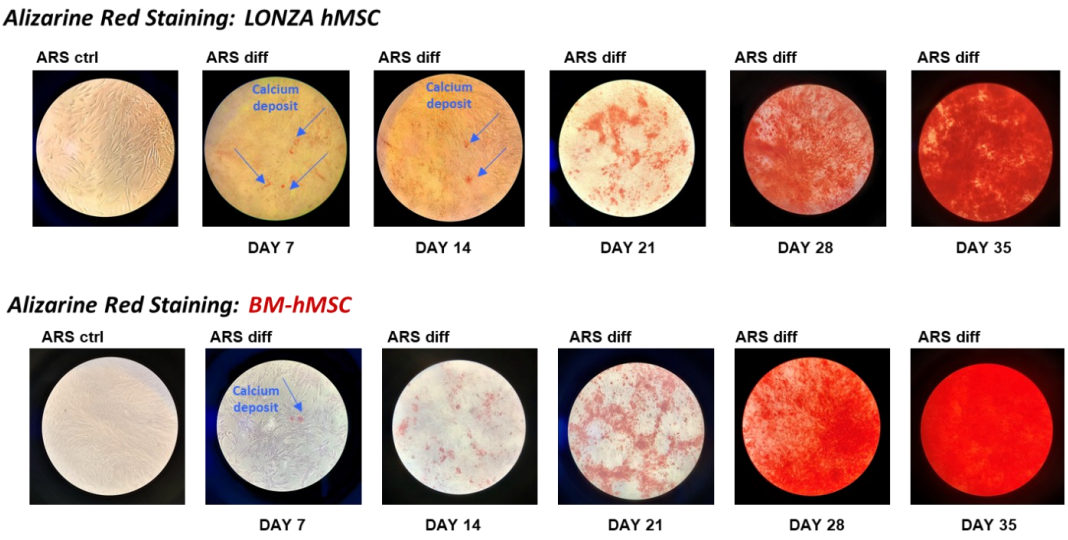

Figure 67. ARS assay of commercial LONZA hMSCs and patient-derived BM-hMSC. The blue arrow show the visible calcium deposits.

ARS assay on MSCs treated with Hh agonists

MSC cultures were subsequently treated with the SMO agonists SAG, **GSA-10**, compound **1**, and compound **2**. Initial screening utilized a 10 µM concentration, which was later adjusted to 3 µM to prevent cytotoxic effects. The assay showed visible calcium accumulation and mineralized matrix deposition (**Figure 68**).

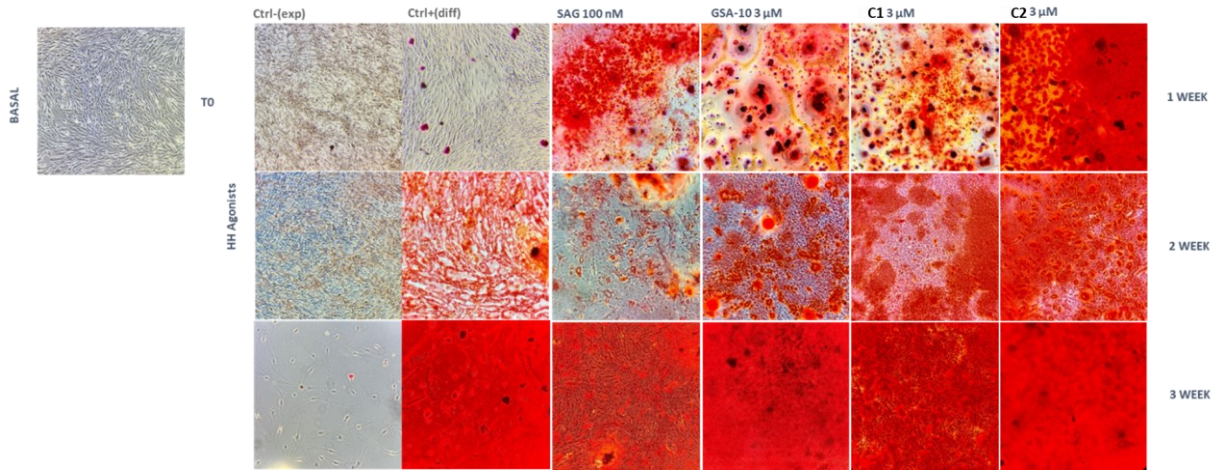

Figure 68. ARS assay of patient-derived BM-hMSCs treated with Hh agonists SAG, **GSA-10**, **1** (C1) and **2** (C2).

Hh agonist testing and pathway activation

Successful pharmacological activation of SMO was verified by real-time polymerase chain reaction (RT-qPCR) analysis of the canonical Hh pathway downstream targets, PTCH1 and GLI1 after 48 h and 21 days (**Figure 69**). The hypothesis is that enhanced Hh signaling promotes the expression of osteogenic genes (such as RUNX2 and COL1A1) and accelerates bone matrix formation.

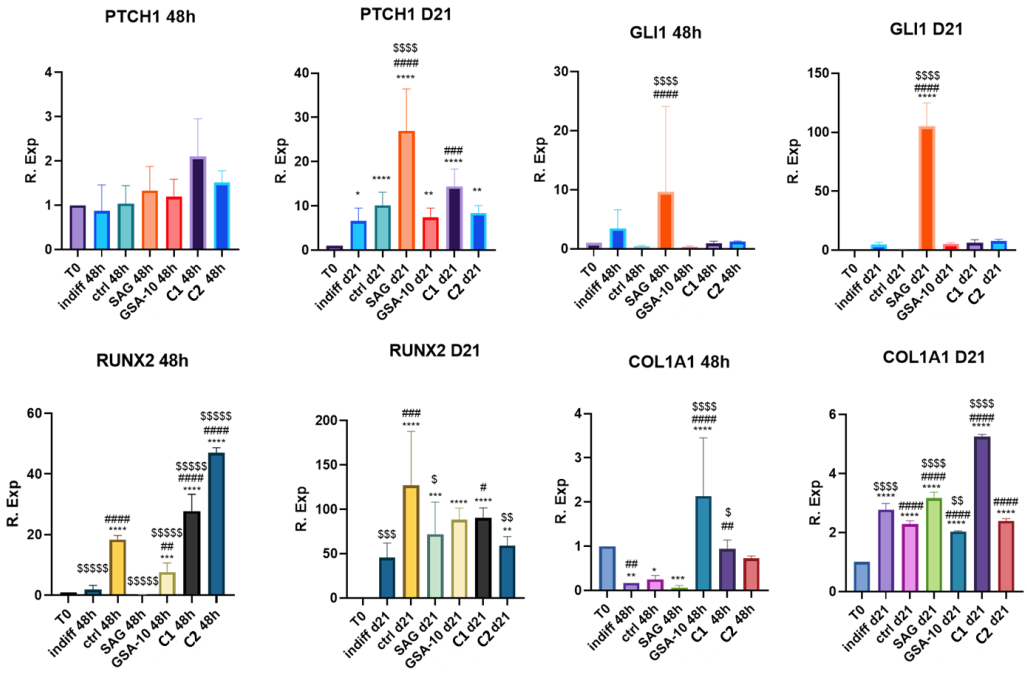

Figure 69. RT-qPCR of canonical Hh targets (PTCH1 and GLI1) and of osteogenic genes (COL1A1 and RUNX2).

SAG robustly increased GLI1 expression, confirming canonical pathway activation. However, the quinolone derivatives often produced stronger osteogenic outcomes despite weaker canonical transcriptional activation. This observation aligns with emerging evidence that Hh signalling is not binary but tunable and that distinct SMO conformations may bias downstream outputs.

Evaluation of early osteogenic commitment

To quantify the early osteogenic activity induced by the agonists, an Alkaline Phosphatase (ALP) activity assay was performed. The ALP assay quantifies the enzymatic conversion of a colorimetric substrate, correlating with the upregulation of ALP during the initial phases of osteoblast differentiation. Elevated ALP activity after treatment with the SMO agonists provided biochemical evidence that Hh pathway activation successfully facilitates osteogenic maturation, thus demonstrating increased enzymatic activity, suggesting enhanced osteogenic commitment (**Figure 70**).

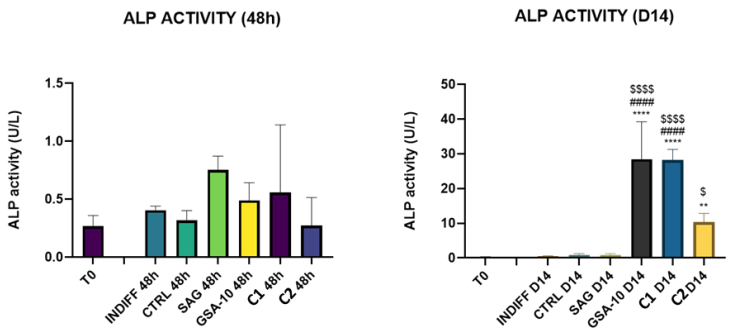

Figure 70. ALP assay after 2 and 14 days, showing significant results after the treatment with **GSA-10**, compound **1** (C1) and compound **2** (C2).

Evaluation of osteogenic potential in 3D scaffold systems

The transition from 2D *in vitro* cultures to 3D scaffold systems is a fundamental step in evaluating the translational potential of new osteoinductive molecules. The osteogenic effects of Hh signalling activation were further investigated using 3D scaffold-based constructs. Specifically, when hMSCs were cultured on Poly(ε-caprolactone) (PCL) 5:1 scaffolds (RegenLab) and treated with Hh agonists SAG, **GSA-10**, **1** and **2**, the results of the ARS assay successfully mirrored the promising outcomes observed in 2D cultures (**Figure 71**). The treated constructs exhibited homogeneous mineral deposition throughout the structure, significantly improved organization of the extracellular matrix (ECM) and enhanced spatial distribution of the mineralized matrix. These findings are particularly significant as many osteoinductive strategies lose efficacy within the diffusion-limited environments characteristic of 3D systems. The persistence of Hh-mediated osteogenesis under these constraints underscores the biological robustness of the pathway and highlights the clinical potential of these quinolone-based derivatives for bone tissue engineering applications.

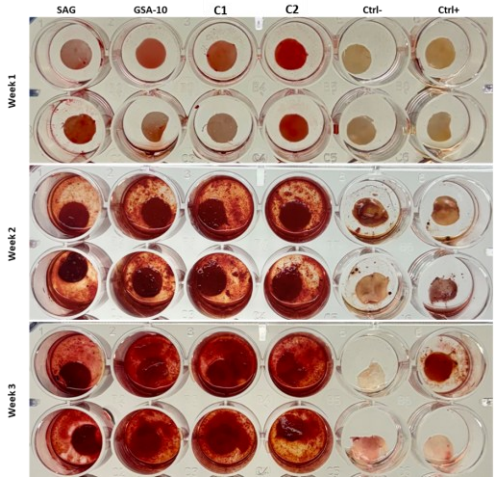

Figure 71. ARS assay performed on PCL 5:1 scaffolds treated with SAG, **GSA-10**, **1** (C1) and **2** (C2).

CHAPTER 3. CONCLUSIONS

The first section of this thesis was based on the design, synthesis, and application of novel Antibody-Drug Conjugates. The research presented herein was driven by the goal of enhancing the therapeutic potential of promising small molecule inhibitors by leveraging the specificity of monoclonal antibodies, while simultaneously advancing the fundamental methodologies of bioconjugation.

A primary focus of this research has been the development of innovative ADCs charged with our in-house developed Hh signalling pathway inhibitors. Recognizing the therapeutic promise of these potent compounds, which was hampered by suboptimal PK profiles, we successfully integrated them into an ADC platform. This endeavor involved the strategic chemical modification of the Hh inhibitors to allow for linker attachment, the synthesis and evaluation of various linker technologies, including both cleavable and non-cleavable systems, and their final conjugation to a selected monoclonal antibody. The challenges encountered and overcome during this process have provided valuable insights into the critical interplay between payload, linker, and antibody in designing a successful ADC. In the end, four ADCs have been successfully synthesized (**Scheme 48**). Looking ahead, these results open up several perspectives for future research. ADCs **95** and **96** showed promising preliminary biological results, with IC_{50} values in the nanomolar range (37.58 nM for **95** and 109.7 nM for **96**) and a significant induction of early and late apoptosis. Nevertheless, the novel ADCs developed need further *in vitro* and *in vivo* evaluation to fully assess their therapeutic efficacy and safety. This evaluation process is under development in collaboration with Dr. Barbara Stecca at Istituto per lo Studio, la Prevenzione e la Rete Oncologica (ISPRO) in Florence.

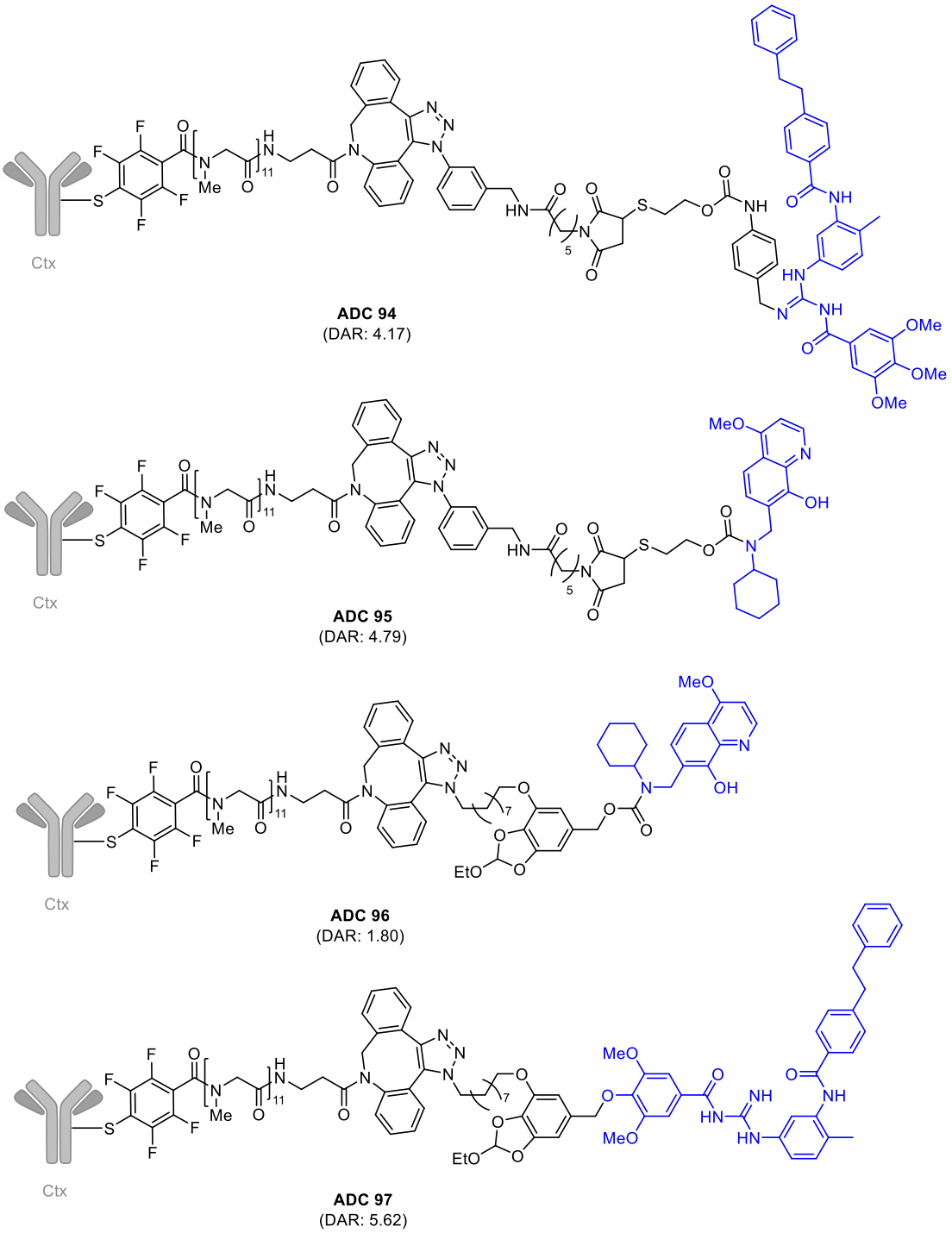

Scheme 48. Structures of ADCs charged with Hh inhibitors synthesized. Payload in blue.

In parallel to the development of Hh inhibitor-based ADCs, novel chemical strategies for the stable and efficient linkage of payloads to antibodies have systematically been explored and optimized. This investigation was not confined to a single class of therapeutic agents but was extended to a variety of linker-payload systems aimed at different cellular targets and employing diverse mechanisms of action. In particular, the natural alkaloid cyclopamine, two different Gemcitabine-ProTide scaffolds, and ERK inhibitor XMD8-92 have been bioconjugated (**Scheme**

49). This approach has allowed us to build a versatile and robust ADC technology platform, adaptable for the targeted delivery of a wide range of therapeutic agents.

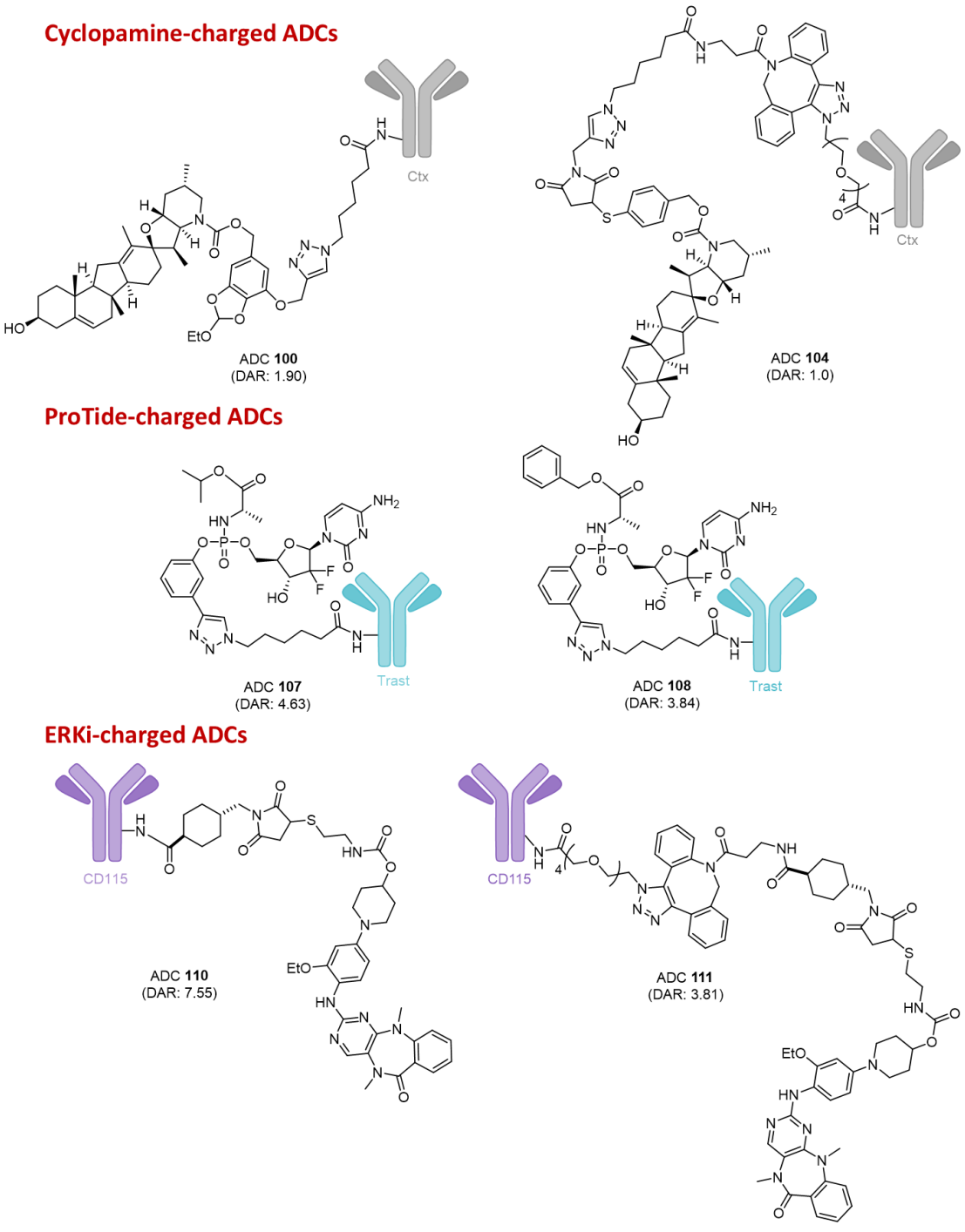

Scheme 49. ADCs synthesized charged with cyclopamine, ProTide systems and ERK inhibitors.

Furthermore, this research has acknowledged the complex and dualistic nature of the Hh signalling pathway, aiming to deepen our understanding of its role beyond oncology. Our previously developed compounds (**GSA-10**, compound **1** and compound **2**) have been furtherly studied and evaluated for their potential application in regenerative medicine, specifically for their osteogenic capabilities. The preliminary steps taken towards understanding the role of Hh pathway agonists in osteogenesis set the stage for a new research direction in this understudied field.

CHAPTER 4. EXPERIMENTAL PART

4.1. SYNTHESIS OF NEW ADCs CHARGED WITH Hh INHIBITORS

4.1.1. General experimental procedures, materials and instruments

All reagents were used as purchased from commercial suppliers without further purification. The reactions were carried out in oven dried vessels. Solvents were dried and purified by conventional methods prior use or, if available, purchased in anhydrous form.

Flash column chromatography was performed with Merck silica gel Å 60, 0.040-0.063 mm (230-400 mesh). MPLC Syncore Büchi on highly resistant PP cartridges Normal Phase silica gel NP 40 - 63 µm particle size and 60 Å pore size (Si60) withstand a maximum pressure of 10 bar (145 psi) column with PE (Eluent A) and EtOAc (Eluent B) as mobile phase. Merck aluminum backed plates pre-coated with silica gel 60 (UV254) were used for analytical thin layer chromatography and were visualized by staining with a $KMnO_4$ or Ninidrine solution.

NMR spectra were recorded at 25 °C or at 37 °C with 400 or 600 MHz for 1H and 101 or 151 MHz for 13C Brücker Advance NMR spectrometers. The solvent is specified for each spectrum. Splitting patterns are designated as s, singlet; d, doublet; t, triplet; q, quartet; m, multiplet; bs, broad singlet. Chemical shifts (δ) are given in ppm relative to the resonance of their respective residual solvent peaks.

High and low resolution mass spectroscopy analyses were recorded by electrospray ionization with a mass spectrometer Q-exactive Plus.

HPLC analyses were performed on a LC/MSD system Agilent InfinityLab LC/MSD iQ, Column: InfinityLab PoroShell 120 EC-C18 2.1 x 50mm x 2.7µm. Flow: 0.4 mL/min. Eluent A/B: H_2O/MeCN. Gradient: 5% B to 95% B in 10 minutes, 4 minutes at 95 % B and 3 minutes of re-equilibration. Detection: 254 nm and 210 nm

HIC analyses were performed on a HPLC system Agilent 1260 Infinity II, Column: TSKgel Butyl-NPR 4.6 mm x 35 mm, P/N 14947 4.6 x 35 mm. Flow: 0.8 mL/min. Eluent A: $Na_2HPO_4{\cdot}2H_2O$ 50 mM pH 7, Eluent B: $(NH_4)_2SO_4$ 2 M/ $Na_2HPO_4{\cdot}2H_2O$ 50 mM pH 7, Eluent C: IPA . Gradient: A/B/C 27.5/70/2.5 to A/B/C 38.8/55/6.2 in 2 minutes, to A/B/C 75/0/25 in 10 minutes, A/B/C 75/0/25 for 2 minutes, to A/B/C 75/0/25 in 3 minutes. Detection: 260 nm and 280 nm. Commercially available ADC brentuximab vedotin (Adcdetris®) was used as control.

MALDI analysis were performed on a Brucker UltrafleX/TOF in linear mode, voltage polarity Pos. Samples preparation: the matrix solutions were prepared at two different concentrations, and both were used in parallel. 20.0 mg or 25 mg of Super DHB were dissolved in a solution of MeCN (150 µL), H_2O (350 µL) and TFA (0.05 µL) and deposited in a stainless-steel target placed in a termoblock set at 39 °C. When the sample was dried, 1.65 µL of matrix solution was added and once completely dried and crystalized, the target plate was removed from the thermoblock. The target plate was analyzed with MALDI-TOF set in linear mode at 83% of laser intensity. The *m/z* range was from 30 kDa to 200 kDa. For each sample spot, 10 shots were acquired to improve the spectra quality and mass accuracy.

SK-MEL-5 cell line was kindly provided by Dr. Laura Poliseno (CRL-ISPRO, Pisa, Italy). Cells were cultured in Dulbecco's modified Eagle's medium (DMEM) (Euroclone, Milan, Italy) with 10% fetal bovine serum (FBS), 1% Penicillin-Streptomycin, and 1% Glutamine (Lonza, Basel, Switzerland).

4.1.2. Synthetic procedures

_N_-(2-methyl-5-(3-(3,4,5-trimethoxybenzoyl)thioureido)phenyl)-[1,1'-biphenyl]-4-carboxamide hydrochloride (21)

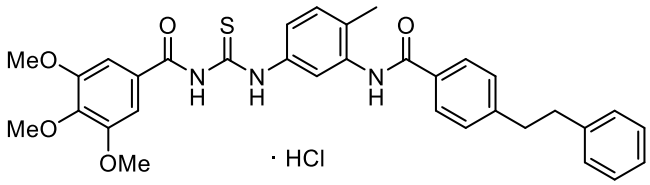

The product was prepared according to the literature.[373]

^{1}H NMR (400 MHz, DMSO-d_6, δ ppm, *J* Hz): δ 11.00 (s, 1H), 9.12 (s, 1H), 8.80 (s, 1H), 7.70-7.00 (m, 12H), 6.87 (s, 2H), 3.96 (s, 9H), 2.10 (s, 3H).

^{13}C NMR (101 MHz, DMSO- d_6, δ ppm): δ 180.4, 166.5, 164.3,156.9, 142.6, 142.1, 142.0, 140.4, 136.7, 135.4, 128.8, 128.7, 126.8, 125.6, 121.1, 118.7, 110.1, 61.2, 57.6, 20.1.

ESI: m/z 556 $[M+H]^+$

(4-azidophenyl)methanol (32)

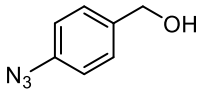

4-Aminobenzyl alcohol (3 g, 24.35 mmol) was dissolved in a solution of H_2SO_4 2 M (20 mL) at 0 °C and to the resulting mixture, a solution of $NaNO_2$ (2.52 g, 36.52 mmol) in H_2O (10 mL) was added. The reaction was stirred at 0 °C for 15 min and a H_2O solution (10 mL) of NaN_3 (2.36 g, 36.52 mmol) was added dropwise. The mixture was stirred at r.t. in the dark for 1 h. The crude was extracted with Et_2O (2 x 30 mL). The combined organic layers were washed with HCl 1 N (20 mL), H_2O (20 mL) and brine (30 mL), dried over anhydrous Na_2SO_4, filtered, and concentrated under reduced pressure to provide compound **32** (3.55 g, 23.86 mmol, 98% yield) as a yellow oil without further purification.

^{1}H NMR (400 MHz, Chloroform-*d*$_1$, δ ppm, *J* Hz): δ 7.42 (d, *J* = 8.0, 2H), 6.97 (d, *J* = 8.0, 2H), 4.57 (s, 2H), 1.87 (bs, 1H).

^{13}C NMR (101 MHz, Chloroform-*d*$_1$, δ ppm): δ 139.01, 137.45, 128.36, 118.88, 64.05.

1-azido-4-(bromomethyl)benzene (33)

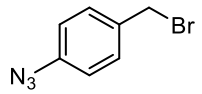

Compound **32** (1.7 g, 11.4 mmol) was dissolved in CH_2Cl_2 (25 mL) at 0 °C and PBr_3 (1.3 mL, 13.7 mmol) was added dropwise. The resulting solution was stirred at r.t. for 30 min. The crude was quenched with Na_2CO_3ss (25 mL). The phases were separated, and the aqueous phase was extracted with CH_2Cl_2 (3 x 30 mL). The combined organic layers were dried over anhydrous Na_2SO_4, filtered, and concentrated under reduced pressure to provide compound **33** (2.05 g, 9.7 mmol, 85% yield) as a bright orange oil without further purification.

^{1}H NMR (400 MHz, Chloroform-*d*$_1$, δ ppm, *J* Hz): δ 7.33 (d, J = 8.0, 2H), 6.95 (d, J = 8.0, 2H), 4.42 (s, 2H).

2-(4-azidobenzyl)isoindoline-1,3-dione (34)

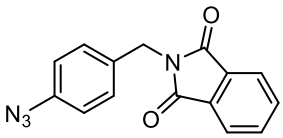

The bromide **33** (1.8 g, 8.5 mmol) was solubilized in dry DMF (15 mL), under N_2, and phthalimide (1.25 g, 8.5 mmol) and K_2CO_3 (2.35 g, 17 mmol) were added at r.t. The reaction was heated at 80 °C for 16 h. After completion of the reaction, the mixture was cooled to r.t. and filtered on a Büchner funnel to remove precipitated salts. The residue was dissolved in CH_2Cl_2 (20 mL) and washed with H_2O (2 x 20 mL) and $NaCl_{SS}$ (20 mL). The organic phase was dried over anhydrous Na_2SO_4, filtered, and concentrated under reduced pressure. The phthalimide derivative **34** was purified by means of flash chromatography on silica gel eluting 0-60% gradient of EtAOc in petroleum ether (2.2 g, 8.1 mmol, 81% yield).

^{1}H NMR (400 MHz, Chloroform-*d_1*, δ ppm, *J* Hz): δ 7.82 (dd, *J* = 5.6, 3.1 Hz, 2H), 7.68 (dd, *J* = 5.6, 3.1 Hz, 2H), 7.41 (d, *J* = 8.2 Hz, 2H), 6.94 (d, *J* = 8.4 Hz, 2H), 4.79 (s, 2H).

(4-azidophenyl)methanamine (22)

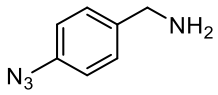

The phthalimide derivative **34** (2.2 g, 8 mmol) and hydrazine monohydrate (1.2 mL, 24 mmol) were solubilized in EtOH (25 mL). The reaction mixture was carried out at reflux for 4 h and was concentred under vacuum after cooled at r.t. The residue was diluted in EtOAc (15 mL), filtered on a Buchner funnel. The organic layer was dried over anhydrous Na_2SO_4, filtered, and concentrated under reduced pressure to provide the desired compound **22** as orange solid (955 mg, 6.45 mmol, 81% yield).

^{1}H NMR (400 MHz, Chloroform-*d_1*, δ ppm, *J* Hz): δ 7.26 (d, *J* = 8.0, 2H), 6.95 (d, *J* = 8.0, 2H), 3.80 (s, 2H), 1.91 (bs, 2H).

^{13}C NMR (101 MHz, Chloroform-*d_1*, δ ppm): δ 137.85, 134.61, 129.37 (2C), 118.65 (2C), 31.33.

(*E*)-*N*-(*N*'-(4-azidobenzyl)-*N*-(4-methyl-3-(4-phenethylbenzamido)phenyl)carbamimidoyl)-3,4,5-trimethoxybenzamide (35)

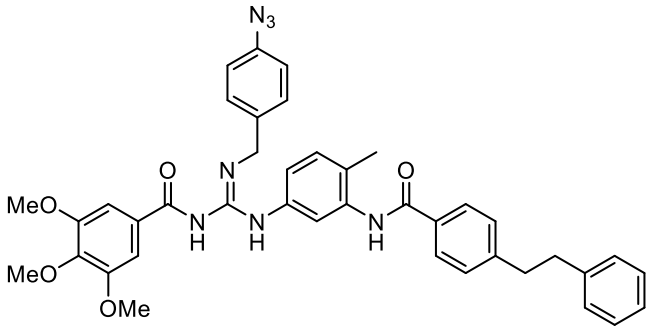

The thiourea **21** (574 mg, 1.03 mmol) and the benzyl amine **22** (153 mg, 1.03 mmol) were solubilized in dry DMF (10 mL), and Et_3N (287 µL, 2.06 mmol) and $HgCl_2$ (280 mg, 1.03 mmol) were added at 0 °C. The mixture was stirred at r.t. for 16 h and was concentered under reduced pressure. The residue was diluted in EtOAc (30 mL) and washed with H_2O (2 x 40 mL) and brine (30 mL). The organic layer was dried over anhydrous Na_2SO_4, filtered and concentrated under reduced pressure. Product **35** was purified by flash chromatography on silica gel eluting 0-5% gradient of MeOH in CH_2Cl_2 (629 mg, 0.94 mmol, 91% yield).

^{1}H NMR (400 MHz, Chloroform-*d*$_1$, δ ppm, *J* Hz): 12.01 (bs, 1H), 9.26 (bs, 1H), 7.98-7.91 (m, 6H), 7,68 (d, *J* = 8.4, 2H), 7.60 (d, *J* = 8.0, 1H), 7.49 (s, 2H), 7.45 (d, *J* = 8.0, 2H), 7.40 (t, *J* = 7.6, 1H), 7.24 (t, *J* = 4.0, 2H), 6.97 (s, 2H), 4.66 (s, 2H), 3.84 (s, 3H), 3.79 (s, 6H), 2.28 (s, 3H).

ESI: *m/z* 670 $[M + H]^+$.

(*E*)-*N*-(*N*'-(4-aminobenzyl)-*N*-(4-methyl-3-(4-phenethylbenzamido)phenyl)carbamimidoyl)-3,4,5-trimethoxybenzamide (20)

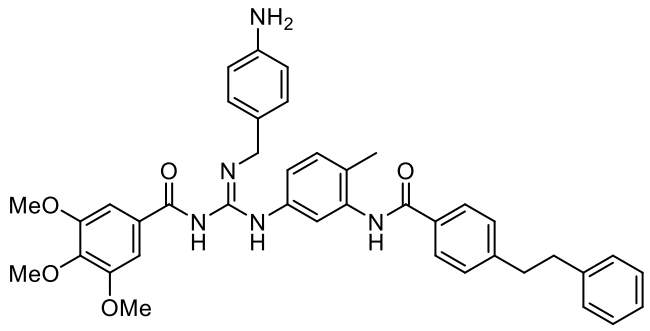

The azide **35** (90 mg, 0.13 mmol) was solubilized in CH_2Cl_2 (5 mL), and $P(Me)_3$ (400 µL, 3.2 mmol) and H_2O (7 µL, 3.2 mmol) were added. The mixture was stirred at r.t. for 16 h. The crude was

concentrated under vacuum and the product **20** was achieved by precipitation with PE:Et_2O 3:1 (20 mL)(51 mg, 0.08 mmol, 60% yield).

^{1}H NMR (400 MHz, Chloroform-*d_1*, δ ppm, *J* Hz): 12.07 (bs, 1H), 7.94 (d, *J* = 8.0, 2H), 7.71 (d, *J* = 4.0, 4H), 7.63-7.49 (m, 6H), 7.41 (d, *J* = 5.2, 2H), 7.23 (d, *J* = 5.6, 1H), 7.20 (d, *J* = 6.0, 1H), 6.62 (d, *J* = 7.2, 2H), 4.63 (s, 2H), 3.88 (s, 9 H), 2.33 (s, 3H).

ESI: *m/z* 644 $[M + H]^+$, 666 $[M + Na]^+$.

1-(prop-2-yn-1-yl)-1*H*-pyrrole-2,5-dione (36)

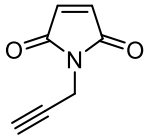

Maleic anhydride (700 mg, 7.14 mmol) and propargylamine (0.5 mL, 7.85 mmol) were dissolved in glacial acetic acid (14 mL) and stirred at r.t. for 16 h. The reaction mixture was concentrated under reduced pressure, the resulting residue was suspended in acetic anhydride (5 mL) and NaOAc (311 mg, 3.57 mmol) was added. The reaction vessel was heated at 65 °C for 2 h. After cooling to r.t., the reaction mixture was diluted in H_2O (70 mL) and extracted with Et_2O (3 × 100 mL). The combined organic phases were dried over Na_2SO_4, filtered, and evaporated under vacuum. Compound **36** was purified via chromatography on silica gel eluting 0-50 % gradient of EtOAc in PE, and obtained as a transparent oil (582 g, 4.28 mmol, 60% yield).

^{1}H NMR (400 MHz, Chloroform-*d_1*, δ ppm, *J* Hz) δ 6.66 (s, 2H), 4.12 (s, 2H), 2.13 (s, 1H).

3-((2-hydroxyethyl)thio)-1-(prop-2-yn-1-yl)pyrrolidine-2,5-dione (19)

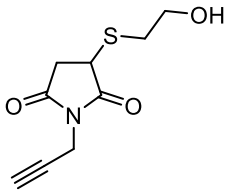

Compound **36** (1.39 g, 10.3 mmol) was solubilized in MeCN (40 mL) and 2-mercaptoethanol (1.44 mL, 20.6 mmol) was added dropwise. The reaction mixture was stirred at r.t. for 16 h. Product **19** was purified via chromatography on silica gel eluting 0-100 % gradient of EtOAc in PE, and obtained as a transparent oil (1.91 g, 8.03 mmol, 78% yield).

^{1}H NMR (400 MHz, Chloroform-*d_1*, δ ppm, *J* Hz): δ 4.15 (s, 2H), 3.75 (t, *J* = 7.0 Hz, 2H), 3.24 - 3.12 (m, 2H), 2.88 (ddd, *J* = 83.2, 14.3, 7.2 Hz, 2H), 2.50 (dd, *J* = 19.0, 3.6 Hz, 1H), 2.19 (s, 1H).

General procedure for the synthesis of carbamates (GP1)

The desired linker (0.4 mmol) was solubilized in dry THF or dry CH_2Cl_2 (5 mL) at r.t under N_2. At 0 ° C *p*-nitrophenyl chloroformate (89 mg, 0.44 mmol) and DMAP (98 mg, 0.8 mmol) were added, and the resulting mixture was stirred for 30-50 min at 0 °C. The activated compound was checked by TLC and was dropped into a solution of the desired amine or aniline (0.6 mmol) and DIPEA (209 µL, 1.2 mmol) at 0 °C. The reaction was stirred at r.t. for 0.15-16 h. The solvent was evaporated under reduced pressure and the residue was dissolved in EtOAc (10 mL) and washed with H_2O (5 mL) and brine (5 mL). The organic phase was dried over anhydrous Na_2SO_4, filtered, and evaporated under vacuum.

2-((2,5-dioxo-1-(prop-2-yn-1-yl)pyrrolidin-3-yl)thio)ethyl (*Z*)-(4-(((((4-methyl-3-(4-phenethylbenzamido)phenyl)amino)(3,4,5-trimethoxybenzamido)methylene)amino)methyl)phenyl)carbamate (17)

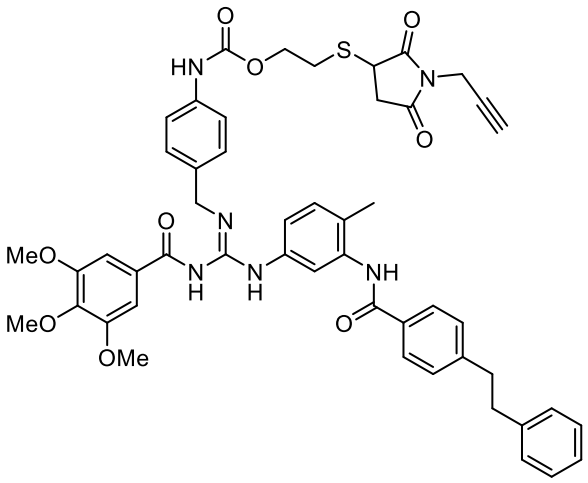

Prepared according to **GP1** from linker **19** and payload **20** in dry THF. Reaction time 3 h.

Carbamate **17** was purified by flash chromatography on silica gel eluting 0-100 % gradient of EtAOc in PE (114 mg, 0.13 mmol, 32% yield).

^{1}H NMR (400 MHz, Chloroform-*d*$_1$, δ ppm, *J* Hz): δ 12.05 (bs, 1H), 7.93 (d, *J* = 8.0, 2H), 7.70 (d, *J* = 8.01, 2H), 7.63-7.49 (m, 8H), 7.54 (d, *J* = 5.2, 2H), 7.46 (d, *J* = 7.5, 1H), 7.32 (d, *J* = 6.0, 1H), 6.61 (d, *J* = 8.0, 2H), 4.68 (s, 2H), 4.32 (t, *J* = 7.0 Hz, 2H), 4.24 (s, 2H), 3.88 (s, 9 H), 3.06 (m, 2H), 3.00 - 2.79 (m, 3H), 2.32 (s, 3H), 2.14 (s, 1H).

ESI: *m/z* 906 $[M + Na]^+$.

6-azidohexanoic acid (18)

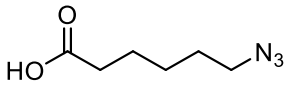

6-bromohexanoic acid (1 g, 5.1 mmol) was solubilized in dry DMF (5 mL) and NaN_3 (1.67 g, 25.7 mmol) was added at the mixture at r.t. The reaction was stirred for 16 h at 80 ° C. EtOAc (100 mL) was added at the crude, filtered on Büchner and washed with $KHSO_4$ 1 M (2 x 50 mL), H_2O (2 x 30 mL) and brine (30 mL). The organic phase was dried over anhydrous Na_2SO_4, filtered, and evaporated under reduced pressure. The product was obtained as yellow oil (727 mg, 4.6 mmol, 90% yield).

^{1}H NMR (400 MHz, Chloroform-*d*$_1$, δ ppm, *J* Hz): δ 10.93 (bs, 1H), 3.19 (t, *J* = 6.8 Hz, 2H), 2.28 (t, *J* = 7.4 Hz, 2H), 1.60-1.56 (m, 4H), 1.44-1.26 (m, 2H).

ESI: *m/z* 156 $[M-H]^-$

General procedure for CuCAAC reactions (GP2)

The desired alkyne (0.07 mmol) and the azide **18** (9 mg, 0.056 mmol) were dissolved in dry DMF (2 mL) under argon. The solution was degassed with three cycles of argon/vacuum. To this solution, a freshly prepared aqueous mixture (2 mL) of $Cu(OAc)_2$ (4 mg, 0.021 mmol) and Na ascorbate (8 mg, 0.042 mmol), previously degassed by argon/vacuum cycles, was added dropwise. The reaction mixture was degassed and left to stir under argon at r.t. for 16 h. The solvent was evaporated and the crude was purified by silica gel flash chromatography eluting 0-10 % gradient of MeOH in CH_2Cl_2 to provide the desired compound.

(*Z*)-6-(5-((3-((2-(((4-((((((4-methyl-3-(4-phenethylbenzamido)phenyl)amino)(3,4,5-trimethoxybenzamido)methylene)amino)methyl)phenyl)carbamoyl)oxy)ethyl)thio)-2,5-dioxopyrrolidin-1-yl)methyl)-1*H*-1,2,3-triazol-1-yl)hexanoic acid (16)

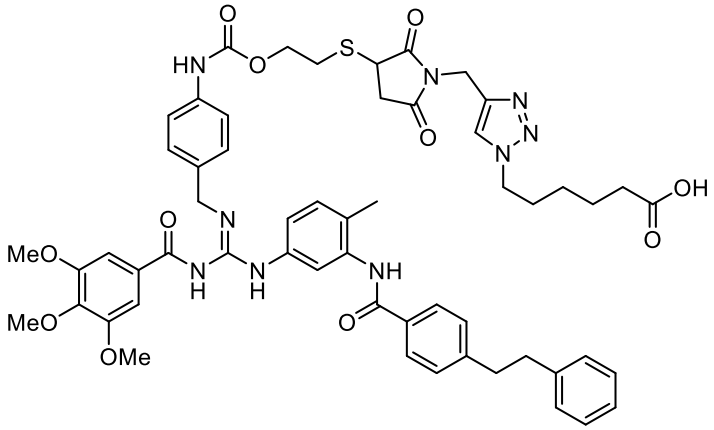

Prepared according to **GP2** from azide **16** and compound **17**.

Obtained: 41 mg, 0.4 mmol, 71% yield.

ESI: *m/z* 1041 $[M + H]^+$.

3-((4-(hydroxymethyl)phenyl)thio)-1-(prop-2-yn-1-yl)pyrrolidine-2,5-dione (38)

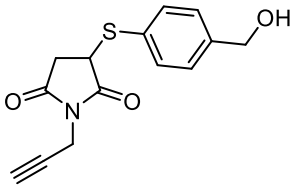

The compound **36** (600 mg, 4.36 mmol) and 4-mercaptoethanol (350 mg, 2.57 mmol) were solubilized in MeCN (15 mL) and a catalytic amount of Et_3N (18 µL, 0.1 mmol) was added dropwise. The reaction mixture was stirred at r.t. for 16 h and after the crude was concentrated under reduced pressure. Product **38** was purified via chromatography on silica gel eluting 0-100 % gradient of EtAOc in PE, as a transparent oil (594 mg, 2.16 mmol, 84% yield).

^{1}H NMR (400 MHz, Chloroform-*d*$_1$, δ ppm, *J* Hz): δ 7.47 (d, *J* = 7.9 Hz, 2H), 7.30 (d, *J* = 7.7 Hz, 2H), 4.66 (s, 2H), 4.15 (s, 2H), 3.99 (dd, *J* = 9.2, 4.1 Hz, 1H), 3.14 (dd, *J* = 18.8, 9.2 Hz, 1H), 2.67 (dd, *J* = 18.8, 4.2 Hz, 1H), 2.13 (s, 1H).

ESI: *m/z* 276 $[M+H]^+$, 298 $[M+Na]^+$.

3-((4-(bromomethyl)phenyl)thio)-1-(prop-2-yn-1-yl)pyrrolidine-2,5-dione (39)

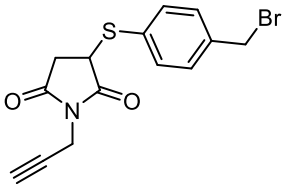

Compound **38** (110 mg, 0.4 mmol) was dissolved in CH_2Cl_2 (10 mL) at 0 °C and PBr_3 (56 µL, 0.60 mmol) was added dropwise. The resulting solution was stirred at r.t. for 30 min. The mixture was concentered under N_2 and quickly filtrated on a pad of silica gel using PE:EtOAc 1:1 mixture. The resulting filtrate was concentered under reduced pressure and the bromide **39** was immediately used for the next step without further purification (135 mg, 0.4 mmol).

General procedure for phenols alkylation (GP3)

The desired phenol (0.038 mmol) was dissolved in MeOH (1 mL) and NaOH 10N (8 µL, 0.076 mmol) was added. The resulting mixture was stirred for 10 min and then added to the bromide or chloride compound (0.115 mmol). The reaction was carried out at r.t. for 0.08-3 h. The base was neutralized with HCl 1 N, diluted with CH_2Cl_2, dried over anhydrous Na_2SO_4, filtered and evaporated under vacuum. The crude was purified by silica gel flash chromatography eluting 0-10% gradient of MeOH in CH_2Cl_2 to provide corresponding product.

4-((4-((2,5-dioxo-1-(prop-2-yn-1-yl)pyrrolidin-3-yl)thio)benzyl)oxy)-3,5-dimethoxy-*N*-(*N*-(4-methyl-3-(4-phenethylbenzamido)phenyl)carbamimidoyl)benzamide (40)

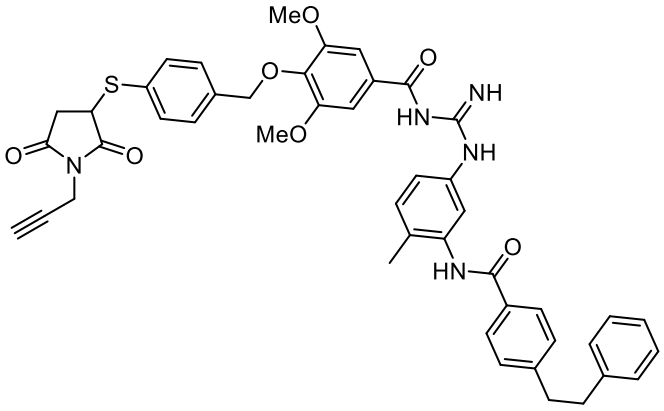

Prepared according to **GP3** from bromide **39** and payload **15**.

Obtained 16 mg, 0.02 mmol, 45% yield.

^{1}H NMR (400 MHz, Chloroform-d_1, δ ppm, *J* Hz): δ 7.77 (d, *J* = 8.0 Hz, 2H), 7.55 (s, 2H), 7.42 (dt, *J* = 13.5, 6.8 Hz, 2H), 7.32 - 7.22 (m, 6H), 7.21 - 7.07 (m, 6H), 5.06 (s, 2H), 3.92 (s, 6H), 3.07 - 2.80 (m, 4H), 2.28 (s, 3H).

^{13}C NMR (101 MHz, Chloroform-d_1, δ ppm): δ 174.20, 173.01, 165.90, 165.46, 156.20, 153.41, 146.78, 141.00, 139.06, 137.25, 134.30, 132.66, 132.34, 131.64, 129.75, 129.14, 128.47, 127.31, 126.20, 121.60, 119.58, 106.46, 82.51, 74.17, 74.04, 71.84, 63.03, 56.81, 52.06, 47.89, 44.08, 37.68, 37.40, 36.42, 36.12, 36.04, 29.70, 28.12, 17.52, 1.02.

ESI: *m/z* 810 $[M + H]^+$, 832 $[M + Na]^+$.

6-(4-((3-((4-((2,6-dimethoxy-4-((N-(4-methyl-3-(4-phenethylbenzamido)phenyl)carbamimidoyl)carbamoyl)phenoxy)methyl)phenyl)thio)-2,5-dioxopyrrolidin-1-yl)methyl)-1*H*-1,2,3-triazol-1-yl)hexanoic acid (41)

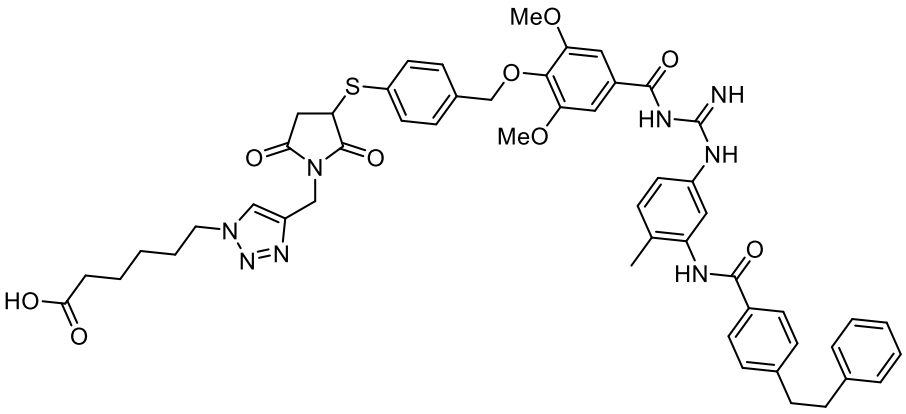

Prepared according to **GP2** from azide **18** and compound **40**.

Obtained: 29 mg, 0.03 mmol, 56% yield.

ESI: *m/z* 967 $[M + H]^+$.

(2-ethoxy-7-(prop-2-yn-1-yloxy)benzo[*d*][1,3]dioxol-5-yl)methanol (44, HMPO)

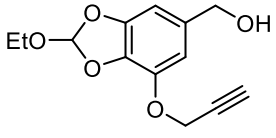

The product was prepared according to the literature.[80]

Obtained 915 mg, 3.66 mmol, 95% yield.

^{1}H NMR (600 MHz, Chloroform-d_1, δ ppm, *J* Hz): δ 6.89 (s, 1H), 6.67 (s, 1H), 6.63 (s, 1H), 4.81 (s, 2H), 4.58 (s, 2H), 3.75 (q, *J* = 7.1 Hz, 2H), 2.52 (s, 1H), 1.26 (t, *J* = 7.1 Hz, 3H).

^{13}C NMR (151 MHz, Chloroform-d_1, δ ppm): δ 147.68, 140.58, 135.42, 133.89, 119.50, 108.82, 101.75, 78.39, 75.94, 65.23, 59.37, 57.39, 14.82.

ESI: *m/z* 273 $[M+Na]^+$.

6-(chloromethyl)-2-ethoxy-4-(prop-2-yn-1-yloxy)benzo[d][1,3]dioxole (45)

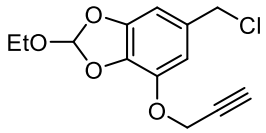

Compound **44** (100 mg, 0.4 mmol) was solubilized in dry CH_2Cl_2 (6 mL) at 0 °C and $SOCl_2$ (70 µL, 0.96 mmol) and Et_3N (145 µL, 1.04 mmol), both freshly distilled, were added carefully. The reaction was carried out at 0 °C for 30 min. After 30 min, the mixture was concentered under N_2 and quickly filtrated on a pad of silica gel using PE:EtOAc 1:1 mixture. The filtrate was concentered under reduced pressure and was immediately used for the next step without further purification.

4-((2-ethoxy-7-(prop-2-yn-1-yloxy)benzo[d][1,3]dioxol-5-yl)methoxy)-3,5-dimethoxy-N-(N-(4-methyl-3-(4-phenethylbenzamido)phenyl)carbamimidoyl)benzamide (46)

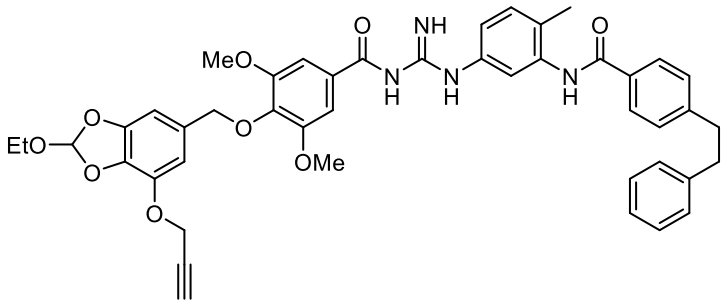

Prepared according to **GP3** from chloride **45** and payload **15**.

^{1}H NMR (400 MHz, Chloroform-d_1, δ ppm, *J* Hz): 7.76 (d, *J* = 8.2 Hz, 1H), 7.48 (s, 2H), 7.31 - 7.07 (m, 5H), 6.86 (s, 1H), 6.77 - 6.59 (m, 7H), 6.53 (s, 1H), 4.95 (s, 2H), 4.29 (s, 2H), 3.88 (s, 6H), 3.69 (q, *J* = 7.3 Hz, 2H), 3.06 - 2.78 (m, 4H), 2.27 (s, 3H), 2.50 (s, 1H), 1.21 (t, *J* = 7.1 Hz, 3H).

^{13}C NMR (101 MHz, Chloroform-d_1, δ ppm): 165.90, 153.16, 147.40, 146.66, 145.14, 144.37, 141.02, 140.39, 140.27, 137.01, 134.29, 131.99, 129.75, 129.11, 128.47, 127.26, 126.18, 121.36,

119.44, 110.39, 109.48, 106.21, 104.67, 103.28, 76.08, 75.93, 74.85, 74.58, 59.08, 57.85, 57.37, 57.22, 56.34, 37.68, 37.43, 29.72, 24.05, 17.41, 14.83, 1.02.

ESI: *m/z* 785 $[M + H]^+$.

6-(5-(((6-((2,6-dimethoxy-4-((*N*-(4-methyl-3-(4-phenethylbenzamido)phenyl)carbamimidoyl)carbamoyl)phenoxy)methyl)-2-ethoxybenzo[d][1,3]dioxol-4-yl)oxy)methyl)-1*H*-1,2,3-triazol-1-yl)hexanoic acid (47)

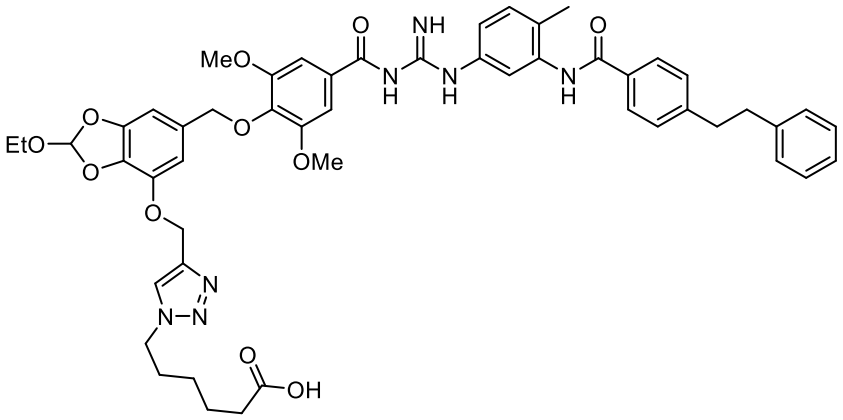

Prepared according to **GP2** from azide **18** and compound **46**.

Obtained: 28 mg, 0.03 mmol, 48% yield.

ESI: *m/z* 942 $[M + H]^+$, 964 $[M + Na]^+$.

***tert*-butyl (2-aminoethyl)carbamate (*N*-Boc-ethylendiamine)**

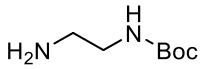

Di-*tert*-butyl dicarbonate (44 mg, 1 mmol) was dissolved in $CHCl_3$ (10 mL), and was added dropwise to a solution of ethane-1,2-diamine (133 µL, 2 mmol) in $CHCl_3$ (10), cooled to 0 °C using an ice bath. The resulting mixture was stirred at r.t. for 3 h. The mixture was washed with H_2O (3 x 20 mL) and brine (20 mL), then the organic phase was dried over anhydrous Na_2SO_4, filtered, and evaporated under reduced pressure. The desired product was obtained pure as a yellow oil without further purification (155 mg, 0.97 mmol, 97% yield).

^{1}H NMR (400 MHz, Chloroform-*d*$_1$, δ ppm, *J* Hz) δ 3.05-3.09 (d, 2H), 2.68-2.71 (t, 2H), 1.35 (s, 9H).
^{13}C NMR (100 MHz, Chloroform-*d*$_1$, δ ppm) δ 28.22, 41.55, 43.08, 78.65, 156.28.
ESI: *m/z* 161 $[M+H]^+$.

6-(2,5-dioxo-2,5-dihydro-1*H*-pyrrol-1-yl)hexanoyl chloride

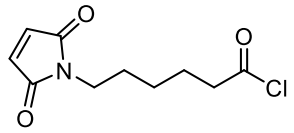

6-maleimidohexanoic acid (106 mg, 0.5 mmol) was solubilized in anhydrous CH_2Cl_2 (2 mL), under N_2, and cooled to 0 °C. Then thionyl dichloride (181 µL, 2.5 mmol) was added and the mixture stirred at r.t. for 3 h. After completion of the reaction, the solvent and thionyl dichloride were evaporated under reduced pressure and the product was obtained as a colorless oil and used directly without further purification.

ESI: *m/z* 230 $[M+H]^+$

***tert*-butyl (2-(6-(2,5-dioxo-2,5-dihydro-1*H*-pyrrol-1-yl)hexanamido)ethyl)carbamate (51)**

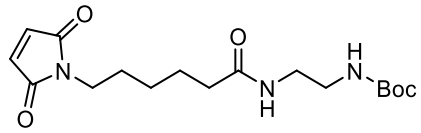

N-Boc-ethylendiamine (384 mg, 2.4 mmol) was dissolved in anhydrous CH_2Cl_2 (3 mL) and cooled to 0 °C, under N_2. Et_3N (335 µL, 2.4 mmol) was added and the mixture stirred at 0 °C for 30 min. The mixture obtained was added dropwise to a solution of 6-(2,5-dioxo-2,5-dihydro-1*H*-pyrrol-1-yl)hexanoyl chloride (460 mg, 2 mmol) in anhydrous CH_2Cl_2 (4 mL), at 0 °C under N_2. The resulting mixture was stirred at r.t. for 16 h, then it was washed with H_2O (3 x 10 mL) and brine (10 mL). The organic phase was dried over anhydrous Na_2SO_4, filtered, and evaporated under vacuum. The crude was purified by silica gel flash-chromatography eluting 0-0.5% gradient of MeOH in CH_2Cl_2, providing product **51** as a colorless oil (423 mg, 1.2 mmol, 60% yield).

^{1}H NMR (400 MHz, Chloroform-d_1, δ ppm, *J* Hz) δ 6.64 (s, 2H), 6.34 (bs, 1H), 5.10 (t, *J* = 5.9 Hz, 1H), 3.45 (t, *J* = 7.2 Hz, 2H), 3.28 (dd, *J* = 7.7, 3.9 Hz, 2H), 3.20 (d, *J* = 5.7 Hz, 2H), 2.11 (t, *J* = 7.6 Hz, 2H), 1.67 - 1.45 (m, 4H), 1.38 (s, 9H), 1.33 - 1.13 (m, 2H).

^{13}C NMR (100 MHz, Chloroform-d_1, δ ppm) δ 24.99, 26.26, 28.17, 28.31, 36.24, 37.52, 40.24, 40.46, 79.42, 134.01, 156.84, 170.77, 173.47.

ESI: *m/z* 354 $[M+H]^+$, 376 $[M+Na]^+$

_N_-(2-aminoethyl)-6-(2,5-dioxo-2,5-dihydro-1_H_-pyrrol-1-yl)hexanamide trifluoroacetate (52)

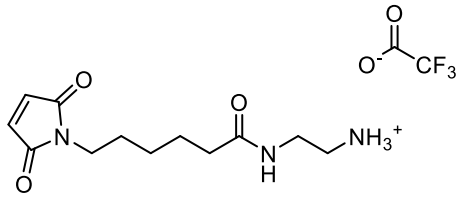

Compound **51** (200 mg, 0.56 mmol) was solubilized in a mixture of TFA:CH_2Cl_2 1:9 (8 mL) and stirred at r.t. for 16 h. After completion of the reaction, the solvent was evaporated under vacuum and the product was obtained as a TFA salt and used without further purification.

2,5-dioxopyrrolidin-1-yl 6-azidohexanoate (53)

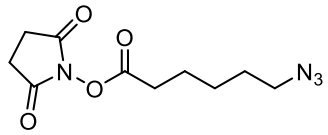

A solution of compound **18** (100 mg, 0.63 mmol) in anhydrous CH_2Cl_2 (3 mL), under N_2, was cooled to 0 °C, then EDC·HCl (182 mg, 0.95 mmol) and *N*-hydroxysuccinimide (110 mg, 0.95 mmol) were added. The resulting mixture was stirred at r.t. for 16 h, then it was washed with H_2O (3 x 10 mL). The organic phase was dried over Na_2SO_4, filtered, and evaporated under reduced pressure. The product was obtained pure as a colorless oil (160 mg, 0.63 mg, 99% yield) and used without further purification.

ESI: *m/z* 255 $[M+H]^+$

6-azido-_N_-(2-(6-(2,5-dioxo-2,5-dihydro-1_H_-pyrrol-1-yl)hexanamido)ethyl)hexanamide (54)

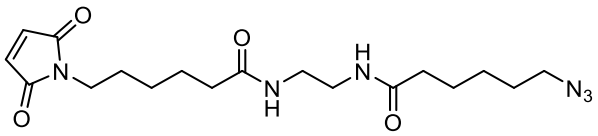

Activated acid **53** (184 mg, 0.5 mmol) and compound **52** (127 mg, 0.5 mmol) were dissolved in anhydrous CH_2Cl_2 (3 mL), the resulting mixture was cooled to 0°C, under N_2, then DIPEA (530 µL, 3 mmol) was added slowly. The reaction mixture was stirred at r.t. for 16 h, then it was diluted with CH_2Cl_2 (5 mL) washed with $NaHCO_{3SS}$ (2 x 10 mL), HCl 0.5 N (2 x 10 mL) and brine (10 mL). The organic phase was dried over Na_2SO_4, filtered, and evaporated under reduced pressure. The crude was purified by silica gel flash-chromatography eluting 1-5% gradient of MeOH in $CHCl_3$, providing product **54** as a colorless oil (28 mg, 0.07 mmol, 14% yield).

^{1}H NMR (400 MHz, Chloroform-d_1, δ ppm, *J* Hz): δ 6.69 (s, 2H), 6.43 (bs, 1H), 6.32 (bs, 1H), 3.51 (t, *J* = 7.15 Hz, 2H), 3.38 (m, 4H), 2.33 (t, *J* = 7.46, 2H), 2.19 (t, *J* = 7.54, 2H), 1.70-1.56 (m, 4H), 1.47-1.34 (m, 2H), 0.96-0.74 (m, 8H).

ESI: *m/z* 415 $[M+Na]^+$

5-(2,5-dioxo-2,5-dihydro-1*H*-pyrrol-1-yl)pentyl acetate (56)

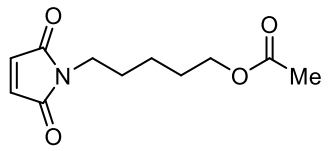

Maleic anhydride (493 mg, 5 mmol) was dissolved in glacial acetic acid (10 mL), 5-amino-1-pentanol (545 uL, 5 mmol) was added and the resulting mixture was refluxed for 2 h. Acetic acid was then removed under vacuum, the obtained residue was dissolved in acetic anhydride (10 mL) and AcONa (247 mg, 3 mmol) was added. The mixture was stirred at reflux temperature for 16 h. The reaction mixture was cooled to 0 °C, neutralized with $NaHCO_{3SS}$ and extracted with Et_2O (3 x 20 mL). The combined organic layers were dried over Na_2SO_4, filtered, and evaporated under reduced pressure. The crude was purified by silica gel flash-chromatography eluting 1-4% gradient of AcOEt in CH_2Cl_2, providing product **56** as a colorless oil (787 mg, 3.5 mmol, 70% yield).

^{1}H NMR (400 MHz, Methanol-d_4, δ ppm, *J* Hz): δ 6.78 (s, 2H), 4.02 (t, *J* = 6.5 Hz, 2H), 3.48 (t, *J* = 7.0 Hz, 2H), 1.99 (s, 3H), 1.60 (ddt, *J* = 19.9, 14.7, 7.0 Hz, 4H), 1.39-1.28 (m, 2H).
ESI: *m/z* 248 $[M+Na]^+$

1-(5-hydroxypentyl)-1*H*-pyrrole-2,5-dione (57)

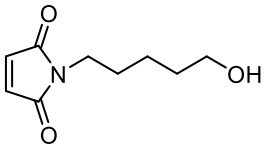

Compound **56** (200 mg, 0.9 mmol) was dissolved in a mixture of THF:HCl 5 N (1:2 - 3 mL) and stirred at r.t. for 3 h. The reaction was cooled to 0 °C and quenched with $NaHCO_{3SS}$, then THF was removed under vacuum and the product was extracted with EtOAc (3 x 20 mL). The organic phases were combined and dried over Na_2SO_4, filtered, and evaporated under reduced pressure. Product **57** was obtained pure as a pale-yellow solid (129 mg, 0.7 mmol, 79% yield) without further purification.

^{1}H NMR (400 MHz, Methanol-*d*$_4$, δ ppm, *J* Hz): δ 6.78 (s, 2H), 3.49 (dt, *J* = 16.0, 6.8 Hz, 4H), 1.65 - 1.45 (m, 4H), 1.39 - 1.28 (m, 3H).

ESI: *m/z* 182 $[M-H]^-$

***N*-(4-azidobenzyl)-6-(2,5-dioxo-2,5-dihydro-1*H*-pyrrol-1-yl)hexanamide (60)**

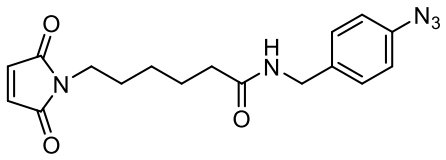

6-maleimidohexanoic acid (570 mg, 2.7 mmol) was solubilized in anhydrous EtOAc (15 mL), under N_2. Then azide **22** (400 mg, 2.7 mmol), DIPEA (1.4 mL, 8 mmol) and propylphosphonic anhydride solution 50% in EtOAc (2.4 mL, 4.05 mmol) were added, and the resulting mixture was stirred at r.t. for 30 min. The mixture was washed with H_2O (2 x 20 mL) and $NaHCO_{3SS}$ (2 x 20 mL). The organic phase was dried over Na_2SO_4, filtered, and evaporated under reduced pressure. The crude was purified by silica gel flash-chromatography eluting 0-2% gradient of MeOH in CH_2Cl_2, providing product **60** as a white solid (430 mg, 1.26 mmol, 47% yield).

^{1}H NMR (400 MHz, Methanol-*d*$_4$, δ ppm, *J* Hz): δ 8.36 (s, 1H), 7.28 (d, *J* = 8.15 Hz, 2H), 7.00 (d, *J* = 8.5 Hz, 2H), 6.77 (s, 2H), 4.30 (d, *J* = 5.87 Hz, 2H), 3.45 (t, *J* = 7.1 Hz, 2H), 2.20 (t, *J* = 7.4 Hz, 2H), 1.59 (dp, *J* = 25.2, 7.4 Hz, 4H), 1.32 - 1.20 (m, 2H).

ESI: *m/z* 342 $[M + H]^+$, 364 $[M + Na]^+$

***N*-(4-azidobenzyl)-6-(3-((2-hydroxyethyl)thio)-2,5-dioxopyrrolidin-1-yl)hexanamide (61)**

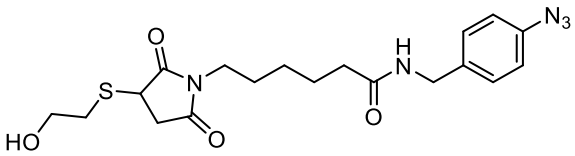

Compound **60** (200 mg, 0.6 mmol) was suspended in MeCN (3 mL), under N_2, and 2-mercaptoethanol (67 µL, 0.95 mmol) was added. The resulting mixture was stirred at r.t. for 16 h. After completion of the reaction, the solvent was evaporated under reduced pressure. The crude was purified by silica gel flash-chromatography eluting 0-4% gradient of MeOH in CH_2Cl_2, providing product **61** as a pale yellow solid (207 mg, 0.49 mmol, 82% yield).

^{1}H NMR (400 MHz, Methanol-*d*$_4$, δ ppm, *J* Hz): δ 7.27 (d, *J* = 8.2 Hz, 2H), 7.00 (d, *J* = 8.5 Hz, 2H), 4.30 (s, 2H), 3.91 (dd, *J* = 9.0, 3.7 Hz, 1H), 3.73 (td, *J* = 6.4, 1.2 Hz, 2H), 3.44 (t, *J* = 7.1 Hz, 2H), 3.15

(t, *J* = 8.0, 7.3 Hz, 1H), 3.01 (dt, *J* = 13.6, 6.3 Hz, 1H), 2.80 (dd, *J* = 13.2, 5.9 Hz, 1H), 2.46 (dd, *J* = 18.5, 3.8 Hz, 1H), 2.20 (t, *J* = 7.4 Hz, 2H), 1.66 - 1.50 (m, 4H), 1.32 - 1.24 (m, 2H).

^{13}C NMR (100 MHz, Methanol-d_4, δ ppm, *J* Hz): δ 177.57, 175.65, 174.36, 138.87, 135.72, 128.79, 118.68, 60.81, 42.06, 39.18, 38.17, 35.78, 35.37, 33.64, 26.84, 25.89, 25.03.

ESI: *m/z* 442 $[M + Na]^+$

***N*-(4-azidobenzyl)-6-(3-((4-(hydroxymethyl)phenyl)thio)-2,5-dioxopyrrolidin-1-yl)hexanamide (62)**

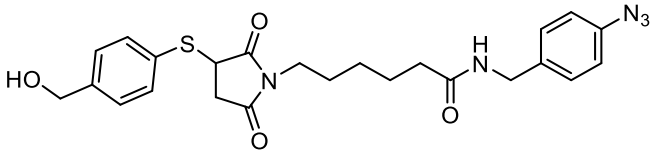

Compound **60** (100 mg, 0.3 mmol) was suspended in MeCN (3 mL), under N_2, and 4-mercaptoethanol (63 mg, 0.45 mmol) was added. The resulting mixture was stirred at r.t. for 16 h. After completion of the reaction, the solvent was evaporated under reduced pressure. The crude was purified by silica gel flash-chromatography eluting 0-2% gradient of MeOH in CH_2Cl_2, providing product **62** as a white solid (106 mg, 0.22 mmol, 73% yield).

^{1}H NMR (400 MHz, Methanol-d_4, δ ppm, *J* Hz): δ 7.47 (d, *J* = 8.2 Hz, 2H), 7.30 (dd, *J* = 15.5, 8.4 Hz, 4H), 7.00 (d, *J* = 8.6 Hz, 2H), 4.57 (s, 2H), 4.30 (s, 2H), 4.12 (dd, *J* = 9.1, 3.8 Hz, 1H), 3.33 (t, *J* = 7.2 Hz, 2H), 3.17 (dd, *J* = 18.7, 9.2 Hz, 1H), 2.62 (dd, *J* = 18.6, 4.0 Hz, 1H), 2.17 (t, *J* = 7.4 Hz, 2H), 1.65 - 1.50 (m, 2H), 1.45 - 1.31 (m, 2H), 1.21 - 1.07 (m, 2H).

^{13}C NMR (101 MHz, 150 MHz, Methanol-d_4, δ ppm) δ 152.37, 147.50, 142.43, 133.07, 132.77, 128.79, 128.58, 127.50, 125.95, 119.20, 112.83, 107.45, 106.18, 100.09, 69.68, 60.63, 59.50, 55.81, 51.36, 37.37, 29.55, 29.24, 28.95, 25.72.

ESI: *m/z* 504 $[M + Na]^+$

2-((1-(6-((4-azidobenzyl)amino)-6-oxohexyl)-2,5-dioxopyrrolidin-3-yl)thio)ethyl (4-(((((4-methyl-3-(4-phenethylbenzamido)phenyl)amino)(3,4,5-trimethoxybenzamido)methylene)amino)methyl)phenyl)carbamate (64)

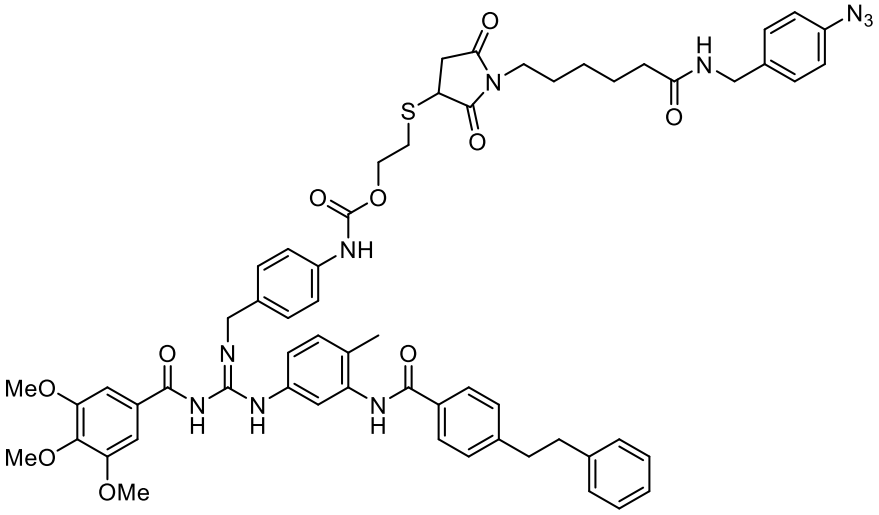

Prepared according to **GP1** from linker **61** and payload **20** in dry CH_2Cl_2. Reaction time 16 h.

The obtained crude was purified by silica gel flash-chromatography eluting 0-2% gradient of MeOH in CH_2Cl_2, providing product **64** as a white solid (26 mg, 0.02 mmol, 20% yield).

^{1}H NMR (600 MHz, Methanol-*d*$_4$, δ ppm, *J* Hz): δ 7.85 (d, *J* = 8.25 Hz, 2H), 7.42-7.05 (m, 20H), 6.98 - 6.93 (m, 3H), 4.59 (s, 2H), 4.55 (s, 1H), 4.36 (dt, *J* = 11.28, 6.35 Hz, 1H), 4.28 (m, 3H), 3.95 (m, 1H), 3.43 (t, *J* = 7.11 Hz, 2H), 3.24-3.09 (m, 3H), 3.01-2.90 (m, 6H), 2.43 (dd, *J* = 18.59, 3.78 Hz, 1H), 2.29 (s, 3H), 2.17 (t, *J* = 7.40 Hz, 2H), 1.56 (m, 4H), 1.27 (m, 2H).

^{13}C NMR (150 MHz, Methanol-*d*$_4$, δ ppm): 152.42, 141.16, 138.87, 135.69, 129.43, 128.78, 128.58, 128.20, 127.94, 127.41, 125.61, 122.91, 118.68, 118.40, 106.07, 59.70, 55.16, 53.38, 46.55, 42.07, 41.17, 39.05, 38.19, 37.44, 37.18, 35.54, 35.36, 30.22, 28.75, 27.46, 26.83, 25.87, 25.01, 21.98, 21.57, 20.09, 18.42, 16.36, 13.22, 12.96, 7.81.

ESI: *m/z* 1118 $[M + H]^+$

***N*-(4-azidobenzyl)-6-(3-((4-(chloromethyl)phenyl)thio)-2,5-dioxopyrrolidin-1-yl)hexanamide (65)**

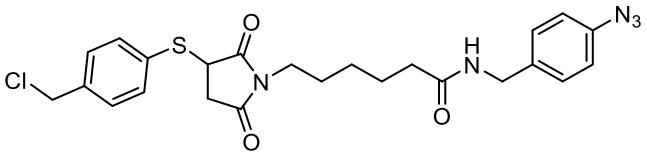

Compound **62** (100 mg, 0.2 mmol) was suspended in anhydrous CH_2Cl_2 (2 mL), under N_2, and cooled to 0°C. Then $SOCl_2$ (30 µL, 0.42 mmol) was added. The resulting mixture was stirred at r.t. for 1 h. After completion of the reaction, the solvent was evaporated under reduced pressure. The crude was used without further purification.

ESI: *m/z* 500 $[M^{35}Cl + H]^+$, 502 $[M^{37}Cl + H]^+$.

4-((4-((1-(6-((4-azidobenzyl)amino)-6-oxohexyl)-2,5-dioxopyrrolidin-3-yl)thio)benzyl)oxy)-3,5-dimethoxy-*N*-(*N*-(4-methyl-3-(4-phenethylbenzamido)phenyl)carbamimidoyl)benzamide (66)

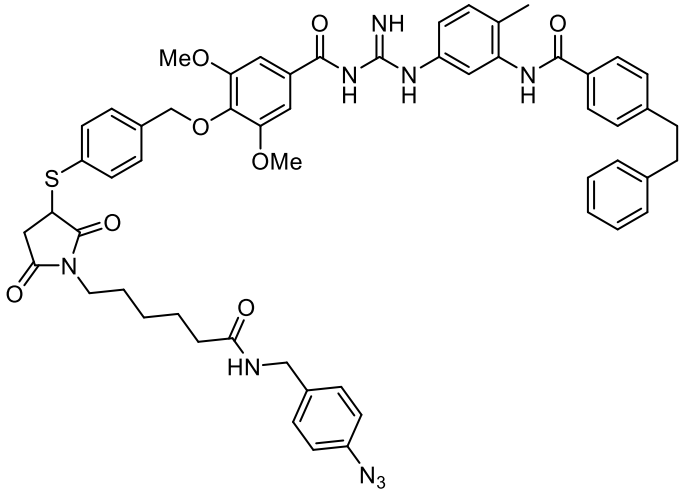

Prepared according to **GP3** from chloride **65** and payload **15**. Reaction time 96 h.

The obtained crude was purified by pTLC 20 x 20 cm eluting 3% mixture of MeOH in CH_2Cl_2, providing product **66** as a white solid (6.7 mg, 0.006 mmol, 20% yield).

^{1}H NMR (600 MHz, Chloroform-d_1, δ ppm, *J* Hz): δ d 8.07 (bs, 1H), 7.82 (d, *J* = 7,92 Hz, 3H), 7.56 (s, 2H), 7.49 (dd, *J* = 8,04, 18.48 Hz, 5H),7.34-7.30 (m, 5H), 7.23 (d, *J* = 8,04 Hz, 3H), 7.19 (d, *J* = 7,44 Hz, 2H), 6.97 (d, *J* = 8,28 Hz, 2H), 5.99 (bs, 1H), 4.36 (d, *J* = 5,82 Hz, 2H), 4.01 (dd, *J* = 4,08, 13.2 Hz, 1H), 3.95 (s, 6H), 3.42 (t, *J* = 7.26, 2H), 3.13 (q, *J* = 9.12 Hz, 1H)3.04 (d, *J* = 7.92, 2H),2.99 (d, *J* = 7,86 Hz, 2H), 2.70 (dd, *J* = 4,14, 18.66 Hz, 1H) 2.39 (s, 2H), 2.36 (t, *J* = 7.44 Hz, 3H), 2.06-2.03 (m, 6H).

ESI: *m/z* 1016 $[M + H]^+$; 1038 $[M + Na]^+$.

7-((cyclohexylamino)methyl)-4-methoxyquinolin-8-ol (14)

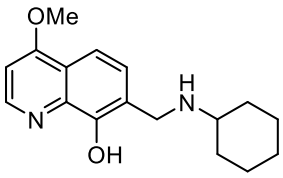

The product was prepared according to the literature.[393]

^{1}H NMR: (600 MHz, Methanol-d_4 δ ppm): δ 8.59 (d, *J* = 4.8 Hz, 1H), 7.52 (d, *J* = 8.4 Hz, 1H), 7.28 (d, *J* = 9 Hz, 1H), 6.92 (d, *J* = 4.8 Hz, 1H), 4.12 (s, 2H), 4.06 (s, 3H), 2.61-2.57 (m, 1H), 2.01 (d, *J* = 10.8 Hz, 2H), 1.76 (d, *J* = 12.6 Hz, 2H), 1.28-1.19 (m, 6H).

^{13}C NMR: (150 MHz, Methanol-d_4 δ ppm): δ 162.90, 149.02, 140.13, 126.93, 121.43, 110.09, 100.36, 55.60, 55.00, 45.80, 31.73, 25.66, 24.62.

2-((1-(6-((4-azidobenzyl)amino)-6-oxohexyl)-2,5-dioxopyrrolidin-3-yl)thio)ethyl cyclohexyl((8-hydroxy-4-methoxyquinolin-7-yl)methyl)carbamate (67)

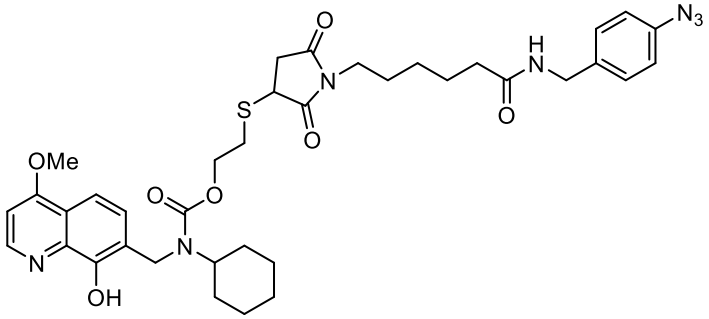

Prepared according to **GP1** from linker **61** and payload **14** in dry CH_2Cl_2. Reaction time 16 h.

The obtained crude was purified by silica gel flash-chromatography in CH_2Cl_2, providing product **67** as a grey oil (23 mg, 0.032 mmol, 42 % yield).

^{1}H NMR (600 MHz, Methanol-d_4, δ ppm, *J* Hz): δ 8.60 (d, *J* = 5.1 Hz, 1H), 7.55 (d, *J* = 8.7 Hz, 1H), 7.35 - 7.25 (m, 3H), 6.99 (t, *J* = 8.1 Hz, 3H), 6.90 (d, *J* = 5.2 Hz, 1H), 4.65 (s, 2H), 4.47 - 4.19 (m, 4H), 4.03 (s, 3H), 3.94 (ddd, *J* = 8.9, 3.7, 1.8 Hz, 1H), 3.45 (dd, *J* = 9.6, 4.7 Hz, 2H), 3.25 - 3.09 (m, 2H), 2.99 - 2.70 (m, 2H), 2.44 (dd, *J* = 18.5, 3.7 Hz, 1H), 2.19 (q, *J* = 7.5 Hz, 2H), 1.79 - 1.40 (m, 8H), 1.37 - 1.16 (m, 8H).

ESI: *m/z* 732 $[M + H]^+$.

ethyl 2-ethoxy-7-hydroxybenzo[d][1,3]dioxole-5-carboxylate (43)

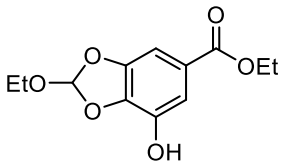

Under N_2 atmosphere, Amberlyst® 15 (62 mg) was suspended in dry toluene (80 mL). After 30 minutes, ethyl gallate (1 g, 5.046 mmol) and triethyl orthoformate (2.5 mL, 15.098 mmol) were added at r.t. and then the mixture was heated to reflux for 16 h. The reaction was cooled to r.t., filtered on Celite pad and toluene was evaporated under reduced pressure. The crude was purified by silica gel flash-chromatography eluting 0-30% gradient of AcOEt in PE, providing product **43** as a white solid (1.06 g, 4.19 mmol, 83% yield).

^{1}H NMR (400 MHz, Chloroform-*d_1*, δ ppm, *J* Hz): δ 7.42 (d, *J* = 1.5 Hz, 1H), 7.15 (d, *J* = 1.5 Hz, 1H), 6.92 (s, 1H), 4.32 (q, *J* = 7.1 Hz, 2H), 3.71 (q, *J* = 1.6 Hz, 2H), 1.34 (t, *J* = 7.1 Hz, 3H), 1.23 (t, *J* = 1.9 Hz, 3H).

^{13}C NMR (151 MHz, Chloroform-*d_1*, δ ppm): δ 165.72, 147.33, 140.23, 138.48, 124.69, 120.12, 112.32, 104.19, 77.87, 76.30, 61.02, 59.59, 57.37, 14.77, 14.32.

ESI: *m/z* 301 $[M + Na]^+$.

9-azidononan-1-ol (68)

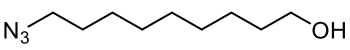

9-bromononan-1-ol (500 mg, 2.24 mmol) was solubilized in dry DMF (10 mL), then NaN_3 (730 mg, 11.2 mmol) was added. The resulting mixture was heated at 70 °C and stirred for 16 h. After reaction completion, H_2O was added (10 mL) and the organic phase was extracted with EtOAc (3 x 25 mL). The organic layers were unified and washed again with H_2O (25 mL). Then the organic phase was dried over Na_2SO_4, filtered, and evaporated under reduced pressure. Compound **68** was obtained as a yellow oil (384 mg, 2.07 mmol, 92% yield) and pure enough, therefore it did not require further purification.

^{1}H NMR (400 MHz, Chloroform-*d_1*, δ ppm, *J* Hz): δ 3.53 (t, *J* = 6.6 Hz, 2H), 3.18 (t, *J* = 6.9 Hz, 2H), 1.55 3 1.44 (m, 4H), 1.35 3 1.18 (m, 10H).

ethyl 7-((9-azidononyl)oxy)-2-ethoxybenzo[*d*][1,3]dioxole-5-carboxylate (69)

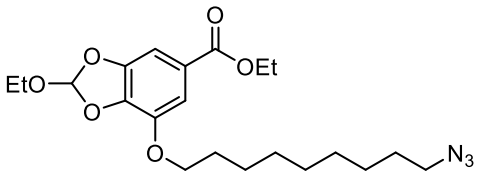

Under N_2 atmosphere, compound **43** (1.45 g, 4.5 mmol) and compound **68** (1 g, 5.4 mmol) were dissolved in dry CH_2Cl_2 (86 mL). To the resulting solution PPh_3 (2.36 g, 9 mmol) was added. Then the mixture was cooled to 0 °C and a solution of DIAD (1.77 mL, 9 mmol) in CH_2Cl_2 (28 mL) was added dropwise. The resulting reaction mixture was heated to r.t. and stirred for 2 h. Solvent was removed under reduced pressure and the crude was purified by silica gel flash-chromatography eluting 0-30% gradient of EtOAc in PE, providing product **69** as a orange oil (1.8 g, 4.27 mmol, 95% yield).

^{1}H NMR: (400 MHz, Chloroform-d_1, δ ppm, *J* Hz): δ 7.29 (d, *J* = 1.5 Hz, 1H), 7.19 (d, *J* = 1.5 Hz 1H), 6.90 (s, 1H), 4.30 (q, *J* = 7.1 Hz, 2H), 4.08 (t, *J* = 6.6 Hz, 2H), 3.70 (q, *J* = 1.3 Hz, 2H), 3.21 (t, *J* = 6.9 Hz, 2H), 1.77 (m, 2H), 1.54 (m, 2H), 1.45 3 1.25 (m, 13H), 1.22 (t, *J* = 7.1 Hz, 3H).

ESI: *m/z* 444 $[M + Na]^+$.

(7-((9-azidononyl)oxy)-2-ethoxybenzo[d][1,3]dioxol-5-yl)methanol (70)

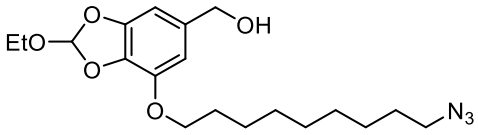

Under N_2 atmosphere, compound **69** (1.24 g, 2.94 mmol) was dissolved in dry THF (40 mL). The resulting solution was cooled to 0 °C, and a solution of DIBAL 1M in toluene (5.89 mL, 5.89 mmol) was added dropwise. The reaction mixture was stirred at r.t. for 4 h. At the end of the reaction, 30 mL of saturated solution of potassium sodium tartrate tetrahydrate were added and the mixture was stirred for 30 min. The organic layer was separated, dried over Na_2SO_4, filtered and evaporated under reduced pressure. The crude was purified by silica gel flash-chromatography eluting 0-30% gradient of AcOEt in PE, providing product **70** as a yellow oil (832 mg, 2.06 mmol, 70% yield).

^{1}H NMR: (400 MHz, Chloroform-*d_1*, δ ppm, *J* Hz): δ 7.24 (s, 1H), 6.86 (s, 1H), 6.55 (s, 1H), 4.56 (s, 2H), 4.07 (t, *J* = 6.6 Hz, 2H), 3.72 (q, *J* = 7.1 Hz, 2H), 3.24 (t, *J* = 7 Hz, 2H), 1.77 (m, 2H), 1.63-1.27 (m, 12H), 1.24 (t, *J* = 7.1 Hz, 3H).

ESI: *m/z* 402 $[M + Na]^+$.

4-((9-azidononyl)oxy)-6-(chloromethyl)-2-ethoxybenzo[d][1,3]dioxole (72)

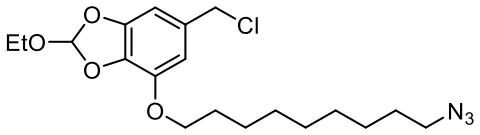

Compound **70** (50 mg, 0.13 mmol) was solubilized in anhydrous CH_2Cl_2 (1.5 mL), under N_2, and the obtained solution was cooled to 0°C. Then Et_3N (18 µL, 0.13 mmol), DMAP (20 mg, 0.16 mmol) and *p*-TsCl (45 mg, 0.23 mmol) were added. The mixture was stirred at 0°C for 1h. Then, the solvent was evaporated under reduced pressure. The crude was quickly purified by silica gel flash-chromatography eluting isocratic PE:EtOAc mixture (9:1), providing product **72** as a colorless oil (44 mg, 0.11 mmol, 85% yield).

^{1}H NMR (400 MHz, Chloroform-*d_1*, δ ppm, *J* Hz): δ δ 7.24 (s, 1H), 6.86 (s, 1H), 6.55 (s, 1H), 4.55 (s, 2H), 4.07 (t, *J* = 6.6 Hz, 2H), 3.72 (q, *J* = 7.1 Hz, 2H), 3.24 (t, *J* = 7 Hz, 2H), 1.77 (m, 2H), 1.63-1.27 (m, 12H), 1.24 (t, *J* = 7.1 Hz, 3H).

***N*-(*N*'-(4-(((7-((9-azidononyl)oxy)-2-ethoxybenzo[d][1,3]dioxol-5-yl)methyl)amino)benzyl)-*N*-(4-methyl-3-(4-phenethylbenzamido)phenyl)carbamimidoyl)-3,4,5-trimethoxybenzamide (75)**

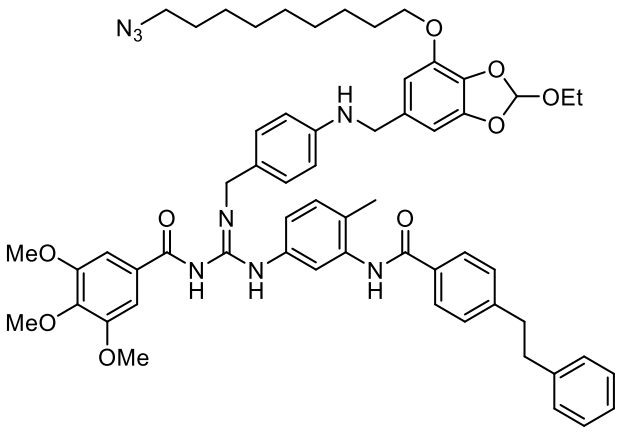

Chloride **72** (15 mg, 0.038 mmol) was solubilized in anhydrous CH_2Cl_2 (1 mL), under N_2, then compound **20** (21 mg, 0.031 mmol) and DIPEA (9 µL, 0.068 mmol) were added. The resulting mixture was stirred at reflux temperature for 48 h, until the disappearance of the starting

material was observed. The solvent was evaporated under reduced pressure. The crude was purified by silica gel flash-chromatography eluting 0-1% gradient of MeOH in CH_2Cl_2, providing product **75** as a white solid (7.8 mg, 0.0075 mmol, 24% yield).

^{1}H NMR (400 MHz, Chloroform-*d_1*, δ ppm, *J* Hz): δ 7.84 - 7.77 (m, 3H), 7.58 (s, 1H), 7.30 - 7.25 (m, 6H), 7.23 - 7.16 (m, 5H), 6.82 (d, *J* = 1.9 Hz, 1H), 6.67 (d, *J* = 8.1 Hz, 1H), 6.39 (d, *J* = 9.9 Hz, 4H), 4.64 (s, 1H), 4.45 (s, 2H), 4.02 (t, *J* = 6.6 Hz, 2H), 3.89 (d, *J* = 6.6 Hz, 9H), 3.73 (q, *J* = 7.1 Hz, 2H), 3.25 (t, *J* = 6.8 Hz, 2H), 3.05 - 2.88 (m, 4H), 2.32 (s, 3H), 2.20 - 2.13 (m, 6H), 1.81 (s, 3H), 1.73 (p, *J* = 6.7 Hz, 2H), 1.64 - 1.54 (m, 2H), 1.44 - 1.22 (m, 6H).

^{13}C NMR (101 MHz, 150 MHz, Methanol-*d_4*, δ ppm) δ 176.65, 152.40, 152.38, 147.51, 146.38, 142.43, 141.04, 134.22, 133.08, 132.78, 128.79, 128.58, 128.36, 128.26, 127.50, 125.96, 119.20, 112.84, 107.45, 106.19, 100.09, 69.68, 60.63, 59.50, 55.80, 54.26, 51.35, 49.22, 37.63, 37.37, 31.79, 29.54, 29.24, 29.12, 28.94, 28.69, 26.57, 25.71, 22.54, 17.18, 14.56.

ESI: *m/z* 1033 $[M + H]^+$, 1071 $[M + K]^+$.

4-((7-((9-azidononyl)oxy)-2-ethoxybenzo[d][1,3]dioxol-5-yl)methoxy)-3,5-dimethoxy-*N*-(*N*-(4-methyl-3-(4-phenethylbenzamido)phenyl)carbamimidoyl)benzamide (76)

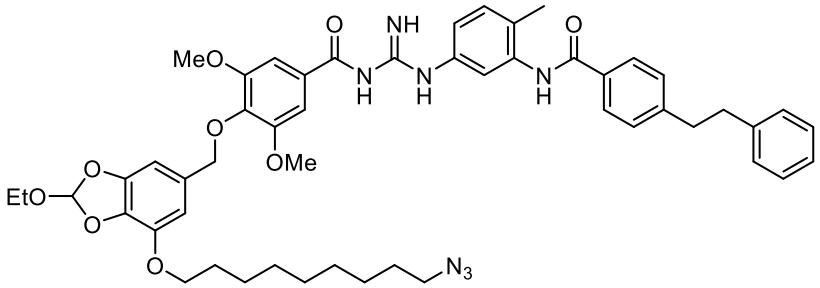

Prepared according to **GP3** from chloride **72** and payload **15**. Reaction time 16 h.

The obtained crude was purified by flash-chromatography 0-0.1% gradient of MeOH in $CHCl_3$, providing product **76** as a white solid (18 mg, 0.02 mmol, 33% yield).

^{1}H NMR (600 MHz, Chloroform-*d_1*, δ ppm, *J* Hz): δ d 8.00 (bs, 1H), 7.77 (d, *J* = 12,06 Hz, 2H), 7.72 (bs, 1H), 7.47 (s, 2H), 7.28-7.24 (m, 5H), 7.20 -7.13 (m, 4H), 6.98-6.96 (m, 1H), 6.85 (s, 1H), 6.70 (s, 2H), 4.95 (s, 2H), 4.06 (t, *J* = 9.96, 2H), 3.90 (s, 6H), 3.69 (q, *J* = 10.56, 2H), 3.23 (t, *J* = 10.44, 2H), 3.02-2.92 (m, 4H), 2.32 (s, 3H), 1.78-1.74 (m, 4H), 1.61-1.54 (m, 6H), 1.42-1.21 (m, 7H).

^{13}C NMR (600 MHz, Chloroform-*d_1*, δ ppm, *J* Hz): δ d 152.9, 147.0, 146.6, 142.1, 141.0, 137.0, 133.8, 132.1, 132.0, 131.9, 129.2, 128.5, 128.4, 127.1, 126.2, 119.2, 109.3, 106.0, 102.2, 75.1,

69.5, 58.9, 56.1, 51.5, 37.7, 37.4, 31.9, 30.9, 30.0, 29.7, 29.6, 29.4, 29.37, 29.35, 29.3, 29.1, 28.8, 28.4, 28.0, 27.8, 26.7, 25.9, 22.7, 17.4, 14.9, 14.2.

ESI: *m/z* 915 $[M + H]^+$; 936 $[M + Na]^+$.

4-(((7-((9-azidononyl)oxy)-2-ethoxybenzo[d][1,3]dioxol-5-yl)methyl)amino)benzyl cyclohexyl((8-hydroxy-4-methoxyquinolin-7-yl)methyl)carbamate (77)

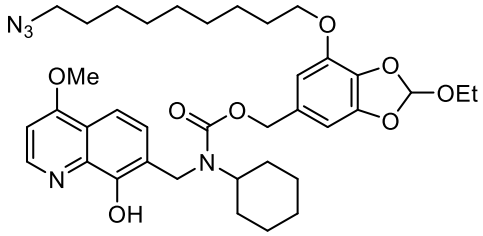

Prepared according to **GP1** from linker **70** and payload **14** in dry CH_2Cl_2. Reaction time 16 h.

The obtained crude was purified by silica gel flash-chromatography eluting 0-1% gradient of MeOH in CH_2Cl_2, providing product **77** as a colorless oil (19 mg, 0.027 mmol, 34% yield).

^{1}H NMR (400 MHz, Chloroform-*d*$_1$, δ ppm, *J* Hz): δ 8.58 (d, *J* = 5.2 Hz, 1H), 7.52 (d, *J* = 8.5 Hz, 1H), 7.43 - 7.25 (m, 1H), 6.92 - 6.78 (m, 1H), 6.72 (d, *J* = 5.2 Hz, 1H), 6.64 - 6.50 (m, 1H), 6.40 (s, 1H), 5.12 (s, 1H), 5.02 (s, 1H), 4.72 (s, 1H), 4.67 (s, 1H), 4.01 (s, 3H), 3.81 (s, 2H), 3.75 - 3.62 (m, 2H), 3.23 (t, *J* = 7.0 Hz, 2H), 1.88 - 0.90 (m, 28H).

^{13}C NMR (101 MHz, 150 MHz, Chloroform-*d*$_1$, δ ppm) δ 162.67, 156.31, 149.01, 147.84, 147.05, 142.23, 138.76, 133.56, 131.03, 125.39, 121.67, 120.00, 119.29, 111.36, 108.29, 101.43, 100.43, 69.21, 66.96, 59.05, 56.45, 55.74, 51.44, 41.23, 40.74, 31.13, 30.64, 26.67, 25.82, 25.36, 14.79.

ESI: *m/z* 692 $[M + H]^+$.

***trans*-4-{[6-(2,5-Dioxo-2,5-dihydro-1*H*-pyrrol-1-yl)hexanamido]methyl}cyclohexane-1-carboxylic acid (81)**

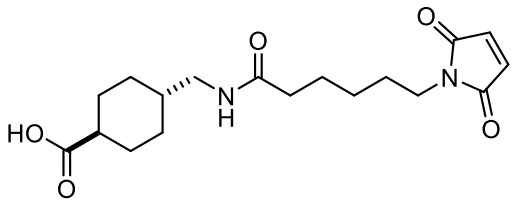

EDC·HCl (1.054 g, 5.5 mmol) and *N*-hydroxysuccinimide (576 mg, 5 mmol) were added at 0 °C, under N_2, to a solution of 6-maleimidohexanoic acid (1.056 g, 5 mmol) in dry CH_2Cl_2 (6 mL) and the mixture stirred at r.t. for 16 h. The reaction mixture was washed with HCl 0.1 N and H_2O, then

dried over Na_2SO_4 and the solvent removed under reduced pressure. The activated acid was obtained as a white solid without further purification (1.46 g, 4.7 mmol, 94% yield).

ESI: *m/z* 309 $[M + H]^+$.

The obtained solid was dissolved into glacial acetic acid (10 mL) and *trans*-4-(aminomethyl)-cyclohexane carboxylic acid (1.06 g, 6.75 mmol) was added at r.t. The reaction mixture was stirred at r.t. for 16 h. Acetic acid was removed under reduced pressure, the residue diluted with MeOH (10 mL) and filtered through a short pad of Celite. H_2O (40 mL) was slowly added to the MeOH solution and the mixture stirred at r.t. for 30 min. The solid was combined by filtration and dried under vacuum to give pure compound **81** (510 mg, 1.46 mmol, 32% yield).

^{1}H NMR (400 MHz, Methanol-*d*$_4$, δ ppm, *J* Hz) δ 6.85, (s, 2H), 3.54 (t, *J* = 7.2 Hz, 2H), 3.07 (d, *J* = 7.0 Hz, 2H), 2.27 - 2.21 (m, 2H), 2.05 (dd, *J* = 14.0, 3.5 Hz, 2H), 1.87 (dd, *J* = 13.3, 3.6 Hz, 2H), 1.69-1.62 (m, 4H), 1.49 - 1.32 (m, 6H), 1.05 (m, 2H).

^{13}C NMR (100 MHz, Methanol-*d*$_4$, δ ppm) δ 178.04, 174.19, 170.74, 133.52, 44.59, 42.61, 36.80, 36.61, 35.03, 29.14, 28.05, 27.46, 25.55, 24.76.

ESI: *m/z* 349 $[M - H]^-$.

***trans*-4-({5-[3-(3-{2-Azatricyclo[10.4.0.0^{4,9}]hexadeca-1(12),4(9),5,7,13,15-hexaen-10-yn-2-yl}-3-oxopropylamino)-2,5-dioxo-1-pyrrolidinyl]pentylcarbonylamino}methyl)cyclohexanecarboxylic acid (78)**

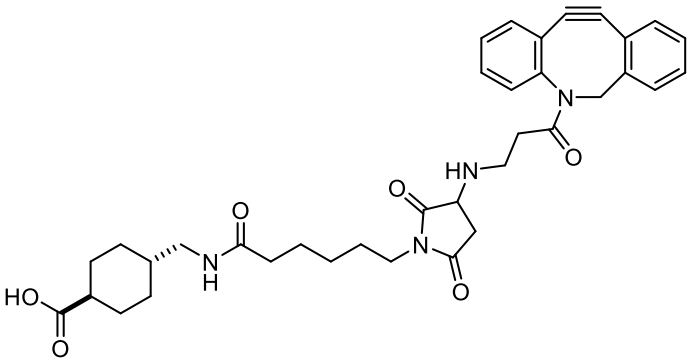

To a solution of DBCO-amine (91 mg, 0.33 mmol) in dry MeCN (2 mL), Et_3N (46 µL, 0.33 mmol) was added dropwise, at r.t. under N_2. The resulting mixture was stirred for 15 min, then compound **81** (100 mg, 0.3 mmol) was slowly added. The mixture was stirred at r.t. for 16 h and then the crude was concentrated under vacuum. The crude was purified by silica gel flash-chromatography eluting 2% mixture of MeOH in CH_2Cl_2, to provide pure compound **78** as a yellow solid (144 mg, 0.23 mmol, 70% yield).

^{1}H NMR (400 MHz, Methanol-*d*$_4$, δ ppm, *J* Hz) δ 7.91 (d, *J* = 6.49 Hz, 1H), 7.65 (t, *J* = 6.53 Hz, 1H), 7.50-7.47 (m, 1H), 7.44-7.40 (m, 2H), 7.32-7.29 (m, 2H), 7.20 (td, *J* = 8.48, 7.97, 1,49 Hz, 1H), 5.13 (dd, *J* = 14.03, 3.09 Hz, 1H), 3.70 (dd, *J* = 13.91, 3.99 Hz, 1H), 3.58 (dd, *J* = 8.45, 4.84 Hz, 1H), 3.40 (qd, *J* = 7.85, 7.19, 4.56 Hz, 2H), 2.99 (q, *J* = 5.57, 2H), 2.78-2.45 (m, 4H), 2.27-2.16 (m, 4H), 2.10-1.85 (m, 3H), 1.79 (d, *J* = 13.08 Hz, 2H), 1.66-1.49 (m, 4H), 1.48-1.25 (m, 4H), 0.96 (1, *J* = 12.87 Hz, 2H)

ESI: *m/z* 625 $[M - H]^-$.

***N*-[3-(2-azatricyclo[10.4.0.0^{4,9}]hexadeca-1(16),4,6,8,12,14-hexaen-10-yn-2-yl)-3-oxopropyl]-6-(2,5-dioxopyrrol-1-yl)hexanamide (79)**

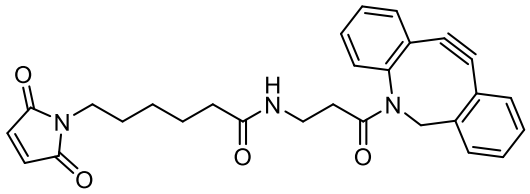

6-maleimidohexanoic acid (38 mg, 0.18 mmol) and DBCO-amine (40 mg, 0.14 mmol) were solubilized in anhydrous CH_2Cl_2 (2 mL), under N_2, and the resulting mixture was cooled to 0°C. Then EDC·HCl (52 mg, 0.27 mmol), HOBt (36 mg, 0.27 mmol) and Et_3N (38 µL, 0.27 mmol) were added. The resulting mixture was stirred at r.t. for 16 h. After completion of the reaction, the solvent was evaporated under reduced pressure. The crude was purified by silica gel flash-chromatography eluting 1% mixture of MeOH in CH_2Cl_2, providing product **79** as a yellow oil (58 mg, 0.12 mmol, 86 % yield).

^{1}H NMR (400 MHz, Chloroform-*d*$_1$, δ ppm, *J* Hz): δ 7.65 (dd, *J* = 7.6, 1.3 Hz, 1H), 7.41 - 7.25 (m, 7H), 6.66 (s, 2H), 5.94 (t, *J* = 6.1 Hz, 1H), 5.11 (d, *J* = 13.9 Hz, 1H), 3.67 (d, *J* = 13.9 Hz, 1H), 3.47 (t, *J* = 7.3 Hz, 2H), 3.31 (dddd, *J* = 13.7, 7.5, 6.3, 3.8 Hz, 1H), 3.18 (dddd, *J* = 13.5, 7.5, 5.9, 3.7 Hz, 1H), 2.42 (ddd, *J* = 16.6, 7.5, 3.8 Hz, 1H), 1.97 - 1.84 (m, 3H), 1.61 - 1.40 (m, 4H), 1.21 (ttd, *J* = 10.2, 7.4, 6.7, 3.5 Hz, 2H).

^{13}C NMR (101 MHz, Chloroform-*d*$_1$, δ ppm) δ 172.51, 172.29, 170.81, 150.99, 147.97, 134.06, 134.05, 132.08, 129.03, 128.61, 128.30, 127.84, 127.24, 125.54, 122.93, 122.46, 114.71, 55.51, 37.70, 37.66, 36.34, 35.12, 34.82, 28.26, 28.25, 26.36, 25.03, 24.34.

ESI: *m/z* 470 $[M + H]^+$.

Quantitative Fmoc Loading Determination by UV-Vis Spectroscopy

This protocol is used to determine the substitution level (loading) of the first Fmoc-amino acid attached to the solid support. The Fmoc group is cleaved from a known weight of resin using a piperidine 20% solution in CH_2Cl_2. This reaction releases dibenzofulvene (DBF), which reacts with piperidine to form a DBF-piperidine adduct that strongly absorbs UV light around 301 nm. The concentration, and thus the resin loading, can be calculated using the Beer-Lambert law.

Colorimetric assay for secondary amines

Two solutions were prepared:

A. 2% (v/v) acetaldehyde in DMF;
B. 2% (w/w) chloranil (2,3,5,6-tetrachloro-1,4-benzoquinone) in DMF.

To assess the presence of free amine few beads of resin were sampled and washed with DMF and MeOH. Then 2 drops of solution A and two drops of solution B were added to the washed resin. After 5 min, the color of the resin was analysed via microscope. The presence of blue beads reveals a positive test.[406]

Loading 2-chlorotrityl chloride resin with Fmoc-SAR-OH

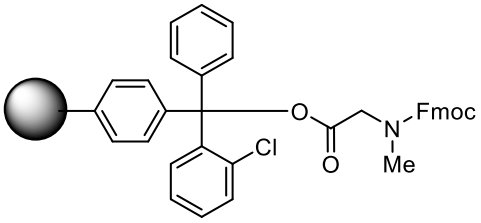

CTC resin (1 g, 100-200 mesh, 1% DVB, 1.1 mmol/g) was swollen in dry CH_2Cl_2 (10 mL) for 10 min. Then, a solution of Fmoc-SAR-OH (411 mg, 1.32 mmol) and DIPEA (0.960 mL, 5.5 mmol) in dry CH_2Cl_2 (10 mL) was added. The obtained mixture was stirred by bubbling N_2 for 2 h at r.t. After 2 h, solvent was removed by filtration under vacuum and the resin was washed with CH_2Cl_2 (3 x 10 mL x 10 min), DMF (3 x 10 mL x 10 min) and MeOH (3 x 10 mL x 10 min), and finally dried.

Fmoc deprotection

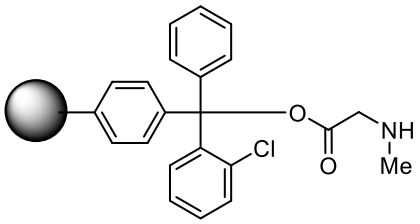

SAR-loaded resin was treated with a solution of piperidine 20% in DMF (1 mL/100 mg of resin) and stirred by bubbling N_2 for 30 min at r.t. This step was repeated again stirring for 15 min. At the end of the reaction, the resin was washed with DMF (4 x 5 mL x 5 min) and CH_2Cl_2 (4 x 5 mL x 5 min). The successful deprotection was verified via colorimetric assay for free secondary amines.

Amide coupling (chain elongation)

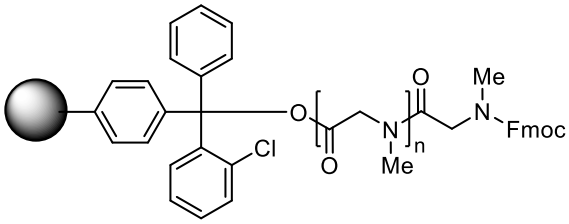

Deprotected resin was treated with a solution of Fmoc-SAR-OH or Fmoc-SAR-SAR-OH (3 equiv), HATU (3 equiv), DIPEA (3 equiv) in dry DMF (1 mL/100 mg of resin). The resulting mixture was stirred by bubbling N_2 for 2 h at r.t. At the end of the reaction the resin was washed with DMF (5 x 5 mL x 5 min) and CH_2Cl_2 (5 x 5 mL x 5 min). The successfull introduction of the Fmoc-protected peptide was verified via colorimetric assay.

The steps of Fmoc-deprotection and amide coupling were repeated until the desired lenght was reached, providing product **85**.

PSAR11-PFB (86)

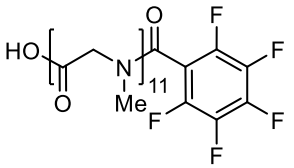

SAR-loaded resin was treated with a solution of piperidine 20% in DMF (1 mL/100 mg of resin) and stirred by bubbling N_2 for 30 min at r.t. This step was repeated again stirring for 15 min. At

the end of the reaction, the resin was washed with DMF (4 x 5 mL x 5 min) and CH_2Cl_2 (4 x 5 mL x 5 min). Then the resin was treated with a solution of pentafluorobenzoic acid (3 equiv), EDC·HCl (3 equiv), HOBt (3 equiv) and DIPEA (6 equiv) in DMF (1 mL/ 100 mg of resin), and the resulting mixture was stirred by bubbling N_2 for 2 h at r.t. The resin was washed with DMF (5 x 5 mL x 5 min) and CH_2Cl_2 (5 x 5 mL x 5 min). To cleave the product from the resin a solution of HFIP 20% and TIS 2% in CH_2Cl_2 (1 mL/ 100 mg of resin) was added and stirred by bubbling N_2 for 1h. The solution was filtered and the step was repeated for 30 min. The final filtrate was evaporated under vacuum, then the product was precipitated by adding Et_2O. The resulting suspension was centrifuged at 3000 rpm for 5 min, washing with Et_2O two times, and finally the obtained solid was dried under vacuum for 24 h.

ESI: *m/z* 992 $[M - H]^-$.

DBCO-PSAR11-PFB (87)

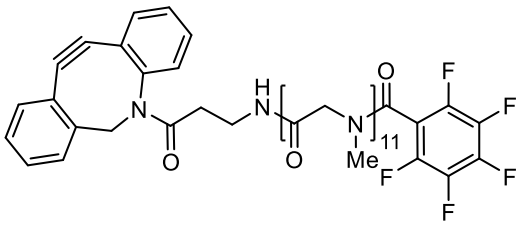

Compound **86** (35 mg, 0.035 mmol) was solubilized in dry DMF (500 μL), then HATU (15 mg, 0.0385 mmol) and DIPEA (25 μL, 0.14 mmol) were added, and the resulting mixture was stirred at r.t. for 5 min. Then DBCO-amine (12 mg, 0.042 mmol) was added, and the mixture was stirred under N_2, in the dark, for 16 h. At the end of the reaction, the solvent was removed under vaccum and the resulting crude was purified via preparative-HPLC eluting a 0-60% gradient of MeCN in H_2O. The product was obtained as a pink solid (15 mg, 35% yield).

ESI: *m/z* 1252 $[M + H]^+$.

General procedure for SPAAC click reactions (GP4)

Linker-payload systems (1 equiv) solubilized in DMF (500 µL) was reacted with a solution of compound **87** in DMSO. The resulting mixture was stirred at r.t. for 16 h. The reaction mixture was purified via preparative-HPLC.

2-((2,5-dioxo-1-(6-oxo-6-((3-(8-(2,5,8,11,14,17,20,23,26,29,32-undecamethyl-1,4,7,10,13,16,19,22,25,28,31,34-dodecaoxo-1-(perfluorophenyl)-2,5,8,11,14,17,20,23,26,29,32,35-dodecaazaoctatriacontan-38-oyl)-8,9-dihydro-3H-dibenzo[b,f][1,2,3]triazolo[4,5-d]azocin-3-yl)benzyl)amino)hexyl)pyrrolidin-3-yl)thio)ethyl (E)-(4-(((((4-methyl-3-(4-phenethylbenzamido)phenyl)amino)(3,4,5-trimethoxybenzamido)methylene)amino)methyl)phenyl)carbamate (88)

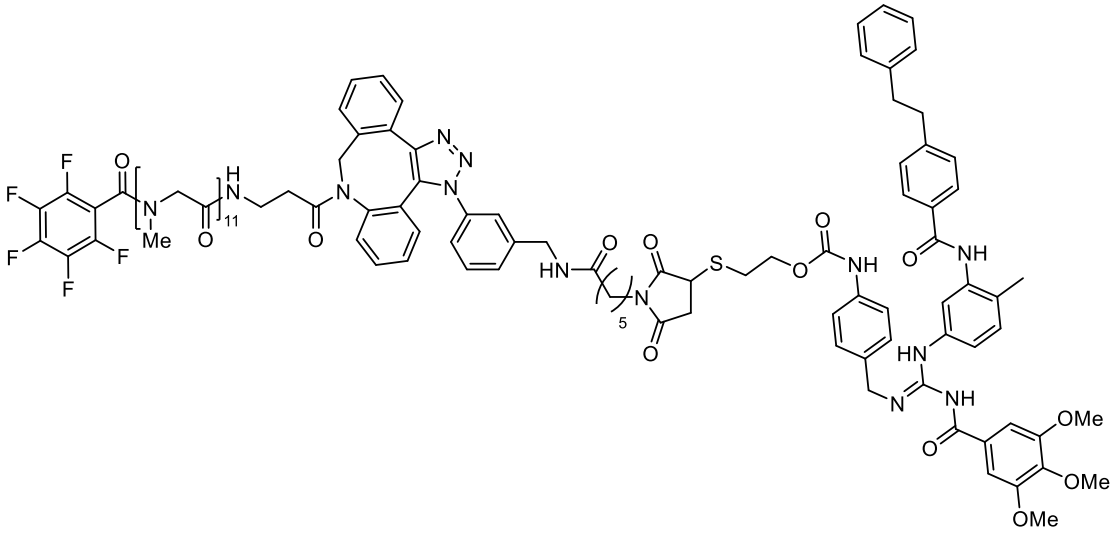

Prepared according to **GP4** from linker-payload **64**.

ESI: *m/z* 1186 $[M + 2H]^{2+}$.

2-((2,5-dioxo-1-(6-oxo-6-((3-(8-(2,5,8,11,14,17,20,23,26,29,32-undecamethyl-1,4,7,10,13,16,19,22,25,28,31,34-dodecaoxo-1-(perfluorophenyl)-2,5,8,11,14,17,20,23,26,29,32,35-dodecaazaoctatriacontan-38-oyl)-8,9-dihydro-3H-dibenzo[b,f][1,2,3]triazolo[4,5-d]azocin-3-yl)benzyl)amino)hexyl)pyrrolidin-3-yl)thio)ethyl cyclohexyl((8-hydroxy-4-methoxyquinolin-7-yl)methyl)carbamate (89)

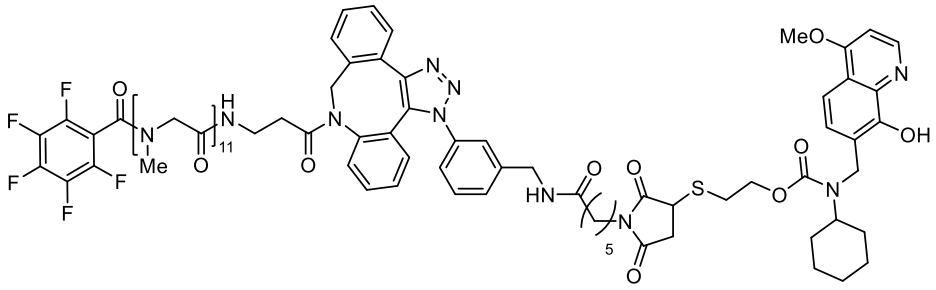

Prepared according to **GP4** from linker-payload **67**.

ESI: *m/z* 993 $[M+2H]^{2+}$.

(2-ethoxy-7-((9-(8-(2,5,8,11,14,17,20,23,26,29,32-undecamethyl-1,4,7,10,13,16,19,22,25,28,31,34-dodecaoxo-1-(perfluorophenyl)-2,5,8,11,14,17,20,23,26,29,32,35-dodecaazaoctatriacontan-38-oyl)-8,9-dihydro-3H-dibenzo[b,f][1,2,3]triazolo[4,5-d]azocin-3-yl)nonyl)oxy)benzo[d][1,3]dioxol-5-yl)methyl cyclohexyl((8-hydroxy-4-methoxyquinolin-7-yl)methyl)carbamate (90)

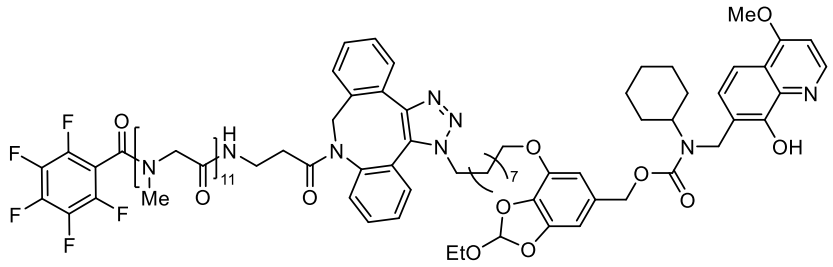

Prepared according to **GP4** from linker-payload **77**.

ESI: *m/z* 973 $[M+2H]^{2+}$.

***N*-(36-(3-(9-((6-((2,6-dimethoxy-4-((*N*-(4-methyl-3-(4-phenethylbenzamido)phenyl)carbamimidoyl)carbamoyl)phenoxy)methyl)-2-ethoxybenzo[d][1,3]dioxol-4-yl)oxy)nonyl)-3,9-dihydro-8H-dibenzo[b,f][1,2,3]triazolo[4,5-d]azocin-8-yl)-3,6,9,12,15,18,21,24,27,30-decamethyl-2,5,8,11,14,17,20,23,26,29,32,36-dodecaoxo-3,6,9,12,15,18,21,24,27,30,33-undecaazahexatriacontyl)-2,3,4,5,6-pentafluoro-N-methylbenzamide (91)**

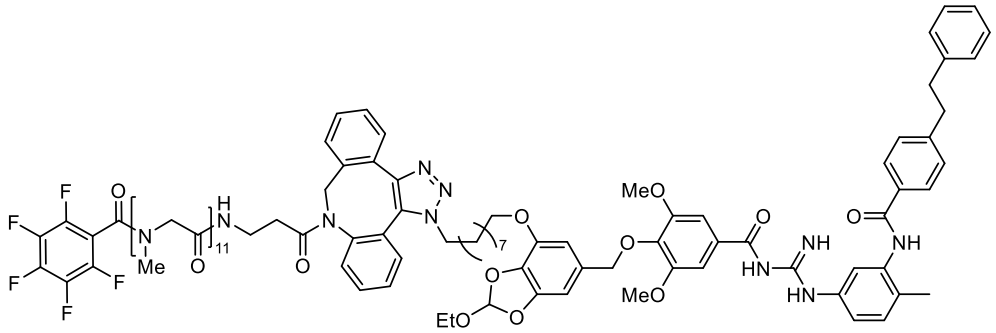

Prepared according to **GP4** from linker-payload **76**.

ESI: *m/z* 1135 $[M+2H]^{2+}$.

4.1.3. Bioconjugation procedures

General procedure for preparation of ADCs 48-50, 83 and 84.

The carboxylic acid moiety of linker-payload system (28 µL, 10 mM in DMSO) was activated by adding S-NHS (5 µL, 100 mM in mQ) and EDC·HCl (5 µL, 100 mM in mQ). The reaction was stirred for 16 h at r.t.

The resulting solution was added to a solution 10 mg/mL of Cetuximab or Bevacizumab in PBS (pH 7.4, 35 µL). The mixture was stirred at r.t. for 1 h. The excess of linker-payload was quenched adding 20 mM glycine aqueous solution (27 µL). The obtained ADCs were purified by ultrafiltration using 10 kDa cutoff dialysis membrane removing the unreacted excess of small molecules. DAR was determined by MALDI analysis.

General procedure for preparation of ADCs 94-97.

To a solution 5mg/mL of Cetuximab in TRIS buffer (pH 8.0, 100 µL) a solution of TCEP (6.6 µL, 10 mM in mQ) was added and the mixture was stirred at r.t. for 2 h. The excess of reductant was removed by ultrafiltration using 10 kDa cutoff dialysis membrane. Immediately after filtration, solution of compounds **88-91** in DMSO was added to the reduced mAb, and the mixture was

stirred at 4 °C for 16 h. The obtained ADCs were purified by ultrafiltration using 10 kDa cutoff dialysis membrane removing the unreacted excess of small molecules and the resulting bioconjugates were analysed via HIC.

Cell viability assay on ADCs 95 and 96.

$3x10^3$/well SK- MEL-5 melanoma cells were seeded in triplicate in 96-well plates (Corning) with complete DMEM medium. After 24h cells were treated in 2.5% FBS DMEM with Cetuximab, JC19, unconjugated linker-payload systems and ADCs **95** and **96** at different concentrations to compare the effect of ADCs with the single components. After 72 h of treatment the culture medium was removed, cells were fixed in paraformaldehyde (Kaltek Srl) for 10 minutes and then stained with Crystal Violet (Sigma- Aldrich) (0.1% Crystal Violet, 20% Methanol, dH2O) for 15 minutes in mild agitation. After 24 h, cells were bleached with 10% glacial acetic acid RPE (Carlo Erba) for 15 minutes in mild agitation, then the absorbance, which is proportional to the number of viable cells within every well, was measured at 595 nm with VICTOR X5 (Multilabel Plate Reader, PerkinElmer).

Cytofluorimetric analysis of cell apoptosis on ADCs 95 and 96.

For analysis of cellular apoptosis was used a double staining with Annexin V and 7-Aminoactinomycin D (7-AAD) (BD PharmingenTM). SK-MEL-5 melanoma cells were seeded in 6-multiwell plates (Corning) in complete medium and after 24 h were treated with Cetuximab, JC19, unconjugated linker-payload systems and ADCs at 200 µg/mL concentration. After 72 h of treatment culture medium has been collected, cells have been detached with Accutase (Thermo Scientific) and resuspended in 50 µL of 1X Binding Buffer (BD PharmingenTM). Cells were stained with 1 µL of Annexin V and 2.5 µL of 7- Aminoactinomycin D (BD PharmingenTM) for 15 minutes in the dark and added with 200 µL of 1X Binding Buffer for the analysis with CytoFLEXS (BD Beckman Coulter).

4.2. EXPLORATION AND DEVELOPMENT OF BIOCONJUGATION METHODOLOGIES

4.2.1. General experimental procedures, materials and instruments

All reagents were used as purchased from commercial suppliers without further purification. The reactions were carried out in oven dried vessels. Solvents were dried and purified by conventional methods prior use or, if available, purchased in anhydrous form.

MALDI analysis were performed with the MALDI-TOF in linear mode set at 83% of laser intensity. Samples preparation: the matrix solutions were prepared at two different concentrations, and both were used in parallel. 20.0 mg or 25 mg of Super DHB were dissolved in a solution of MeCN (150 µL), H_2O (350 µL) and TFA (0.05 µL) and deposited in a stainless-steel target placed in a termoblock set at 39 °C. When the sample was dried, 1.65 µL of matrix solution was added and once completely dried and crystalized, the target plate was removed from the termoblock. The target plate was analyzed with MALDI-TOF set in linear mode at 83% of laser intensity. The *m/z* range was from 30 kDa to 200 kDa. For each sample spot, 10 shots were acquired to improve the spectra quality and mass accuracy.

4.2.2. Bioconjugation procedures

Preparation of ADC 100

To a 10 mM DMSO solution of compound **98** (10 mM in DMSO), an aqueous solution of S-NHS (2 eq, 100 mM in mQ) and an aqueous solution of EDC·HCl (2 equiv, 100 mM in mQ) were added, and the mixture was stirred at r.t for 16 h. Subsequently, 250 µL of Cetuximab (0.025 equiv, 10 mg/mL, EPPS pH 8.0) were added, and the mixture was gently mixed at r.t. for 1 h. An aqueous solution of glycine (2 equiv, 40 mM in mQ) was added to quench the unreacted linker-payload system, and the mixture was stirred at r.t. for 5 min. The obtained ADCs were purified by ultrafiltration using 10 kDa cutoff dialysis membrane removing the unreacted excess of small molecules. DAR was determined by MALDI analysis.

Pre-functionalization of Cetuximab

To 400 µL of Cetuximab (0.05 equiv, 10 mg/mL, PBS pH 7.4) was added a 10 mM solution in DMSO of 14-azido-3,6,9,12-tetraoxatetradecanoic acid (**103**). The mixture was stirred at r.t. for 1 h. An aqueous solution of glycine (2 equiv, 40 mM in mQ) was added to quench the unreacted linker-payload system, and the mixture was stirred at r.t. for 5 min. The resulting bioconjugate (**Ctx-N_3**) was purified by ultrafiltration using 10 kDa cutoff dialysis membrane and analysed by MALDI mass spectrometry.

Preparation of ADC 104

To 450 µL of the functionalized **Ctx-N_3** (5.7 mg/mL in PBS pH 7.4) was added a DMSO solution of the linker-payload system (**102**, 80 equiv), and the mixture was gently mixed at 4 °C for 16 h. The resulting bioconjugate was purified by ultrafiltration using 10 kDa cutoff dialysis membrane and analysed by MALDI mass spectrometry.

Preparation of ADCs 107-108

The proper carboxylic acid (**105** or **106**, 0.01 mmol) was dissolved in anhydrous DMF (0.5 mL) in a round bottom flask under N_2 and magnetic stirring. DCC (3 mg, 0.014 mmol) and NHS (2 mg, 0.014 mmol) were added to the solution and the mixture stirred at r.t. for 16 h. The white solid was removed by filtration and the solvent removed under vacuum, to provide a white solid (MS(ESI): m/z 881 $[M + Na]^+$ for activated **105**, 833 $[M + Na]^+$ for activated **106** that was dissolved in DMSO in order to obtain a 10 mM solution.

To a solution of Trastuzumab (in PBS pH 7.4) was added a DMSO solution of the activated linker-payload system (**105** or **106**, mM in DMSO, 20 equiv), and the mixture was gently mixed at r.t. for 1 h. An aqueous solution of glycine (2 equiv, 40 mM in mQ) was added to quench the unreacted linker-payload system, and the mixture was stirred at r.t. for 5 min. The resulting bioconjugate (**107** and **108**) was purified by ultrafiltration using 10 kDa cutoff dialysis membrane and analysed by MALDI mass spectrometry.

Preparation of ADC 110

To a solution of anti-CD115 mAb (100 µL in PBS pH 7.4) was added a DMSO solution of the activated linker-payload system (**109**, mM in DMSO, 20 equiv), and the mixture was gently mixed at r.t. for 1 h. An aqueous solution of glycine (2 equiv, 40 mM in mQ) was added to quench the unreacted linker-payload system, and the mixture was stirred at r.t. for 5 min. The resulting

bioconjugate was purified by ultrafiltration using 10 kDa cutoff dialysis membrane and analysed by MALDI mass spectrometry.

Pre-functionalization of anti-CD115 mAb

To 100 µL of anti-CD115 mAb (0.1 equiv, 2 mg/mL, PBS pH 7.4) was added a 10 mM solution in DMSO of 14-azido-3,6,9,12-tetraoxatetradecanoic acid (1.4 µL). The mixture was stirred at r.t for 1 h. An aqueous solution of glycine (2 equiv, 20 mM in mQ) was added to quench the unreacted linker-payload system, and the mixture was stirred at r.t. for 5 min. The resulting bioconjugate (**CD115-N_3**) was purified by ultrafiltration using 10 kDa cutoff dialysis membrane and analysed by MALDI mass spectrometry.

Preparation of ADC 111

To 100 µL of the functionalized **CD115-N_3** (1.9 mg/mL in PBS pH 7.4) was added a DMSO solution of the linker-payload system (**112**, 40 equiv), and the mixture was gently mixed at 4 °C for 16 h. The resulting bioconjugate was purified by ultrafiltration using 10 kDa cutoff dialysis membrane and analysed by MALDI mass spectrometry.

4.3. SYNTHESIS AND EVALUATION OF Hh AGONISTS FOR OSTEOGENIC APPLICATIONS

4.3.1. General experimental procedures, materials and instruments

All reagents were used as purchased from commercial suppliers without further purification. The reactions were carried out in oven dried vessels. Solvents were dried and purified by conventional methods prior use or, if available, purchased in anhydrous form.

Flash column chromatography was performed with Merck silica gel Å 60, 0.040-0.063 mm (230-400 mesh). MPLC Syncore Büchi on highly resistant PP cartridges Normal Phase silica gel NP 40 - 63 µm particle size and 60 Å pore size (Si60) withstand a maximum pressure of 10 bar (145 psi) column with PE (Eluent A) and EtOAc (Eluent B) as mobile phase. Merck aluminum backed plates pre-coated with silica gel 60 (UV254) were used for analytical thin layer chromatography and were visualized by staining with a $KMnO_4$ or Ninidrine solution.

NMR spectra were recorded at 25 °C or at 37 °C with 400 or 600 MHz for 1H and 101 or 151 MHz for 13C Brücker Advance NMR spectrometers. The solvent is specified for each spectrum. Splitting patterns are designated as s, singlet; d, doublet; t, triplet; q, quartet; m, multiplet; bs, broad singlet. Chemical shifts (δ) are given in ppm relative to the resonance of their respective residual solvent peaks.

High and low resolution mass spectroscopy analyses were recorded by electrospray ionization with a mass spectrometer Q-exactive Plus.

HPLC analyses were performed on a LC/MSD system Agilent InfinityLab LC/MSD iQ, Method: Column: InfinityLab PoroShell 120 EC-C18 2.1 x 50mm x 2.7µm. Flow: 0.4 mL/min. Eluent A/B: H_2O/MeCN. Gradient: 5% B to 95% B in 10 minutes, 4 minutes at 95 % B and 3 minutes of re-equilibration. Detection: 254 nm and 210 nm.

4.3.2. Synthetic procedures

propyl 4-(1-hexyl-4-hydroxy-2-oxo-1,2-dihydroquinoline-3-carboxamido)benzoate (GSA-10)

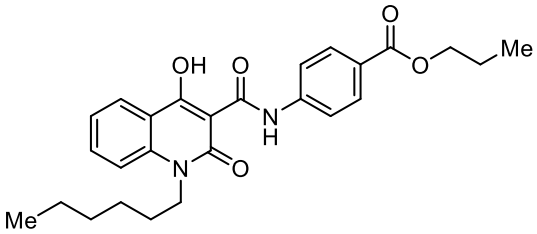

The product was prepared according to the literature.[311]

^{1}H NMR (400 MHz, Chloroform-*d*$_3$, δ ppm, *J* Hz): δ 16.30 (bs, 1H), 15.71 (bs, 1H), 8.24 (d, *J* = 8.0 Hz, 1H), 7.85 (d, *J* = 8.4 Hz, 2H), 7.77 (t, *J* = 8.4 Hz, 1H), 7.44-7.24 (m, 2H), 6.52 (d, *J* = 8.8 Hz, 2H), 4.27 (t, *J* = 7.6 Hz, 2H), 4.19 (t, *J* = 6.4 Hz, 2H), 2.85-2.80 (m, 2H), 1.76-1.71 (m, 2H), 1.45-1.23 (m, 6H), 0.98 (t, *J* = 7.6 Hz, 3H), 0.89 (t, *J* = 6.8 Hz, 3H).

^{13}C NMR (400 MHz, Chloroform-*d*$_3$, δ ppm): δ 197.23, 173.05, 170.67, 164.25, 141.28, 139.13, 134.52, 130.97, 125.94, 123.06, 115.64, 92.11 72.54, 65.95, 42.32, 29.71, 26.54, 26.11, 22.01 21.95, 13.53, 10.11.

ESI: *m*/*z* 473 $[M + Na]^+$, 449 $[M - H]^-$.

4-(1-hexyl-4-hydroxy-2-oxo-1,2-dihydroquinoline-3-carboxamido)benzoic acid (2)

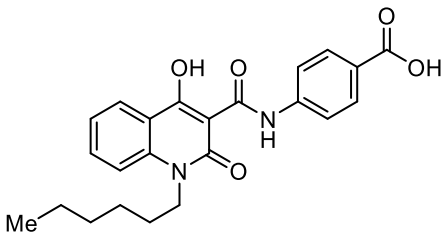

The product was prepared according to the literature.[311]

^{1}H NMR (400 MHz, Methanol-*d*$_4$, δ ppm, *J* Hz): δ 16.37 (bs, 1H), 15.82 (bs, 1H), 8.24 (d, *J* = 8.0 Hz, 1H), 7.87 (d, *J* = 8.4 Hz, 2H), 7.77 (t, *J* = 8.4 Hz, 1H), 7.44-7.24 (m, 2H), 6.52 (d, *J* = 8.8 Hz, 2H), 4.27 (t, *J* = 7.6 Hz, 2H), 2.85-2.80 (m, 2H), 1.49-1.23 (m, 6H), 0.89 (t, *J* = 6.8 Hz, 3H).

^{13}C NMR (400 MHz, Methanol-*d*$_4$, δ ppm): δ 197.21, 173.05, 170.67, 169.23, 139.13, 134.58, 130.92, 128.81, 125.99, 123.06, 115.62, 72.53, 42.32, 30.58, 29.71, 26.11, 19.13, 13.49.

ESI: *m*/*z* 407 $[M - H]^-$, 443 $[M + Cl]^-$.

propyl 4-(4-hydroxy-6,7-dimethoxy-2-oxo-1-propyl-1,2-dihydroquinoline-3-carboxamido)benzoate (1)

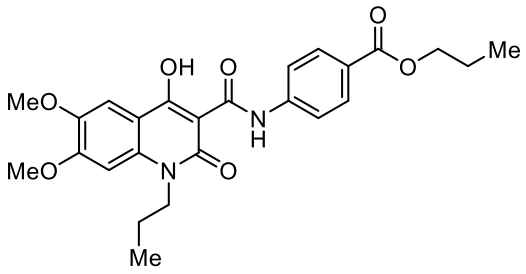

The product was prepared according to the literature.[311]

^{1}H NMR (400 MHz, Chloroform-d_3, δ ppm, *J* Hz): δ 16.28 (bs, 1H), 12.87 (bs, 1H), 8.02 (d, *J* = 8.4 Hz, 2H), 7.76 (d, *J* = 8.8 Hz, 2H), 7.55 (s, 1H), 6.72 (s, 1H), 4.24 (q, *J* = 6.4 Hz, 4H), 4.00 (s, 3H), 3.96 (s, 3H), 1.82 - 1.75 (m, 4H), 1.50 - 0.92 (m, 6H).

^{13}C NMR (400 MHz, Chloroform-d_3, δ ppm): δ 171.19, 170.00, 166.25, 162.49, 155.14, 145.74, 141.64, 135.66, 130.68, 126.19, 125.70, 120.30, 109.07, 105.33, 96.92, 95.82, 77.33, 77.01, 76.69, 66.44, 56.25, 44.18, 20.17, 11.44, 10.54.

ESI: *m/z* 469 $[M + H]^+$, 491 $[M + Na]^+$, 507 $[M + K]^+$.

SECTION B - DEVELOPMENT OF PHOTOREDOX METHODOLOGY USING SULFUR HEXAFLUORIDE FOR NUCLEOPHILIC FLUORINATION OF ALKOXYAMINES

CHAPTER 1. INTRODUCTION

1.1. THE IMPORTANCE OF FLUORINE IN PHARMACEUTICAL AND AGROCHEMICAL SCIENCES

The strategic introduction of fluorine into organic molecules has become a cornerstone of modern medicinal and agrochemical chemistry. While fluorine-containing compounds are rare in nature, their synthesis and application in the design of bioactive substances are now considered indispensable. This prominence stems from the unique physicochemical and stereoelectronic properties of the fluorine atom and the carbon-fluorine (C-F) bond. Fluorine possesses the highest electronegativity on the Pauling scale, and its atomic radius is the second smallest, comparable to that of hydrogen[412]. These fundamental characteristics enable fluorine to form an exceptionally strong single bond with carbon, with a bond energy of approximately 485 $kJmol^{-1}$.[413]

These properties allow the fluorine atom to act as a potent modulator of a molecule's biological behavior. The introduction of fluorine can dramatically alter a compound's properties, influencing its acidity, lipophilicity, stability, and overall reactivity.[414–416] Such enhancements can manifest in improved binding to target receptors, more efficient transport to the site of action, and increased resistance to metabolic deactivation.[417]

1.1.1. Physicochemical and stereoelectronic properties

Fluorine's high electronegativity and the resulting polarity of the C-F bond, which has a large dipole moment (μ=1.51D), have significant electronic and conformational effects on a molecule.[418] A primary effect is the modulation of acidity; the electron-withdrawing nature of fluorine can stabilize a conjugate base, thereby altering the molecule's pKa value and its interactions with biological targets, such as through hydrogen bonding.[419] Furthermore, fluorine atoms play a critical role in controlling a molecule's lipophilicity. As a consequence, fluorine can improve its permeability through biological membranes, facilitating its transport to the intended site of action.[420] A prominent example is the use of trifluoromethyl (CF_3) and trifluoromethoxy (OCF_3) groups, which have been shown to improve the penetration of active ingredients into the CNS. Beyond electronic effects, the small size of the fluorine atom, which is similar to that of hydrogen, allows for subtle but significant stereoelectronic and conformational changes. The substitution of a hydrogen atom with a fluorine atom often results in a minimal steric

perturbation while altering the molecule's electronic landscape.[421] For instance, high quantum mechanical level calculations have demonstrated that polyfluorinated isopropyl moieties induce a preference for a coplanar arrangement of the phenyl ring and the C-F bonds, with rotational barriers of approximately 7.74 and 6.62 kcalmol^{-1} for heptafluoro-iso-propyl and 1-methoxy-heptafluoro-iso-propyl groups, respectively.[422] These conformational changes can be crucial for optimizing the fit of an active ingredient into its receptor's binding pocket.

1.1.2. Bioisosteric replacement and metabolic stabilization

A fundamental strategy in drug and agrochemical design is bioisosteric replacement, where an atom or group is substituted with another that has similar size, shape, and electronic properties.[423] The fluorine atom is the perfect bioisostere for hydrogen due to their comparable atomic radii. The trifluoromethyl group (CF_3) is a widely used bioisostere for a methyl group (CH_3), a strategy particularly effective for enhancing metabolic stability.[424] This strategic replacement of hydrogen with fluorine or methyl with a trifluoromethyl group can block or significantly decrease oxidation processes, particularly those mediated by cytochrome P450 monooxygenases.[424] This deliberate modification prevents the molecule from being prematurely metabolized and deactivated, thereby increasing its half-life and overall efficacy in the body. A classic example of this is the drug ezetimibe, where key metabolic sites are strategically replaced by fluorine atoms to achieve metabolic stabilization and an enhanced PK profile.[425]

1.1.3. Fluorine in modern agrochemicals

Agrochemicals launched in the period from 2016 to 2022 reveal the sustained and growing importance of fluorine in this sector. Approximately 64% of all new halogenated agrochemicals introduced during this time were fluorinated, with a clear preference for specific fluorine-containing motifs. The trifluoromethyl group was found in approximately 52% of these products, the difluoromethyl (CHF_2) group in 20%, and the trifluoromethoxy (OCF_3) group in 4%.[426] The trifluoromethylpyridine (TFMP) fragment is particularly noteworthy, being a biologically active fragment in about 30 marketed pesticides.[427]

Fluorinated herbicides often function by mimicking natural plant hormones or by inhibiting key biosynthetic pathways. The precise placement of fluorine is critical for their efficacy.

- Auxin Mimics (Florpyrauxifen-benzyl): The herbicide florpyrauxifen-benzyl (**Figure 71a**) acts as a synthetic mimic of the naturally occurring plant growth hormone indole-3-acetic

acid (IAA).[428] Its development hinged on a detailed SAR study that demonstrated the significant value of a fluorine atom at a specific position on the pyridine ring. The introduction of a fluorine at the 5-position of the pyridine ring led to optimized effectiveness against dicotyledonous weeds. A direct comparison of herbicidal activity with other halogens showed a clear ranking: 5−Br<5−Cl<5−H<5−F.[429] This finding underscores that the biological effect is not due to a generic halogen but is a highly specific interaction requiring the unique electronic and steric properties of the fluorine atom at that precise location.

- Protoporphyrinogen Oxidase (PPO) Inhibitors (Trifludimoxazin): Trifludimoxazin (**Figure 71b**) is a PPO inhibitor that contains a novel gem-difluorinated 3-oxo-2H-1,4-benzoxazine ring system.[430] This motif is central to its high efficacy. A comparative analysis with its non-fluorinated des-F2 analog revealed a significant enhancement in activity against problematic weeds such as velvetleaf and redroot pigweed, highlighting that the gem-difluorination is an activity-enhancing structural feature. The fluorine atoms in this ring are believed to influence the dynamics of the PPO2 binding pocket, leading to a more favorable affinity with the herbicide ligand and, consequently, reduced affinity with the target enzyme.[431]

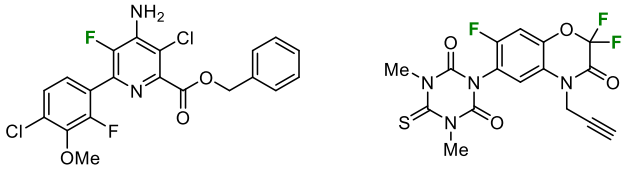

(a) - florpyrauxifen-benzyl **(b) -** trifludimoxazin

Figure 71. Structure of fluorinated herbicides **a)** florpyrauxifen-benzyl and **b)** trifludimoxazin.

Fungicides represent the largest class of new fluorinated agrochemicals, with a particular emphasis on heterocyclic scaffolds.

- Succinate Dehydrogenase Inhibitors (SDHIs): This class of fungicides (**Figure 72**), which targets complex II of the respiratory chain, has seen a significant rise in fluorinated compounds.[432] A common and highly effective structural motif is the pyrazole-4-carboxamide moiety, particularly when featuring a difluoromethyl (CHF_2) group. Prominent examples include pydiflumetofen, isoflucypram, inpyrfluxam, and fluindapyr.[426] In the case of isoflucypram, a specific SAR study showed that the 5-fluoro-

3-difluoromethyl pyrazole is particularly beneficial and significantly more active than its trifluoromethyl counterpart.[433]

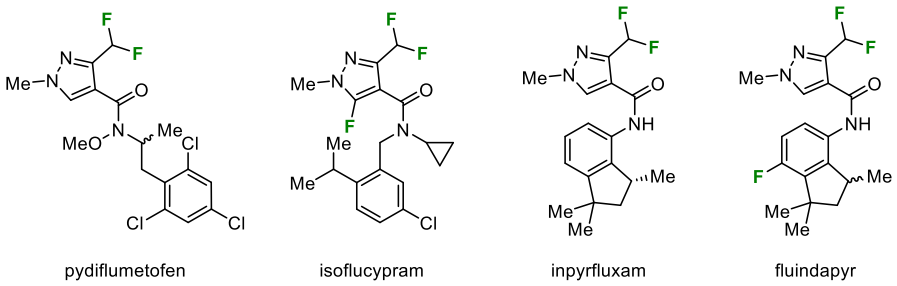

Figure 72. Structure of some fluorinated fungicides SDHIs.

1.1.4. Fluorine in pharmaceuticals

The importance of fluorine in pharmaceutical chemistry is a central theme in modern drug design. The strategic placement of fluorine atoms in bioactive molecules has been shown to enhance key PK parameters such as bioavailability, lipophilicity, and metabolic resistance.[434]

This is a widely used strategy to replace a hydrogen atom without causing significant steric changes to the molecule, while still dramatically altering its electronic profile, or improving its metabolic stability. The efficacy of this approach is evident in a number of recently approved FDA drugs that contain fluorinated moieties, suggesting that these groups contribute significantly to their biological activity and optimized PK profiles. These include:

- Tovorafenib (**Figure 73a**): A selective RAF kinase inhibitor with anti-tumor activity, used to treat pediatric low-grade glioma with specific genetic mutations. It works by inhibiting the RAF-mediated signalling pathways, such as the RAS-RAF-MEK-ERK pathway, which are often dysregulated in cancer. Tovorafenib is also noted for its ability to cross the BBB. [435]
- Vorasidenib (**Figure 73b**): A first-in-class dual inhibitor of mutant isocitrate dehydrogenase-1 (IDH1) and -2 (IDH2). This drug works by blocking the overproduction of D-2-hydroxyglutarate (2-HG), an oncometabolite that contributes to oncogenesis and tumor growth. Vorasidenib demonstrates improved brain penetration and higher drug exposure compared to other IDH inhibitors, making it effective for treating low-grade glioma.[436]

- Other approved drugs such as inavolisib, acoramidis, ensartinib, danicopan, and seladelpar also feature fluorine-containing moieties, which may contribute to their optimized biological and pharmacokinetic profiles.[434]

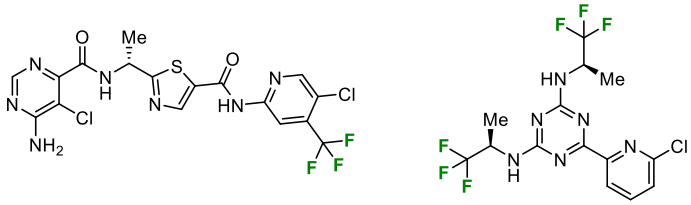

(a) - Tovorafenib **(b)** - Vorasidenib

Figure 73. Structure of two fluorinated drugs **a)** Tovorafenib and **b)** Vorasidenib.

The development of new fluorinated bioactive compounds is inextricably linked to the evolution of synthetic methodologies. While traditional methods for incorporating fluorine remain foundational, modern chemistry is increasingly turning to more efficient and sustainable approaches to address the challenges of complexity and scale.

1.2. TRADITIONAL FLUORINATING REAGENTS: CHALLENGES AND LIMITATIONS

The two primary approaches for synthesizing fluorinated organic compounds are: 1) the "fluorinated synthon" method, which involves incorporating a pre-fluorinated molecule, and 2) the direct fluorination method, which creates new carbon-fluorine bonds in a pre-existing molecule.[437] Over 90% of fluorinated drugs and agrochemicals are produced using the building-block method, where fluorine is introduced as part of a raw material.[437] However, a significant amount of research has focused on the direct fluorination approach to overcome the limitations of traditional methods.

For this reason the development of advanced fluorinating reagents is continously evolving. These newer reagents are designed for enhanced thermal stability, operational simplicity, and chemoselectivity, making them suitable for late-stage fluorination of complex, biologically active molecules. In addition, multicomponent reactions (MCRs) have emerged as powerful tools for synthesizing fluorinated compounds.[434] These "one-pot" processes combine three or more reagents to build complex scaffolds, including fluorine-containing polyheterocycles, efficiently and sustainably. They are praised for their high atom economy, minimal need for purification, and alignment with green chemistry principles.

The formation of the carbon-fluorine bond is often a significant challenge in organic synthesis due to the unique physicochemical properties of fluorine and the inherent limitations of traditional fluorination methods. The choice of reagent is critical and depends on the specific transformation required, whether it be nucleophilic, electrophilic, or radical-mediated.

1.2.1. Nucleophilic fluorinating reagents

A key class of nucleophilic reagents includes sulfur trifluoride derivatives, which are particularly effective for deoxyfluorination, the conversion of hydroxyl groups into fluorine atoms. The most well-known is diethylaminosulfur trifluoride (DAST - **Figure 74a**)[438] , which has been a popular choice for fluorinating alcohols and other substrates due to its versatility and ease of handling. However, DAST can be thermally unstable and prone to decomposition. This led to the development of more stable and safer alternatives, such as bis(2-methoxyethyl)aminosulfur trifluoride (Deoxo-Fluor - **Figure 74b**)[439] and 2,2-difluoro-1,3-dimethylimidazolidine (DFI - **Figure 74c**)[440], which are more amenable to large-scale industrial applications. Beyond these, simple fluoride sources like alkali metal fluorides and quaternary ammonium fluorides have been studied. For instance, anhydrous tetrabutylammonium fluoride (TBAF) in DMSO has been shown to be effective for the fluorodenitration of activated ring systems under mild conditions.[441] A significant challenge with such reagents is the dual nature of the fluoride ion, which can act as both a nucleophile and a strong base, potentially leading to undesirable side reactions.

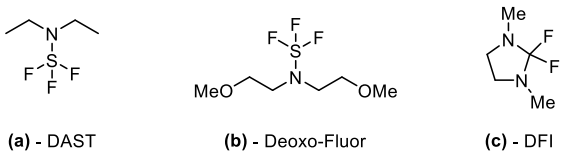

Figure 74. Structure of nucleophilic fluorinating agents **a)** DAST, **b)** Deoxo-Fluor and **c)** DFI.

1.2.2. Electrophilic fluorinating reagents

To circumvent the use of highly reactive and corrosive elemental fluorine gas (F_2), a range of user-friendly, bench-stable electrophilic reagents have been introduced. These reagents, often referred to as N-F reagents, function as a stoichiometric source of positive fluorine (F^+) and have revolutionized benchtop fluorination chemistry. A prominent example is Selectfluor (1-chloromethyl-4-fluoro-1,4-diazoniabicyclo[2.2.2]octane bis(tetrafluoroborate) - **Figure 75a**)[442], which is used in the enantioselective fluorination of β-ketoesters with high yields and enantiomeric excess in the presence of titanium complexes. Another widely used reagent is *N*-

fluorobenzenesulfonimide (NFSI - **Figure 75b**)[443], a stable crystalline solid that can be employed to fluorinate alkyl radicals and has also been applied in the synthesis of a steroid derivative.

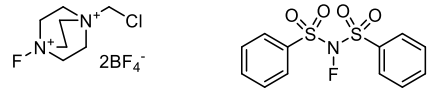

(a) - Selectfluor **(b)** - NSFI

Figure 75. Structure of electrophilic fluorinating agents **a)** Selectfluor, **b)** NSFI.

1.2.3. Radical-mediated fluorination

A variety of strategies have been developed to generate carbon-centered radicals for fluorination. For example, some methods utilize manganese-catalyzed C(sp^3)-H fluorination with silver fluoride (AgF) as the fluoride source and iodosobenzene as a stoichiometric oxidant.[444,445] Another notable approach is copper-catalyzed C(sp^3)-H fluorination via a Hydrogen Atom Transfer (HAT) mechanism, which proceeds through a transient Cu(III) fluoride intermediate.[446] Radical chemistry can also be initiated by photocatalysis, which uses visible light to drive reactions under mild conditions. This has enabled new routes for decarboxylative fluorination from carboxylic acids and allows for the selective fluorination of highly substituted aliphatic substrates that are challenging to synthesize using other methods. Radical-mediated fluorination has emerged as a powerful, complementary approach to traditional ionic methods, overcoming previous limitations associated with the lack of selective radical fluorinating agents. These innovations provide chemists with a broader and more selective toolbox for C-F bond formation under mild conditions.

One of the oldest and most fundamental challenges is the difficulty of creating new carbon-fluorine bonds with selective control over the reaction. Traditional fluorination reactions are generally limited to simple molecules and often require harsh conditions such as high temperatures or highly reactive intermediates, which severely restrict their application to more complex, functionalized molecules. Key difficulties are related to the properties of fluorine itself:

- High reactivity and toxicity: Elemental fluorine (F_2) is one of the most powerful and hazardous reagents, and its use is typically limited to specialized laboratories with dedicated equipment due to its corrosive nature and indiscriminately reactive character. This has led to the development of alternative, easier-to-handle reagents, but many of these are still toxic or unstable.

- Poor nucleophilicity: The fluoride ion (F^-) is a weak nucleophile in the presence of protic solvents like water or alcohols because its small size and high charge density cause it to form strong hydrogen bonds. This solvation shell effectively "cloaks" the ion, reducing its reactivity for nucleophilic substitution reactions.
- Dual reactivity: In the absence of hydrogen-bond donors, fluoride becomes a much better nucleophile, but also a strong base, which can lead to undesired side reactions like elimination.
- Harsh reaction conditions: Conventional methods such as the Balz-Schiemann and Halex reactions, used for preparing aryl fluorides, require high temperatures and aggressive conditions. These methods are unsuitable for molecules containing sensitive functional groups that cannot tolerate such a harsh chemical environment. The Halex reaction, for instance, is used industrially to convert electron-poor aromatic chlorides into fluorides using spray-dried potassium fluoride (KF) at high temperatures.
- Challenges in metal-catalyzed reactions: The high bond strength and polarized nature of the metal-fluorine bond make the reductive elimination step, a crucial part of many catalytic cycles, particularly challenging. This increases the activation energy barrier for C-F bond formation and makes it difficult for the desired reaction to outcompete unproductive side reactions, such as hydrolysis of the metal-fluorine bond.

1.3. SULFUR HEXAFLUORIDE (SF_6): A POTENT GREENHOUSE GAS AND A LATENT FLUORINE SOURCE

Sulfur hexafluoride (SF_6) is a molecule with a significant duality in its properties: it is a widely used industrial gas but also the most potent greenhouse gas known. Characterized by its high density, high dielectric constant, low toxicity, and chemical inertness, SF_6 is extensively used as an electrical insulator in high-voltage equipment and in the semiconductor industry.

In 1997, the *Kyoto Protocol* recognized SF_6 as the most potent greenhouse gas, with a global warming potential approximately 23.900 times greater than that of carbon dioxide (CO_2), and an atmospheric lifetime exceeding 3.000 years. As of 2020, atmospheric concentrations of SF_6 have surpassed 10 parts per trillion (ppt), and projections indicate a 75% increase by 2030. This alarming trend highlights the urgent need for innovative strategies to repurpose SF_6 for chemical feedstock production. As previousloy described, currently available fluorinating reagents, such as Selectfluor, DAST, and NFSI, are often cost-prohibitive for large-scale use, chemically unstable, and prone to producing undesirable by-products. In contrast, SF_6 is inexpensive, non-toxic, and possesses an essentially unlimited shelf life.

The chemical inertness of SF_6, particularly the strong $F_5S{-}F$ bond with a dissociation enthalpy of approximately 455 $kJmol^{-1}$, makes its activation challenging and has historically limited its use in organic synthesis to conditions of extremely high temperatures and pressures.[447] However, recent advancements have focused on converting this inert gas into an active fluorinating reagent under milder conditions.

1.3.1. Activation of SF_6 for fluorination

The high chemical and physical stability of SF_6 presents a significant challenge for its activation and subsequent utilization. For these reasons, increasing attention has been directed toward the development of effective methods for the activation and transformation of SF_6. A key strategy involves single-electron reduction (SER) through photocatalytic or electrochemical pathways, which generates the highly reactive SF_6 radical anion (**Figure 76**). This intermediate then fragments into a fluoride anion (F^-) and a pentafluorosulfanyl radical ($SF_5^{\cdot}$). Modern methodologies leverage these principles to achieve various fluorination reactions.

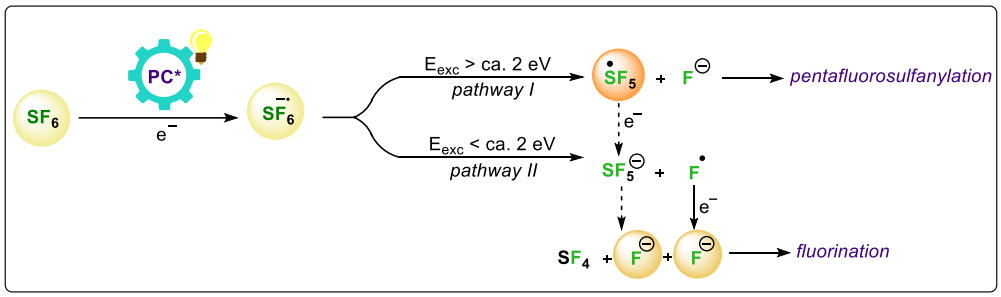

Figure 76. Photoredox activation of SF_6.

A prominent activation strategy is photoredox catalysis, which uses light to initiate the reaction.[448] The photocatalyst, upon excitation by visible light, performs a single-electron transfer to SF_6, generating the highly reactive $SF_6^{\cdot-}$ radical anion.[449] This transient species then fragment into a fluoride anion (F^-) and a pentafluorosulfanyl radical ($SF_5^{\cdot}$), which can then participate in fluorination reactions. This method has been successfully applied to the deoxyfluorination of benzylic, allylic, and propargyl alcohols with high chemoselectivity and functional group tolerance, employing Ru and Ir catalysts (**Scheme 50a**).[449]

Another key approach involves the use of metal-free organic electron donors. Certain highly reducing organic molecules can directly activate SF_6 through single- or two-electron reduction. For instance, 2,2'-bipyridyl-based donors (**Scheme 50b**) can rapidly and selectively reduce SF_6 at ambient temperatures, yielding stable solid ion pairs containing the SF_5^- anion.[450] Similarly, *N*-heterocyclic carbenes (NHCs - **Scheme 50c**) have been shown to activate SF_6 via a single-electron transfer (SET) mechanism under UV light, leading to the fragmentation of the $SF_6^{\cdot-}$ radical anion.[451] A particularly significant advancement is the synthesis of a new SF_5-based reagent by activating SF_6 with tetrakis(dimethylamino)ethylene (TDAE - **Scheme 50d**) under blue LED irradiation, which can then be used for deoxyfluorination and the synthesis of SF_5-containing scaffolds.[452]

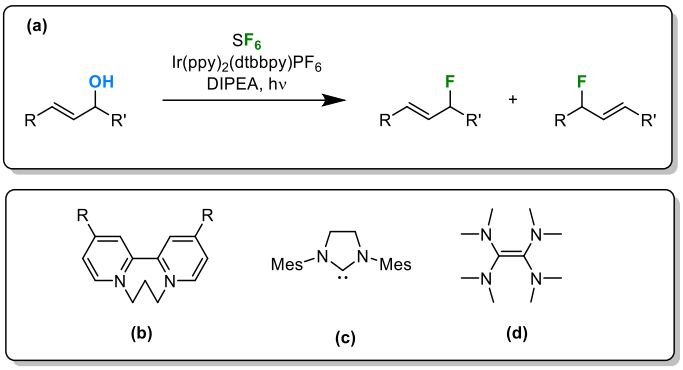

Scheme 50. a) Deoxyfluorination of allylic alcohols by photoredox catalysis using SF_6; **b-d)** Metal-free organic electron donors reported for the activation of SF_6.

Beyond these methods, other activation pathways have also been explored. Electrochemical activation similarly operates via SER to generate reactive intermediates from SF_6.[453] These diverse activation methodologies demonstrate the immense potential of SF_6 not only as a safe and inexpensive fluorinating agent but also as a means to degrade a potent greenhouse gas by converting it into useful chemical building blocks. However, these methods have generally been limited to a narrow range of functional groups, such as activated alcohols and carboxylic acids.

1.4. AIM OF THIS RESEARCH WORK

The strategic introduction of fluorine into organic molecules is crucial in pharmaceutical and agrochemical sciences, as the unique properties of the C-F bond critically modulate a compound's biological profile, stability, and lipophilicity. However, current industrial fluorinating reagents often present drawbacks related to high cost, chemical instability, and hazardous by-products. In contrast stands SF_6, an abundant and highly stable industrial gas recognized as the most potent greenhouse gas, necessitating urgent repurposing strategies. While SF_6 is an appealing alternative due to its low cost, non-toxicity, and abundant availability, its extreme chemical inertness presents a formidable challenge for effective chemical activation.

This research work was carried out in the research group of Prof. Tanja Gulder, at Saarland University, and aims to convert this potent pollutant into a valuable chemical feedstock. The core objective is to develop efficient and versatile methodologies for the catalytic activation and transformation of SF_6 (**Figure 77**).

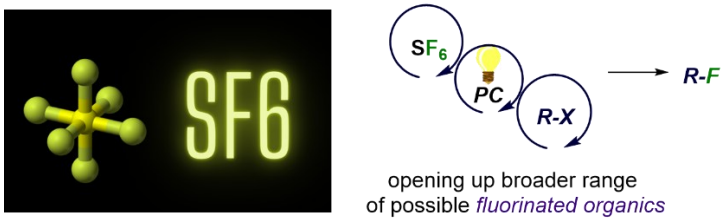

Figure 77. Structure of SF_6 and general photoactivation for the fluorination of organic substrates.

Specifically, this work focuses on the utilization of SF_6 within photoredox catalysis as a benign, inexpensive, and readily available source of fluoride. The primary synthetic goal involves exploring a novel methodology for the nucleophilic fluorination of alkoxyamines, a key transformation that contributes to the synthesis of highly valuable fluorinated building blocks. For this class of substrates, Ortalli and coworkers proposed a mechanism for the fluorination of TEMPO-functionalised alkoxyamines, which implies mesolytic cleavage of the substrate, which bypasses the formation of reactive carbon-centered radicals (**Scheme 51**).[454] From a synthetic perspective, the TEMPO group is also noteworthy for its facile installation in a single step from a wide variety of substrate classes.

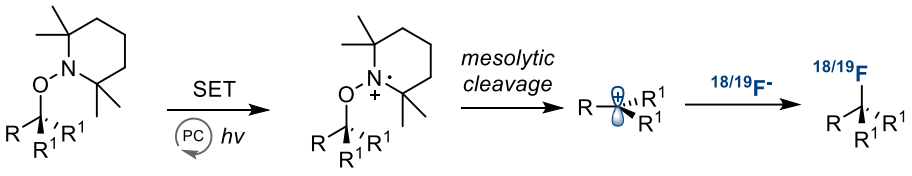

Scheme 51. Reported (radio)fluorination of TEMPO-functionalised alkoxyamines.

By successfully implementing a mild, photoredox-driven activation pathway, this work seeks not only to provide a sustainable solution for a critical environmental problem but also to establish a new, scalable, and operationally simple strategy for accessing fluorinated organic compounds crucial for modern drug discovery.

CHAPTER 2. RESULTS AND DISCUSSION

2.1. REACTION OPTIMIZATION

2.1.1. Photocatalyst screening

The initial efforts directed at developing our SF_6-mediated fluorination methodology focused on screening available, well-established photocatalysts on a model substrate. The choice of the ideal catalyst was governed by the need to participate in two fundamental, processes (**Scheme 52**):

- Reduction of SF_6 : The catalyst must effectively reduce the fluorinating agent, SF_6 , via a SET mechanism to generate the radical anion $SF_6^{\cdot-}$. This intermediate undergoes spontaneous dissociation to generate the crucial nucleophilic fluoride anion (F^-);
- Oxidation of substrate: Within the same catalytic cycle, the photocatalyst must simultaneously oxidize the TEMPO-functionalized substrate, providing the corresponding radical cation. This oxidative step is necessary to induce the subsequent mesolytic cleavage and the generation of the target carbon cation intermediate.

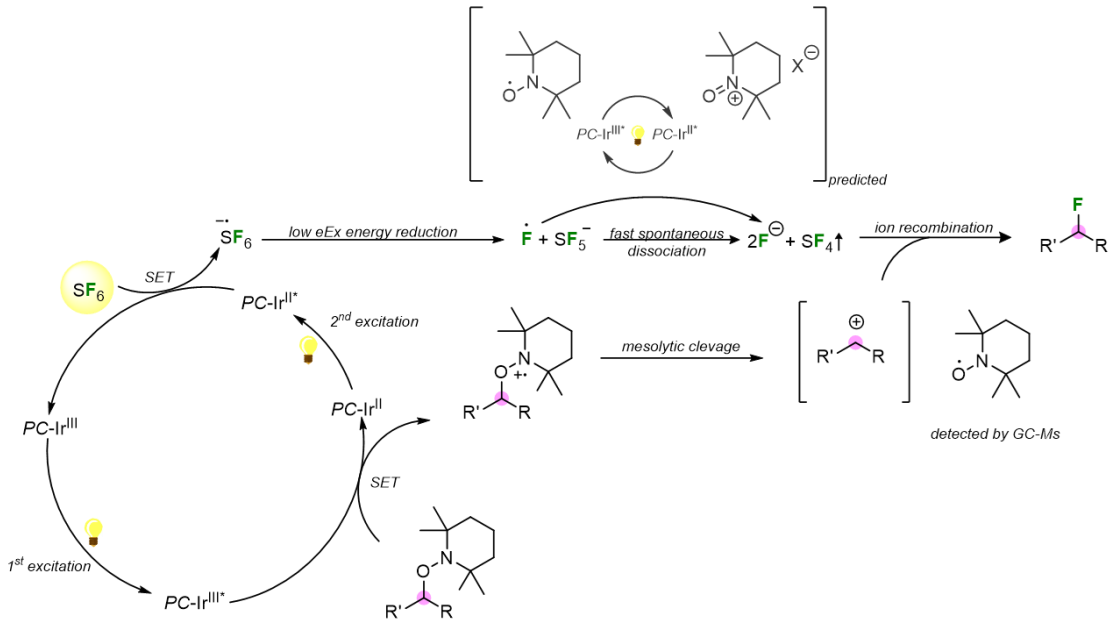

Scheme 52. Possible photocatalytic cycle.

Based on the state of the art in photoredox catalysis, a defined library of candidates was assembled and screened using compound **123** as the model substrate (**Scheme 53**). In addition to the most commonly employed Iridium catalysts, the library included one Ruthenium catalyst and an acridinium salt to ensure a broad evaluation of distinct photoredox properties. Compound

123 was solubilized in deoxygenated 1,2-dichloroethane (DCE), photocatalyst (PC) was added, then the reaction vessel was filled with gaseous SF_6, via a baloon and the resulting mixture was stirred and irradiated with 456 nm LED for 6 hours. Results obtained are summarized in **Table 12**.

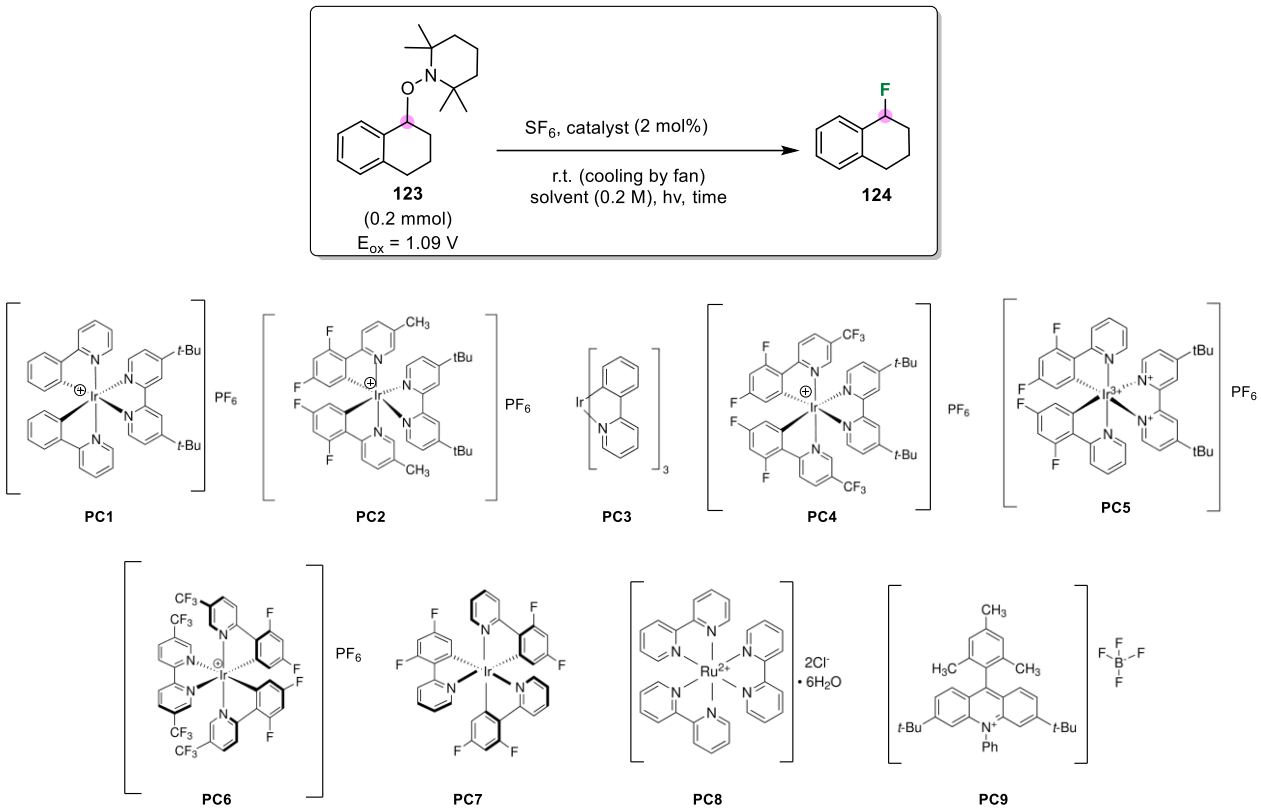

Scheme 53. SF_6-enabled fluorination of compound **123**. For the initial optimization of reaction conditions catalysts **PC1-9** have been screened.

Table 12. Catalyst screening.

Entry[a]	*Catalyst (2 mol%)*	*Solvent*	*Light (nm)*	*Time (h)*	*Yield*[b] *(%)*
1	PC1	DCE	456	06	17
2	PC2	DCE	456	06	39
3	PC3	DCE	456	06	No reaction
4	PC4	DCE	456	06	67
5	PC5	DCE	456	06	62
6	PC6	DCE	456	06	12
7	PC7	DCE	456	06	04
8	PC8	DCE	456	06	No reaction
9	PC9	DCE	456	06	9

[a]Reaction conditions: Substrate, PC, SF_6 baloon, 456 nm LED, r.t. (cooled by overhead fan), solvent (0.2 M) deoxygenated by N_2 flow; [b]Yield determined by ^{19}F NMR using external standard 1F-napthalene.

The initial screening of the photocatalyst library demonstrated varying levels of efficiency for the target fluorination reaction. While catalysts **PC3** and **PC8** showed no detectable reactivity (entries **3** and **8**), catalysts **PC3**, **PC6**, and **PC7** did afford the desired fluorinated product **124** , but in very poor yields (< 20% yield) (entries **1**, **6**, and **7**).

Significantly more promising results were observed using catalysts **PC2**, **PC4**, and **PC5** (entries **2**, **4**, and **5**). Among these working catalysts, **PC4** stood out as the most effective, delivering the fluorinated product in the highest yield (67%) and exhibiting the highest redox potential (**Figure 78**). Consequently, **PC4** was selected as the optimal photocatalyst to be carried forward into the following stages of reaction optimization.

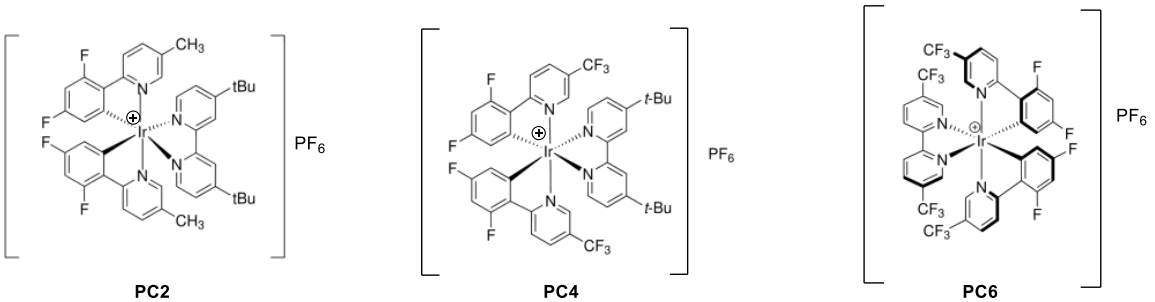

Figure 78. Redox potentials of the best performing catalysts. E_{redox} vs SCE in MeCN.

2.1.2. Light wavelenght and solvent optimization

Having successfully identified a suitable photocatalyst (**PC4**), the next critical parameter to investigate was the light source (**Table 13**). As expected, the reaction did not proceed in the dark (entry **14**), unequivocally confirming the fundamental role of photocatalytic activation for both the substrate and the fluorinating agent. We subsequently screened different wavelengths as well as distinct light sources operating at the same wavelength. The two best outcomes were achieved using the 440 (entry **11**) and 456 nm (entry **16**) Kessil lamps. This improved performance is likely attributed to enhanced light penetration, better absorption efficiency by the photocatalyst, and a slight increase in the reaction temperature. Overall, the 456 nm Kessil lamp provided the optimal condition, yielding the desired product in a 68% yield.

Table 13. Light wavelenght optimization.

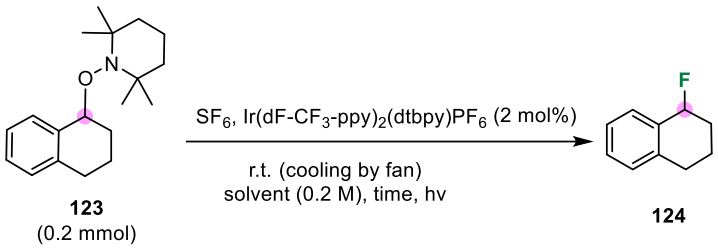

123 (0.2 mmol)

124

Entry[a]	*Solvent*	*Light (nm)*	*Time (h)*	*Yield*[b] *(%)*
10	DCE	405	06	45
11	DCE	Kessil 440	06	68
12	DCE	Kessil 390	06	53
13	DCE	528	06	03
14	DCE	In Dark	06	-
15	DCE	CFL (2*48 W bulbs)	06	Traces
16	DCE	Kessil 456	06	71

[a]Reaction conditions: Substrate, PC, SF_6 baloon, irradiation, r.t. (cooled by overhead fan), solvent (0.2 M) deoxygenated by N_2 flow; [b]Yield determined by ^{19}F NMR using external standard 1F-napthalene; CFL: Compact Fluorescent Lamp

Additionally, a brief screening of various solvents was carried out (**Table 14**). However, every alternative solvent tested yielded the fluorinated product in a significantly lower yield when compared to DCE. For this reason, DCE was definitively selected as the optimal solvent for the current methodology, as it provided the best balance of solubility, stability, and efficiency for the photoredox system.

Table 14. Solvent screening.

Entry[a]	*Solvent*	*Light (nm)*	*Time (h)*	*Yield*[b] *(%)*
17	Toluene	456	06	14
18	DCM	456	06	51
19	MeCN	456	06	23
20	THF	456	06	17
21	HFIP	456	06	Traces
22	1,4 dioxane	456	06	08
23	$MeNO_2$	456	06	37
24	DME	456	06	25
25	$CHCl_3$	456	S1	39
26	EtOAc	456	06	Traces
27	Et_2O	456	06	Traces
28	$PhCF_3$	456	06	44

[a]Reaction conditions: Substrate, PC, SF_6 baloon, irradiation, rt (cooled by overhead fan), solvent (0.2 M) deoxygenated by N_2 flow; [b]Yield determined by ^{19}F NMR using external standard 1F-napthalene.

2.1.3. Screening of reaction conditions

To finalize the optimization of this process on compound, systematic deviations from the established standard conditions were screened (**Table 15**). This analysis was crucial for defining the operational constraints and key mechanistic requirements of the developed photoredox methodology.

Table 15. Condition screening.

Entry[a]	*Deviation from std conditions*	*Light (nm)*	*Time (h)*	*Yield*[b] *(%)*
29	$Cu(OTf)_2$	456	06	09
30	HFIP (5 equiv.)	456	06	23
31	DIPEA (1 equiv.)	456	06	Traces
32	H_2O (5 equiv.)	456	06	04
33	No degassing	456	06	43
34	No cooling fan	456	06	65
35	Std. LED plates*2	456	06	68
36	Catalyst (2.5 mol%)	456	08	74[#]
37	High pressure setup**	456	12	85

[a]Reaction conditions: Substrate, SF_6 baloon, irradiation, r.t. (cooled by overhead fan), solvent (0.2 M) deoxygenated by N_2 flow; [b]Yield determined by ^{19}F NMR using external standard 1F-napthalene.

** *J Young* type flask, pressurized to 2.8 bar with SF_6

[#] average yield after 3 runs.

The data strongly underscores the non-trivial nature and high specificity of the entire catalytic system: Substituting the optimized photocatalyst with a different metal-based catalyst, such as $Cu(OTf)_2$ (entry **29**), caused a near-complete shutdown of the reaction, resulting in a yield of only 9%. This confirms that the redox potential of **PC4** is irreplaceable for simultaneously performing the required oxidation of the substrate and the reduction of SF_6. The presence of even small amounts of protic or basic species proved detrimental, confirming the delicate balance of the nucleophilic mechanism:

- Protic solvents: The addition of H_2O (5 equiv., entry **32**) reduced the yield to 4%. This necessitates performing the reaction under anhydrous conditions to prevent the quenching of the nucleophilic fluoride anion or competing protic side reactions.

- Base interference: The presence of DIPEA (1 equiv., entry **31**) yielded only traces of the product. This failure is likely due to acting as a competitive electron donor, intercepting the excited **PC4** and generating the radical cation $DIPEA^{\cdot+}$. This competitive quenching impedes the required oxidation of the TEMPO-substrate and the generation of the carbocationic intermediate. As a base, DIPEA could also quench any successfully formed carbon cation, leading to undesirable side products (e.g., elimination) instead of fluorination.
- Oxygen exclusion: Performing the reaction without degassing (entry **33**) led to a significant drop in yield, from 68% to 43%. This confirms that the fluorination proceeds via a radical mechanism highly susceptible to inhibition by atmospheric oxygen.

The final optimization attempts (entries **36**, **37**) identified the rate-limiting factors for maximum conversion: The highest yield achieved was 85% (entry **37**) by extending the reaction time to 12 h and utilizing a high-pressure setup (to increase the concentration of SF_6). This confirms that the final stages of conversion are kinetically slow and limited by the sustained availability of the gaseous fluorinating agent. In addition, a slight increase in yield was observed even when increasing the catalyst loading (entry **36**, 2.5%). Finally, the reaction is relatively tolerant to modest temperature variations; running it without a cooling fan (entry **34**, ≈40°C) caused only a minimal drop in yield (65%).

2.2. SCOPE EXPANSION

Having successfully optimized the fluorination conditions utilizing the photocatalytic activation of gaseous SF_6 on the model substrate **123**, the focus shifted to the synthesis of a diverse library of substrates for scope expansion.

The synthesis of TEMPO-functionalized alkoxyamines is a well-established procedure in literature, and various methods exist for their preparation, offering access to a wide variety of structural motifs for fluorination (**Scheme 54**). For instance, the reaction can be performed via direct functionalization of C-H bonds in common starting materials, such as ketones, esters, nitriles, toluene, ethylbenzene, heterocycles, cyclohexene, and cyclohexanes. This is achieved efficiently using a copper(II)/*tert*-butyl hydroperoxide catalyst system [(Bpy)Cu(II)/TBHP] under mild, ambient air conditions (**Scheme 54a**).[455] Alternatively, carboxylic acids can be converted into the desired TEMPO-alkoxyamines via several advanced methods:

- An iron-catalyzed, light-driven decarboxylative alkoxyamination (**Scheme 54b-c**).[456,457]
- A ruthenium-catalyzed process that converts the carboxylic acid into an *N*-(acyloxy)phthalimide intermediate (**Scheme 54d**).[458]

These available synthetic routes provide the necessary versatility to prepare a broad range of TEMPO-functionalized substrates, allowing a thorough investigation of the functional group tolerance and mechanistic limitations of the newly developed SF_6-based photoredox fluorination.

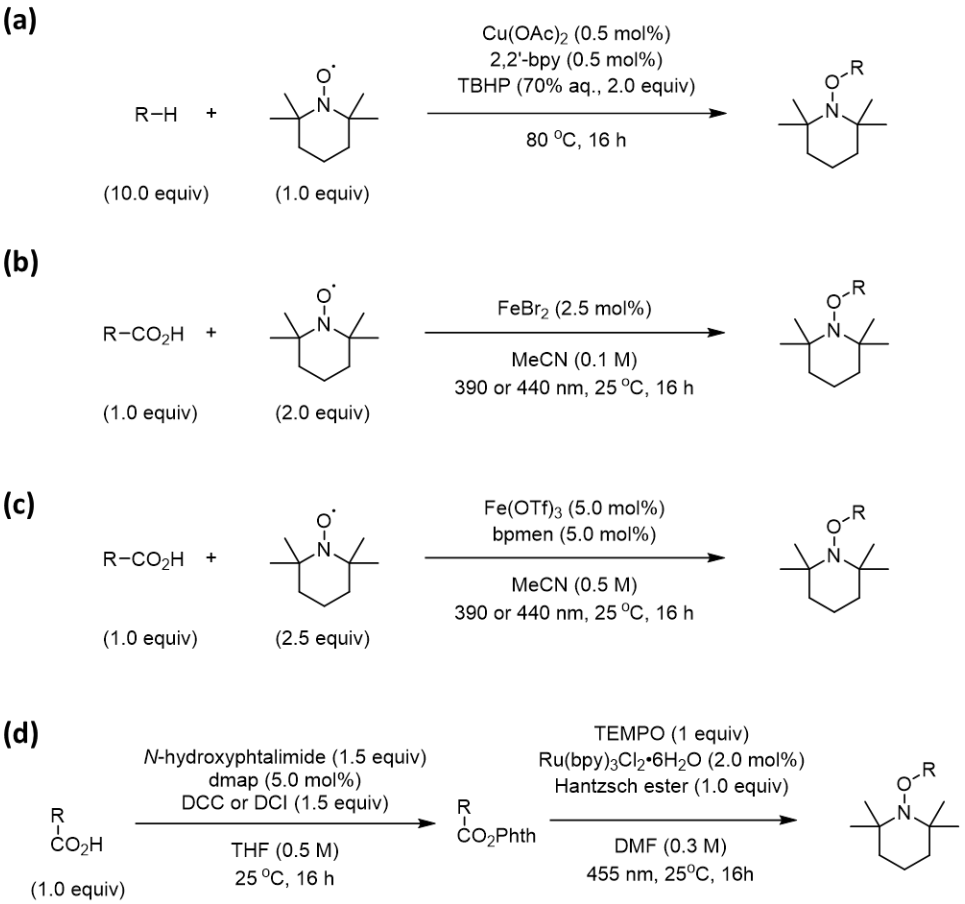

Scheme 54. Some reported methods for the synthesis of TEMPO-functionalized compounds.

Employing these efficient procedures a wide scope of substrates has been prepared (**Scheme 55**), some of which (G3) containing scaffolds of APIs:

G1:

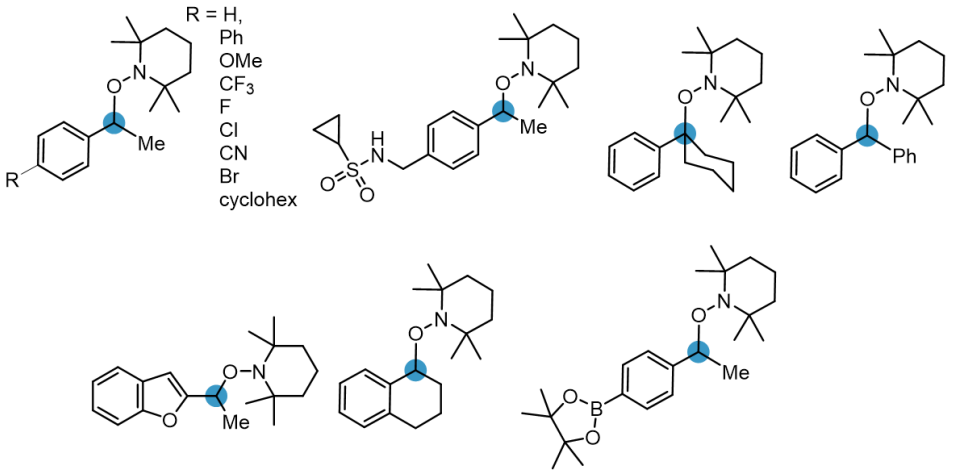

G2

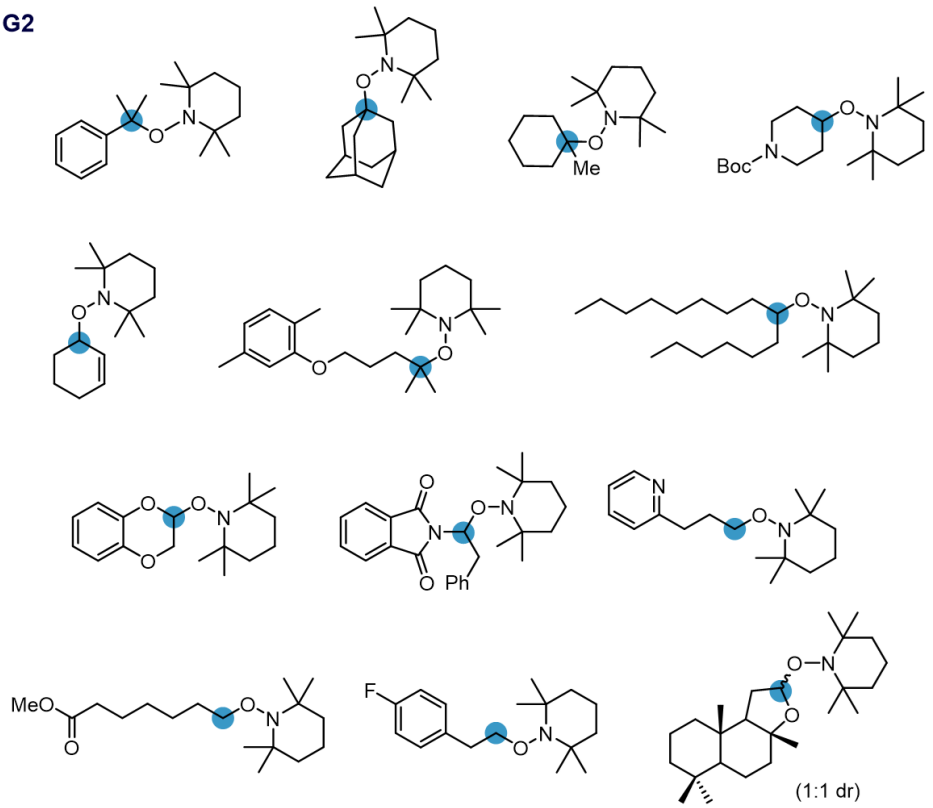

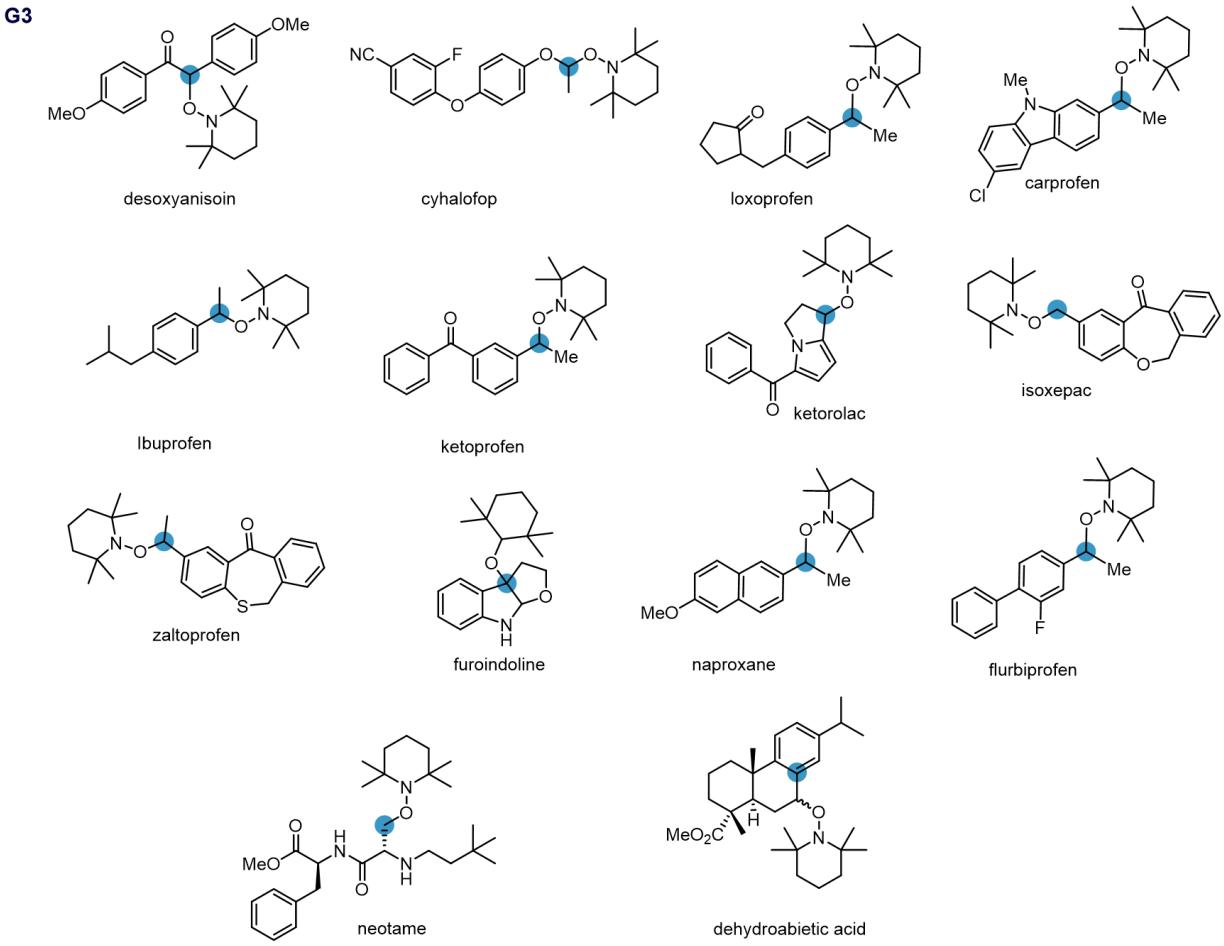

Scheme 55. Substrates prepared for the expansion of the scope.

So far, 15 compounds of this scope have been tested (**S1**-**S15**), carrying out the fluorination in the optimized conditions (**Scheme 56**).

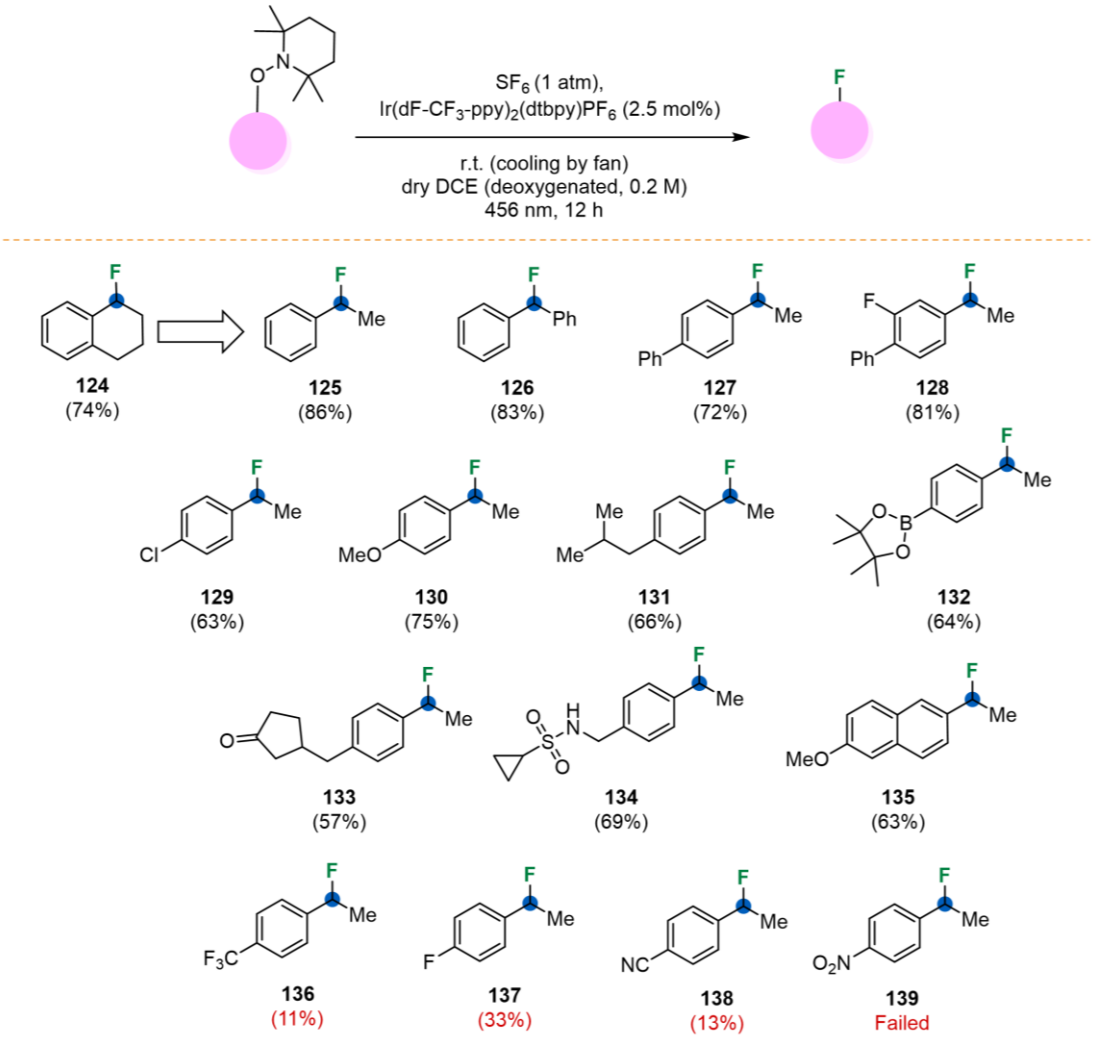

Scheme 56. General fluorination protocol carried out and obtained products. Yield determined by ^{19}F NMR using external standard 1F-napthalene.

For 11 out of the 15 tested substrates, the developed protocol successfully yielded the desired fluorinated products (**124-135**) with good to excellent yields (57-86%). However, the yields were significantly lower for three substrates (products **136-138**, 11-33%), and the reaction completely failed for the synthesis of product **137**.

Given that the photocatalytic activation of SF_6 to generate the nucleophilic fluoride source resulted efficient under these conditions, we hypothesized that the turnover-limiting step for the overall reaction is primarily determined by the ease of forming the carbocation intermediate. The stability of this carbocation is particularly sensitive to the electronic nature of the aromatic substituent. The observed yield trend strongly correlates with the π-electron-donating ability of the aromatic substituent, confirming the carbocation-mediated nature of the bond formation.

Electron-Donating Groups (EDGs) stabilize the positive charge, facilitating the reaction, whereas Electron-Withdrawing Groups (EWGs) destabilize it, leading to diminished reactivity.

Specifically, the strong EWGs, -CF_3 (product **136**, 11%), -CN (product **138**, 13%), and -NO_2 (product **139**, 0%), severely destabilize the developing positive charge on the benzylic carbon. This destabilization renders the mesolytic cleavage step highly unfavorable, dramatically slowing the reaction or preventing it entirely. In the extreme case of the highly deactivating group, the energetic barrier for carbocation formation is so high that the process is completely unfavored in respect to competitive radical pathways, resulting in zero conversion to the desired product. Ongoing efforts are focused on exploring the application of this procedure to the remaining substrate scope and investigating strategies to overcome the limitations imposed by these highly deactivating groups.

CHAPTER 3. CONCLUSIONS

The central objective of this project has been the design and implementation of a photoredox-catalyzed strategy for the nucleophilic fluorination of alkoxyamines using the greenhouse gas SF_6. Our investigation into photocatalysts revealed that the reaction's success is critically dependent on the catalyst's specific redox properties, with **PC4** being identified as capable of simultaneously oxidizing the TEMPO-functionalized substrate and reducing the exceptionally inert SF_6. By carefully controlling each parameter, we developed a robust protocol capable of affording the desired fluorinated product in high yield, notably reaching 85% under an optimized high-pressure SF_6 atmosphere. Testing this methodology on a modest scope of substrates has provided satisfactory results for most compounds, and less successful substrates provided further insight on the reaction.

The successful development of this methodology provides more than just a new synthetic tool; it offers a compelling proof-of-concept for the chemical valorization of SF_6, a problematic pollutant that can be turned into a functional reagent for a high-value chemical transformation. This work lays a solid foundation for future investigations. The scope of this photoredox activation could be expanded to other classes of substrates, potentially unlocking new pathways for the synthesis of diverse fluorinated molecules.

CHAPTER 4. EXPERIMENTAL PART

4.1. General experimental procedures, materials and instruments

All reagents were used as purchased from commercial suppliers without further purification. The reactions were carried out in oven dried vessels. Solvents were dried and purified by conventional methods prior use or, if available, purchased in anhydrous form.

Flash column chromatography was performed with Macherey-Nagel silica gel 60 M, 0.040-0.063 mm. Merck aluminum backed plates pre-coated with silica gel 60 (UV254) were used for analytical thin layer chromatography and were visualized by staining with a $KMnO_4$ or Ninidrine solution.

NMR spectra were recorded at 25 °C or at 37 °C with 400 MHz for 1H, 101 MHz for 13C and 282 MH for 19F, using Brücker AV II NMR spectrometer. The solvent is specified for each spectrum. Splitting patterns are designated as s, singlet; d, doublet; t, triplet; q, quartet; m, multiplet; bs, broad singlet. Chemical shifts (δ) are given in ppm relative to the resonance of their respective residual solvent peaks.

4.2. Synthetic procedures for the preparation of TEMPO-functionalized alkoxyamines

General procedure 1 (GP1)[455]

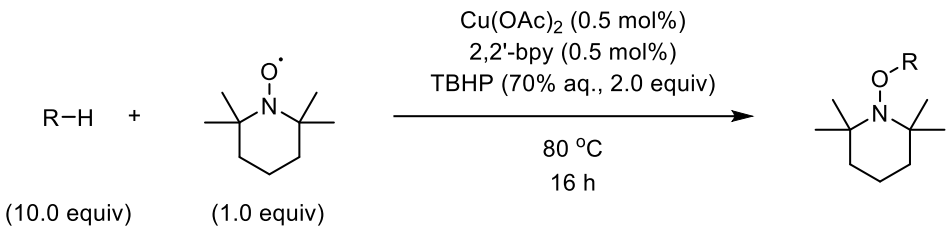

Under air, TEMPO (1.0 equiv), substrate (10.0 equiv), $Cu(OAc)_2$ (0.5 mol%), 2,2'-bpy (0.5 mol%), TBHP (70% aq, 2.0 equiv) were added into a round bottom flask equipped with a magnetic stirrer. The reaction was stirred at 80 °C until its color turned from dark red to light green (indication of the consumption of TEMPO starting material). Upon completion, the mixture was diluted with Et_2O and washed with brine solution twice. The organic phase was dried over Na_2SO_4 and evaporated under reduced pressure. The crude product was purified by silica gel flash-column chromatography.

General procedure 2 (GP2)[456]

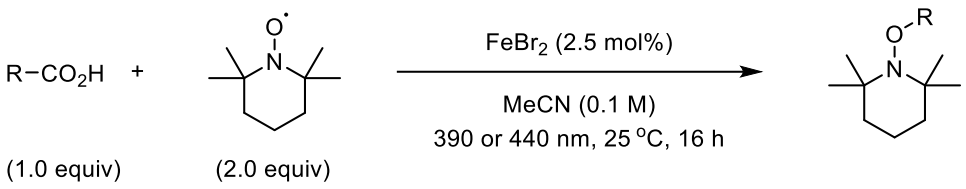

The carboxylic acid (1.0 equiv), TEMPO (2.0 equiv) and $FeBr_2$ (2.5 mol%) were added in an oven-dried Schlenk flask. The flask was flushed with argon and anhydrous and degassed MeCN (0.1 M) was added. The reaction was allowed to stir at r.t. for 16 h under light irradiation (390 or 440 nm). After 16 h, the reaction mixture was concentrated under reduced pressure and the resulting crude material was purified by silica gel flash-column chromatography.

General procedure 3 (GP3)[457]

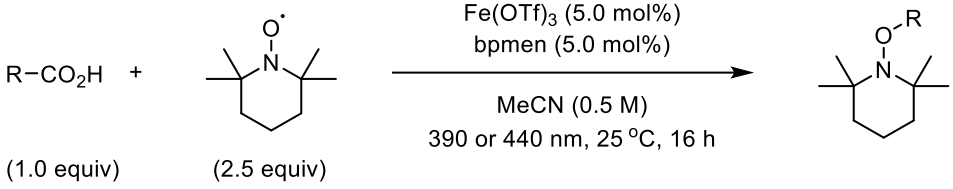

An oven-dried Schlenk flask equipped with a magnetic stirring bar was charged with the carboxylic acid (1.0 equiv). The flask was flushed with argon and anhydrous and degassed MeCN (0.5 M) was added. Then, to the flask were added solutions in MeCN of *N*,*N*-dimethyl-*N*,*N*-bis(pyridin-2-ylmethyl)ethane1,2-diamine (bpmen) (5.0 mol%, 40 mM) followed by the addition of $Fe(OTf)_3$ (5.0 mol%, 40 mM) and TEMPO (2.5 equiv, 0.50 M). The resulting mixture was stirred under light irradiation (390 or 440 nm) at r.t. for 16 h. Then, the solvent was evaporated, and to the crude was added CH_2Cl_2, the resulting solution was washed with saturated solution of $NaHCO_3$, the organic layer was dried over Na_2SO_4, and concentrated under reduced pressure. The crude product was purified by silica gel column chromatography.

General procedure 4 (GP4)[458]

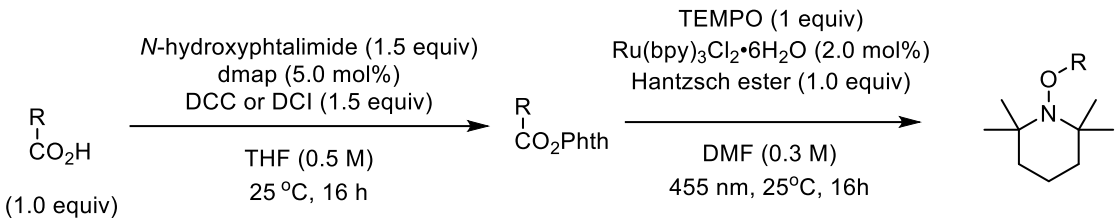

The alkyl redox active esters were synthesized according to the following method: the corresponding carboxylic acids (1.0 equiv), *N*-hydroxyphthalimide (1.5 equiv), and 4-dimethylaminopyridine (5 mol %) were mixed in a flask with a magnetic stirring bar, then CH_2Cl_2 was added. Then a solution of DCC or DCI (1.5 equiv) in CH_2Cl_2 was added slowly at r.t. The reaction mixture was stirred at r.t. for 16 h. When the *N*-hydroxyphthalimide was completely converted, the white precipitate was filtered off and the solution was concentrated under reduced pressure. The residue was purified by flash column chromatography to give corresponding redox active esters.

Redox-active ester (1.0 equiv), TEMPO (1 equiv), $Ru(bpy)_3Cl_2{\cdot}6H_2O$ (2 mol %), Hantzsch ester (1 equiv) were placed in a dry transparent Schlenk tube equipped with a stirring bar. The tube was evacuated and filled with argon (three times). To these solids, dry DMF was added via a gas-tight syringe under argon atmosphere. The reaction mixture was stirred under the irradiation (455 nm) at r.t. for 16 h. After reaction completion, the mixture was quenched with brine and extracted with EtOAc. The organic layers were combined and concentrated under reduced pressure. The product was purified by flash column chromatography on silica gel.

2,2,6,6-tetramethyl-1-((1,2,3,4-tetrahydronaphthalen-1-yl)oxy)piperidine (123)

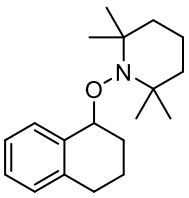

Following the general procedure **GP4**, the product was obtained in 96% yield as a white solid.

^{1}H NMR (400 MHz, Chloroform-*d*$_3$, δ ppm, *J* Hz): δ 7.63 - 7.61 (m, 1H), 7.21 - 7.03 (m, 3H), 4.89 - 4.86 (m, 1H), 2.91 - 2.64 (m, 2H), 2.11 - 1.91 (m, 3H), 1.75 - 1.66 (m, 1H), 1.61 - 1.12 (m, 15H), 0.72 (s, 3H).

^{13}C NMR (101 MHz, Chloroform-*d*$_3$, δ ppm): δ 137.8, 137.7, 129.8, 128.5, 127.2, 124.8, 78.3, 60.2, 59.9, 40.4, 34.7, 33.3, 29.2, 29.1, 20.9, 20.6, 19.2, 17.4.

2,2,6,6-tetramethyl-1-(1-phenylethoxy)piperidine (S1)

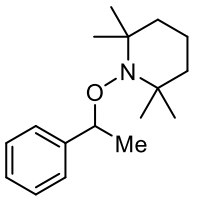

Following the general procedure **GP1**, the product was obtained in 90% yield as a colorless solid.

^{1}H NMR (400 MHz, Chloroform-*d*$_3$, δ ppm, *J* Hz): δ 7.28-7.14 (m, 5H), 4.72 (q, *J* = 6.7 Hz, 1H), 1.59-1.19 (m, 6H), 1.43 (d, *J* = 6.7 Hz, 3H), 1.24 (s, 3H), 1.12 (s, 3H), 0.97 (s, 3H), 0.60 (s, 3H).

^{13}C NMR (101 MHz, Chloroform-*d*$_3$): δ 146.0, 128.1 (2C), 126.9, 126.7 (2C), 83.3, 59.8 (2C), 40.5 (2C), 34.6, 34.3, 23.7, 20.5 (2C), 17.4.

1-(benzhydryloxy)-2,2,6,6-tetramethylpiperidine (S2)

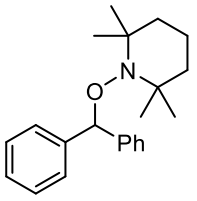

Following the general procedure **GP3** (440 nm), the product was obtained in 93% yield as a colorless solid.

^{1}H NMR (400 MHz, Chloroform-*d*$_3$, δ ppm, *J* Hz): δ 7.44 - 7.38 (m, 4H), 7.30 (t, *J* = 7.4 Hz, 4H), 7.20 (tt, *J* = 7.4, 1.3 Hz, 2H), 5.69 (s, 1H), 1.68 - 1.28 (m, 6H), 1.20 (s, 6H), 0.79 (s, 6H).

^{13}C NMR (101 MHz, Chloroform-*d*$_3$): δ 145.0, 128.2, 126.8, 126.6, 90.8, 60.0, 40.5, 34.0, 20.5, 17.2.

1-(1-([1,1'-biphenyl]-4-yl)ethoxy)-2,2,6,6-tetramethylpiperidine (S3)

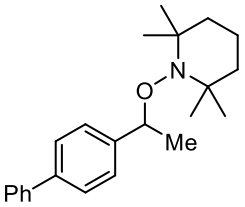

4-(1-bromoethyl)-1,1'-biphenyl (1.0 equiv), $Cu(OTf)_2$ (2.5 mol%), 4,4'-di-*tert*-butyl-2,2'-bipyridine (10.0 mol%), Cu powder (2.0 equiv) and TEMPO (1.3 equiv) were added into a flame-dried round bottom flask equipped with a magnetic stirrer. The flask was evacuated and backfilled with N_2 three times. Anhydrous and degassed benzene (0.5 M) was added. The reaction mixture was stirred at 75°C for 16 h under N_2, then cooled to r.t., filtered over a short silica pad with the aid of some Et_2O and concentrated under reduced pressure. The crude product was purified by silica gel column chromatography eluting a gradient 0-2% mixture of EtOAc in pentane to give the product as a white solid in 47% yield.

^{1}H NMR (400 MHz, Chloroform-*d*$_3$, δ ppm, *J* Hz): δ 7.63-7.59 (m, 2H), 7.57-7.53 (m, 2H), 7.45-7.37 (m, 4H), 7.35-7.30 (m, 1H), 4.84 (q, *J* = 6.6 Hz, 1H), 1.52 (d, *J* = 6.7 Hz, 6H), 1.38 (bs, 2H), 1.31 (bs, 4H), 1.19 (bs, 3H), 1.06 (bs, 3H), 0.72 (bs, 3H).

^{13}C NMR (101 MHz, Chloroform-*d*$_3$): δ 145.1, 141.3, 139.8, 128.9, 127.2, 127.2, 126.9, 82.9, 59.9, 40.6, 34.7, 34.5 23.7, 20.6, 17.4;

1-(1-(2-fluoro-[1,1'-biphenyl]-4-yl)ethoxy)-2,2,6,6-tetramethylpiperidine (S4)

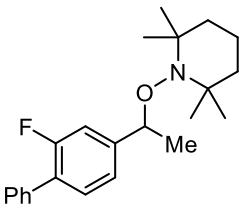

Following the general procedure **GP2** (390 nm), the product was obtained in 99% yield as a colorless solid.

^{1}H NMR (400 MHz, Chloroform-*d*$_3$, δ ppm, *J* Hz): δ 7.61-7.57 (m, 2H), 7.48-7.44 (m, 2H), 7.43-7.35 (m, 2H), 7.19 (s, 1H), 7.17-7.16 (m, 1H), 4.85 (q, *J* = 6.7 Hz, 1H), 1.55-1.29 (m, 6H), 1.53 (d, *J* = 6.6 Hz, 3H), 1.45 (s, 3H), 1.21 (s, 3H), 1.10 (s, 3H), 0.79 (s, 3H).

^{13}C NMR (101 MHz, Chloroform-d_3): δ 159.6, 147.4, 136.0,130.3, 129.1 (2C), 128.5, 127.6, 127.4, 127.2, 122.5, 114.10, 82.4, 59.9 (2C), 40.5 (2C), 34.6, 34.3, 23.5, 20.5 (2C), 17.3.

1-(1-(4-chlorophenyl)ethoxy)-2,2,6,6-tetramethylpiperidine (S5)

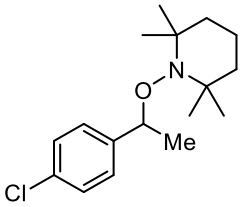

Following the general procedure **GP2** (390 nm), the product was obtained in 90% yield as a colorless oil.

^{1}H NMR (400 MHz, Chloroform-d_3, δ ppm, *J* Hz): δ 7.32 (d, *J* = 1.9 Hz, 4H), 4.81 (s, 2H), 1.68-1.49 (m, 5H), 1.38 (m, 1H), 1.26 (s, 6H), 1.17 (s, 6H).

^{13}C NMR (101 MHz, Chloroform-d_3): δ 36.6, 132.8, 128.6 (2C), 128.2 (2C), 77.8, 59.8 (2C), 39.5 (2C), 32.9 (2C), 20.1 (2C), 16.9.

1-(1-(4-methoxyphenyl)ethoxy)-2,2,6,6-tetramethylpiperidine (S6)

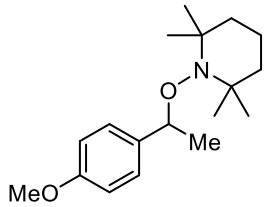

Following the general procedure **GP2** (440 nm), the product was obtained in 91% yield as a colorless solid.

^{1}H NMR (400 MHz, Chloroform-d_3, δ ppm, *J* Hz): δ 7.31-7.23 (m, 2H), 6.92-6.83 (m, 2H), 4.77 (q, *J* = 6.7 Hz, 1H), 3.82 (s, 3H), 1.54-1.49 (m, 3H), 1.49 (d, *J* = 6.7 Hz, 3H), 1.43-1.37 (m, 2H), 1.35-1.28 (m, 4H), 1.19 (s, 3H), 1.05 (s, 3H), 0.69 (s, 3H).

^{13}C NMR (101 MHz, Chloroform-d_3): δ 158.6, 138.1, 127.9 (2C), 113.4 (2C), 82.6, 59.8 (2C), 55.3, 40.5 (2C), 34.4(2C), 23.4, 20.4 (2C), 17.4.

1-(1-(4-isobutylphenyl)ethoxy)-2,2,6,6-tetramethylpiperidine (S7)

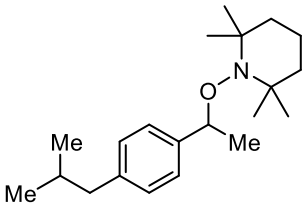

Following the general procedure **GP2** (440 nm), the product was obtained in 85% yield as a colorless oil.

^{1}H NMR (400 MHz, Chloroform-*d*$_3$, δ ppm, *J* Hz): δ 7.24 (d, *J* = 8.0 Hz, 2H), 7.08 (d, *J* = 8.1 Hz, 2H), 4.76 (q, *J* = 6.7 Hz, 1H), 2.46 (d, *J* = 7.3 Hz, 2H), 1.86 (dp, *J* = 13.6, 6.8 Hz, 1H), 1.49 (d, *J* = 6.7 Hz, 6H), 1.42 (d, *J* = 9.0 Hz, 2H), 1.32 (dd, *J* = 14.2, 7.1 Hz, 4H), 1.17 (s, 3H), 1.03 (s, 3H), 0.94 (d, *J* = 6.7 Hz, 6H), 0.63 (s, 3H).

^{13}C NMR (101 MHz, Chloroform-*d*$_3$, δ ppm): δ 143.09, 140.29, 128.81, 126.62, 82.96, 59.87, 59.67, 45.31, 40.50, 34.54, 34.19, 30.39, 23.38, 22.51, 20.48, 17.39.

2,2,6,6-tetramethyl-1-(1-(4-(4,4,5,5-tetramethyl-1,3,2-dioxaborolan-2-yl)phenyl)ethoxy)piperidine (S8)

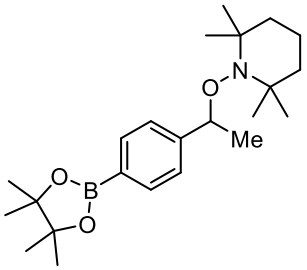

To a flame-dried Schlenk tube equipped with a magnetic stirrer were added 1-(1-(4-bromophenyl)ethoxy)-2,2,6,6-tetramethylpiperidine (340 mg, 1.0 mmol, 1.0 equiv), B_2Pin_2 (762 mg, 3.0 mmol, 3.0 equiv), K_3PO_4 (637 mg, 3.0 mmol, 3.0 equiv), $Pd(OAc)_2$ (5 mg, 0.02 mmol, 2.0 mol%) and Sphos (21 mg, 0.05 mmol, 5.0 mol%). The tube vas evacuated and backfilled with N_2 three times prior to the addition of dry 1,4-dioxane (2.0 mL, 0.5 M). The reaction mixture was stirred at r.t. under N_2 for 16 h, then filtered through a short celite pad and washed with EtOAc. The filtrate was then evaporated under reduced pressure and the crude product was purified by silica gel column chromatography eluting a gradient 0% to 1% mixture of EtOAc in pentane, to give the product as a white solid (88 mg, 0.23 mmol, 23% yield).

^{1}H NMR (400 MHz, Chloroform-*d*$_3$, δ ppm, *J* Hz): δ 7.76 (d, *J* = 8.1 Hz, 2H), 7.32 (d, *J* = 8.1 Hz, 2H), 4.78 (q, *J* = 6.7 Hz, 1H), 1.46 (d, *J* = 6.7 Hz, 6H), 1.34 (s, 15H), 1.29 (bs, 3H), 1.16 (bs, 3H), 1.01 (bs, 3H), 0.65 (bs, 3H).

^{13}C NMR (101 MHz, Chloroform-*d*$_3$, δ ppm): δ 167.3, 151.3, 129.6, 128.7, 126.6, 83.12, 59.9, 52.1, 40.5, 34.6, 34.3, 23.7, 20.4, 17.3;

3-(4-(1-((2,2,6,6-tetramethylpiperidin-1-yl)oxy)ethyl)benzyl)cyclopentan-1-one (S9)

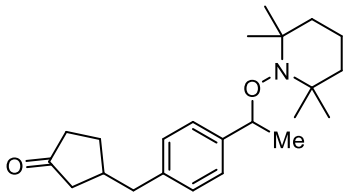

To a flame-dried round bottom flask equipped with a magnetic stirrer were added Loxoprofen (1.0 equiv), TEMPO (2.0 equiv), K_2CO_3 (1.5 equiv) and $K_2S_2O_8$ (1.0 equiv). The flask was evacuated and backfilled with N_2 three times prior to the addition of DCE and H_2O (0.1 M, 3:1 v/v). The reaction mixture was then stirred at 80 °C for 20 h under N_2. Upon completion, the reaction mixture was extracted with EtOAc three times. The combined organic layers were washed with brine, dried over Na_2SO_4 and evaporated under reduced pressure. The crude product was purified by silica gel column chromatography eluting a gradient 0% to 2% mixture of EtOAc in pentane to give the product.as a clear oil in 57% yield (diastereomers not resolved).

^{1}H NMR (400 MHz, Chloroform-*d*$_3$, δ ppm, *J* Hz): δ 7.22 (d, *J* = 8.1 Hz, 2H), 7.09 (d, *J* = 8.1 Hz, 2H), 4.74 (q, *J* = 6.6 Hz, 1H), 3.12 (dd, *J* = 13.9, 4.1 Hz, 1H), 2.52 (dd, *J* = 13.9, 9.6 Hz, 1H), 2.40-2.28 (m, 2H), 2.15-2.01 (m, 2H), 1.98-1.88 (m, 1H), 1.78-1.67 (m, 1H), 1.61-1.51 (m, 2H), 1.46 (d, *J* = 6.6 Hz, 5H), 1.36 (bs, 2H), 1.28 (bs, 4H), 1.15 (bs, 3H), 1.01 (bs, 3H), 0.62 (bs, 3H).

^{13}C NMR (101 MHz, Chloroform-*d*$_3$, δ ppm): δ 220.5, 143.6, 143.6, 138.4, 138.4, 128.6, 126.8, 82.8, 59.8 (br), 59.6 (br), 51.1, 40.4, 38.4, 35.4, 34.4 (br), 34.1 (br), 29.1, 23.3, 23.3, 20.6, 20.4, 17.3;

***N*-(4-(1-((2,2,6,6-tetramethylpiperidin-1-yl)oxy)ethyl)benzyl)cyclopropanesulfonamide (S10)**

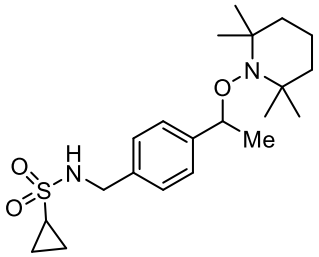

To a flame-dried round bottom flask equipped with a magnetic stirrer was added (4-(1((2,2,6,6-tetramethylpiperidin-1-yl)oxy)ethyl)phenyl)methanamine (250 mg, 0.86 mmol, 1.0 equiv). The flask was evacuated and backfilled with N_2 three times prior to the addition of dry CH_2Cl_2 (4.3 mL, 0.2 M), anhydrous Et_3N (240 µL, 1.72 mmol, 2.0 equiv) and cyclopropanesulfonyl chloride (105 µL, 1.03 mmol, 1.2 equiv). The reaction mixture was stirred at r.t. under N_2 for 48 h, then washed with a saturated aqueous $NaHCO_3$ solution, an aqueous 1 M HCl solution, and brine. The organic layer was dried over Na_2SO_4 and evaporated under reduced pressure. The crude product was purified by silica gel column chromatography eluting a gradient 0% to 40% mixture of EtOAc in pentane to give the product.as a white solid in 71% yield

^{1}H NMR (400 MHz, Chloroform-*d*$_3$, δ ppm, *J* Hz): δ 7.30 (s, 4H), 4.77 (q, *J* = 6.7 Hz, 1H), 4.54 (t, *J* = 6.2 Hz, 1H), 4.32 (d, *J* = 6.2 Hz, 2H), 2.31 (tt, *J* = 8.0, 4.9 Hz, 1H), 1.46 (d, *J* = 6.7 Hz, 6H), 1.37 (bs, 2H), 1.29 (bs, 4H), 1.21-1.09 (m, 5H), 0.95-0.86 (m, 2H), 0.62 (bs, 3H).

^{13}C NMR (101 MHz, Chloroform-*d*$_3$, δ ppm): δ 146.0, 135.6, 127.7, 127.2, 83.0, 59.8, 47.4, 40.5, 34.6, 34.4, 30.7, 23.8, 20.5, 17.3, 5.7

1-(1-(6-methoxynaphthalen-2-yl)ethoxy)-2,2,6,6-tetramethylpiperidine (S11)

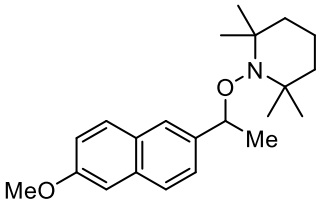

Following the general procedure **GP3** (440nm), the product was obtained in 89% yield as an white solid.

^{1}H NMR (400 MHz, Chloroform-*d*$_3$, δ ppm, *J* Hz): δ 7.74-7.69 (m, 2H), 7.65 (bs, 1H), 7.47 (dd, *J* = 8.5, 1.8 Hz, 1H), 7.15-7.10 (m, 2H), 4.91 (q, *J* = 6.6 Hz, 1H), 3.92 (s, 3H), 1.55 (d, *J* = 6.6 Hz, 4H), 1.51 (bs, 2H), 1.34 (bs, 6H), 1.20 (bs, 3H), 1.03 (bs, 3H), 0.61 (bs, 3H)

^{13}C NMR (101 MHz, Chloroform-*d*$_3$, δ ppm): δ 157.5, 141.2, 133.8, 129.5, 128.8, 126.8, 125.9, 125.1, 118.7, 105.8, 83.4, 60.0, 59.7, 55.4, 40.5, 34.8, 34.4, 23.7, 20.5, 17.4.

2,2,6,6-tetramethyl-1-(1-(4-(trifluoromethyl)phenyl)ethoxy)piperidine (S12)

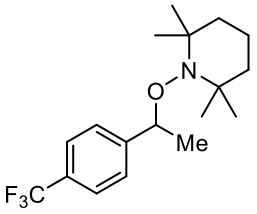

Following the general procedure **GP1**, the product was obtained in 75% yield as a white solid.

^{1}H NMR (400 MHz, Chloroform-*d*$_3$, δ ppm, *J* Hz): δ 7.62-7.56 (m, 2H), 7.45 (d, *J* = 8.1 Hz, 2H), 4.86 (q, *J* = 6.7 Hz, 1H), 1.57-1.26 (m, 6H), 1.50 (d, *J* = 6.5 Hz, 3H), 1.32 (s, 3H), 1.19 (s, 3H), 1.05 (s, 3H), 0.67 (s, 3H).

^{13}C NMR (101 MHz, Chloroform-*d*$_3$, δ ppm): δ 149.8, 126.7, 125.0 , 82.7, 59.7, 40.3, 34.5, 34.2, 23.6, 20.3, 17.2.

^{19}F NMR (282 MHz, Chloroform-*d*$_3$, δ ppm) δ -61.45.

1-(1-(4-fluorophenyl)ethoxy)-2,2,6,6-tetramethylpiperidine (S13)

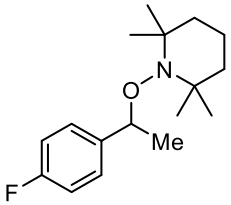

Following the general procedure **GP3** (440nm), the product was obtained in 97% yield as an orange oil.

^{1}H NMR (400 MHz, Chloroform-*d*$_3$, δ ppm, *J* Hz): δ 7.35-7.30 (m, 2H), 7.05-7.00 (m, 2H), 4.78 (s, 2H), 1.64-1.25 (m, 6H), 1.25 (s, 6H), 1.15 (s, 6H).

^{13}C NMR (101 MHz, Chloroform-*d*$_3$, δ ppm): δ 162.3, 134.2, 129.3, 115.2, 78.2, 60.1, 39.9, 33.3, 20.4, 17.3.

^{19}F NMR (282 MHz, Chloroform-*d*$_3$, δ ppm): δ -115.3.

4-(1-((2,2,6,6-tetramethylpiperidin-1-yl)oxy)ethyl)benzonitrile (S14)

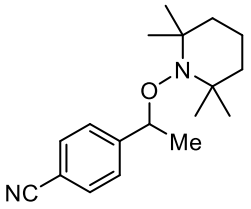

$Cu(OTf)_2$ (2.5 mol%), 4,4'-di-tert-butyl-2,2'-bipyridine (10.0 mol%), Cu powder (2.0 equiv) and TEMPO (1.3 equiv) were added into a flame-dried round bottom flask equipped with a magnetic stirrer. The flask was evacuated and backfilled with N_2 three times. Anhydrous and degassed benzene (0.5 M) was added followed by 4-(1-bromoethyl)benzonitrile (1.0 equiv). The reaction mixture was stirred at 75 °C for 16 h under N_2, then cooled to r.t., filtered over a short silica pad with the aid of some Et_2O and concentrated under reduced pressure. The crude product was purified by silica gel column chromatography eluting a gradient 0-5% mixture of EtOAc in pentane, to give the product in 55% as a white solid.

^{1}H NMR (400 MHz, Chloroform-*d*$_3$, δ ppm, *J* Hz): δ 7.60 (d, *J* = 8.1 Hz, 2H), 7.41 (d, *J* = 8.4 Hz, 2H), 4.82 (q, *J* = 6.7 Hz, 1H), 1.46 (d, *J* = 6.7 Hz, 6H), 1.37 (bs, 2H), 1.28 (bs, 4H), 1.16 (bs, 3H), 1.01 (bs, 3H), 0.60 (bs, 3H);

^{13}C NMR (101 MHz, Chloroform-*d*$_3$, δ ppm): δ 151.3, 132.2, 127.3, 119.2, 110.7, 82.9, 59.9, 40.4, 34.6, 34.3, 23.6, 20.4, 17.3;

2,2,6,6-tetramethyl-1-(1-(4-nitrophenyl)ethoxy)piperidine (S15)

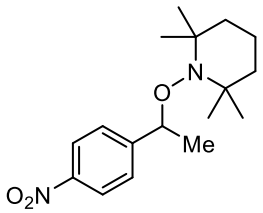

Following the general procedure **GP2** (390 nm), the product was obtained in 68% yield as a colorless oil

^{1}H NMR (400 MHz, Chloroform-*d*$_3$, δ ppm, *J* Hz): δ 8.18 (m, 2H), 7.47 (m, 2H), 4.88 (q, *J* = 6.7 Hz, 1H), 1.64-1.24 (m, 6H), 1.49 (d, *J* = 6.7 Hz, 3H), 1.29 (s, 3H), 1.17 (s, 3H), 1.02 (s, 3H), 0.61 (s, 3H).

^{13}C NMR (101 MHz, Chloroform-*d*$_3$, δ ppm): δ 153.4, 147.0, 127.3 (2C), 123.6 (2C), 82.7,59.9 (2C), 40.4 (2C), 34.5, 34.4, 23.7, 20.4 (2C), 17.2.

4.3. Fluorination of alkoxyamines via SF_6 photocatalytic activation

General procedure for fluorination

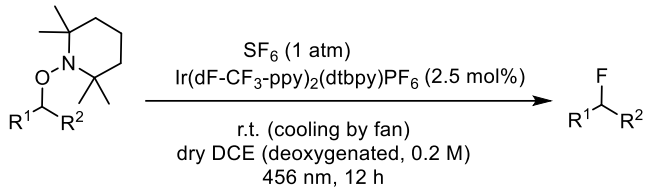

An oven-dried Schlenk flask equipped with a magnetic stirring bar was charged with the TEMPO-functionalized substrate (1.0 equiv) and **PC4** (2.5 mol%). The flask was flushed with N_2 and anhydrous and degassed DCE (0.2 M) was added. The flask was subjected to three cycles of vacuum/N_2 and subsequently sparged with SF_6 via a baloon. The obtained mixture was stirred under irradiation (456 nm) at r.t. (cooling by fan) for 12 h. Then, the solvent was evaporated and the crude product was purified by silica gel flash column chromatography.

1-fluoro-1,2,3,4-tetrahydronaphthalene (124)

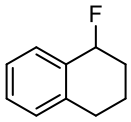

Yield of 74% determined by ^{19}F NMR using external standard 1F-napthalene.

Full degradation of the product was observed upon attempted purification by silica gel chromatography. Hence, the crude product was dissolved in pentane and filtered through a celite pipette plug, which was washed with further pentane. The filtrate was evaporated under reduced pressure and was not subjected to further purification.

^{1}H NMR (400 MHz, Chloroform-*d_3*, δ ppm, *J* Hz): δ (benzylic proton) 5.53 (dt, *J* = 51.6, 4.0 Hz, 1H).

^{19}F NMR (282 MHz, Chloroform-*d_3*, δ ppm): δ -155.85 (m).

(1-fluoroethyl)benzene (125)

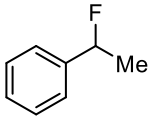

Purified by silica gel flash column chromatography eluting pentane, to give product **125** in 86% yield as a clear oil.

^{1}H NMR (400 MHz, Chloroform-*d_3*, δ ppm, *J* Hz): δ 7.43-7.30 (m, 5H), 5.64 (dq, *J* = 47.6, 6.3 Hz, 1H), 1.66 (dd, *J* = 23.9, 6.4 Hz, 3H).

^{13}C NMR (101 MHz, Chloroform-*d*$_3$, δ ppm): δ 141.6 (d, *J* = 19.5 Hz), 128.6, 128.4 (d, *J* = 2.3 Hz), 125.4 (d, *J* = 6.8 Hz), 91.1 (d, *J* = 167.6 Hz), 23.1 (d, *J* = 25.0 Hz).

^{19}F NMR (282 MHz, Chloroform-*d*$_3$, δ ppm, *J* Hz): δ -167.06 (dq, *J* = 47.7, 24.3 Hz);

(fluoromethylene)dibenzene (126)

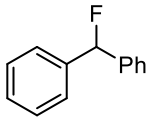

Purified by silica gel flash column chromatography eluting pentane, to give product **126** in 83% yield as a clear oil.

^{1}H NMR (400 MHz, Chloroform-*d*$_3$, δ ppm, *J* Hz): δ 7.42-7.32 (m, 10H), 6.49 (d, *J* = 47.3 Hz, 1H).

^{13}C NMR (101 MHz, Chloroform-*d*$_3$, δ ppm): δ 140.0 (d, *J* = 21.3 Hz), 128.6, 128.6 (d, *J* = 2.3 Hz), 126.7 (d, *J* = 6.4 Hz), 94.6 (d, *J* = 172.6 Hz)

^{19}F NMR (282 MHz, Chloroform-*d*$_3$, δ ppm, *J* Hz): δ -166.70 (d, J = 46.8 Hz)

4-(1-fluoroethyl)-1,1'-biphenyl (127)

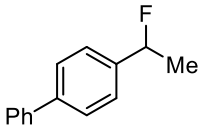

Purified by silica gel flash column chromatography eluting a gradient 0% to 20% of CH_2Cl_2 in pentane, to give product **127** in 72% yield as a white solid.

^{1}H NMR (400 MHz, Chloroform-*d*$_3$, δ ppm, *J* Hz): δ 7.68-7.58 (m, 4H), 7.51-7.43 (m, 4H), 7.41-7.35 (m, 1H), 5.70 (dq, *J* = 47.7, 6.4 Hz, 1H), 1.71 (dd, *J* = 23.8, 6.5 Hz, 3H).

^{13}C NMR (101 MHz, Chloroform-*d*$_3$, δ ppm): δ 141.3 (d, *J* = 2.4 Hz), 140.8, 140.5 (d, *J* = 19.5 Hz), 128.9, 127.6, 127.4, 127.3, 125.9 (d, *J* = 6.8 Hz), 90.9 (d, *J* = 167.3 Hz), 23.0 (d, *J* = 25.4 Hz).

^{19}F NMR (282 MHz, Chloroform-*d*$_3$, δ ppm, *J* Hz): δ -166.60 (dq, J = 48.2, 24.1 Hz).

2-fluoro-4-(1-fluoroethyl)-1,1'-biphenyl (128)

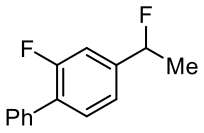

Purified by silica gel column chromatography eluting pentane, to give product **128** in 81% yield as a clear oil.

^{1}H NMR (400 MHz, Chloroform-*d*$_3$, δ ppm, *J* Hz): δ 7.55 (d, *J* = 7.3 Hz, 2H), 7.46 (t, *J* = 7.7 Hz, 3H), 7.38 (t, *J* = 7.4 Hz, 1H), 7.18 (t, *J* = 8.9 Hz, 2H), 5.66 (dq, *J* = 47.4, 6.5 Hz, 1H), 1.68 (dd, *J* = 23.9, 6.4 Hz, 3H).

^{13}C NMR (101 MHz, Chloroform-*d*$_3$, δ ppm): δ 159.9 (d, *J* = 248.9 Hz), 143.1 (dd, *J* = 20.2, 7.5 Hz), 135.5, 131.0 (d, *J* = 4.1 Hz), 129.1 (d, *J* = 2.7 Hz), 128.9 (dd, *J* = 13.6, 1.8 Hz), 128.6, 128.0, 121.2 (dd, *J* = 6.8, 3.6 Hz), 113.2 (dd, *J* = 24.3, 7.5 Hz), 90.1 (dd, *J* = 169.2, 1.6 Hz), 23.0 (d, *J* = 25.0 Hz).

^{19}F NMR (282 MHz, Chloroform-*d*$_3$, δ ppm, *J* Hz): δ -117.43-117.38 (m, 1F), -168.33 (dq, *J* = 47.7, 23.4 Hz, 1F).

1-chloro-4-(1-fluoroethyl)benzene (129)

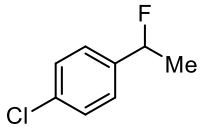

Purified by silica gel column chromatography eluting pentane, to give product **129** in 63% yield as a colorless oil.

^{1}H NMR (400 MHz, Chloroform-*d*$_3$, δ ppm, *J* Hz): δ 7.35 (d, 2H, J = 8.4 Hz, Ph H-2,6), 7.28 (d, 2H, J = 8.4 Hz, Ph H-3,5), 5.60 (dq, 1H, 2JH,F = 47.5 Hz, 3JH,H = 6.5 Hz, CHF), 1.62 (dd, 3H, 3JH,F = 23.8 Hz, 3JH,H = 6.4 Hz, CH3).

^{13}C NMR (101 MHz, Chloroform-*d*$_3$, δ ppm): δ 140.1 (d, *J* = 20.0 Hz), 134.2 (d, *J* = 1.7 Hz), 128.8 (2C), 126.8 (d, 2C, *J* = 6.9 Hz), 90.4 (d, *J* = 168.2 Hz), 23.0 (d, *J* = 28.3 Hz).

^{19}F NMR (282 MHz, Chloroform-*d*$_3$, δ ppm, *J* Hz): δ -167.5 (dq, *J* = 47.9 Hz, 23.9 Hz).

1-(1-fluoroethyl)-4-methoxybenzene (130)

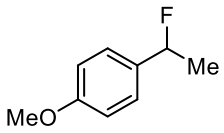

Purified by silica gel column chromatography eluting pentane, to give product **130** in 75% yield as a colorless oil.

^{1}H NMR (400 MHz, Chloroform-*d*$_3$, δ ppm, *J* Hz): δ 7.26-7.33 (m, 4H), 5.48 (dq, *J* = 40.5, 5.4 Hz, 1H), 3.86 (s, 3H), 1.59 (dd, *J* = 23.6, 5.8 Hz, 3H).

^{13}C NMR (101 MHz, Chloroform-*d*$_3$, δ ppm): δ 160.0, 128.2, 127.9, 116.1, 90.0 (d, *J* = 166.8 Hz), 55.7, 22.6 (d, *J* = 25.4 Hz).

^{19}F NMR (282 MHz, Chloroform-*d*$_3$, δ ppm, *J* Hz): δ -167.7 (dq, *J* = 40.5, 23.6 Hz).

1-(1-fluoroethyl)-4-isobutylbenzene (131)

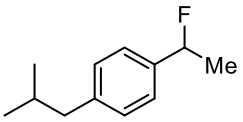

Purified by silica gel column chromatography eluting pentane, to give product **131** in 66% yield as a colorless oil.

^{1}H NMR (400 MHz, Chloroform-*d*$_3$, δ ppm, *J* Hz): δ 7.28 (d, *J* = 8.1 Hz, 2H), 7.17 (d, *J* = 8.1 Hz, 2H), 5.62 (dq, *J* = 48.0, 6.5 Hz, 1H), 2.49 (d, *J* = 7.2 Hz, 2H), 1.88 (hept, *J* = 6.5 Hz, 1H), 1.65 (dd, *J* = 23.9, 6.5 Hz, 3H), 0.92 (d, *J* = 6.6 Hz, 6H).

^{13}C NMR (101 MHz, Chloroform-*d*$_3$, δ ppm): δ 142.01 (d, *J* = 2.4 Hz), 138.78 (d, *J* = 19.9 Hz), 129.34, 125.32 (d, *J* = 6.4 Hz), 91.16 (d, *J* = 166.5 Hz), 45.26, 30.36, 22.90 (d, *J* = 25.8 Hz), 22.50.

^{19}F NMR (282 MHz, Chloroform-*d*$_3$, δ ppm, *J* Hz): δ -164.62 (dq, *J* = 47.7, 23.8 Hz).

2-(4-(1-fluoroethyl)phenyl)-4,4,5,5-tetramethyl-1,3,2-dioxaborolane (132)

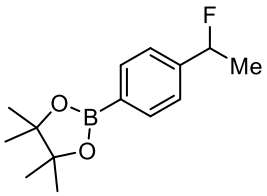

Purified by silica gel column chromatography eluting CH_2Cl_2, to give product **132** in 64% yield as a white solid.

^{1}H NMR (400 MHz, Chloroform-*d*$_3$, δ ppm, *J* Hz): δ 7.83 (d, *J* = 7.6 Hz, 2H); 7.35 (d, *J* = 7.8 Hz, 2H), 5.64 (dq, *J* = 47.7, 6.5 Hz, 1H), 1.63 (dd, *J* = 23.9, 6.5 Hz, 3H), 1.35 (s, 12H).

^{13}C NMR (101 MHz, Chloroform-*d*$_3$, δ ppm): δ 144.7 (d, *J* = 19.5 Hz), 135.1, 124.5 (d, *J* = 7.2 Hz), 91.0 (d, *J* = 168.1 Hz), 84.0, 25.0, 23.2 (d, *J* = 25.0 Hz).

^{19}F NMR (282 MHz, Chloroform-*d*$_3$, δ ppm, *J* Hz): δ -169.59 (dq, *J* = 47.7, 23.8 Hz).

3-(4-(1-fluoroethyl)benzyl)cyclopentan-1-one (133)

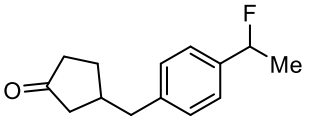

Purified by silica gel column chromatography eluting a gradient 0-10% mixture of EtOAc in pentane, to give product **133** in 57% yield as a light-yellow oil (diastereomers not resolved).

^{1}H NMR (400 MHz, Chloroform-*d*$_3$, δ ppm, *J* Hz): δ 7.27 (d, *J* = 7.4 Hz, 2H), 7.18 (d, *J* = 8.2 Hz, 2H), 5.60 (dq, *J* = 47.7, 6.4 Hz, 1H), 3.15 (dd, *J* = 14.0, 4.2 Hz, 1H), 2.55 (dd, *J* = 14.0, 9.4 Hz, 1H), 2.39-2.30 (m, 2H), 2.15-2.04 (m, 2H), 2.0-1.92 (m, 1H), 1.79-1.69 (m, 1H), 1.63 (dd, *J* = 23.8, 6.4 Hz, 3H), 1.60-1.51 (m, 1H).

^{13}C NMR (101 MHz, Chloroform-*d*$_3$, δ ppm): δ (C=O not visible) 140.3 (d, *J* = 2.2 Hz), 139.4 (d, *J* = 19.5 Hz), 129.2, 125.6 (d, *J* = 6.4 Hz), 91.0 (d, *J* = 166.7 Hz), 51.1, 38.3, 35.4, 29.3, 22.9 (d, *J* = 25.4 Hz), 20.7.

^{19}F NMR (282 MHz, Chloroform-*d*$_3$, δ ppm, *J* Hz): δ -165.41 (dp, *J* = 47.7, 24.3 Hz).

***N*-(4-(1-fluoroethyl)benzyl)cyclopropanesulfonamide (134)**

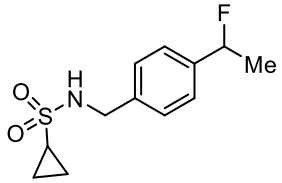

Purified by silica gel column chromatography eluting a gradient 0-20% mixture of EtOAc in pentane, to give product **134** in 69% yield as a white solid.

^{1}H NMR (400 MHz, Chloroform-*d*$_3$, δ ppm, *J* Hz): δ 7.41-7.32 (m, 4H), 5.63 (dq, *J* = 47.6, 6.5 Hz, 1H), 4.54 (t, *J* = 6.3 Hz, 1H), 4.35 (d, *J* = 6.2 Hz, 2H), 2.36 (tt, *J* = 8.1, 4.8 Hz, 1H), 1.63 (dd, *J* = 23.9, 6.5 Hz, 3H) 1.19-1.14 (m, 2H), 0.98-0.92 (m, 2H).

^{13}C NMR (101 MHz, Chloroform-*d*$_3$, δ ppm): δ 141.3 (d, *J* = 18.9 Hz), 137.4, 128.0, 125.8 (d, *J* = 6.5 Hz), 90.7 (d, *J* = 167.5 Hz), 47.0, 30.6, 23.0 (d, *J* = 25.4 Hz), 5.6.

^{19}F NMR (282 MHz, Chloroform-*d*$_3$, δ ppm, *J* Hz): δ -167.50 (dt, *J* = 47.7, 24.1 Hz).

2-(1-fluoroethyl)-6-methoxynaphthalene (135)

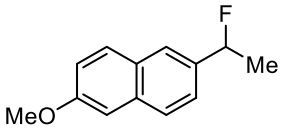

Purified by silica gel column chromatography eluting a 10% mixture of PE in pentane, to give product **135** in 63% yield as a white solid.

^{1}H NMR (400 MHz, Chloroform-*d*$_3$, δ ppm, *J* Hz): δ 7.77-7.72 (m, 3H), 7.45 (dd, *J* = 8.5, 1.8 Hz, 1H), 7.17 (dd, *J* = 8.8, 2.5 Hz, 1H), 7.14 (d, *J* = 2.5 Hz, 1H), 5.76 (dq, *J* = 47.6, 6.4 Hz, 1H), 3.93 (s, 3H), 1.73 (dd, *J* = 23.7, 6.4 Hz, 3H).

^{13}C NMR (101 MHz, Chloroform-*d*$_3$, δ ppm): δ 158.1, 136.6 (d, *J* = 19.4 Hz), 134.6 (d, *J* = 1.6 Hz), 129.7, 128.6, 127.3, 124.4 (d, *J* = 7.7 Hz), 123.9 (d, *J* = 5.4 Hz), 119.3, 105.8, 91.4 (d, *J* = 166.9 Hz), 55.5, 22.3 (d, *J* = 25.5 Hz).

^{19}F NMR (282 MHz, Chloroform-*d*$_3$, δ ppm, *J* Hz): δ -164.98 (dq, J = 47.6, 23.6 Hz).

1-(1-fluoroethyl)-4-(trifluoromethyl)benzene (136)

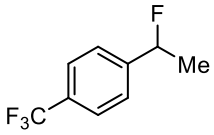

Purified by silica gel column chromatography eluting pentane, to give product **136** in 11% yield as a colorless oil.

^{1}H NMR (400 MHz, Chloroform-*d*$_3$, δ ppm, *J* Hz): δ 7.62 (d, *J* = 8.0 Hz, 2H), 7.45 (d, *J* = 8.0 Hz, 2H), 5.66 (dq, *J* = 47.5, 6.5 Hz, 1H), 1.63 (dd, *J* = 24.0, 6.5 Hz, 3H).

^{13}C NMR (101 MHz, Chloroform-*d*$_3$, δ ppm): δ 145.6 (d, *J* = 19.1 Hz), 130.4 (q, *J* = 32.2 Hz), 125.6 (q, *J* = 3.6 Hz), 125.4 (d, *J* = 7.2 Hz), 124.1 (q, *J* = 270.7 Hz), 90.2 (d, *J* = 168.1 Hz), 22.5 (d, *J* = 25.0 Hz

^{19}F NMR (282 MHz, Chloroform-*d*$_3$, δ ppm, *J* Hz): δ -62.5 (s, 3F), -171.0 (dq, *J* = 47.9, 23.7 Hz).

1-fluoro-4-(1-fluoroethyl)benzene (137)

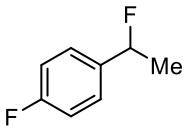

Purified by silica gel column chromatography eluting pentane, to give product **137** in 33% yield as a colorless oil.

^{1}H NMR (400 MHz, Chloroform-*d*$_3$, δ ppm, *J* Hz): δ 7.44 - 7.38 (2H, m), 7.16-7.10 (2H, m), S 19 5.65 (1H, dq, *J* = 47.7 Hz, 6.4 Hz), 1.59 (3H, dd, *J* = 24.0 Hz, 6.4 Hz);

^{19}F NMR (282 MHz, Chloroform-*d*$_3$, δ ppm, *J* Hz): δ -115.6 (m), -164.3 (dq, *J* = 48.6 Hz, 24.3 Hz).

4-(1-fluoroethyl)benzonitrile (138)

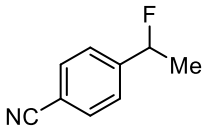

Purified by silica gel column chromatography eluting pentane, to give product **138** in 13% yield as a colorless oil.

^{1}H NMR (400 MHz, Chloroform-*d*$_3$, δ ppm, *J* Hz): δ 7.67 (d, J = 8.1 Hz, 2H), 7.44 (d, J = 8.7 Hz, 2H); 5.67 (dq, J = 47.5, 6.6 Hz, 1H), 1.64 (dd, J = 24.0, 6.4 Hz, 3H);

^{13}C NMR (101 MHz, Chloroform-*d*$_3$, δ ppm): δ 146.8 (d, J = 20.0 Hz), 132.5, 125.7 (d, J = 7.7 Hz), 118.7, 112.1 (d, J = 1.8 Hz), 90.0 (d, J = 170.8 Hz), 23.1 (d, J = 24.5 Hz).

^{19}F NMR (282 MHz, Chloroform-*d*$_3$, δ ppm, *J* Hz): δ -172.58 (tdd, J = 48.0, 25.3, 8.5 Hz).

SECTION C - BIBLIOGRAPHY

(1) Wild, C. P.; Weiderpass, E.; Stewart, B. W. *Cancer research for cancer prevention World Cancer Report* **2020**, IARC.

(2) *Our world in data - https://ourworldindata.org/*.

(3) *World Health Organization - https://www.who.int/health-topics/cancer*.

(4) *International Agency for Research on Cancer - https://gco.iarc.who.int/tomorrow/*.

(5) Jia, Q.; Wang, A.; Yuan, Y.; Zhu, B.; Long, H. *Exp Hematol Oncol* **2022**, *11* (1), 24.

(6) Huang, R.-X.; Zhou, P.-K. *Signal Transduct Target Ther* **2020**, *5* (1), 60.

(7) Zhou, J.; Lei, N.; Tian, W.; Guo, R.; Chen, M.; Qiu, L.; Wu, F.; Li, Y.; Chang, L. *Front Oncol* **2022**, *12*, 999643.

(8) Alam, S. M.; Chollet-Hinton, L.; Thompson, J.; Holzbeierlein, J. M. *World J Urol* **2022**, *40* (3), 719–725.

(9) Hanley, R.; Pagliari, F.; Garcia-Calderón, D.; Fernandes Guerreiro, J.; Genard, G.; Jansen, J.; Nisticò, C.; Marafioti, M. G.; Tirinato, L.; Seco, J. *Radiation Oncology* **2023**, *18* (1), 1–14.

(10) DeVita, V. T.; Chu, E. *Cancer Res* **2008**, *68* (21), 8643–8653.

(11) Ehrlich, P. *Chemotherapy*, Pergamon Press, London, **1960**.

(12) Withrow, S. J.; Vail, D. M.; Page, R. Saunders, 2012.

(13) Tannock, I. F. *Lancet* **1998**, *351*, SII9-SII16.

(14) Seledtsov, V. I.; von Delwig, A. *Expert Opin Biol Ther* **2021**, *21* (3), 323–342.

(15) Cole, K.; Al-Kadhimi, Z.; Talmadge, J. E. *Int Immunopharmacol* **2023**, *117*, 109882.

(16) Ma, W.; Xue, R.; Zhu, Z.; Farrukh, H.; Song, W.; Li, T.; Zheng, L.; Pan, C. xian. *Exp Hematol Oncol* **2023**, *12* (1), 1–19.

(17) Tan, S.; Li, D.; Zhu, X. *Biomedicine & Pharmacotherapy* **2020**, *124*, 109821.

(18) Waldmann, T. A. *Nat Med* **2003**, *9* (3), 269–277.

(19) Zahavi, D.; Weiner, L. *Antibodies **2020**, 9* (3), 34.

(20) Weiner, L. M.; Dhodapkar, M. V.; Ferrone, S. *The Lancet*. **2009**, 1033–1040.

(21) Carter, P. J.; Lazar, G. A. *Nat Rev Drug Discov* **2018**, *17* (3), 197–223.

(22) Strebhardt, K.; Ullrich, A. *Nat Rev Cancer* **2008**, *8* (6), 473–480.

(23) Sochaj, A. M.; Świderska, K. W.; Otlewski, J. *Biotechnol Adv* **2015**, *33* (6), 775–784.

(24) Giansanti, F.; Flavell, D. J.; Angelucci, F.; Fabbrini, M. S.; Ippoliti, R. *Toxins* **2018**, *10* (2), 82.

(25) Joubert, N.; Beck, A.; Dumontet, C.; Denevault-Sabourin, C. *Pharmaceuticals (Basel)* **2020**, *13* (9), 1–30.

(26) Peters, C.; Brown, S. *Biosci Rep* **2015**, *35* (4).

(27) Kalim, M.; Chen, J.; Wang, S.; Lin, C.; Ullah, S.; Liang, K.; Ding, Q.; Chen, S.; Zhan, J. B. *Drug Des Devel Ther* **2017**, *11*, 2265–2276.

(28) Gerber, H. P.; Gangwar, S.; Betts, A. *MAbs* **2023**, *15* (1), 2230618.

(29) Dumontet, C.; Reichert, J. M.; Senter, P. D.; Lambert, J. M.; Beck, A. *Nat Rev Drug Discov* **2023**, *22* (8), 641–661.

(30) Li, F.; Emmerton, K. K.; Jonas, M.; Zhang, X.; Miyamoto, J. B.; Setter, J. R.; Nicholas, N. D.; Okeley, N. M.; Lyon, R. P.; Benjamin, D. R.; Law, C. L. *Cancer Res* **2016**, *76* (9), 2710–2719.

(31) Giugliano, F.; Corti, C.; Tarantino, P.; Michelini, F.; Curigliano, G. *Curr Oncol Rep* **2022**, *24* (7), 809–817.

(32) Mathe, G.; Tran Ba, L.; Bernard, J. *C R Hebd Seances Acad Sci* **1958**, *246* (10), 1626–1628.

(33) Ghose, T.; Path, M. R. C.; Nigam, S. P. *Cancer* **1972**, *29*(5), 1398-400.

(34) Rowland, G. F.; O'Neill, G. J.; Davies, D. A. L. *Nature* **1975**, *255* (5508), 487–488.

(35) Riechmann, L.; Clark, M.; Waldmann, H.; Winter, G. *Nature* **1988**, *332* (6162), 323–327.

(36) Sievers, E. L.; Larson, R. A.; Stadtmauer, E. A.; Estey, E.; Löwenberg, B.; Dombret, H.; Karanes, C.; Theobald, M.; Bennett, J. M.; Sherman, M. L.; Berger, M. S.; Eten, C. B.; Loken, M. R.; Van Dongen, J. J. M.; Bernstein, I. D.; Appelbaum, F. R. *J Clin Oncol* **2001**, *19* (13), 3244–3254.

(37) Castaigne, S.; Pautas, C.; Terré, C.; Raffoux, E.; Bordessoule, D.; Bastie, J. N.; Legrand, O.; Thomas, X.; Turlure, P.; Reman, O.; De Revel, T.; Gastaud, L.; De Gunzburg, N.; Contentin, N.; Henry, E.; Marolleau, J. P.; Aljijakli, A.; Rousselot, P.; Fenaux, P.; Preudhomme, C.; Chevret, S.; Dombret, H. *The Lancet* **2012**, *379* (9825), 1508–1516.

(38) Younes, A.; Bartlett, N. L.; Leonard, J. P.; Kennedy, D. A.; Lynch, C. M.; Sievers, E. L.; Forero-Torres, A. *N Engl J Med* **2010**, *363* (19), 1812–1821.

(39) Senter, P. D.; Sievers, E. L. *Nat Biotechnol* **2012**, *30* (7), 631–637.

(40) Verma, S.; Miles, D.; Gianni, L.; Krop, I. E.; Welslau, M.; Baselga, J.; Pegram, M.; Oh, D.-Y.; Diéras, V.; Guardino, E.; Fang, L.; Lu, M. W.; Olsen, S.; Blackwell, K. *N Engl J Med* **2012**, *367* (19), 1783–1791.

(41) LoRusso, P. M.; Weiss, D.; Guardino, E.; Girish, S.; Sliwkowski, M. X. *Clin Cancer Res* **2011**, *17* (20), 6437–6447.

(42) Shitara, K.; Bang, Y.-J.; Iwasa, S.; Sugimoto, N.; Ryu, M.-H.; Sakai, D.; Chung, H.-C.; Kawakami, H.; Yabusaki, H.; Lee, J.; Saito, K.; Kawaguchi, Y.; Kamio, T.; Kojima, A.; Sugihara, M.; Yamaguchi, K. *N Engl J Med* **2020**, *382* (25), 2419–2430.

(43) Cortés, J.; Kim, S.-B.; Chung, W.-P.; Im, S.-A.; Park, Y. H.; Hegg, R.; Kim, M. H.; Tseng, L.-M.; Petry, V.; Chung, C.-F.; Iwata, H.; Hamilton, E.; Curigliano, G.; Xu, B.; Huang, C.-S.; Kim, J. H.; Chiu, J. W. Y.; Pedrini, J. L.; Lee, C.; Liu, Y.; Cathcart, J.; Bako, E.; Verma, S.; Hurvitz, S. A. *N Engl J Med* **2022**, *386* (12), 1143–1154.

(44) Modi, S.; Jacot, W.; Yamashita, T.; Sohn, J.; Vidal, M.; Tokunaga, E.; Tsurutani, J.; Ueno, N. T.; Prat, A.; Chae, Y. S.; Lee, K. S.; Niikura, N.; Park, Y. H.; Xu, B.; Wang, X.; Gil-Gil, M.; Li, W.; Pierga, J.-Y.; Im, S.-A.; Moore, H. C. F.; Rugo, H. S.; Yerushalmi, R.; Zagouri, F.; Gombos, A.; Kim, S.-B.; Liu, Q.; Luo, T.; Saura, C.; Schmid, P.; Sun, T.; Gambhire, D.; Yung, L.; Wang, Y.; Singh, J.; Vitazka, P.; Meinhardt, G.; Harbeck, N.; Cameron, D. A. *N Engl J Med* **2022**, *387* (1), 9–20.

(45) Bhushan, A.; Misra, P. *Curr Oncol Rep* **2024**, *26* (10), 1224–1235.

(46) Thurston, D. E.; Jackson, P. J. M. *Cytotoxic Payloads for Antibody–Drug Conjugates* **2019**, Royal Society of Chemistry.

(47) Schuurman, J.; Parren, P. W. H. I. *Curr Opin Immunol* **2016**, *40*, vii–xiii.

(48) Vidarsson, G.; Dekkers, G.; Rispens, T. *Front Immunol* **2014**, 117227.

(49) Yu, J.; Song, Y.; Tian, W. *J Hematol Oncol* **2020**, *13* (1).

(50) Agarwal, P.; Bertozzi, C. R. *Bioconjug Chem* **2015**, *26* (2), 176–192.

(51) Hoffmann, R. M.; Coumbe, B. G. T.; Josephs, D. H.; Mele, S.; Ilieva, K. M.; Cheung, A.; Tutt, A. N.; Spicer, J. F.; Thurston, D. E.; Crescioli, S.; Karagiannis, S. N. *Oncoimmunology* **2017**, *7* (3).

(52) Peters, C.; Brown, S. *Biosci Rep* **2015**, *35* (4).

(53) Senter, P. D. *Curr Opin Chem Biol* **2009**, *13* (3), 235–244.

(54) Paul, S.; Konig, M. F.; Pardoll, D. M.; Bettegowda, C.; Papadopoulos, N.; Wright, K. M.; Gabelli, S. B.; Ho, M.; van Elsas, A.; Zhou, S. *Nat Rev Cancer* **2024**, *24* (6), 399–426.

(55) Leung, D.; Wurst, J. M.; Liu, T.; Martinez, R. M.; Datta-Mannan, A.; Feng, Y. *Antibodies (Basel)* **2020**, *9* (1).

(56) Alley, S. C.; Okeley, N. M.; Senter, P. D. *Curr Opin Chem Biol* **2010**, *14* (4), 529–537.

(57) Kovtun, Y. V.; Audette, C. A.; Ye, Y.; Xie, H.; Ruberti, M. F.; Phinney, S. J.; Leece, B. A.; Chittenden, T.; Blättler, W. A.; Goldmacher, V. S. *Cancer Res* **2006**, *66* (6), 3214–3221.

(58) Cheson, B. D.; Leonard, J. P. *N Engl J Med* **2008**, *359* (6), 613–626.

(59) Weiner, L. M.; Surana, R.; Wang, S. *Nat Rev Immunol* **2010**, *10* (5), 317–327.

(60) Van den Eynde, B. J. & S. A. M. Encyclopedia of Immunology, **1998** Academic Press: London.

(61) Van Cutsem, E.; Köhne, C.-H.; Hitre, E.; Zaluski, J.; Chang Chien, C.-R.; Makhson, A.; D'Haens, G.; Pintér, T.; Lim, R.; Bodoky, G.; Roh, J. K.; Folprecht, G.; Ruff, P.; Stroh, C.; Tejpar, S.; Schlichting, M.; Nippgen, J.; Rougier, P. *N Engl J Med* **2009**, *360* (14), 1408–1417.

(62) Hudis, C. A. *N Engl J Med* **2007**, *357* (1), 39–51.

(63) Schoeberl, B.; Pace, E. A.; Fitzgerald, J. B.; Harms, B. D.; Xu, L.; Nie, L.; Linggi, B.; Kalra, A.; Paragas, V.; Bukhalid, R.; Grantcharova, V.; Kohli, N.; West, K. A.; Leszczyniecka, M.; Feldhaus, M. J.; Kudla, A. J.; Nielsen, U. B. *Sci Signal* **2009**, *2* (77).

(64) Cañadas, I.; Rojo, F.; Arumí-Uría, M.; Rovira, A.; Albanell, J.; Arriola, E. *Clin Transl Oncol* **2010**, *12* (4), 253–260.

(65) Scartozzi, M.; Bianconi, M.; Maccaroni, E.; Giampieri, R.; Berardi, R.; Cascinu, S. *Curr Opin Mol Ther* **2010**, *12* (3), 361–371.

(66) Vearing, C.; Lee, F. T.; Wimmer-Kleikamp, S.; Spirkoska, V.; To, C.; Stylianou, C.; Spanevello, M.; Brechbiel, M.; Boyd, A. W.; Scott, A. M.; Lackmann, M. *Cancer Res* **2005**, *65* (15), 6745–6754.

(67) Fulda, S. *Adv Exp Med Biol* **2014**, *818*, 167–180.

(68) Neri, D.; Schliemann, C. *Recent Results Cancer Res* **2010**, *180*, 201–216.

(69) Scott, A. M.; Wiseman, G.; Welt, S.; Adjei, A.; Lee, F.-T.; Hopkins, W.; Divgi, C. R.; Hanson, L. H.; Mitchell, P.; Gansen, D. N.; Larson, S. M.; Ingle, J. N.; Hoffman, E. W.; Tanswell, P.; Ritter, G.; Cohen, L. S.; Bette, P.; Arvay, L.; Amelsberg, A.; Vlock, D.; Rettig, W. J.; Old, L. J. *Clin Cancer Res* **2003**, *9* (5), 1639–1647.

(70) Jungbluth, A. A.; Stockert, E.; Huang, H. J. S.; Collins, V. P.; Coplan, K.; Iversen, K.; Kolb, D.; Johns, T. J.; Scott, A. M.; Gullick, W. J.; Ritter, G.; Cohen, L.; Scanlan, M. J.; Cavanee, W. K.; Old, L. J. *Proc Natl Acad Sci U S A* **2003**, *100* (2), 639–644.

(71) Weiner, L. M.; Surana, R.; Wang, S. *Nat Rev Immunol* **2010**, *10* (5), 317–327.

(72) Lee, B. C.; Chalouni, C.; Doll, S.; Nalle, S. C.; Darwish, M.; Tsai, S. P.; Kozak, K. R.; Del-Rosario, G.; Yu, S. F.; Erickson, H.; Vandlen, R. *Bioconjug Chem* **2018**, *29* (7), 2468–2477.

(73) Ducry, L. *Antibody-drug conjugates*, **2013**, Humana Press.

(74) Estrella, V.; Chen, T.; Lloyd, M.; Wojtkowiak, J.; Cornnell, H. H.; Ibrahim-Hashim, A.; Bailey, K.; Balagurunathan, Y.; Rothberg, J. M.; Sloane, B. F.; Johnson, J.; Gatenby, R. A.; Gillies, R. J. *Cancer Res* **2013**, *73* (5), 1524–1535.

(75) McMahon, H. T.; Boucrot, E. *Nat Rev Mol Cell Biol* **2011**, *12* (8), 517–533.

(76) Hoffmann, R. M.; Coumbe, B. G. T.; Josephs, D. H.; Mele, S.; Ilieva, K. M.; Cheung, A.; Tutt, A. N.; Spicer, J. F.; Thurston, D. E.; Crescioli, S.; Karagiannis, S. N. *Oncoimmunology* **2017**, *7* (3).

(77) DiJoseph, J. F.; Dougher, M. M.; Kalyandrug, L. B.; Armellino, D. C.; Boghaert, E. R.; Hamann, P. R.; Moran, J. K.; Damle, N. K. *Clin Cancer Res* **2006**, *12* (1), 242–249.

(78) Govindan, S. V.; Cardillo, T. M.; Sharkey, R. M.; Tat, F.; Gold, D. V.; Goldenberg, D. M. *Mol Cancer Ther* **2013**, *12* (6), 968–978.

(79) Bargh, J. D.; Isidro-Llobet, A.; Parker, J. S.; Spring, D. R. *Chem Soc Rev* **2019**, *48* (16), 4361–4374.

(80) Migliorini, F.; Cini, E.; Dreassi, E.; Finetti, F.; Ievoli, G.; Macrì, G.; Petricci, E.; Rango, E.; Trabalzini, L.; Taddei, M. *Chem Comm* **2022**, *58* (75), 10532–10535.

(81) Dubikovskaya, E. A.; Thorne, S. H.; Pillow, T. H.; Contag, C. H.; Wender, P. A. *PNAS* **2008**, *105* (34), 12128–12133.

(82) Groot, F.; Damen, E.; Scheeren, H. *Curr Med Chem* **2001**, *8* (9), 1093–1122.

(83) Kellogg, B. A.; Garrett, L.; Kovtun, Y.; Lai, K. C.; Leece, B.; Miller, M.; Payne, G.; Steeves, R.; Whiteman, K. R.; Widdison, W.; Xie, H.; Singh, R.; Chari, R. V. J.; Lambert, J. M.; Lutz, R. J. *Bioconjug Chem* **2011**, *22* (4), 717–727.

(84) Lewis Phillips, G. D.; Li, G.; Dugger, D. L.; Crocker, L. M.; Parsons, K. L.; Mai, E.; Blättler, W. A.; Lambert, J. M.; Chari, R. V. J.; Lutz, R. J.; Wong, W. L. T.; Jacobson, F. S.; Koeppen, H.; Schwall, R. H.; Kenkare-Mitra, S. R.; Spencer, S. D.; Sliwkowski, M. X. *Cancer Res* **2008**, *68* (22), 9280–9290.

(85) McCombs, J. R.; Owen, S. C. *AAPS J* **2015**, *17* (2), 339–351.

(86) Gondi, C. S.; Rao, J. S. *Expert Opin Ther Targets* **2013**, *17* (3), 281–291.

(87) Lu, J.; Jiang, F.; Lu, A.; Zhang, G. *Int J Mol Sci* **2016**, *17* (4), 561.

(88) Burke, P. J.; Senter, P. D.; Meyer, D. W.; Miyamoto, J. B.; Anderson, M.; Toki, B. E.; Manikumar, G.; Wani, M. C.; Kroll, D. J.; Jeffrey, S. C. *Bioconjug Chem* **2009**, *20* (6), 1242–1250.

(89) Dubowchik, G. M.; Firestone, R. A.; Padilla, L.; Willner, D.; Hofstead, S. J.; Mosure, K.; Knipe, J. O.; Lasch, S. J.; Trail, P. A. *Bioconjug Chem* **2002**, *13* (4), 855–869.

(90) Dubowchik, G. M.; Radia, S.; Mastalerz, H.; Walker, M. A.; Firestone, R. A.; Dalton King, H.; Hofstead, S. J.; Willner, D.; Lasch, S. J.; Trail, P. A. *Bioorg Med Chem Lett* **2002**, *12* (11), 1529–1532.

(91) Doronina, S. O.; Toki, B. E.; Torgov, M. Y.; Mendelsohn, B. A.; Cerveny, C. G.; Chace, D. F.; DeBlanc, R. L.; Gearing, R. P.; Bovee, T. D.; Siegall, C. B.; Francisco, J. A.; Wahl, A. F.; Meyer, D. L.; Senter, P. D. *Nat Biotechnol* **2003**, *21* (7), 778–784.

(92) Jeffrey, S. C.; Andreyka, J. B.; Bernhardt, S. X.; Kissler, K. M.; Kline, T.; Lenox, J. S.; Moser, R. F.; Nguyen, M. T.; Okeley, N. M.; Stone, I. J.; Zhang, X.; Senter, P. D. *Bioconjug Chem* **2006**, *17* (3), 831–840.

(93) Bargh, J. D.; Walsh, S. J.; Isidro-Llobet, A.; Omarjee, S.; Carroll, J. S.; Spring, D. R. *Chem Sci* **2020**, *11* (9), 2375–2380.

(94) Bargh, J. D.; Walsh, S. J.; Ashman, N.; Isidro-Llobet, A.; Carroll, J. S.; Spring, D. R. *Chem Commun (Camb)* **2021**, *57* (28), 3457–3460.

(95) Kern, J. C.; Cancilla, M.; Dooney, D.; Kwasnjuk, K.; Zhang, R.; Beaumont, M.; Figueroa, I.; Hsieh, S. C.; Liang, L.; Tomazela, D.; Zhang, J.; Brandish, P. E.; Palmieri, A.; Stivers, P.; Cheng, M.; Feng, G.; Geda, P.; Shah, S.; Beck, A.; Bresson, D.; Firdos, J.; Gately, D.; Knudsen, N.; Manibusan, A.; Schultz, P. G.; Sun, Y.; Garbaccio, R. M. *J Am Chem Soc* **2016**, *138* (4), 1430–1445.

(96) Lee, H. K.; Kim, B.; Chang, H. W.; Kim, S. Y.; Byun, Y. *Cancer Res* **2024**, *84*, 4700–4700.

(97) Miller, J. T.; Vitro, C. N.; Fang, S.; Benjamin, S. R.; Tumey, L. N. *Bioconjug Chem* **2021**, *32* (4), 842–858.

(98) Zana, A.; Galbiati, A.; Gilardoni, E.; Bocci, M.; Millul, J.; Sturm, T.; Stucchi, R.; Elsayed, A.; Nadal, L.; Cirillo, M.; Roll, W.; Stegger, L.; Asmus, I.; Backhaus, P.; Schäfers, M.; Neri, D.; Cazzamalli, S. *Clin Cancer Res* **2022**, *28* (24), 5440–5454.

(99) Tang, S. C.; Wynn, C.; Le, T.; McCandless, M.; Zhang, Y.; Patel, R.; Maihle, N.; Hillegass, W. *Cancer Metastasis Rev* **2024**, *44* (1).

(100) Lu, J.; Jiang, F.; Lu, A.; Zhang, G. *Int J Mol Sci* **2016**, *17* (4).

(101) Chalouni, C.; Doll, S. *J Exp Clin Cancer Res* **2018**, *37* (1).

(102) Lei, Y.; Zheng, M.; Chen, P.; Seng Ng, C.; Peng Loh, T.; Liu, H. *Chem Med Chem* **2025**, *20* (15).

(103) Ding, H.; Altai, M.; Rinne, S. S.; Vorobyeva, A.; Tolmachev, V.; Gräslund, T.; Orlova, A. *Cancers (Basel)* **2019**, *11* (8).

(104) Tedeschini, T.; Campara, B.; Grigoletto, A.; Bellini, M.; Salvalaio, M.; Matsuno, Y.; Suzuki, A.; Yoshioka, H.; Pasut, G. *J Control Release* **2021**, *337*, 431–447.

(105) Giese, M. W.; Woodman, R. H.; Hermanson, G. T.; Davis, P. D. In *Chemical Linkers in Antibody–Drug Conjugates (ADCs),* **2021**, The Royal Society of Chemistry.

(106) Garay, R. P.; El-Gewely, R.; Armstrong, J. K.; Garratty, G.; Richette, P. *Expert Opin Drug Deliv* **2012**, *9* (11), 1319–1323.

(107) Yang, Q.; Lai, S. K. *Wiley Interdiscip Rev Nanomed Nanobiotechnol* **2015**, *7* (5), 655–677.

(108) Hoogenboom, J.; Van Berkel, S. S. *RSC Drug Discovery Series* **2021**, 81, 377–421.

(109) Verkade, J. M. M.; Wijdeven, M. A.; van Geel, R.; Janssen, B. M. G.; van Berkel, S. S.; van Delft, F. L. *Antibodies (Basel)* **2018**, *7* (1).

(110) Ding, H.; Altai, M.; Rinne, S. S.; Vorobyeva, A.; Tolmachev, V.; Gräslund, T.; Orlova, A. *Cancers (Basel)* **2019**, *11* (8).

(111) Yurkovetskiy, A. V.; Bodyak, N. D.; Yin, M.; Thomas, J. D.; Clardy, S. M.; Conlon, P. R.; Stevenson, C. A.; Uttard, A.; Qin, L. L.; Gumerov, D. R.; Ter-Ovanesyan, E.; Bu, C.; Johnson, A. J.; Gurijala, V. R.; McGillicuddy, D.; DeVit, M. J.; Poling, L. L.; Protopopova, M.; Xu, L.; Zhang, Q.; Park, P. U.; Bergstrom, D. A.; Lowinger, T. B. *Mol Cancer Ther* **2021**, *20* (5), 885–895.

(112) Conilh, L.; Fournet, G.; Fourmaux, E.; Murcia, A.; Matera, E. L.; Joseph, B.; Dumontet, C.; Viricel, W. *Pharmaceuticals (Basel)* **2021**, *14* (3).

(113) Birke, A.; Huesmann, D.; Kelsch, A.; Weilbächer, M.; Xie, J.; Bros, M.; Bopp, T.; Becker, C.; Landfester, K.; Barz, M. *Biomacromolecules* **2014**, *15* (2), 548–557.

(114) Lau, K. H. A.; Ren, C.; Sileika, T. S.; Park, S. H.; Szleifer, I.; Messersmith, P. B. *Langmuir* **2012**, *28* (46), 16099–16107.

(115) Sano, K.; Ohashi, M.; Kanazaki, K.; Makino, A.; Ding, N.; Deguchi, J.; Kanada, Y.; Ono, M.; Saji, H. *Bioconjug Chem* **2017**, *28* (4), 1024–1030.

(116) Hu, Y.; Hou, Y.; Wang, H.; Lu, H. *Bioconjug Chem* **2018**, *29* (7), 2232–2238.

(117) Viricel, W.; Fournet, G.; Beaumel, S.; Perrial, E.; Papot, S.; Dumontet, C.; Joseph, B. *Chem Sci* **2019**, *10* (14), 4048–4053.

(118) Gisbert-Garzarán, M.; Manzano, M.; Vallet-Regí, M. *Chemical Engineering Journal* **2018**, *340*, 24–31.

(119) Alouane, A.; Labruère, R.; Le Saux, T.; Schmidt, F.; Jullien, L. *Angew Chem Int Ed Engl* **2015**, *54* (26), 7492–7509.

(120) Alouane, A.; Labruère, R.; Silvestre, K. J.; Le Saux, T.; Schmidt, F.; Jullien, L. *Chem Asian J* **2014**, *9* (5), 1334–1340.

(121) Lee, H. Y.; Jiang, X.; Lee, D. *Org Lett* **2009**, *11* (10), 2065–2068.

(122) De Groot, F. M. H.; Albrecht, C.; Koekkoek, R.; Beusker, P. H.; Scheeren, H. W. *Angew Chem Int Ed Engl* **2003**, *42* (37), 4490–4494.

(123) Erez, R.; Shabat, D. *Org Biomol Chem* **2008**, *6* (15), 2669–2672.

(124) Senter, P. D.; Pearce, W. E.; Greenfield, R. S. *J Org Chem* **2002**, *55* (9), 2975–2978.

(125) Weinstain, R.; Segal, E.; Satchi-Fainaro, R.; Shabat, D. *Chem Comm* **2010**, *46* (4), 553–555.

(126) Gnaim, S.; Shabat, D. *Acc Chem Res* **2014**, *47* (10), 2970–2984.

(127) de Gracia Lux, C.; McFearin, C. L.; Joshi-Barr, S.; Sankaranarayanan, J.; Fomina, N.; Almutairi, A. *ACS Macro Lett* **2012**, *1* (7), 922–926.

(128) Shan, D.; Nicolaou, M. G.; Borchardt, R. T.; Wang, B. *J Pharm Sci* **1997**, *86* (7), 765–767.

(129) Grether, U.; Waldmann, H. *Chem Eur J* **2001**, 7, 959-971 .

(130) Zheng, A.; Shan, D.; Shi, X.; Wang, B. *J Org Chem* **1999**, *64* (20), 7459–7466.

(131) DeWit, M. A.; Gillies, E. R. *J Am Chem Soc* **2009**, *131* (51), 18327–18334.

(132) Flygare, J. A.; Pillow, T. H.; Aristoff, P. *Chem Biol Drug Des* **2013**, *81* (1), 113–121.

(133) Hollander, I.; Kunz, A.; Hamann, P. R. *Bioconjug Chem* **2008**, *19* (1), 358–361.

(134) King, H. D.; Dubowchik, G. M.; Mastalerz, H.; Willner, D.; Hofstead, S. J.; Firestone, R. A.; Lasch, S. J.; Trail, P. A. *J Med Chem* **2002**, *45* (19), 4336–4343.

(135) Zhao, R. Y.; Wilhelm, S. D.; Audette, C.; Jones, G.; Leece, B. A.; Lazar, A. C.; Goldmacher, V. S.; Singh, R.; Kovtun, Y.; Widdison, W. C.; Lambert, J. M.; Chari, R. V. J. *J Med Chem* **2011**, *54* (10), 3606–3623.

(136) Hitchcock, S. A. *J Med Chem* **2012**, *55* (11), 4877–4895.

(137) Widdison, W. C.; Chari, R. V. J. *Antibody-Drug Conjugates and Immunotoxins: From Pre-Clinical Development to Therapeutic Applications* **2013**, Humana Press.

(138) Zhao, R. Y.; Wilhelm, S. D.; Audette, C.; Jones, G.; Leece, B. A.; Lazar, A. C.; Goldmacher, V. S.; Singh, R.; Kovtun, Y.; Widdison, W. C.; Lambert, J. M.; Chari, R. V. J. *J Med Chem* **2011**, *54* (10), 3606–3623.

(139) Kanellos, J.; Pietersz, G. A.; McKenzie, I. F. *J Natl Cancer Inst* **1985**, *75* (2), 319–332.

(140) Saleh, M. N.; Sugarman, S.; Murray, J.; Ostroff, J. B.; Healey, D.; Jones, D.; Daniel, C. R.; LeBherz, D.; Brewer, H.; Onetto, N.; LoBuglio, A. F. *J Clin Oncol* **2000**, *18* (11), 2282–2292.

(141) Starling, J. J.; Maciak, R. S.; Law, K. L.; Hinson, N. A.; Briggs, S. L.; Laguzza, B. C.; Johnson, D. A. *Cancer Res* **1991**, *51* (11), 2965–2972.

(142) Trail, P. A.; Willner, D.; Lasch, S. J.; Henderson, A. J.; Hofstead, S.; Casazza, A. M.; Firestone, R. A.; Hellström, I.; Hellström, K. E. *Science* **1993**, *261* (5118), 212–215.

(143) Liu, C.; Tadayoni, B. M.; Bourret, L. A.; Mattocks, K. M.; Derr, S. M.; Widdison, W. C.; Kedersha, N. L.; Ariniello, P. D.; Goldmacher, V. S.; Lambert, J. M.; Blättler, W. A.; Chari, R. V. J. *Proc Natl Acad Sci U S A* **1996**, *93* (16), 8618–8623.

(144) Senter, P. D. *Curr Opin Chem Biol* **2009**, *13* (3), 235–244.

(145) Lambert, J. M.; Chari, R. V. J. *J Med Chem* **2014**, *57* (16), 6949–6964.

(146) Oroudjev, E.; Lopus, M.; Wilson, L.; Audette, C.; Provenzano, C.; Erickson, H.; Kovtun, Y.; Chari, R.; Jordan, M. A. *Mol Cancer Ther* **2010**, *9* (10), 2700–2713.

(147) Issell, B. F.; Crooke, S. T. *Cancer Treat Rev* **1978**, *5* (4), 199–207.

(148) Waight, A. B.; Bargsten, K.; Doronina, S.; Steinmetz, M. O.; Sussman, D.; Prota, A. E. *PLoS One* **2016**, *11* (8).

(149) Shor, B.; Gerber, H. P.; Sapra, P. *Mol Immunol* **2015**, *67* (2), 107–116.

(150) Ricart, A. D. *Clin Cancer Res* **2011**, *17* (20), 6417–6427.

(151) Ogitani, Y.; Aida, T.; Hagihara, K.; Yamaguchi, J.; Ishii, C.; Harada, N.; Soma, M.; Okamoto, H.; Oitate, M.; Arakawa, S.; Hirai, T.; Atsumi, R.; Nakada, T.; Hayakawa, I.; Abe, Y.; Agatsuma, T. *Clin Cancer Res* **2016**, *22* (20), 5097–5108.

(152) Sharkey, R. M.; McBride, W. J.; Cardillo, T. M.; Govindan, S. V.; Wang, Y.; Rossi, E. A.; Chang, C. H.; Goldenberg, D. M. *Clin Cancer Res* **2015**, *21* (22), 5131–5138.

(153) Pietersz, G. A.; Rowland, A.; Smyth, M. J.; McKenzie, I. F. C. *Adv Immunol* **1994**, *56*, 301–387.

(154) Tolcher, A. W.; Sugarman, S.; Gelmon, K. A.; Cohen, R.; Saleh, M.; Isaacs, C.; Young, L.; Healey, D.; Onetto, N.; Slichenmyer, W. *J Clin Oncol* **1999**, *17* (2), 478–484.

(155) Kolakowski, R. V.; Young, T. D.; Howard, P. W.; Jeffrey, S. C.; Senter, P. D. *Tetrahedron Lett* **2015**, *56* (30), 4512–4515.

(156) Miller, M. L.; Fishkin, N. E.; Li, W.; Whiteman, K. R.; Kovtun, Y.; Reid, E. E.; Archer, K. E.; Maloney, E. K.; Audette, C. A.; Mayo, M. F.; Wilhelm, A.; Modafferi, H. A.; Singh, R.; Pinkas, J.; Goldmacher, V.; Lambert, J. M.; Chari, R. V. J. *Mol Cancer Ther* **2016**, *15* (8), 1870–1878.

(157) Dokter, W.; Ubink, R.; van der Lee, M.; van der Vleuten, M.; van Achterberg, T.; Jacobs, D.; Loosveld, E.; van den Dobbelsteen, D.; Egging, D.; Mattaar, E.; Groothuis, P.; Beusker, P.; Coumans, R.; Elgersma, R.; Menge, W.; Joosten, J.; Spijker, H.; Huijbregts, T.; de Groot, V.; Eppink, M.; de Roo, G.; Verheijden, G.; Timmers, M. *Mol Cancer Ther* **2014**, *13* (11), 2618–2629.

(158) Valeur, E.; Knerr, L.; Ölwegård-Halvarsson, M.; Lemurell, M. *Drug Discov Today* **2017**, *22* (6), 841–847.

(159) Dunny, E.; O'Connor, I.; Bones, J. *Drug Discov Today* **2017**, *22* (6), 947–951.

(160) Cazaly, E.; Charlesworth, J.; Dickinson, J. L.; Holloway, A. F. *Mol Med* **2015**, *21* (1), 400–409.

(161) Cini, E.; Faltoni, V.; Petricci, E.; Taddei, M.; Salvini, L.; Giannini, G.; Vesci, L.; Milazzo, F. M.; Anastasi, A. M.; Battistuzzi, G.; De Santis, R. *Chem Sci* **2018**, *9* (31), 6490–6496.

(162) Giannini, G.; Vesci, L.; Battistuzzi, G.; Vignola, D.; Milazzo, F. M.; Guglielmi, M. B.; Barbarino, M.; Santaniello, M.; Fantò, N.; Mor, M.; Rivara, S.; Pala, D.; Taddei, M.; Pisano, C.; Cabri, W. *J Med Chem* **2014**, *57* (20), 8358–8377.

(163) Cianferotti, C.; Faltoni, V.; Cini, E.; Ermini, E.; Migliorini, F.; Petricci, E.; Taddei, M.; Salvini, L.; Battistuzzi, G.; Milazzo, F. M.; Anastasi, A. M.; Chiapparino, C.; De Santis, R.; Giannini, G. *Chem Comm* **2021**, *57* (7), 867–870.

(164) Rambaldi, A.; Dellacasa, C. M.; Finazzi, G.; Carobbio, A.; Ferrari, M. L.; Guglielmelli, P.; Gattoni, E.; Salmoiraghi, S.; Finazzi, M. C.; Di Tollo, S.; D'Urzo, C.; Vannucchi, A. M.; Barosi, G.; Barbui, T. *Br J Haematol* **2010**, *150* (4), 446–455.

(165) Subramanian, S.; Bates, S. E.; Wright, J. J.; Espinoza-Delgado, I.; Piekarz, R. L. *Pharmaceuticals (Basel)* **2010**, *3* (9), 2751–2767.

(166) Zhao, R.-J.; Fan, X.-X. *Int J Mol Sci* **2025**, *26* (4), 1440.

(167) Kaczanowska, S.; Joseph, A. M.; Davila, E. *J Leukoc Biol* **2013**, *93* (6), 847–863.

(168) Amouzegar, A.; Chelvanambi, M.; Filderman, J. N.; Storkus, W. J.; Luke, J. J. *Cancers (Basel)* **2021**, *13* (11).

(169) Turaj, A. H.; Dahal, L. N.; Beers, S. A.; Cragg, M. S.; Lim, S. H. *Cancer Res* **2017**, *77* (12), 3376–3378.

(170) Ackerman, S. E.; Pearson, C. I.; Gregorio, J. D.; Gonzalez, J. C.; Kenkel, J. A.; Hartmann, F. J.; Luo, A.; Ho, P. Y.; LeBlanc, H.; Blum, L. K.; Kimmey, S. C.; Luo, A.; Nguyen, M. L.; Paik, J. C.; Sheu, L. Y.; Ackerman, B.; Lee, A.; Li, H.; Melrose, J.; Laura, R. P.; Ramani, V. C.; Henning, K. A.; Jackson, D. Y.; Safina, B. S.; Yonehiro, G.; Devens, B. H.; Carmi, Y.; Chapin, S. J.; Bendall, S. C.; Kowanetz, M.; Dornan, D.; Engleman, E. G.; Alonso, M. N. *Nat Cancer* **2021**, *2* (1), 18–33.

(171) Tsuchikama, K.; Anami, Y.; Ha, S. Y. Y.; Yamazaki, C. M. *Nat Rev Clin Oncol* **2024**, *21* (3), 203–223.

(172) Yu, S.; Lim, A.; Tremblay, M. S. *Cancer Drug Discovery and Development* **2018**, 321–347.

(173) McColl, A.; Michlewska, S.; Dransfield, I.; Rossi, A. G. *Sci World J* **2007**, *7*, 1165–1181.

(174) Graversen, J. H.; Svendsen, P.; Dagnæs-Hansen, F.; Dal, J.; Anton, G.; Etzerodt, A.; Petersen, M. D.; Christensen, P. A.; Møller, H. J.; Moestrup, S. K. *Mol Ther* **2012,** *20* (8), 1550–1558.

(175) Graversen, J. H.; Moestrup, S. K. *Membranes (Basel)* **2015**, *5* (2), 228–252.

(176) Schade, A. E.; Schieven, G. L.; Townsend, R.; Jankowska, A. M.; Susulic, V.; Zhang, R.; Szpurka, H.; Maciejewski, J. P. *Blood* **2008**, *111* (3), 1366–1377.

(177) Lee, K. C.; Ouwehand, I.; Giannini, A. L.; Thomas, N. S.; Dibb, N. J.; Bijlmakers, M. J. *Leukemia* **2010**, *24* (4), 896–900.

(178) Conchon, M.; Moura, C. M. B. de F.; Rego, M. A. do C.; Braga, J. W. R. *Rev Bras Hematol Hemoter* **2011**, *33* (2), 131–139.

(179) Wang, R. E.; Liu, T.; Wang, Y.; Cao, Y.; Du, J.; Luo, X.; Deshmukh, V.; Kim, C. H.; Lawson, B. R.; Tremblay, M. S.; Young, T. S.; Kazane, S. A.; Wang, F.; Schultz, P. G. *J Am Chem Soc* **2015**, *137* (9), 3229–3232.

(180) Lehar, S. M.; Pillow, T.; Xu, M.; Staben, L.; Kajihara, K. K.; Vandlen, R.; DePalatis, L.; Raab, H.; Hazenbos, W. L.; Hiroshi Morisaki, J.; Kim, J.; Park, S.; Darwish, M.; Lee, B. C.; Hernandez, H.; Loyet, K. M.; Lupardus, P.; Fong, R.; Yan, D.; Chalouni, C.; Luis, E.; Khalfin, Y.; Plise, E.; Cheong, J.; Lyssikatos, J. P.; Strandh, M.; Koefoed, K.; Andersen, P. S.; Flygare, J. A.; Wah Tan, M.; Brown, E. J.; Mariathasan, S. *Nature* **2015**, *527* (7578), 323–328.

(181) Peck, M.; Rothenberg, M. E.; Deng, R.; Lewin-Koh, N.; She, G.; Kamath, A. V.; Carrasco-Triguero, M.; Saad, O.; Castro, A.; Teufel, L.; Dickerson, D. S.; Leonardelli, M.; Tavel, J. A. *Antimicrob Agents Chemother* **2019**, *63* (6).

(182) Dong, W.; Wang, W.; Cao, C. *Chem Med Chem* **2024**, *19* (17).

(183) Anderson, G. W.; Zimmerman, J. E.; Callahan, F. M. *J Am Chem Soc* **2002**, *86* (9), 1839–1842.

(184) Wang, L.; Amphlett, G.; Blättler, W. A.; Lambert, J. M.; Zhang, W. *Protein Sci* **2005**, *14* (9), 2436–2446.

(185) Mädler, S.; Bich, C.; Touboul, D.; Zenobi, R. *J Mass Spectrom* **2009**, *44* (5), 694–706.

(186) Swaim, C. L.; Smith, J. B.; Smith, D. L. *J Am Soc Mass Spectrom* **2004**, *15* (5), 736–749.

(187) Dovgan, I.; Ursuegui, S.; Erb, S.; Michel, C.; Kolodych, S.; Cianférani, S.; Wagner, A. *Bioconjug Chem* **2017**, *28* (5), 1452–1457.

(188) Narayanan, A.; Jones, L. H. *Chem Sci* **2015**, *6* (5), 2650–2659.

(189) Hao, L.; Zhou, Q.; Piao, Y.; Zhou, Z.; Tang, J.; Shen, Y. *J Controll Release* **2021**, *330*, 362–371.

(190) Diethelm, S.; Schafroth, M. A.; Carreira, E. M. *Org Lett* **2014**, *16* (15), 3908–3911.

(191) Zhang, Y.; Liang, Y.; Huang, F.; Zhang, Y.; Li, X.; Xia, J. *Biochemistry* **2019**, *58* (7), 1010–1018.

(192) Nakamura, T.; Kawai, Y.; Kitamoto, N.; Osawa, T.; Kato, Y. *Chem Res Toxicol* **2009**, *22* (3), 536–542.

(193) Yi, S.; Wei, S.; Wu, Q.; Wang, H.; Yao, Z. J. *Angew Chem Int Ed Engl* **2022**, *61* (6).

(194) Teng, S.; Ng, E. W. H.; Zhang, Z.; Soon, C. N.; Xu, H.; Li, R.; Hirao, H.; Loh, T. P. *Sci Adv* **2023**, *9* (17).

(195) Tiwari, S.; Senthil, S.; Khanna, S.; Duraisamy, S.; Vechalapu, S. K.; Chandra Mallojjala, S.; Allimuthu, D. *Cell Rep Phys Sci* **2024**, *5* (11), 102260.

(196) Liu, H.; May, K. *MAbs* **2012**, *4* (1), 17–23.

(197) Schumacher, F. F.; Nunes, J. P. M.; Maruani, A.; Chudasama, V.; Smith, M. E. B.; Chester, K. A.; Baker, J. R.; Caddick, S. *Org. Biomol. Chem.* **2014**, *12* (37), 7261–7269.

(198) Szijj, P. A.; Bahou, C.; Chudasama, V. *Drug Discov Today Technol* **2018**, *30*, 27–34.

(199) Lyon, R. P.; Setter, J. R.; Bovee, T. D.; Doronina, S. O.; Hunter, J. H.; Anderson, M. E.; Balasubramanian, C. L.; Duniho, S. M.; Leiske, C. I.; Li, F.; Senter, P. D. *Nat Biotechnol* **2014**, *32* (10), 1059–1062.

(200) Christie, R. J.; Fleming, R.; Bezabeh, B.; Woods, R.; Mao, S.; Harper, J.; Joseph, A.; Wang, Q.; Xu, Z. Q.; Wu, H.; Gao, C.; Dimasi, N. *J Controll Release* **2015**, *220* (Pt B), 660–670.

(201) Christie, R. J.; Tiberghien, A. C.; Du, Q.; Bezabeh, B.; Fleming, R.; Shannon, A.; Mao, S.; Breen, S.; Zhang, J.; Zhong, H.; Harper, J.; Wu, H.; Howard, P. W.; Gao, C. *Antibodies (Basel)* **2017**, *6* (4).

(202) Abbas, A.; Xing, B.; Loh, T. P. *Angew Chem Int Ed Engl* **2014**, *53* (29), 7491–7494.

(203) Pichon, M. M.; Drelinkiewicz, D.; Lozano, D.; Moraru, R.; Hayward, L. J.; Jones, M.; McCoy, M. A.; Allstrum-Graves, S.; Balourdas, D.-I.; Joerger, A. C.; Whitby, R. J.; Goldup, S. M.; Wells, N.; Langley, G. J.; Herniman, J. M.; Baud, M. G. J. *Bioconjug Chem* **2023**, *34* (9), 1679–1687.

(204) Embaby, A. M.; Schoffelen, S.; Kofoed, C.; Meldal, M.; Diness, F. *Angew Chem Int Ed Engl* **2018**, *57* (27), 8022–8026.

(205) Lazar, A. C.; Wang, L.; Blättler, W. A.; Amphlett, G.; Lambert, J. M.; Zhang, W. *Rapid Commun Mass Spectrom* **2005**, *19* (13), 1806–1814.

(206) Boylan, N. J.; Zhou, W.; Proos, R. J.; Tolbert, T. J.; Wolfe, J. L.; Laurence, J. S. *Bioconjug Chem* **2013**, *24* (6), 1008–1016.

(207) Lee, M. T. W.; Maruani, A.; Baker, J. R.; Caddick, S.; Chudasama, V. *Chem Sci* **2016**, *7* (1), 799–802.

(208) Nunes, J. P. M.; Morais, M.; Vassileva, V.; Robinson, E.; Rajkumar, V. S.; Smith, M. E. B.; Pedley, R. B.; Caddick, S.; Baker, J. R.; Chudasama, V. *Chem Comm* **2015**, *51* (53), 10624–10627.

(209) Maruani, A.; Smith, M. E. B.; Miranda, E.; Chester, K. A.; Chudasama, V.; Caddick, S. *Nat Commun* **2015**, *6*.

(210) Bryant, P.; Pabst, M.; Badescu, G.; Bird, M.; McDowell, W.; Jamieson, E.; Swierkosz, J.; Jurlewicz, K.; Tommasi, R.; Henseleit, K.; Sheng, X.; Camper, N.; Manin, A.; Kozakowska, K.; Peciak, K.; Laurine, E.; Grygorash, R.; Kyle, A.; Morris, D.; Parekh, V.; Abhilash, A.; Choi, J. W.; Edwards, J.; Frigerio, M.; Baker, M. P.; Godwin, A. *Mol Pharm* **2015**, *12* (6), 1872–1879.

(211) Behrens, C. R.; Ha, E. H.; Chinn, L. L.; Bowers, S.; Probst, G.; Fitch-Bruhns, M.; Monteon, J.; Valdiosera, A.; Bermudez, A.; Liao-Chan, S.; Wong, T.; Melnick, J.; Theunissen, J.-W.; Flory, M. R.; Houser, D.; Venstrom, K.; Levashova, Z.; Sauer, P.; Migone, T.-S.; van der Horst, E. H.; Halcomb, R. L.; Jackson, D. Y. *Mol Pharm* **2015**, *12* (11), 3986–3998.

(212) Junutula, J. R.; Bhakta, S.; Raab, H.; Ervin, K. E.; Eigenbrot, C.; Vandlen, R.; Scheller, R. H.; Lowman, H. B. *J Immunol Methods* **2008**, *332* (1–2), 41–52.

(213) Zacharias, N.; Podust, V. N.; Kajihara, K. K.; Leipold, D.; Del Rosario, G.; Thayer, D.; Dong, E.; Paluch, M.; Fischer, D.; Zheng, K.; Lei, C.; He, J.; Ng, C.; Su, D.; Liu, L.; Masih, S.; Sawyer, W.; Tinianow, J.; Marik, J.; Yip, V.; Li, G.; Chuh, J.; Morisaki, J. H.; Park, S.; Zheng, B.; Hernandez-Barry, H.; Loyet, K. M.; Xu, M.; Kozak, K. R.; Phillips, G. L.; Shen, B. Q.; Wu, C.; Xu, K.; Yu, S. F.; Kamath, A.; Rowntree, R. K.; Reilly, D.; Pillow, T.; Polson, A.; Schellenberger, V.; Hazenbos, W. L. W.; Sadowsky, J. *Chem Sci* **2022**, *13* (11), 3147–3160.

(214) Arnér, E. S. J. *Exp Cell Res* **2010**, *316* (8), 1296–1303.

(215) Nilchan, N.; Li, X.; Pedzisa, L.; Nanna, A. R.; Roush, W. R.; Rader, C. *Antib Ther* **2019**, *2* (4), 1–8.

(216) Huang, Y.; Liu, T. *Synth Syst Biotechnol* **2018**, *3* (3), 150–158.

(217) Kularatne, S. A.; Deshmukh, V.; Ma, J.; Tardif, V.; Lim, R. K. V.; Pugh, H. M.; Sun, Y.; Manibusan, A.; Sellers, A. J.; Barnett, R. S.; Srinagesh, S.; Forsyth, J. S.; Hassenpflug, W.; Tian, F.; Javahishvili, T.; Felding-Habermann, B.; Lawson, B. R.; Kazane, S. A.; Schultz, P. G. *Angew Chem Int Ed Engl* **2014**, *53* (44), 11863–11867.

(218) Manabe, S.; Yamaguchi, Y. *Chem Rec* **2021**, *21* (11), 3005–3014.

(219) Zhang, X.; Ou, C.; Liu, H.; Prabhu, S. K.; Li, C.; Yang, Q.; Wang, L. X. *ACS Chem Biol* **2021**, *16* (11), 2502–2514.

(220) Dong, W.; Wang, W.; Cao, C. *Chem Med Chem* **2024**, *19* (17).

(221) Ton-That, H.; Liu, G.; Mazmanian, S. K.; Faull, K. F.; Schneewind, O. *Proc Natl Acad Sci U S A* **1999**, *96* (22), 12424–12429.

(222) Strop, P. *Bioconjug Chem* **2014**, *25* (5), 855–862.

(223) Dennler, P.; Chiotellis, A.; Fischer, E.; Brégeon, D.; Belmant, C.; Gauthier, L.; Lhospice, F.; Romagne, F.; Schibli, R. *Bioconjug Chem* **2014**, *25* (3), 569–578.

(224) Kolb, H. C.; Finn, M. G.; Sharpless, K. B. *Angew Chem Int Ed* **2001**, 2004–2021.

(225) Nwe, K.; Brechbiel, M. W. *Cancer Biother Radiopharm* **2009**, *24* (3), 289–302.

(226) Tornøe, C. W.; Christensen, C.; Meldal, M. *J Org Chem* **2002**, *67* (9), 3057–3064.

(227) Meldal, M.; Tomøe, C. W. *Chem Rev* **2008**, *108* (8), 2952–3015.

(228) Hong, V.; Steinmetz, N. F.; Manchester, M.; Finn, M. G. *Bioconjug Chem* **2010**, *21* (10), 1912–1916.

(229) Agard, N. J.; Prescher, J. A.; Bertozzi, C. R. *J Am Chem Soc* **2004**, *126* (46), 15046–15047.

(230) Dommerholt, J.; Rutjes, F. P. J. T.; van Delft, F. L. *Top Curr Chem* **2016**, *374* (2), 16.

(231) Dommerholt, J.; Schmidt, S.; Temming, R.; Hendriks, L. J. A.; Rutjes, F. P. J. T.; van Hest, J. C. M.; Lefeber, D. J.; Friedl, P.; van Delft, F. L. *Angew Chem Int Ed* **2010**, *49* (49), 9422–9425.

(232) Debets, M. F.; van der Doelen, C. W. J.; Rutjes, F. P. J. T.; van Delft, F. L. *ChemBioChem* **2010**, *11* (9), 1168–1184.

(233) Ning, X.; Guo, J.; Wolfert, M. A.; Boons, G. *Angew Chem Int Ed* **2008**, *47* (12), 2253–2255.

(234) Lyon, R. P.; Bovee, T. D.; Doronina, S. O.; Burke, P. J.; Hunter, J. H.; Neff-Laford, H. D.; Jonas, M.; Anderson, M. E.; Setter, J. R.; Senter, P. D. *Nat Biotechnol* **2015**, *33* (7), 733–735.

(235) Harding, F. A.; Stickler, M. M.; Razo, J.; DuBridge, R. B. *MAbs* **2010**, *2* (3), 256–265.

(236) Pineda, C.; Castañeda Hernández, G.; Jacobs, I. A.; Alvarez, D. F.; Carini, C. *BioDrugs* **2016**, *30* (3), 195–206.

(237) Hamblett, K. J.; Senter, P. D.; Chace, D. F.; Sun, M. M. C.; Lenox, J.; Cerveny, C. G.; Kissler, K. M.; Bernhardt, S. X.; Kopcha, A. K.; Zabinski, R. F.; Meyer, D. L.; Francisco, J. A. *Clin Cancer Res* **2004**, *10* (20), 7063–7070.

(238) Kraynov, E.; Kamath, A. V.; Walles, M.; Tarcsa, E.; Deslandes, A.; Iyer, R. A.; Datta-Mannan, A.; Sriraman, P.; Bairlein, M.; Yang, J. J.; Barfield, M.; Xiao, G.; Escandon, E.; Wang, W.; Rock, D. A.; Chemuturi, N. V.; Moore, D. J. *Drug Metab Dispos* **2016**, *44* (5), 617–623.

(239) Drake, P. M.; Rabuka, D. *BioDrugs* **2017**, *31* (6), 521–531.

(240) Donaghy, H. *MAbs* **2016**, *8* (4), 659–671.

(241) Panowski, S.; Bhakta, S.; Raab, H.; Polakis, P.; Junutula, J. R. *MAbs* **2014**, *6* (1), 34–45.

(242) Shah, D. K.; Betts, A. M. *MAbs* **2013**, *5* (2), 297–305.

(243) Yip, V.; Palma, E.; Tesar, D. B.; Mundo, E. E.; Bumbaca, D.; Torres, E. K.; Reyes, N. A.; Shen, B. Q.; Fielder, P. J.; Prabhu, S.; Khawli, L. A.; Boswell, C. A. *MAbs* **2014**, *6* (3), 689–696.

(244) Herbertson, R. A.; Tebbutt, N. C.; Lee, F. T.; MacFarlane, D. J.; Chappell, B.; Micallef, N.; Lee, S. T.; Saunder, T.; Hopkins, W.; Smyth, F. E.; Wyld, D. K.; Bellen, J.; Sonnichsen, D. S.; Brechbiel, M. W.; Murone, C.; Scott, A. M. *Clinical Cancer Research* **2009**, *15* (21), 6709–6715.

(245) Lu, D.; Joshi, A.; Wang, B.; Olsen, S.; Yi, J. H.; Krop, I. E.; Burris, H. A.; Girish, S. *Clin Pharmacokinet* **2013**, *52* (8), 657–672.

(246) Han, T. H.; Gopal, A. K.; Ramchandren, R.; Goy, A.; Chen, R.; Matous, J. V.; Cooper, M.; Grove, L. E.; Alley, S. C.; Lynch, C. M.; O'connor, O. A. *J Clin Pharmacol* **2013**, *53* (8), 866–877.

(247) Collins, D. M.; Bossenmaier, B.; Kollmorgen, G.; Niederfellner, G. *Cancers (Basel)* **2019**, *11* (3).

(248) Ashman, N.; Bargh, J. D.; Spring, D. R. *Chem Soc Rev* **2022**, *51* (22), 9182–9202.

(249) Barok, M.; Joensuu, H.; Isola, J. *Breast Cancer Res* **2014**, *16* (2).

(250) Loganzo, F.; Tan, X.; Sung, M.; Jin, G.; Myers, J. S.; Melamud, E.; Wang, F.; Diesl, V.; Follettie, M. T.; Musto, S.; Lam, M. H.; Hu, W.; Charati, M. B.; Khandke, K.; Kim, K. S. K.; Cinque, M.; Lucas, J.; Graziani, E.; Maderna, A.; O'Donnell, C. J.; Arndt, K. T.; Gerber, H. P. *Mol Cancer Ther* **2015**, *14* (4), 952–963.

(251) Poison, A. G.; Calemine-Fenaux, J.; Chan, P.; Chang, W.; Christensen, E.; Clark, S.; De Sauvage, F. J.; Eaton, D.; Elkins, K.; Michael Elliott, J.; Frantz, G.; Fuji, R. N.; Gray, A.; Harden, K.; Ingle, G. S.; Kljavin, N. M.; Koeppen, H.; Nelson, C.; Prabhu, S.; Raab, H.; Ross, S.; Stephan, J. P.; Scales, S. J.; Spencer, S. D.; Vandlen, R.; Wranik, B.; Yu, S. F.; Zheng, B.; Ebens, A. *Cancer Res* **2009**, *69* (6), 2358–2364.

(252) Gébleux, R.; Stringhini, M.; Casanova, R.; Soltermann, A.; Neri, D. *Int J Cancer* **2017**, *140* (7), 1670–1679.

(253) Matsumura, Y. *Adv Drug Deliv Rev* **2012**, *64* (8), 710–719.

(254) Yasunaga, M.; Manabe, S.; Tarin, D.; Matsumura, Y. *Bioconjug Chem* **2011**, *22* (9), 1776–1783.

(255) Joubert, N.; Denevault-Sabourin, C.; Bryden, F.; Viaud-Massuard, M. C. *Eur J Med Chem* **2017**, *142*, 393–415.

(256) Matsuda, Y. *J Sep Sci* **2022**, *45* (1), 27–37.

(257) Wakankar, A.; Chen, Y.; Gokarn, Y.; Jacobson, F. S. *MAbs* **2011**, *3* (2), 161–172.

(258) Nobbmann, U.; Connah, M.; Fish, B.; Varley, P.; Gee, C.; Mulot, S.; Chen, J.; Zhou, L.; Lu, Y.; Sheng, F.; Yi, J.; Harding, S. E. *Biotechnol Genet Eng Rev* **2007**, *24* (1), 117–128.

(259) Acchione, M.; Kwon, H.; Jochheim, C. M.; Atkins, W. M. *MAbs* **2012**, *4* (3), 362–372.

(260) Siegel, M. M.; Tabei, K.; Kunz, A.; Hollander, I. J.; Hamann, P. R.; Bell, D. H.; Berkenkamp, S.; Hillenkamp, F. *Anal Chem* **1997**, *69* (14), 2716–2726.

(261) Hutchins, B. M.; Kazane, S. A.; Staflin, K.; Forsyth, J. S.; Felding-Habermann, B.; Schultz, P. G.; Smider, V. V. *J Mol Biol* **2011**, *406* (4), 595–603.

(262) Hamann, P. R.; Hinman, L. M.; Hollander, I.; Beyer, C. F.; Lindh, D.; Holcomb, R.; Hallett, W.; Tsou, H. R.; Upeslacis, J.; Shochat, D.; Mountain, A.; Flowers, D. A.; Bernstein, I. *Bioconjug Chem* **2002**, *13* (1), 47–58.

(263) Garnett, M. C.; Embleton, M. J.; Jacobs, E.; Baldwin, R. W. *Int J Cancer* **1983**, *31* (5), 661–670.

(264) Greenfield, R. S.; Kaneko, T.; Daues, A.; Edson, M. A.; Fitzgerald, K. A.; Olech, L. J.; Grattan, J. A.; Spitalny, G. L.; Braslawsky, G. R. *Cancer Res* **1990**, *50* (20), 6600–6607.

(265) Valliere-Douglass, J.; Wallace, A.; Balland, A. *J Chromatogr A* **2008**, *1214* (1–2), 81–89.

(266) Liu, J.; Zhao, H.; Volk, K. J.; Klohr, S. E.; Kerns, E. H.; Lee, M. S. *J Chromatogr A* **1996**, *735* (1–2), 357–366.

(267) Sun, M. M. C.; Beam, K. S.; Cerveny, C. G.; Hamblett, K. J.; Blackmore, R. S.; Torgov, M. Y.; Handley, F. G. M.; Ihle, N. C.; Senter, P. D.; Alley, S. C. *Bioconjug Chem* **2005**, *16* (5), 1282–1290.

(268) Shen, B. Q.; Xu, K.; Liu, L.; Raab, H.; Bhakta, S.; Kenrick, M.; Parsons-Reponte, K. L.; Tien, J.; Yu, S. F.; Mai, E.; Li, D.; Tibbitts, J.; Baudys, J.; Saad, O. M.; Scales, S. J.; McDonald, P. J.; Hass, P. E.; Eigenbrot, C.; Nguyen, T.; Solis, W. A.; Fuji, R. N.; Flagella, K. M.; Patel, D.; Spencer, S. D.; Khawli, L. A.; Ebens, A.; Wong, W. L.; Vandlen, R.; Kaur, S.; Sliwkowski, M. X.; Scheller, R. H.; Polakis, P.; Junutula, J. R. *Nat Biotechnol* **2012**, *30* (2), 184–189.

(269) Boswell, C. A.; Tesar, D. B.; Mukhyala, K.; Theil, F. P.; Fielder, P. J.; Khawli, L. A. *Bioconjug Chem* **2010**, *21* (12), 2153–2163.

(270) Junutula, J. R.; Raab, H.; Clark, S.; Bhakta, S.; Leipold, D. D.; Weir, S.; Chen, Y.; Simpson, M.; Tsai, S. P.; Dennis, M. S.; Lu, Y.; Meng, Y. G.; Ng, C.; Yang, J.; Lee, C. C.; Duenas, E.; Gorrell, J.; Katta, V.; Kim, A.; McDorman, K.; Flagella, K.; Venook, R.; Ross, S.; Spencer, S. D.; Lee Wong, W.; Lowman, H. B.; Vandlen, R.; Sliwkowski, M. X.; Scheller, R. H.; Polakis, P.; Mallet, W. *Nat Biotechnol* **2008**, *26* (8), 925–932.

(271) McDonagh, C. F.; Turcott, E.; Westendorf, L.; Webster, J. B.; Alley, S. C.; Kim, K.; Andreyka, J.; Stone, I.; Hamblett, K. J.; Francisco, J. A.; Carter, P. *Protein Eng Des Sel* **2006**, *19* (7), 299–307.

(272) Rosati, S.; Yang, Y.; Barendregt, A.; Heck, A. J. R. *Nat Protoc* **2014**, *9* (4), 967–976.

(273) Wang, Y.; Lu, Q.; Wu, S. L.; Karger, B. L.; Hancock, W. S. *Anal Chem* **2011**, *83* (8), 3133–3140.

(274) Safavy, A.; Bonner, J. A.; Waksal, H. W.; Buchsbaum, D. J.; Gillespie, G. Y.; Khazaeli, M. B.; Arani, R.; Chen, D. T.; Carpenter, M.; Raisch, K. P. *Bioconjug Chem* **2003**, *14* (2), 302–310.

(275) Ingham, P. W.; McMahon, A. P. *Genes Dev* **2001**, *15* (23), 3059–3087.

(276) Roessler, E.; Belloni, E.; Gaudenz, K.; Jay, P.; Berta, P.; Scherer, S. W.; Tsui, L. C.; Muenke, M. *Nat Genet* **1996**, *14* (3), 357–360.

(277) Beachy, P. A.; Karhadkar, S. S.; Berman, D. M. *Nature* **2004**, *432* (7015), 324–331.

(278) Rubin, L. L.; de Sauvage, F. J. *Nat Rev Drug Discov* **2006**, *5* (12), 1026–1033.

(279) Nüsslein-volhard, C.; Wieschaus, E. *Nature* **1980**, *287* (5785), 795–801.

(280) Blotta, S.; Jakubikova, J.; Calimeri, T.; Roccaro, A. M.; Amodio, N.; Azab, A. K.; Foresta, U.; Mitsiades, C. S.; Rossi, M.; Todoerti, K.; Molica, S.; Morabito, F.; Neri, A.; Tagliaferri, P.; Tassone, P.; Anderson, K. C.; Munshi, N. C. *Blood* **2012**, *120* (25), 5002–5013.

(281) Choudhry, Z.; Rikani, A. A.; Choudhry, A. M.; Tariq, S.; Zakaria, F.; Asghar, M. W.; Sarfraz, M. K.; Haider, K.; Shafiq, A. A.; Mobassarah, N. J. *Ann Neurosci* **2014**, *21* (1), 28–31.

(282) Rimkus, T. K.; Carpenter, R. L.; Qasem, S.; Chan, M.; Lo, H. W. *Cancers (Basel)* **2016**, *8* (2).

(283) Kinzler, K. W.; Bigner, S. H.; Bigner, D. D.; Trent, J. M.; Law, M. L.; O'Brien, S. J.; Wong, A. J.; Vogelstein, B. *Science* **1987**, *236* (4797), 70–73.

(284) Teglund, S.; Toftgård, R. *Biochim Biophys Acta Rev Cancer* **2010**, *1805* (2), 181–208.

(285) Kim, J.; Kato, M.; Beachy, P. A. *Proc Natl Acad Sci U S A* **2009**, *106* (51), 21666–21671.

(286) Gonnissen, A.; Isebaert, S.; Haustermans, K. *Oncotarget* **2015**, *6* (16), 13899–13913.

(287) Kogerman, P.; Grimm, T.; Kogerman, L.; Krause, D.; Undén, A. B.; Sandstedt, B.; Toftgård, R.; Zaphiropoulos, P. G. *Nat Cell Biol* **1999**, *1* (5), 312–319.

(288) Humke, E. W.; Dorn, K. V.; Milenkovic, L.; Scott, M. P.; Rohatgi, R. *Genes Dev* **2010**, *24* (7), 670–682.

(289) Lauth, M.; Bergström, Å.; Shimokawa, T.; Toftgård, R. *Proc Natl Acad Sci U S A* **2007**, *104* (20), 8455–8460.

(290) Riobó, N. A.; Lu, K.; Ai, X.; Haines, G. M.; Emerson, C. P. *Proc Natl Acad Sci U S A* **2006**, *103* (12), 4505–4510.

(291) Riobo, N. A.; Haines, G. M.; Emerson, C. P. *Cancer Res* **2006**, *66* (2), 839–845.

(292) Mao, J.; Maye, P.; Kogerman, P.; Tejedor, F. J.; Toftgard, R.; Xie, W.; Wu, G.; Wu, D. *J Biol Chem* **2002**, *277* (38), 35156–35161.

(293) Gulino, A.; Di Marcotullio, L.; Canettieri, G.; De Smaele, E.; Screpanti, I. *Vitam Horm* **2012**, *88*, 211–227.

(294) Canettieri, G.; Di Marcotullio, L.; Greco, A.; Coni, S.; Antonucci, L.; Infante, P.; Pietrosanti, L.; De Smaele, E.; Ferretti, E.; Miele, E.; Pelloni, M.; De Simone, G.; Pedone, E. M.; Gallinari, P.; Giorgi, A.; Steinkühler, C.; Vitagliano, L.; Pedone, C.; Schinin, M. E.; Screpanti, I.; Gulino, A. *Nat Cell Biol* **2010**, *12* (2), 132–142.

(295) Archer, T. C.; Weeraratne, S. D.; Pomeroy, S. L. *Journal of Clinical Oncology* **2012**, *30* (17), 2154–2156.

(296) Svärd, J.; Henricson, K. H.; Persson-Lek, M.; Rozell, B.; Lauth, M.; Bergström, Å.; Ericson, J.; Toftgård, R.; Teglund, S. *Dev Cell* **2006**, *10* (2), 187–197.

(297) Lee, Y.; Kawagoe, R.; Sasai, K.; Li, Y.; Russell, H. R.; Curran, T.; McKinnon, P. J. *Oncogene* **2007**, *26* (44), 6442–6447.

(298) Robbins, D. J.; Fei, D. L.; Riobo, N. A. *Sci Signal* **2012**, *5* (246).

(299) Arensdorf, A. M.; Marada, S.; Ogden, S. K. *Trends Pharmacol Sci* **2016**, *37* (1), 62–72.

(300) Lee, H.; Ko, H. W. *Biochem Biophys Res Commun* **2016**, *480* (4), 574–579.

(301) Yuan, X.; Cao, J.; He, X.; Serra, R.; Qu, J.; Cao, X.; Yang, S. *Nat Commun* **2016**, *7*.

(302) Fuchs, S.; Dohle, E.; Kirkpatrick, C. J. *Vitam Horm* **2012**, *88*, 491–506.

(303) Yang, J.; Andre, P.; Ye, L.; Yang, Y.-Z. *Int J Oral Sci* **2015**, *7* (2), 73–79.

(304) Huang, C.; Tang, M.; Yehling, E.; Zhang, X. *Mol Ther* **2014**, *22* (2), 430–439.

(305) Mak, K. K.; Bi, Y.; Wan, C.; Chuang, P.-T.; Clemens, T.; Young, M.; Yang, Y. *Dev Cell* **2008**, *14* (5), 674–688.

(306) Long, F.; Chung, U.; Ohba, S.; McMahon, J.; Kronenberg, H. M.; McMahon, A. P. *Development* **2004**, *131* (6), 1309–1318.

(307) Wang, Q.; Huang, C.; Zeng, F.; Xue, M.; Zhang, X. *Am J Pathol* **2010**, *177* (6), 3100–3111.

(308) Pola, R.; Ling, L. E.; Silver, M.; Corbley, M. J.; Kearney, M.; Blake Pepinsky, R.; Shapiro, R.; Taylor, F. R.; Baker, D. P.; Asahara, T.; Isner, J. M. *Nat Med* **2001**, *7* (6), 706–711.

(309) Nagase, T.; Nagase, M.; Yoshimura, K.; Machida, M.; Yamagishi, M. *J Craniofac Surg* **2006**, *17* (4), 736–744.

(310) Gorojankina, T.; Hoch, L.; Faure, H.; Roudaut, H.; Traiffort, E.; Schoenfelder, A.; Girard, N.; Mann, A.; Manetti, F.; Solinas, A.; Petricci, E.; Taddei, M.; Ruat, M. *Mol Pharmacol* **2013**, *83* (5), 1020–1029.

(311) Manetti, F.; Petricci, E.; Gabrielli, A.; Mann, A.; Faure, H.; Gorojankina, T.; Brasseur, L.; Hoch, L.; Ruat, M.; Taddei, M. *Eur J Med Chem* **2016**, *121*, 747–757.

(312) Hahn, H.; Wicking, C.; Zaphiropoulos, P. G.; Gailani, M. R.; Shanley, S.; Chidambaram, A.; Vorechovsky, I.; Holmberg, E.; Unden, A. B.; Gillies, S.; Negus, K.; Smyth, I.; Pressman, C.; Leffell, D. J.; Gerrard, B.; Goldstein, A. M.; Dean, M.; Toftgard, R.; Chenevix-Trench, G.; Wainwright, B.; Bale, A. E. *Cell* **1996**, *85* (6), 841–851.

(313) Undén, A. B.; Zaphiropoulos, P. G.; Bruce, K.; Toftgård, R.; Ståhle-Bäckdahl, M. *Cancer Res* **1997**, *57* (12), 2336–2340.

(314) Dahmane, N.; Lee, J.; Robins, P.; Heller, P.; Ruiz I Altaba, A. *Nature* **1997**, *389* (6653), 876–881.

(315) Xie, J.; Murone, M.; Luoh, S. M.; Ryan, A.; Gu, Q.; Zhang, C.; Bonifas, J. M.; Lam, C. W.; Hynes, M.; Goddard, A.; Rosenthal, A.; Epstein, E. H.; De Sauvage, F. J. *Nature* **1998**, *391* (6662), 90–92.

(316) Taylor, M. D.; Liu, L.; Raffel, C.; Hui, C. chung; Mainprize, T. G.; Zhang, X.; Agatep, R.; Chiappa, S.; Gao, L.; Lowrance, A.; Hao, A.; Goldstein, A. M.; Stavrou, T.; Scherer, S. W.; Dura, W. T.; Wainwright, B.; Squire, J. A.; Rutka, J. T.; Hogg, D. *Nat Genet* **2002**, *31* (3), 306–310.

(317) Nilsson, M.; Undèn, A. B.; Krause, D.; Malmqwist, U.; Raza, K.; Zaphiropoulos, P. G.; Toftgård, R. *Proc Natl Acad Sci U S A* **2000**, *97* (7), 3438–3443.

(318) Grachtchouk, M.; Mo, R.; Yu, S.; Zhang, X.; Sasaki, H.; Hui, C. C.; Dlugosz, A. A. *Nat Genet* **2000**, *24* (3), 216–217.

(319) Aszterbaum, M.; Epstein, J.; Anthony, O.; Douglas, V.; Leboit, P. E.; Scott, M. P.; Epstein, E. H. *Nat Med* **1999**, *5* (11), 1285–1291.

(320) Blair, A.; Kazerouni, N. *Cancer Causes Control* **1997**, *8* (3), 473–490.

(321) Wu, A. H.; Wan, P.; Bernstein, L. *Cancer Causes Control* **2001**, *12* (8), 721–732.

(322) Uemura, N.; Okamoto, S.; Yamamoto, S.; Matsumura, N.; Yamaguchi, S.; Yamakido, M.; Taniyama, K.; Sasaki, N.; Schlemper, R. J. *N Engl J Med* **2001**, *345* (11), 784–789.

(323) Burak, K.; Angulo, P.; Pasha, T. M.; Egan, K.; Petz, J.; Lindor, K. D. *Am J Gastroenterol* **2004**, *99* (3), 523–526.

(324) Watkins, D. N.; Berman, D. M.; Burkholder, S. G.; Wang, B.; Beachy, P. A.; Baylin, S. B. *Nature* **2003**, *422* (6929), 313–317.

(325) Beachy, P. A.; Karhadkar, S. S.; Berman, D. M. *Nature* **2004**, *432* (7015), 324–331.

(326) Lessard, J.; Sauvageau, G. *Nature* **2003**, *423* (6937), 255–260.

(327) Park, I. K.; Qian, D.; Kiel, M.; Becker, M. W.; Pihalja, M.; Weissman, I. L.; Morrison, S. J.; Clarke, M. F. *Nature* **2003**, *423* (6937), 302–305.

(328) Karhadkar, S. S.; Bova, G. S.; Abdallah, N.; Dhara, S.; Gardner, D.; Maitra, A.; Isaacs, J. T.; Berman, D. M.; Beachy, P. A. *Nature* **2004**, *431* (7009), 707–712.

(329) Leung, C.; Lingbeek, M.; Shakhova, O.; Liu, J.; Tanger, E.; Saremaslani, P.; Van Lohuizen, M.; Marino, S. *Nature* **2004**, *428* (6980), 337–341.

(330) Wang, C.; Wu, H.; Katritch, V.; Han, G. W.; Huang, X. P.; Liu, W.; Siu, F. Y.; Roth, B. L.; Cherezov, V.; Stevens, R. C. *Nature* **2013**, *497* (7449), 338–343.

(331) Kristiansen, K. *Pharmacol Ther* **2004**, *103* (1), 21–80.

(332) Fan, J.; Liu, Y.; Jia, J. *Dev Biol* **2012**, *366* (2), 172–184.

(333) Wang, Y.; Zhou, Z.; Walsh, C. T.; McMahon, A. P. *Proceedings of the National Academy of Sciences* **2009**, *106* (8), 2623–2628.

(334) Marinissen, M. J.; Gutkind, J. S. *Trends Pharmacol Sci* **2001**, *22* (7), 368–376.

(335) Chen, J. K.; Taipale, J.; Cooper, M. K.; Beachy, P. A. *Genes Dev* **2002**, *16* (21), 2743–2748.

(336) Cooper, M. K.; Porter, J. A.; Young, K. E.; Beachy, P. A. *Science* **1998**, *280* (5369), 1603–1607.

(337) Binns, W.; Thacker, E. J.; James, L. F.; Huffman, W. T. *J Am Vet Med Assoc* **1959**, *134* (4), 180–183.

(338) Incardona, J. P.; Gaffield, W.; Kapur, R. P.; Roelink, H. *Development* **1998**, *125* (18), 3553–3562.

(339) Talpale, J.; Chen, J. K.; Cooper, M. K.; Wang, B.; Mann, R. K.; Milenkovic, L.; Scott, M. P.; Beachy, P. A. *Nature* **2000**, *406* (6799), 1005–1009.

(340) Varnat, F.; Duquet, A.; Malerba, M.; Zbinden, M.; Mas, C.; Gervaz, P.; Ruiz I Altaba, A. *EMBO Mol Med* **2009**, *1* (6–7), 338–351.

(341) Feldmann, G.; Dhara, S.; Fendrich, V.; Bedja, D.; Beaty, R.; Mullendore, M.; Karikari, C.; Alvarez, H.; Iacobuzio-Donahue, C.; Jimeno, A.; Gabrielson, K. L.; Matsui, W.; Maitra, A. *Cancer Res* **2007**, *67* (5), 2187–2196.

(342) Sanchez, P.; Ruiz I Altaba, A. *Mech Dev* **2005**, *122* (2), 223–230.

(343) Nagata, R.; Izumi, K. *Jpn J Pharmacol* **1991**, *55* (1), 129–137.

(344) Ruch, J. M.; Kim, E. J. *Drugs* **2013**, *73* (7), 613–623.

(345) Von Hoff, D. D.; LoRusso, P. M.; Rudin, C. M.; Reddy, J. C.; Yauch, R. L.; Tibes, R.; Weiss, G. J.; Borad, M. J.; Hann, C. L.; Brahmer, J. R.; Mackey, H. M.; Lum, B. L.; Darbonne, W. C.; Marsters, J. C.; de Sauvage, F. J.; Low, J. A. *N Engl J Med* **2009**, *361* (12), 1164–1172.

(346) Di Magno, L.; Coni, S.; Di Marcotullio, L.; Canettieri, G. *Biochim Biophys Acta Rev Cancer* **2015**, *1856* (1), 62–72.

(347) Basset-Séguin, N.; Hauschild, A.; Kunstfeld, R.; Grob, J.; Dréno, B.; Mortier, L.; Ascierto, P. A.; Licitra, L.; Dutriaux, C.; Thomas, L.; Meyer, N.; Guillot, B.; Dummer, R.; Arenberger, P.; Fife, K.; Raimundo, A.; Dika, E.; Dimier, N.; Fittipaldo, A.; Xynos, I.; Hansson, J. *Eur J Cancer* **2017**, *86*, 334–348.

(348) Mohan, S. V.; Chang, J.; Li, S.; Solomon Henry, A.; Wood, D. J.; Chang, A. L. S. *JAMA Dermatol* **2016**, *152* (5), 527–532.

(349) Bhutani, T.; Abrouk, M.; Sima, C. S.; Sadetsky, N.; Hou, J.; Caro, I.; Chren, M. M.; Arron, S. T. *J Am Acad Dermatol* **2017**, *77* (4), 713–718.

(350) Chang, A. L. S.; Oro, A. E. *Arch Dermatol* **2012**, *148* (11), 1324–1325.

(351) Jamieson, C.; Martinelli, G.; Papayannidis, C.; Cortes, J. E. *Blood Cancer Discov* **2020**, *1* (2), 134–145.

(352) Rodon, J.; Tawbi, H. A.; Thomas, A. L.; Stoller, R. G.; Turtschi, C. P.; Baselga, J.; Sarantopoulos, J.; Mahalingam, D.; Shou, Y.; Moles, M. A.; Yang, L.; Granvil, C.; Hurh, E.; Rose, K. L.; Amakye, D. D.; Dummer, R.; Mita, A. C. *Clin Cancer Res* **2014**, *20* (7), 1900–1909.

(353) Lear, J. T.; Migden, M. R.; Lewis, K. D.; Chang, A. L. S.; Guminski, A.; Gutzmer, R.; Dirix, L.; Combemale, P.; Stratigos, A.; Plummer, R.; Castro, H.; Yi, T.; Mone, M.; Zhou, J.; Trefzer, U.; Kaatz, M.; Loquai, C.; Kudchadkar, R.; Sellami, D.; Dummer, R. *J Eur Acad Dermatol Venereol* **2018**, *32* (3), 372–381.

(354) Xie, P.; Lefrançois, P. *J Am Acad Dermatol* **2018**, *79* (6), 1089-1100.e17.

(355) Danial, C.; Sarin, K. Y.; Oro, A. E.; Chang, A. L. S. *Clin Cancer Res* **2016**, *22* (6), 1325–1329.

(356) Gan, G. N.; Jimeno, A. *Expert Opin Investig Drugs* **2016**, *25* (10), 1153–1166.

(357) Olive, K. P.; Jacobetz, M. A.; Davidson, C. J.; Gopinathan, A.; McIntyre, D.; Honess, D.; Madhu, B.; Goldgraben, M. A.; Caldwell, M. E.; Allard, D.; Frese, K. K.; DeNicola, G.; Feig, C.; Combs, C.; Winter, S. P.; Ireland-Zecchini, H.; Reichelt, S.; Howat, W. J.; Chang, A.; Dhara, M.; Wang, L.; Rückert, F.; Grützmann, R.; Pilarsky, C.; Izeradjene, K.; Hingorani, S.

R.; Huang, P.; Davies, S. E.; Plunkett, W.; Egorin, M.; Hruban, R. H.; Whitebread, N.; McGovern, K.; Adams, J.; Iacobuzio-Donahue, C.; Griffiths, J.; Tuveson, D. A. *Science* **2009**, *324* (5933), 1457–1461.

(358) Ko, A. H.; LoConte, N.; Tempero, M. A.; Walker, E. J.; Kelley, R. K.; Lewis, S.; Chang, W. C.; Kantoff, E.; Vannier, M. W.; Catenacci, D. V.; Venook, A. P.; Kindler, H. L. *Pancreas* **2016**, *45* (3), 370–375.

(359) Piérard, G. E.; Arrese, J. E.; Piérard-Franchimont, C. *Expert Opin Pharmacother* **2000**, *1* (2), 287–304.

(360) Pantziarka, P. *Ecancermedicalscience* **2015**, *9*.

(361) Kim, D. J.; Kim, J.; Spaunhurst, K.; Montoya, J.; Khodosh, R.; Chandra, K.; Fu, T.; Gilliam, A.; Molgo, M.; Beachy, P. A.; Tang, J. Y. *J Clin Oncol* **2014**, *32* (8), 745–751.

(362) Antonarakis, E. S.; Heath, E. I.; Smith, D. C.; Rathkopf, D.; Blackford, A. L.; Danila, D. C.; King, S.; Frost, A.; Ajiboye, A. S.; Zhao, M.; Mendonca, J.; Kachhap, S. K.; Rudek, M. A.; Carducci, M. A. *Oncologist* **2013**, *18* (2), 163–173.

(363) Tsubamoto, H.; Sonoda, T.; Ikuta, S.; Tani, S.; Inoue, K.; Yamanaka, N. *Anticancer Res* **2015**, *35* (9), 4923–4927.

(364) Tsubamoto, H.; Sonoda, T.; Ikuta, S.; Tani, S.; Inoue, K.; Yamanaka, N. *Anticancer Res* **2015**, *35* (7), 4191–4196.

(365) Tsubamoto, H.; Sonoda, T.; Inoue, K. *Anticancer Res* **2014**, *34* (7), 3839–3844.

(366) Tsubamoto, H.; Sonoda, T.; Yamasaki, M.; Inoue, K. *Anticancer Res* **2014**, *34* (4), 2007–2014.

(367) Sharpe, H. J.; Pau, G.; Dijkgraaf, G. J.; Basset-Seguin, N.; Modrusan, Z.; Januario, T.; Tsui, V.; Durham, A. B.; Dlugosz, A. A.; Haverty, P. M.; Bourgon, R.; Tang, J. Y.; Sarin, K. Y.; Dirix, L.; Fisher, D. C.; Rudin, C. M.; Sofen, H.; Migden, M. R.; Yauch, R. L.; de Sauvage, F. J. *Cancer Cell* **2015**, *27* (3), 327–341.

(368) Yauch, R. L.; Dijkgraaf, G. J. P.; Alicke, B.; Januário, T.; Ahn, C. P.; Holcomb, T.; Pujara, K.; Stinson, J.; Callahan, C. A.; Tang, T.; Bazan, J. F.; Kan, Z.; Seshagiri, S.; Hann, C. L.; Gould, S. E.; Low, J. A.; Rudin, C. M.; De Sauvage, F. J. *Science* **2009**, *326* (5952), 572–574.

(369) Buonamici, S.; Williams, J.; Morrissey, M.; Wang, A.; Guo, R.; Vattay, A.; Hsiao, K.; Yuan, J.; Green, J.; Ospina, B.; Yu, Q.; Ostrom, L.; Fordjour, P.; Anderson, D. L.; Monahan, J. E.; Kelleher, J. F.; Peukert, S.; Pan, S.; Wu, X.; Maira, S. M.; García-Echeverría, C.; Briggs, K. J.; Watkins, D. N.; Yao, Y. M.; Lengauer, C.; Warmuth, M.; Sellers, W. R.; Dorsch, M. *Sci Transl Med* **2010**, *2* (51).

(370) Avery, J. T.; Zhang, R.; Boohaker, R. J. *Front Oncol* **2021**, *11*.

(371) Manetti, F.; Faure, H.; Roudaut, H.; Gorojankina, T.; Traiffort, E.; Schoenfelder, A.; Mann, A.; Solinas, A.; Taddei, M.; Ruat, M. *Mol Pharmacol* **2010**, *78* (4), 658–665.

(372) Roudaut, H.; Traiffort, E.; Gorojankina, T.; Vincent, L.; Faure, H.; Schoenfelder, A.; Mann, A.; Manetti, F.; Solinas, A.; Taddei, M.; Ruat, M. *Mol Pharmacol* **2011**, *79* (3), 453–460.

(373) Solinas, A.; Faure, H.; Roudaut, H.; Traiffort, E.; Schoenfelder, A.; Mann, A.; Manetti, F.; Taddei, M.; Ruat, M. *J Med Chem* **2012**, *55* (4), 1559–1571.

(374) Hoch, L.; Faure, H.; Roudaut, H.; Schoenfelder, A.; Mann, A.; Girard, N.; Bihannic, L.; Ayrault, O.; Petricci, E.; Taddei, M.; Rognan, D.; Ruat, M. *The FASEB Journal* **2015**, *29* (5), 1817–1829.

(375) Wang, C.; Wu, H.; Evron, T.; Vardy, E.; Han, G. W.; Huang, X. P.; Hufeisen, S. J.; Mangano, T. J.; Urban, D. J.; Katritch, V.; Cherezov, V.; Caron, M. G.; Roth, B. L.; Stevens, R. C. *Nat Commun* **2014**, *5* (1), 1–11.

(376) Gorojankina, T.; Hoch, L.; Faure, H.; Roudaut, H.; Traiffort, E.; Schoenfelder, A.; Girard, N.; Mann, A.; Manetti, F.; Solinas, A.; Petricci, E.; Taddei, M.; Ruat, M. *Mol Pharmacol* **2013**, *83* (5), 1020–1029.

(377) Pietrobono, S.; Santini, R.; Gagliardi, S.; Dapporto, F.; Colecchia, D.; Chiariello, M.; Leone, C.; Valoti, M.; Manetti, F.; Petricci, E.; Taddei, M.; Stecca, B. *Cell Death Dis* **2018**, *9* (2), 142.

(378) Vesci, L.; Milazzo, F. M.; Stasi, M. A.; Pace, S.; Manera, F.; Tallarico, C.; Cini, E.; Petricci, E.; Manetti, F.; De Santis, R.; Giannini, G. *Eur J Med Chem* **2018**, *157*, 368–379.

(379) Srivastava, R. K.; Kaylani, S. Z.; Edrees, N.; Li, C.; Talwelkar, S. S.; Xu, J.; Palle, K.; Pressey, J. G.; Athar, M. *Oncotarget* **2014**, *5* (23), 12151–12165.

(380) Shahi, M. H.; Holt, R.; Rebhun, R. B. *PLoS One* **2014**, *9* (5), e96593.

(381) Chen, Q.; Xu, R.; Zeng, C.; Lu, Q.; Huang, D.; Shi, C.; Zhang, W.; Deng, L.; Yan, R.; Rao, H.; Gao, G.; Luo, S. *PLoS One* **2014**, *9* (2), e88386.

(382) Calcaterra, A.; Iovine, V.; Botta, B.; Quaglio, D.; D'Acquarica, I.; Ciogli, A.; Iazzetti, A.; Alfonsi, R.; Lospinoso Severini, L.; Infante, P.; Di Marcotullio, L.; Mori, M.; Ghirga, F. *J Enzyme Inhib Med Chem* **2018**, *33* (1), 349–358.

(383) Vanderburgh, J. P.; Kwakwa, K. A.; Werfel, T. A.; Merkel, A. R.; Gupta, M. K.; Johnson, R. W.; Guelcher, S. A.; Duvall, C. L.; Rhoades, J. A. *J Control Release* **2019**, *311–312*, 257–272.

(384) Infante, P.; Malfanti, A.; Quaglio, D.; Balducci, S.; De Martin, S.; Bufalieri, F.; Mastrotto, F.; Basili, I.; Garofalo, M.; Lospinoso Severini, L.; Mori, M.; Manni, I.; Moretti, M.; Nicoletti, C.; Piaggio, G.; Caliceti, P.; Botta, B.; Ghirga, F.; Salmaso, S.; Di Marcotullio, L. *Cancer Lett* **2021**, *499*, 220–231.

(385) List, A.; Beran, M.; DiPersio, J.; Slack, J.; Vey, N.; Rosenfeld, C. S.; Greenberg, P. *Leukemia* **2003**, *17* (8), 1499–1507.

(386) Beauchamp, E. M.; Ringer, L.; Bulut, G.; Sajwan, K. P.; Hall, M. D.; Lee, Y. C.; Peaceman, D.; Özdemirli, M.; Rodriguez, O.; Macdonald, T. J.; Albanese, C.; Toretsky, J. A.; Üren, A. *J Clin Invest* **2011**, *121* (1), 148–160.

(387) Kim, J.; Lee, J. J.; Kim, J.; Gardner, D.; Beachy, P. A. *Proc Natl Acad Sci U S A* **2010**, *107* (30), 13432–13437.

(388) Han, J. Bin; Sang, F.; Chang, J. J.; Hua, Y. Q.; Shi, W. D.; Tang, L. H.; Liu, L. ming. *Onco Targets Ther* **2013**, *6*, 1129–1138.

(389) Leu, L.; Mohassel, L. *American Journal of Health-System Pharmacy* **2009**, *66* (21), 1913–1918.

(390) Jing, J.; Wu, Z.; Wang, J.; Luo, G.; Lin, H.; Fan, Y.; Zhou, C. *Signal Transduct Target Ther* **2023**, *8* (1), 315.

(391) Manetti, F.; Stecca, B.; Santini, R.; Maresca, L.; Giannini, G.; Taddei, M.; Petricci, E. *ACS Med Chem Lett* **2020**, *11* (5), 832–838.

(392) Manetti, F.; Maresca, L.; Crivaro, E.; Pepe, S.; Cini, E.; Singh, S.; Governa, P.; Maramai, S.; Giannini, G.; Stecca, B.; Petricci, E. *ACS Med Chem Lett* **2022**, *13* (8), 1329–1336.

(393) Maresca, L.; Crivaro, E.; Migliorini, F.; Anichini, G.; Giammona, A.; Pepe, S.; Poggialini, F.; Vagaggini, C.; Giannini, G.; Sestini, S.; Borgognoni, L.; Lapucci, A.; Dreassi, E.; Taddei, M.; Manetti, F.; Petricci, E.; Stecca, B. *Pharmacol Res* **2023**, *195*, 106858.

(394) Mancini, C.; Lori, G.; Mattei, G.; Iozzo, M.; Desideri, D.; Cianchi, F.; Fortuna, L.; Passagnoli, F.; Massi, D.; Ugolini, F.; Messerini, L.; Piscuoglio, S.; Pezone, A.; Magherini, F.; Biagioni, A.; Lottini, T.; Zambardino, D.; Truglio, G. I.; Petricci, E.; Magi, A.; Arcangeli, A.; Maresca, L.; Stecca, B.; Pranzini, E.; Taddei, M. L. *J Exp Clin Cancer Res* **2025**, *44* (1).

(395) De Clercq, E.; Li, G. *Clin Microbiol Rev* **2016**, *29* (3), 695–747.

(396) Shelton, J.; Lu, X.; Hollenbaugh, J. A.; Cho, J. H.; Amblard, F.; Schinazi, R. F. *Chem Rev* **2016**, *116* (23), 14379–14455.

(397) Mehellou, Y.; Balzarini, J.; McGuigan, C. *Chem Med Chem* **2009**, *4* (11), 1779–1791.

(398) Mehellou, Y.; Rattan, H. S.; Balzarini, J. *J Med Chem* **2018**, *61* (6), 2211–2226.

(399) Mehellou, Y.; Mcguigan, D. C. *ChemMedChem* **2016**, *11* (11), 1114–1116.

(401) Li, D.; Sun, X.; Li, Y.; Shang, C.; Dong, Y.; Zhao, R.; Zhang, H.; Wang, Z.; Fan, S.; Ma, C.; Li, X. *Bioorg Med Chem* **2024**, *102*, 117657.

(402) Mattellone, A.; Corbisiero, D.; Ferrazzano, L.; Cantelmi, P.; Martelli, G.; Palladino, C.; Tolomelli, A.; Cabri, W. *Green Chemistry* **2023**, *25* (7), 2563–2571.

(403) Ding, R.; He, Y.; Wang, X.; Xu, J.; Chen, Y.; Feng, M.; Qi, C. *Molecules 2011, Vol. 16, Pages 5665-5673* **2011**, *16* (7), 5665–5673.

(404) Angiolini, L.; Manetti, F.; Spiga, O.; Tafi, A.; Visibelli, A.; Petricci, E. *J Chem Inf Model* **2025**, *65* (12), 5847–5855.

(405) Irwin, J. J.; Duan, D.; Torosyan, H.; Doak, A. K.; Ziebart, K. T.; Sterling, T.; Tumanian, G.; Shoichet, B. K. *J Med Chem* **2015**, *58* (17), 7076–7087.

(406) Gaggini, F.; Porcheddu, A.; Reginato, G.; Rodriquez, M.; Taddei, M. *J Comb Chem* **2004**, *6* (5), 805–810.

(407) Ricciardella, G.; Migliorini, F.; Cini, E.; Ievoli, G.; Petricci, E.; Taddei, M.; Zambardino, D.; Stecca, B.; Maresca, L.; Montalbano, A.; Crivaro, E. *Bioorg Chem*, **Submitted**.

(408) Saiki, Y.; Yoshino, Y.; Fujimura, H.; Manabe, T.; Kudo, Y.; Shimada, M.; Mano, N.; Nakano, T.; Lee, Y.; Shimizu, S.; Oba, S.; Fujiwara, S.; Shimizu, H.; Chen, N.; Nezhad, Z. K.; Jin, G.; Fukushige, S.; Sunamura, M.; Ishida, M.; Motoi, F.; Egawa, S.; Unno, M.; Horii, A. *Biochem Biophys Res Commun* **2012**, *421* (1), 98–104.

(409) Siciliano, S.; Bernardi, C.; Finetti, F.; Guerrini, A.; Monti, M. C.; Morretta, E.; Petricci, E.; Poggialini, F.; Romagnoli, G.; Taddei, M.; Trabalzini, L.; Vinciarelli, G.; Zambardino, D.; Cini, E. *Bioorg Chem*, **Submitted**.

(410) Wang, S.; Wang, J.; Chen, Z.; Luo, J.; Guo, W.; Sun, L.; Lin, L. *NPJ Precis Oncol* **2024**, *8* (1).

(411) Giurisato, E.; Tournier, C. *Cell Cycle* **2016**, *15* (5), 619–620.

(412) Pauling, L. *The Nature of the Chemical Bond, An Introduction to Modern Structural Chemistry* **1960**, Cornell Press.

(413) Corradi, E.; Meille, S. V; Messina, M. T.; Metrangolo, P.; Resnati, G. *Angew Chem Int Ed* **2000**, *39* (10), 1782–1786.

(414) Nie, J.; Guo, H.-C.; Cahard, D.; Ma, J.A. *Chem Rev* **2011**, *111* (2), 455–529.

(415) Müller, K.; Faeh, C.; Diederich, F. *Science* **2007**, *317* (5846), 1881–1886.

(416) Berger, R.; Resnati, G.; Metrangolo, P.; Weber, E.; Hulliger, J. *Chem Soc Rev* **2011**, *40* (7), 3496.

(417) Gillis, E. P.; Eastman, K. J.; Hill, M. D.; Donnelly, D. J.; Meanwell, N. A. *J Med Chem* **2015**, *58* (21), 8315–8359.

(418) Lien, E. J.; Guo, Z. -R; Li, R. -L; Su, C. -T. *J Pharm Sci* **1982**, *71* (6), 641–655.

(419) Jeschke, P.; Gutbrod, O.; Leroux, F. R. *Fluorine in Life Sciences: Pharmaceuticals, Medicinal Diagnostics, and Agrochemicals Progress in Fluorine Science Series* **2019**, Academic Press, 631–651.

(420) Barton, H. A.; Pastoor, T. P.; Baetcke, K.; Chambers, J. E.; Diliberto, J.; Doerrer, N. G.; Driver, J. H.; Hastings, C. E.; Iyengar, S.; Krieger, R.; Stahl, B.; Timchalk, C. *Crit Rev Toxicol* **2006**, *36* (1), 9–35.

(421) Bondi, A. *J Phys Chem* **2002**, *68* (3), 441–451.

(422) El Qacemi, M.; Rendine, S.; Maienfisch, P. *Fluorine in Life Sciences: Pharmaceuticals, Medicinal Diagnostics, and Agrochemicals Progress in Fluorine Science Series* **2019**, Academic Press, 607–629.

(423) Meanwell, N. A. *J Agric Food Chem* **2023**, *71* (47), 18087–18122.

(424) Zhou, Y.; Wang, J.; Gu, Z.; Wang, S.; Zhu, W.; Acenã, J. L.; Soloshonok, V. A.; Izawa, K.; Liu, H. *Chem Rev* **2016**, *116* (2), 422–518.

(425) Han, J.; Kiss, L.; Mei, H.; Remete, A. M.; Ponikvar-Svet, M.; Sedgwick, D. M.; Roman, R.; Fustero, S.; Moriwaki, H.; Soloshonok, V. A. *Chem Rev* **2021**, *121* (8), 4678–4742.

(426) Jeschke, P. *Pest Manag Sci* **2024**, *80* (7), 3065–3087.

(427) Zheng, Z.; Dai, A.; Jin, Z.; Chi, Y. R.; Wu, J. *J Agric Food Chem* **2022**, *70* (36), 11019–11030.

(428) Walsh, T. A.; Schmitzer, P. R.; Masters, R. A.; Lo, W. C.; Gast, R. E.; Claus, J. S.; Finkelstein, B. L. *Modern Crop Protection Compounds: Second Edition* **2012**, Wiley, *1*, 277–304.

(429) Cai, H.; Gan, X.; Jin, Z.; Hao, G. *J Agric Food Chem* **2023**, *71* (26), 9973–9993.

(430) Witschel, M.; Aponte, R.; Armel, G.; Bowerman, P.; Mietzner, T.; Newton, T.; Porri, A.; Simon, A.; Seitz, T. *Recent Highlights in the Discovery and Optimization of Crop Protection Products* **2021**, Academic Press, 501–509.

(431) Porri, A.; Betz, M.; Seebruck, K.; Knapp, M.; Johnen, P.; Witschel, M.; Aponte, R.; Liebl, R.; Tranel, P. J.; Lerchl, J. *Pest Manag Sci* **2023**, *79* (2), 507–519.

(432) Luo, B.; Ning, Y. *J Agric Food Chem* **2022**, *70* (4), 957–975.

(433) Desbordes, P.; Essigmann, B.; Gary, S.; Gutbrod, O.; Maue, M.; Schwarz, H. G. *Pest Manag Sci* **2020**, *76* (10), 3340–3347.

(434) Morales-Salazar, I.; Islas-Jácome, P.; Herrera-Zuñiga, L. D.; Couve-Bonnaire, S.; Jubault, P.; González-Zamora, E.; Bouillon, J.; Islas-Jácome, A. *European J Org Chem* **2025**, *28*(38).

(435) Rastogi, S.; Perino, S.; Lal-Nag, M.; Wang, Y.; Blackman, S. C.; Venetsanakos, E. *Cancer Res Commun* **2025**, *5* (4), 668.

(436) Konteatis, Z.; Artin, E.; Nicolay, B.; Straley, K.; Padyana, A. K.; Jin, L.; Chen, Y.; Narayaraswamy, R.; Tong, S.; Wang, F.; Zhou, D.; Cui, D.; Cai, Z.; Luo, Z.; Fang, C.; Tang, H.; Lv, X.; Nagaraja, R.; Yang, H.; Su, S. S. M.; Sui, Z.; Dang, L.; Yen, K.; Popovici-Muller, J.; Codega, P.; Campos, C.; Mellinghoff, I. K.; Biller, S. A. *ACS Med Chem Lett* **2020**, *11* (2), 101.

(437) Richardson, P. *Expert Opin Drug Discov* **2016**, *11* (10), 983–999.

(438) Middleton, W. J. *J Org Chem* **2002**, *40* (5), 574–578.

(439) Lal, G. S.; Fez, G. P.; Pesaresi, R. J.; Prozonic, F. M. *Chem Comm* **1999**, No. 2, 215–216.

(440) Hayashi, H.; Sonoda, H.; Fukumura, K.; Nagata, T. *Chem Comm* **2002**, *2* (15), 1618–1619.

(441) Champagne, P. A.; Desroches, J.; Hamel, J. D.; Vandamme, M.; Paquin, J. F. *Chem Rev* **2015**, *115* (17), 9073–9174.

(442) Singh, R. P.; Shreeve, J. M. *Acc Chem Res* **2003**, *37* (1), 31–44.

(443) Differding, E.; Ofner, H. *Synlett* **1991**, *1991* (3), 187–189.

(444) Liu, W.; Huang, X.; Groves, J. T. *Nat Protoc* **2013**, *8* (12), 2348–2354.

(445) Liu, W.; Groves, J. T. *Angew Chem Int Ed Engl* **2013**, *52* (23), 6024–6027.

(446) Pitts, C. R.; Bloom, S.; Woltornist, R.; Auvenshine, D. J.; Ryzhkov, L. R.; Siegler, M. A.; Lectka, T. *J Am Chem Soc* **2014**, *136* (27), 9780–9791.

(447) Akhgarnusch, A.; Höckendorf, R. F.; Beyer, M. K. *J Phys Chem A* **2015**, *119* (39), 9978–9985.

(448) Prier, C. K.; Rankic, D. A.; MacMillan, D. W. C. *Chem Rev* **2013**, *113* (7), 5322–5363.

(449) McTeague, T. A.; Jamison, T. F. *Angew Chem Int Ed* **2016**, *55* (48), 15072–15075.

(450) Rueping, M.; Nikolaienko, P.; Lebedev, Y.; Adams, A. *Green Chem* **2017**, *19* (11), 2571–2575.

(451) Tomar, P.; Braun, T.; Kemnitz, E. *Chem Comm* **2018**, *54* (70), 9753–9756.

(452) Taponard, A.; Jarrosson, T.; Khrouz, L.; Médebielle, M.; Broggi, J.; Tlili, A. *Angew Chem Int Ed* **2022**, *61* (27).

(453) Kim, S.; Nagorny, P. *Org Lett* **2022**, *24* (12), 2294–2298.

(454) Ortalli, S.; Ford, J.; Trabanco, A. A.; Tredwell, M.; Gouverneur, V. *J Am Chem Soc* **2024**, *146* (17), 11599–11604.

(455) Li, L.; Yu, Z.; Shen, Z. *Adv Synth Catal* **2015**, *357* (16–17), 3495–3500.

(456) Innocent, M.; Tanguy, C.; Gavelle, S.; Aubineau, T.; Guérinot, A. *Chem Eur J* **2024**, *30* (41).

(457) Denkler, L. M.; Aladahalli Shekar, M.; Ngan, T. S. J.; Wylie, L.; Abdullin, D.; Engeser, M.; Schnakenburg, G.; Hett, T.; Pilz, F. H.; Kirchner, B.; Schiemann, O.; Kielb, P.; Bunescu, A. *Angew Chem Int Ed* **2024**, *63* (32), e202403292.

(458) Zheng, C.; Wang, Y.; Xu, Y.; Chen, Z.; Chen, G.; Liang, S. H. *Org Lett* **2018**, *20* (16), 4824–4827.

ACKNOWLEDGEMENTS

As I reach the conclusion of this journey, I would like to express my deepest gratitude to my supervisor, Prof. Elena Petricci, for her unwavering trust since the very beginning. I am profoundly grateful for the challenges we navigated together throughout these years; her dedication and humanity have served as an inspiring example of excellence within the scientific and academic community.

My sincere thanks also go to Prof. Tanja Gulder for welcoming me into her research group in Saarbrücken. The six months spent under her guidance were an invaluable opportunity that significantly enriched my doctoral path, providing me with an unforgettable professional and personal experience.

I wish to extend my appreciation to Prof. Giulia Berardini, Prof. Fabrizio Manetti, Dr. Barbara Stecca, Prof. Elena Cini, and Prof. Maurizio Taddei. It has been a privilege to collaborate with them and with all the talented scientists I encountered; their expertise and support were fundamental to the realization of our projects.

Finally, a special and heartfelt thank you goes to my colleagues and the many brilliant researchers and students, I have had the privilege to work with. Beyond our shared professional goals this journey has been one of immense personal growth. To those who became true friends: thank you for your constant support, for the brilliant exchanges of ideas, and for making the laboratory feel like home.